ENGINEERING OF
BIOMATERIALS
INŻYNIERIA BIOMATERIAŁÓW
JOURNAL OF POLISH SOCIETY FOR BIOMATERIALS AND FACULTY OF MATERIALS SCIENCE AND CERAMICS AGH-UST
CZASOPISMO POLSKIEGO STOWARZYSZENIA BIOMATERIAŁÓW I WYDZIAŁU INŻYNIERII MATERIAŁOWEJ I CERAMIKI AGH

Number 128-129
Special Issue
Numer 128-129
Numer specjalny
Volume XVII
Rok XVII

DECEMBER 2014
GRUDZIEŃ 2014

ISSN 1429-7248

PUBLISHER:
WYDAWCA:

Polish Society for Biomaterials in Krakow
Polskie Stowarzyszenie Biomateriałów w Krakowie

EDITORIAL COMMITTEE:
KOMITET REDAKCYJNY:

Editor-in-Chief
Redaktor naczelny
Jan Chłopek

Editor
Redaktor
Elżbieta Pamuła

Secretary of editorial
Sekretarz redakcji
Design
Projekt
Katarzyna Trała
Augustyn Powroźnik

ADDRESS OF EDITORIAL OFFICE:
ADRES REDAKCJI:

AGH-UST
30/A3, Mickiewicz Av.
30-059 Krakow, Poland
Akademia Górniczo-Hutnicza
al. Mickiewicza 30/A-3
30-059 Kraków

Issue: 250 copies
Nakład: 250 egz.

Scientific Publishing House AKAPIT
Wydawnictwo Naukowe AKAPIT
e-mail: wn@akapit.krakow.pl

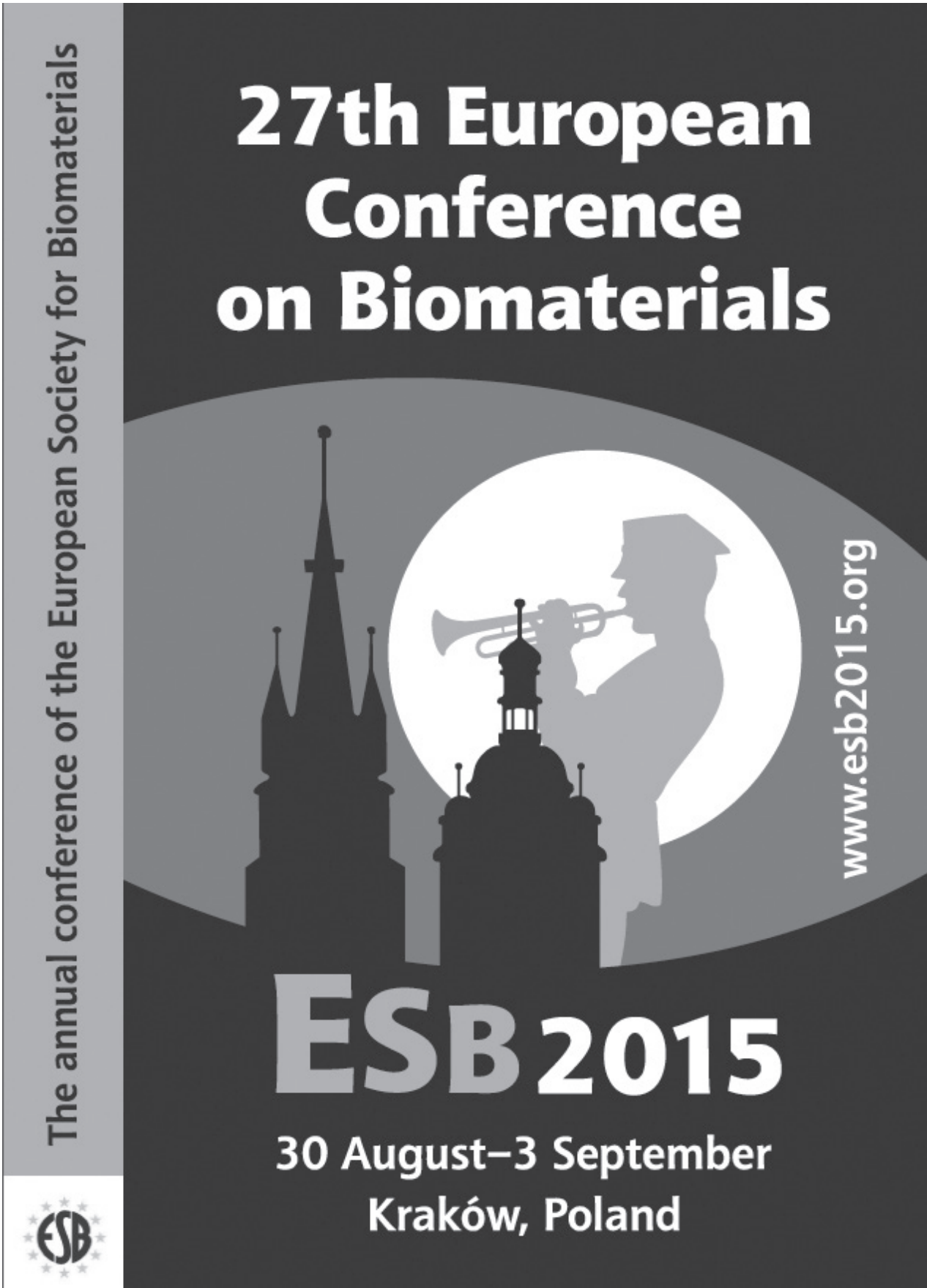

ENGINEERING OF BIOMATERIALS

EDITORIAL BOARD
KOMITET REDAKCYJNY

INTERNATIONAL EDITORIAL BOARD
MIĘDZYNARODOWY KOMITET REDAKCYJNY

25th Conference on

BIOMATERIALS IN MEDICINE AND VETERINARY MEDICINE

13-16 October 2016
Hotel "Perła Południa"
Rytro, Poland
www.biomat.agh.edu.pl

24th Conference on BIOMATERIALS IN MEDICINE AND VETERINARY MEDICINE

9-12 October 2014
Hotel "Perła Południa"
Rytro, Poland
www.biomat.agh.edu.pl

Conference supported by Ministry of Science and Higher Education

SPIS TREŚCI

CONTENTS

Wersja papierowa czasopisma „Engineering of Biomaterials / Inżynieria Biomateriałów" jest jego wersją pierwotną
Printed version of „Engineering of Biomaterials / Inżynieria Biomateriałów" is a primary version of the journal

PHYSIOCHEMICAL AND BIOLOGICAL EVALUATION OF THIN CNTS LAYERS 93
A.Benko, A.Przekora, M.Nocuń, A.Wesełucha-Birczyńska, G.Ginalska, M.Błażewicz

MATERIALS AND METHODS SUPPORTING NERVE REGENERATION IN PERIPHERAL AND CENTRAL NERVOUS SYSTEM 95
J.Laska, P.Bednarz, A.Lis, D.Szarek

THE INFLUENCE OF PRE-COARSENING ON ARCHITECTURAL AND MECHANICAL PROPERTIES OF HIGHLY POROUS TITANIUM DIOXIDE SCAFFOLDS FOR BONE TISSUE ENGINEERING 96
K.Reczyńska, Ł.Rumian, E.Pamuła, H.J.Haugen, H.Tiainen

CARBON FIBROUS MATERIAL FOR CARTILAGE TISSUE TREATMENT 98
J.Markowski, J.Pilch, W.Ścierski, A.Benko, E.Menaszek, M.Błażewicz

CORROSION PROPERTIES OF Ca-DOPED TiO_2 COATINGS 100
B.Burnat, J.Robak, A.Leniart, S.Skrzypek, M.Brycht

STEM CELLS AND THEIR DERIVATIVES - HOPES AND CHALLENGES IN REGENERATIVE MEDICINE 102
E.K.Zuba-Surma

NEW FUNCTIONAL ALIPHATIC POLY-CARBONATES – MATERIALS FOR ADVANCED BIOMEDICAL APPLICATIONS 103
M.Pastusiak, M.Kawalec, J.Jaworska, P.Kurcok, H.Janeczek, P.Dobrzynski

BIOLOGICAL PROPERTIES OF NEW CHITOSAN-FATTY ACIDS DERIVATIVES 107
A.Niemczyk, M.El Fray

OSTEOSYNTHESIS ON THE BASIS OF RESORBABLE POLYMERS IMPLANTS - SELECTED PROBLEMS 108
R.Będziński, J.Chłopek, R.Frątczak, I.Kotela

HYDROGELS BASED ON IONICALLY AND COVALENTLY CROSSLINKED ALGINATES 109
J.Walczak, J.Marchewka, J.Laska

PRELIMINARY STUDY ON THE ELECTROSPUN PLA–BASED NANOFIBRES AS BIOMATERIALS FOR THE TREATMENT OF CARTILAGE 110
A.Magiera, J.Markowski, M.Lesiuk, A.L.Sieron, J.Pilch, S.Błażewicz

THE BIOCOMPATIBILITY IN VITRO STUDY OF AN INNOVATIVE ELASTOMER FOR HEART ASSIST DEVICES CONSTRUCTION 112
M.Kościelniak-Ziemniak, P.Wilczek, R.Kustosz, M.Gonsior, A.Błachowicz, M.El Fray, A.Piegat, M.Piątek-Hnat

THE EFFECT OF SURFACE MODIFICATION ON CORROSION RESISTANCE OF AISI 440B MARTENSITIC STAINLESS STEEL 114
M.Łępicka, M.Grądzka-Dahlke

SYNTHETIC PHOSPHOSERINE-TETHERED HYPERBRANCHED PEPTIDES AS BIOMIMETIC COATINGS FOR MEDICAL IMPLANTS

Stefan Stübinger[1,2], Katja Nuss[1], Alexander Bürki[3], Isabel Mosch[1], Michéle Sidler[1], Steve T. Meikle[4], Brigitte von Rechenberg[1,2], Matteo Santin[4]

[1] Musculoskeletal Research Unit, Equine Hospital, Vetsuisse Faculty ZH, University of Zurich, Winterthurerstrasse 260, CH-8057 Zurich, Switzerland
[2] Center for Applied Biotechnology and Molecular Medicine (CABMM), Vetsuisse Faculty, University of Zurich, Winterthurerstrasse 190, CH-8057 Zurich, Switzerland
[3] Institute for Surgical Biotechnology and Biomechanics, University of Bern, Stauffacherstrasse 78, CH-3014 Bern, Switzerland
[4] Brighton Studies in Tissue-mimicry and Aided Regeneration, Brighton Cluster for Regenerative Medicine, University of Brighton, Huxley Building Lewes Road, Brighton BN2 4GJ, UK

[Engineering of Biomaterials, 128-129, (2014), 1]

Introduction

In orthopedic as well as in oral and maxillofacial surgery there is an increasing demand for a faster osseointegration of implants. To improve the mechanical anchorage and biological-chemical bond between the implant and the surrounding bone, the state-of-the-art increasingly focus on technological innovation of surface treatments at nano-, micro- and macro-scale. While dental implant design, thread pattern and pitch distances are mechanical implant features related to the macro design, surface nanostructuring and biofunctionalization are approaches aiming to enhance biological reactivity through biomimicking topography and biocue presentation. The present study for the first time analyses the in vivo osseointegrative potential of the phosphoserine-tethered dendron coating applied to dental titanium implants.

Materials and methods

Titanium alloy fixtures (diameter 4.1 mm, length 9 mm) underwent the following surface treatments: (i) a sandblasting and etching (SE); (ii) a macro-porous additive manufacturing (AM) achieved by Direct Metal Laser Sintering (DMLS). The AM implants had a solid core, a macroporous shell 500 µm in thickness, and a solid thread over the porous shell thus limiting the exposed porosity present in between the threads. The interthreads length was 1.5 mm. Porosity was designed according to gyroid geometry thus having a geometrically ordered and repeated unit spatial cell consisting in a knot with three arms departing with 120° of angular distance; (iii) Phosphoserine modified dendron coating prepared as described by Meikle et al. . Altogether four different groups were analysed: Sandblasted and etched implants (SE), porous additive manufactured implants (AM), SE with additional dendron functionalisation (SE-PSD) and AM with additional dendron functionalisation (AM-PSD).

Results and discussion

After 2 and 8 weeks the bone-to-implant contact (BIC) total values of SE implants (43.7±12.2%;53.3±9.0%) and SE-PSD (46.7±4.5%;61.7±4.9%) as well as AM implants (20.49±5.1%;43.9±9.7%) and AM-PSD implants (19.7±3.5%;48.3±15.6%) showed no statistically significant differences. For SE-PSD and AM-PSD a separate analysis of only the cancellous BIC demonstrated a statistically significant difference after 2 weeks and 8 weeks. Biomechanical findings proved the overall trend of an increased stability of the porous implants after 8 weeks.

Conclusions

The functionalisation of the implant surface by phosphoserine-tethered dendron increases trabecular bone formation at the interface of metal implants supporting the role played by the implant topography in osseointegration

Acknowledgements

This work has been supported by Eurocoating SpA through the Provincia Autonoma of Trento grant, Biosintering project.

BIOMATERIAL-BASED REGENERATIVE MEDICINE: CHALLENGES & OPPORTUNITIES

Charles James Kirkpatrick

REPAIR-lab, Institute of Pathology, University Medical Center, Johannes Gutenberg University of Mainz, Germany; Sahlgrenska Academy, University of Gothenburg, Sweden
e-mail : kirkpatrick@ukmainz.de

Abstract

For the author there are three major challenges in Regenerative Medicine (RegMed), namely to develop strategies which are translatable, materials which are functional and methods which are predictive. New strategies in RegMed depend on a concerted interdisciplinary effort between the exact and engineering sciences on the one side and the life sciences on the other. As cells synthesize and reside in an extracellular matrix (ECM), which they remodel, a main focus of biomaterial research is the development of injectable, bioresorbable hydrogels containing biological signals which could be released by tissue responses. These interactive materials will certainly increase in importance in the future. However, a major challenge is how to combine them, for example, in composites with load-bearing capacity relevant for human applications. Where synthetic materials such as metals are still essential, as in orthopaedics and traumatology, there is the possibility of adding such responsive materials as coatings to the bulk material. The use of decellularized matrix is also part of the bioinspired approach to developing biomaterials.

In the life sciences great effort is being invested in understanding the so-called „regenerative niche“, which differs from tissue to tissue. Great progress made in stem cell biology has opened up new vistas on the possibility to target

a regenerative niche. Cell-cell and cell-matrix interactions remain a central element of this activity. One of the paradigm shifts we need to master is the step from what is usual even in complex cell biological models, namely the use of purely physiological conditions, to a more realistic situation as would be found in the clinical setting. Thus, we need to understand regeneration in hostile environments, which include post-trauma, cancer and multimorbidity. This will be discussed with examples from the author's own research.

One of the important in vitro methods to investigate the mechanisms involved in regeneration is the use of coculture systems with relevant human cells, usually on tissue culture plastic and, as knowledge progresses, on more complex 3D biomaterial scaffolds. As major limiting factors in bone regeneration are the speed and extent of vascularization, we have established human osteoblast (pOB)-endothelial cell (EC) cocultures to study cellular crosstalk and its possible use for translational strategies [1,2].

Concerning the background, if two cell populations, that is, human pOB and human dermal microvascular EC (HDMEC), are seeded as cell suspensions on an open porous biomaterial scaffold, such as can be made from microfibres of the silk protein fibroin, the two cell types will interact in such a way that lumen-containing, capillary-like structures (CLS) will form as a vascular network [3]. Further molecular studies on the cellular crosstalk revealed that the EC induce an upregulation of growth factor and matrix production in pOB, such as VEGF and collagen type I resp. The EC then respond to these signals by promoting the angiogenic phenotype [4,5].

The following additional approaches have been adopted to study CLS formation: use of early embryonic signals, such as sonic hedgehog (shh), to accelerate both osteo- and angiogenesis [6,7], use of intermittent hypoxia, but not constant hypoxia, to promote vascular sprout formation, and study of possible stimulatory roles for macrophages in the bone regenerative niche [8]. How this is investigated in coculture models will be discussed in the context of future developments. Naturally, all phenomena from in vitro studies require proof of concept in relevant in vivo models, as only this approach can lead to a translational perspective. Thus, we were able to demonstrate that these in vitro pre-formed vessels can rapidly become inosculated, that is, incorporated into the pre-existing microcirculation of host tissue in a subcutaneous implantation model [9]. The major role of the osteoblasts as a natural „drug delivery system" was shown by the fact that host vascular response can be stimulated by these cells even in the absence of a pre-cultivation with endothelial cells [10].

A further aspect offering a promising perspective for the future is NanoMedicine, which uses advances in nanotechnology for medical applications. For reasons of time this will not be addressed in the context of the presentation.

In conclusion, biomaterials, especially so-called responsive biomaterials, are an essential element of modern regenerative medicine, and must be accompanied by state of the art life sciences, from cell and molecular biology to good clinical practice. To achieve this the multidisciplinary approach is a conditio sine qua non.

[Engineering of Biomaterials, 128-129, (2014), 1-2]

Acknowledgements

Supported by the EU Institute of Excellence, EXPERTISSUES, and a research grant from the BMBF/DAAD German-Chinese Cooperation in Regenerative Medicine.

References

[1] Kirkpatrick CJ, Fuchs S, Hermanns MI, Peters K, Unger RE. Cell culture methods of higher complexity in tissue engineering and regenerative medicine. Biomaterials 2007; 28: 5193-5198
[2] Kirkpatrick CJ, Fuchs S, Unger RE. Co-culture systems for vascularization - learning from Nature. Adv Drug Deliv Rev 2011; 63: 291-299
[3] Unger RE, Sartoris A, Peters K, Motta A, Migliaresi C, Kunkel M, Bulnheim U, Rychly J, Kirkpatrick CJ. Tissue-like self-assembly in co-cultures of endothelial cells and osteoblasts and the formation of microcapillary-like structures on three-dimensional porous biomaterials. Biomaterials 2007; 28: 3965-3976
[4] Santos MI, Pashkuleva I, Alves CM, Gomes ME, Fuchs S, Unger RE, Reis RL, Kirkpatrick CJ. Surface-modified 3D starch -based scaffold for improved endothelialization for bone tissue engineering. J Mater Chem 2009; 19: 4091-4101
[5] Santos MI, Unger RE, Sousa RA, Reis RL, Kirkpatrick CJ. Crosstalk between osteoblasts and endothelial cells co-cultured on a polycaprolactone-starch scaffold and the in vitro development of vascularization. Biomaterials 2009; 30: 4407-4415
[6] Dohle E, Fuchs S, Kolbe M, Hofmann A, Schmidt H, Kirkpatrick CJ. Sonic hedgehog promotes angiogenesis and osteogenesis in a co-culture system consisting of primary osteoblasts and outgrowth endothelial cells. Tissue Engineering Part A 2010; 16: 1235-1246
[7] Dohle E, Fuchs S, Kolbe M, Hofmann A, Schmidt H, Kirkpatrick CJ. Comparative study assessing effects of sonic hedgehog and VEGF in a human co-culture model for bone vascularization strategies. E Cells & Mater J 2011; 21: 144-156
[8] Dohle E, Bischoff I, Böse T, Marsano A, Banfi A, Unger RE, Kirkpatrick CJ. Macrophage-mediated angiogenic activation of outgrowth endothelial cells in co-culture with primary osteoblasts. E Cells & Mater J 2014; 27:149-164
[9] Fuchs S, Ghanaati S, Orth C, Barbeck M, Kolbe M, Hofmann A, Eblenkamp M, Gomes M, Reis RL, Kirkpatrick CJ. Outgrowth endothelial cells from human peripheral blood contribute to in vivo vascularization of bone tissue engineered constructs based on starch polycaprolactone scaffolds. Biomaterials 2009; 30: 526-534
[10] Ghanaati S, Unger RE, Webber MJ, Barbeck M, Orth C, Kirkpatrick JA, Booms P, Motta A, Migliaresi C, Sader RA, Kirkpatrick CJ. Scaffold vascularization in vivo driven by primary human osteoblasts in concert with host inflammatory cells. Biomaterials 2011; 32: 8150-8160

NANOFIBROUS MEMBRANE WITH FIBRIN AND COLLAGEN STRUCTURES AS CARRIERS FOR SKIN CELLS

Marketa Bacakova[1,2], Tomas Riedel[3], Denisa Stranska[4], Eduard Brynda[3], Lucie Bacakova[1]

[1]Department of Biomaterials and Tissue Engineering, Institute of Physiology, Academy of Sciences of the Czech Republic, Videnska 1083, 142 20 Prague 4 – Krc, Czech Republic, Tel: +420 296 443 765;
e-mail: marketa.bacakova@biomed.cas.cz
[2]2nd Faculty of Medicine, Charles University in Prague, V Uvalu 84, 150 06, Prague 5, Czech Republic
[3]Institute of Macromolecular Chemistry, Academy of Sciences of the Czech Republic, Heyrovsky Sq. 2, 16206 Prague 6, Czech Republic
[4]Elmarco Ltd., V Horkach 76/18, 460 07 Liberec, Czech Republic

[Engineering of Biomaterials, 128-129, (2014), 2-4]

Introduction

Recently, nanofibrous materials have been interesting for applications in tissue engineering. They better simulate the structure of fibrous component of natural extracellular matrix than conventional flat or microstructured surfaces and they enable adsorption of cell adhesion mediating molecules in an appropriate spatial conformation. The appropriate spatial conformation enables a good accessibility of active sites on these molecules by adhesion receptors on the cell membrane [1,2]. Most of the clinically used skin substitutes consist of non-resorbable material and allogeneic cells thus they cannot provide permanent coverage due to their final rejection. The promising approach could be construction of nanofibrous carriers from biodegradable polymers which will be slowly resorbed in organism and finally replaced by regenerated tissue. The attractiveness of the nanofibrous membrane for adhesion and growth of skin cells can be further promoted by coating the membrane with biomolecules normally presented in natural skin (collagen, hyaluronan) or occurring during wound healing (fibrin).

The study is focused on evaluation of adhesion and growth of human dermal fibroblasts and human immortal HaCaT keratinocytes on polylactide (PLA) nanofibrous membranes coated with fibrin, collagen and fibronectin.

Materials and methods

The PLA membranes were prepared using the novel Nanospider needleless electrospinning technology. We coated the membranes with fibrin, fibrin with fibronectin (cell adhesion-mediating extracellular matrix protein), collagen I or collagen I with fibronectin.

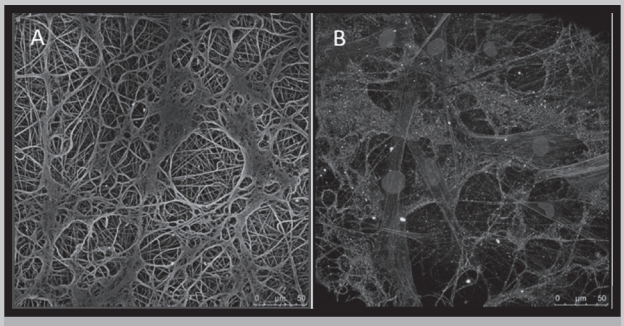

FIG. 1. Immunofluorescence staining of fibrin structure on PLA membranes (A) and phalloidin staining of F-actin (red) and nucleus staining (Hoechst 33342, blue) in human dermal fibroblasts after 24 hours of cultivation on PLA membranes with immunofluorescence stained fibrin structure (green) (B). Leica TCS SPE DM2500 confocal microscope, obj. 40 oil, bar 50 µm.

We evaluated adhesion, morphology, proliferation, metabolic activity (determined by MTS assay) and viability (determined by Live/dead assay) of dermal human fibroblasts and human immortal HaCaT keratinocytes. We also studied collagen production (real-time PCR, immunofluorescence staining) by fibroblasts stimulated by fibrin structure on PLA nanofibrous membrane.

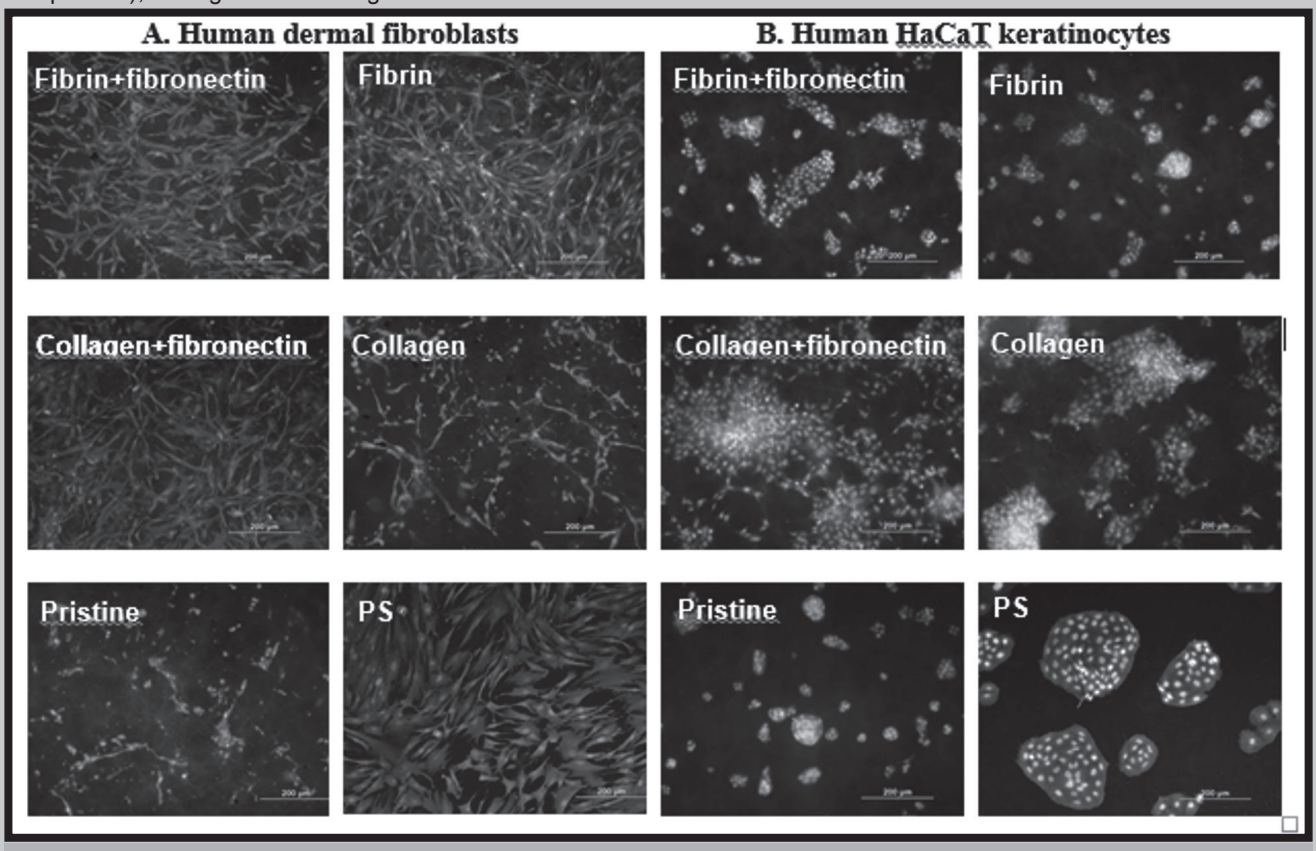

FIG. 2. Morphology of human dermal fibroblasts (A) and human HaCaT keratinocytes (B) after 3 day-cultivation on pristine PLA membranes, PLA membranes with fibrin and fibronectin, fibrin, collagen and fibronectin or collagen. Standard cell culture polystyrene dish (PS) served as a reference material. Cells stained with Texas Red C2-Maleimide and Hoechst #33342. Olympus IX 51 microscope, obj. 10 x, DP 70 digital camera, bar 200 µm.

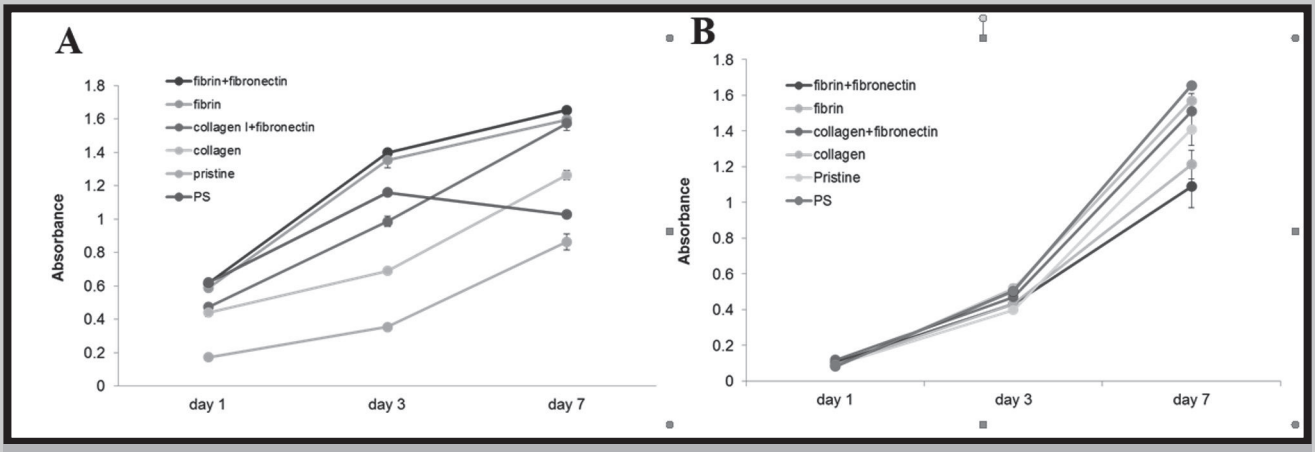

FIG. 3. Mitochondrial activity of human dermal fibroblasts (A) and human HaCaT keratinocytes (B) determined by MTS assay on day 1, 3 and 7 after cell seeding on pristine PLA membranes, PLA membranes with fibrin and fibronectin, fibrin, collagen and fibronectin or collagen. Standard cell culture polystyrene dish (PS) served as a reference material. Arithmetic means ± S.E.M from 9 measurements made on three independent samples for each experimental group and time interval.

Results

Results indicate that PLA nanofibrous membrane promoted adhesion and growth of the skin cells. Fibrin (FIG.1) and collagen structures on PLA membranes further improved adhesion, proliferation and metabolic mitochondrial activity of the skin cells. The human dermal fibroblasts preferentially adhered and were more spread on the membranes coated-with fibrin, fibrin with attached fibronectin on its surface or collagen I with fibronectin than on the membranes coated only with collagen or on the membranes in pristine form (FIG.2A). Moreover, the metabolic activity of human dermal fibroblasts was the highest on the membranes coated with fibrin or fibrin with fibronectin (FIG.3A). In addition, fibrin structures on PLA membranes stimulate fibroblasts to produce collagen I. The membranes coated with collagen I or collagen I with fibronectin promoted spreading of the HaCaT keratinocytes and increased the cell metabolic activity in comparison with pristine membranes or membranes coated with fibrin or fibrin with fibronectin (FIG.2B, 3B). Viability (determined by a Live/Dead assay) of the fibroblasts and the keratinocytes on the membranes was almost 100% on all samples.

Acknowledgements

This study was supported by the Grant Agency of the Charles University in Prague, Czech Republic (GA UK, grant No. 38214) and by the Grant Agency of the Czech Republic (grant No. P108/12/G108).

References

[1] Bacakova L, Filova E, Parizek M, Ruml T and Svorcik V. Modulation of cell adhesion, proliferation and differentiation on materials designed for body implants. Biotechnol. Adv. 2011; 29: 739-67.
[2] Parizek M, Douglas TE, Novotna K, et al. Nanofibrous poly(lactide-co-glycolide) membranes loaded with diamond nanoparticles as promising substrates for bone tissue engineering. Int. J. Nanomed.. 2012; 7: 1931-51.

BLACK ORLON AS PROMISING MATERIAL FOR BONE TISSUE ENEGINEERING

Martin Parizek[1], Miroslav Vetrik[2], Martin Hruby[2], Vera Lisa[1] and Lucie Bacakova[1]

[1] Institute of Physiology, Acad. Sci. Cr, Videnska 1083, 14220 Prague 4-Krc, Czech Republic;
e-mail: parizek@biomed.cas.cz, lucy@biomed.cas.cz
[2] Institute of Macromolecular Chemistry, Acad. Sci. Cr, Heyrovskeho Sq. 2, 16206 Prague 6;
e-mail: Vetrix@Seznam.cz, Mhruby@Centrum.cz

Keywords: *Orlon, polyacrylonitrile, tissue engineering, porous 3D scaffolds, cell adhesion, cell growth, osteoblasts.*
[Engineering of Biomaterials, 128-129, (2014), 4-6]

Introduction

Black Orlon is a promising material for applications in tissue engineering and regenerative medicine. Chemically, it is a carbonized polyacrylonitrile (PAN) containing fibrous ladder structure with chemical functional groups containing oxygen (e.g., hydroxyl, carboxyl), created by heating of Orlon above 300° C in the air atmosphere [1]. Although the biomedical applications of this materials started relatively early (in the seventieth), its potential for these applications has not yet been fully explored. In 1976, black Orlon was tested for construction of blood-contacting anticoagulant surfaces in the form of atrial patches implanted into hearts of experimental dogs [2].

Black Orlon can be relatively easily processed into three-dimensional (3D) scaffolds with microporous structure [3], and also nanofibrous structure created by electrospinning [4]. Microporous 3D scaffolds of carbonized PAN showed excellent osteoinductivity, i.e., they promoted osteogenic differentiation of human bone marrow mesenchymal stem cells without addition of other osteogenic factors [3]. The nanofibrous structure is also of a great importance for bone tissue engineering. It has been reported that nanos-

tructured materials adsorb preferentially vitronectin, which is then recognized by osteoblasts through the KRSR amino acid sequence in the vitronectin molecule (for a review, see [5]). Other properties, which make the black Orlon attractive for bone tissue engineering, are its mechanical resistance and electrical conductivity [4].

Thus, in the present study we investigated the osteoconductivity of microporous 3D black Orlon scaffolds in terms of the adhesion and subsequent growth of human osteoblast-like MG 63 cells in cultures on these materials.

Material and methods

Two types of black Orlon scaffolds were prepared for cytocompatibility tests in vitro, i.e. containing 5 wt.% or 10 wt.% of PAN in succinonitrile, which acted as a porogen. Both mixtures were heated to 35°C, and after stiffening of the material, the succinonitrile was washed out in methanol. The resulting PAN scaffolds with different porosities were further heated to 300 °C, which resulted in the material carbonization, oxidation and establishment of its electrical conductivity.

The materials were cut into samples of 10·10·2 mm in size, sterilized with 70% ethanol for 1 hour, inserted into 24-well plates (TPP, Switzerland; well diameter 1.5 cm) and seeded with human osteoblast-like MG 63 cells (30 000 cells/well, i.e. 17 000 cells/cm^2). Each well contained 1.5 ml of a medium DMEM with 10% of fetal bovine serum and 40 µg/ml of gentamicin. On days 1, 3 and 7 after seeding, the cell number and morphology were evaluated. For each experimental group and time interval, four samples were used. For evaluating the cell number, the cells were trypsinized and counted in Bürker hemocytometer. For evaluating the cell morphology, i.e. the cell shape and the size of cell spreading area, the cells were fixed with 70% ethanol (-20°C, 10 min) and stained with a combination of fluorescence dyes Texas Red C2-maleimide, which stains the cell membrane and cytoplasm, and Hoechst #33342, which stains the cell nuclei. The number and morphology of cells on the sample surface were then evaluated on pictures taken under a Leica TCS SPE DH 2500 confocal microscope. As reference materials, standard tissue culture polystyrene dishes were used.

Results and discussion

Generally, the numbers of cells on the scaffolds prepared from the mixture with 10 wt.% of PAN were significantly higher than on samples with 5 wt.% of PAN. Also the cell spreading areas on 1 day after seeding were significantly larger on the samples with 10 wt.% PAN, and the shape of these cells was mostly polygonal, while the shape of the cells on samples with 5 wt.% of PAN was often rounded (FIG.1). These findings could be explained by a more homogeneous and relatively large size of the pores in the scaffolds based on 10 wt.% of PAN (FIG.2). Our earlier studies revealed that for successful ingrowth of MG 63 cells inside the scaffolds, the pore diameter should be more than 100 µm, optimally 400-600 µm. Smaller pores were usually spanned by cells on the scaffold surface, which led to a lower cell population densities in the scaffolds [6,7].

Nevertheless, in the following days, the cell spreading on samples with 5% of PAN improved, and the cells on both types of scaffolds materials grew continuously without visible cell damage (FIG.2). The cell growth was probably supported by the presence of oxygen-containing groups on the material surface, which promote the adsorption of cell adhesion-mediating proteins in favorable geometrical con-

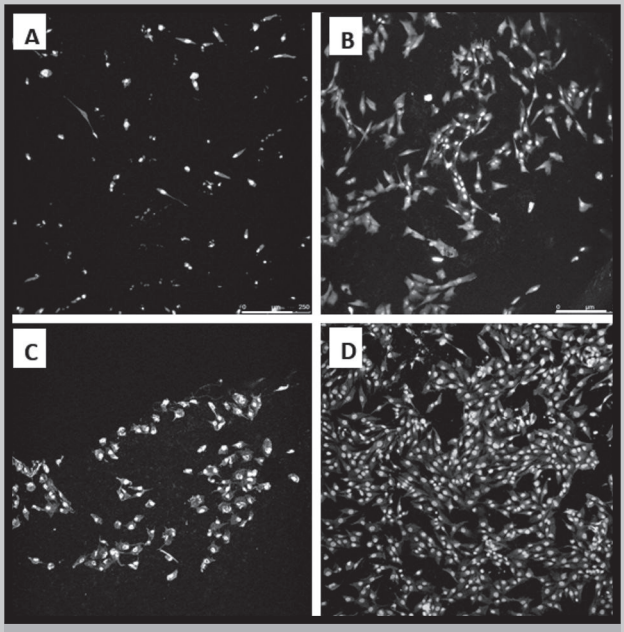

FIG. 1. Morphology of human osteoblast-like MG 63 cells on day 1 (A, B) and on day 3 (C, D) after seeding on black Orlon scaffolds prepared from a mixture containing 5 wt.% of PAN (A, C) or 10 wt.% of PAN (B, D) in succinonitrile. Cells stained with Texas Red C2-maleimide and Hoechst #33342. Leica TCS SPE DH 2500 confocal microscope, obj. 10.0x0.30, bar = 250 µm.

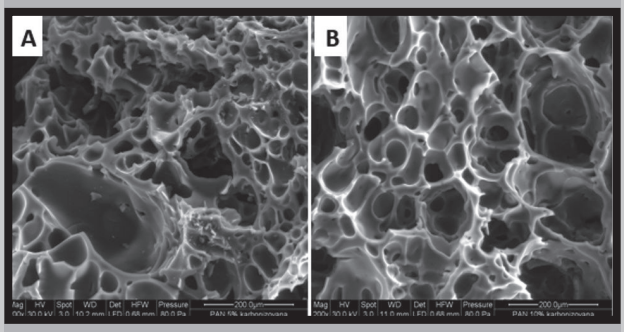

FIG. 2. Morphology of black orlon scaffolds prepared from a mixture containing 5 wt.% of PAN (a) or 10 wt.% of PAN (b) in succinonitrile. Sem microscope quanta 200 feg (fei), bar = 250 µm.

formation. The specific sites in these molecules, e.g. amino acid sequences such as RGD, are better accessible for cell adhesion receptors (for a review, see [5]). Also the material carbonization, i.e. a relative increase of carbon content in the material, and its electrical conductivity can contribute to the enhanced cell adhesion and growth. Similar results were obtained in vascular smooth muscle and endothelial cells grown on polymers modified with ion implantation, also resulting in the polymer oxidation and carbonization [8, 9], or on polymers doped with carbon black [10

Conclusion

It can be concluded that porous scaffolds made of black Orlon provided good support for the adhesion and growth of human bone-derived cells, particularly if they are prepared from matrix with a higher content of PAN, and thus this material is promising for construction of scaffolds for bone tissue engineering. However, these first conclusions need further deeper investigation, e.g. focused on cell cultivation in a

dynamic bioreactor (which enables higher colonization of the inside of the scaffolds), on the depth of penetration of cells inside the scaffolds and on osteogenic cell differentiation. engineering. However, these first conclusions need further deeper investigation, e.g. focused on cell cultivation in a dynamic bioreactor (which enables higher colonization of the inside of the scaffolds), on the depth of penetration of cells inside the scaffolds and on osteogenic cell differentiation.

Acknowledgements

Supported by the Grant Agency of the Czech Republic (grants No. P108/12/1168, P108/10/1106).

References

[1] Rahaman MSA, Ismail AF, Mustafa A: A review of heat treatment on polyacrylonitrile fiber. Polym Degrad Stabil 92: 1421-1432, 2007
[2] Ross JN, Wright JT, Eskin S, Von Koch L, Normann NA: Oxidized orlon as a blood interface. J Biomed Mater Res 10: 583-594, 1976
[3] Ryu S, Lee C, Park J, Lee JS, Kang S, Seo YD, Jang J, Kim BS: Three-dimensional scaffolds of carbonized polyacrylonitrile for bone tissue regeneration. Angew Chem Int Ed Engl 53: 9213-9217, 2014
[4] Chawla S, Naraghi M, Davoudi A. Effect of twist and porosity on the electrical conductivity of carbon nanofiber yarns. Nanotechnology 24: 255708, 2013
[5] Bacakova L, Filova E, Parizek M, Ruml T, Svorcik V: Modulation of cell adhesion, proliferation and differentiation on materials designed for body implants. Biotechnol Adv 29: 739-767, 2011.
[6] Pamula E, Bacakova L, Filova E, Buczynska J, Dobrzynski P, Noskova L Grausova L: The influence of pore size on colonization of poly(L-lactide-glycolide) scaffolds with human osteoblast-like MG 63 cells in vitro. J Mater Sci Mater Med 19: 425-435, 2008
[7] Pamula E, Filova E, Bacakova L, Lisa V, Adamczyk D: Resorbable polymeric scaffolds for bone tissue engineering: The influence of their microstructure on the growth of human osteoblast-like MG 63 cells. J Biomed Mater Res A 89A: 432-443, 2009
[8] Bacakova L, Mares V, Bottone MG, Pellicciari C, Lisa V, Svorcik V: Fluorine-ion-implanted polystyrene improves growth and viability of vascular smooth muscle cells in culture. J Biomed Mater Res 49: 369-379, 2000
[9] Bacakova L, Mares V, Lisa V, Svorcik V: Molecular mechanisms of improved adhesion and growth of an endothelial cell line cultured on polystyrene implanted with fluorine ions. Biomaterials 21: 1173-1179, 2000
[10] Svorcik V, Rybka V, Hnatowicz V, Bacakova L: Polarity, resistivity and biocompatibility of polyethylene doped with carbon black. J Mater Sci Lett 14: 1723-1724, 1995

SILK-COLLAGEN-INSPIRED COPOLYMER: PROMISING BIOMATERIAL PRODUCED BY YEASTS

Małgorzata Włodarczyk-Biegun[1], Marc Werten[2], Frits de Wolf[2], Jeroen van den Beucken[3], Sander Leeuwenburgh[3], Martien Cohen Stuart[1], Marleen Kamperman[1]

[1]Laboratory of Physical Chemistry and Colloid Science, Wageningen University, Wageningen, The Netherlands,
[2]Wageningen UR Food and Biobased Research, Wageningen, The Netherlands,
[3]Department of Biomaterials, Radboud UMC, Nijmegen, The Netherlands

[Engineering of Biomaterials, 128-129, (2014), 6-8]

Introduction

Biomimetic recombinant protein polymers are a new group of materials introduced to regenerative medicine. Due to the high level of precision in the production using recombinant DNA technology, accurate control over material structure and properties is ensured. Importantly, biofunctional domains can be incorporated in a recombinant way. Therefore, the approach may lead to fully functional scaffolds with properties adjusted to a particular biomedical use. In the last three decades several recombinant protein modules for biomedical application were designed, produced and characterized [1,2]. A broad range of them is inspired by nature, such as elastin-like [3,4], collagen-like [3] and silk-like protein sequence [5]. Depending on the DNA sequence, most commonly used hosts organisms to achieve optimal expression are Escherichia coli or yeasts such as Saccharomyces cerevisiae and Pichia Pastoris.

The recombinant protein used in this study is a silk-collagen-inspired copolymer, denoted further as CSC. CSC is expressed by Pichia pastoris in a methanol fed-batch fermentation process and consists of two types of blocks. The silk-inspired block (S) is rich in histidine and is responsible for pH-responsive protein gelation. The S block is flanked by collagen-inspired blocks (C), which stabilize the hydrogel network, due to their hydrophilicity and random coil formation. The resulting CSC protein is soluble in water at low pH, whereas after increasing the pH to physiological values it self-assembles into fibers and at higher concentrations forms a physical hydrogel.

The aim of this study was to synthetize, characterize and evaluate the biological performance of CSC protein polymers. In addition, biofunctionalization of the block copolymer by active sites, such as integrin and proteoglycans binding domains, was performed and the modification effects investigated. It was shown that the obtained scaffolds are self-supporting at low protein concentrations. Our biomaterial appeared to be non-cytotoxic and able to support attachment and proliferation of bone cells. Moreover, the ability to induce a desired cell response by incorporating biofunctionalization was confirmed.

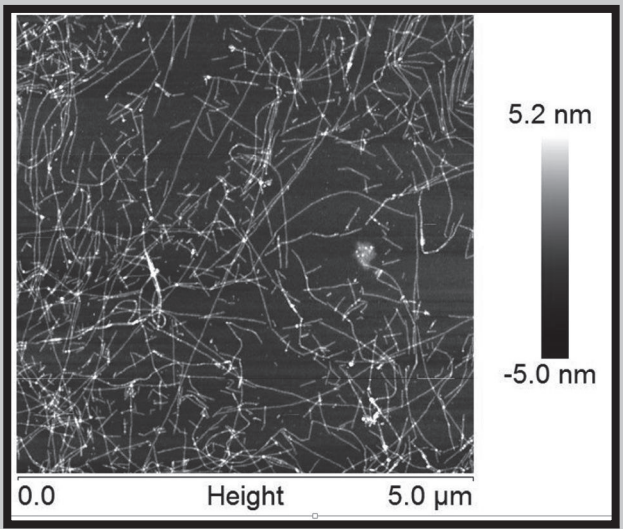

FIG. 1. AFM picture of 1% CSC solution at pH 7.4.

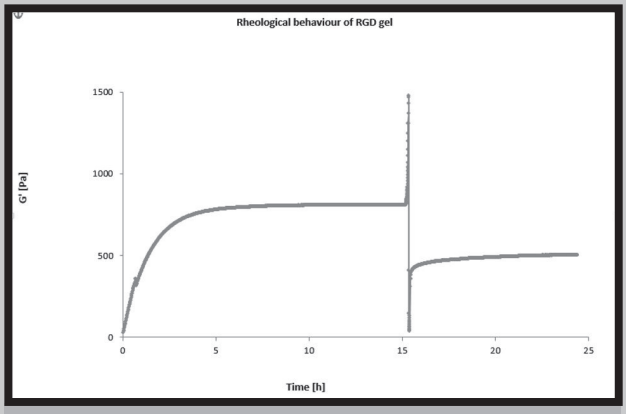

FIG. 2. Rheological data on assembly and healing of 2% CSC-RGD gel at pH 7.4

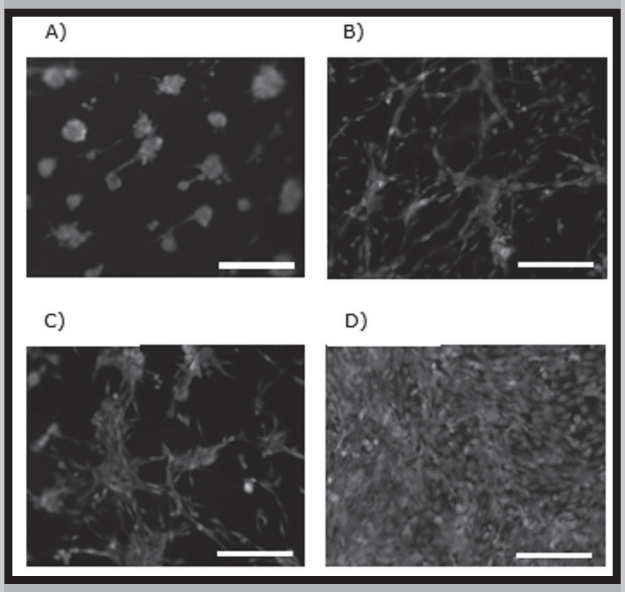

FIG. 3. Cell shape after 5 days of cell culture, visible after staining with Live/Dead assay: A) 100% CSC gel; B) mix of 50% CSC and 50% CSC-RGD gel; C) mix of 50% CSC and 50% CSC-HB gel; D) 100% CSC-HB gel. Scale bar = 200 µm.

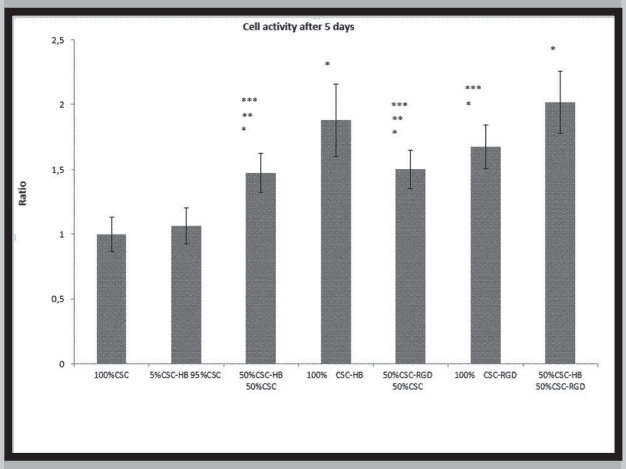

FIG. 4. Cell activity relative to cells on CSC gels after 5 days of cell culture.
*** significant difference in comparison to cells on CSC gels;**
**** significant difference in comparison to cells on 100% CSC-HB gels;**
***** significant difference in comparison to cells on 50% CSC-HB and 50% RGD mixed gels**

Results

Production of CSC protein, and its variants, with recombinantly incorporated integrin binding domains (denoted as CSC-RGD) or heparin binding domains (denoted as CSC-HB), consisted of fixed, consecutive steps, typical for recombinant DNA technology. The process started with the design of peptide sequence, and was followed by construction of encoding genes, transfection to a host organism Pichia pastoris and expression of proteins in methanol fed-batch fermentation of yeasts. To obtain the final product, selective ammonium sulphate precipitation was used for purification, after which the protein was lyophilized. The materials were characterized with a variety of techniques: SDS-PAGE gel analysis, amino acid composition and sugar content analysis, N-terminal sequencing and MALDI-TOF MAS. The analysis confirmed that CSC, CSC-RGD and CSC-HB proteins were successfully obtained in a recombinant way.

To induce fibril formation, an amount of protein was dissolved at low pH, followed by an increase in pH to physiological value of 7.4. The AFM picture (FIG.1) of 1% protein solution (protein concentration 10 g/l) at physiological pH shows fiber formation by the protein after 24 hours incubation time. The driving force in the assembly is stacking of S blocks with uncharged histidine.

The cell culture study showed that cells could survive for 24 days at all variants of CSC gels (FIG.3.). The differences in cell behaviour and activity, depending on the presence and amount of added specific bioactive domains, were clearly visible after 5 days of culture. Although cells were fully viable on the all gel types, plain CSC did not enhance cells spreading. Addition of 50% material with integrin binding domains increased cell spreading; the cell shape was more elongated. Addition of heparin binding domains improved cells spreading and proliferation. The cells seemed to spread a little less but the number of cells was higher on the gels with heparin binding domains. The cell activity test (FIG.4.) confirmed the effectiveness of biofunctional domain incorporation into our biomaterial. Cell activity was significantly higher on the gels containing functional domains than the cell activity of pure CSC gel. However, addition of 5% material with heparin binding domains appeared to be insufficient to improve material performance. According to the obtained results, the addition of heparin binding domains in high concentrations or a combination of heparin and integrin binding domains was most profitable for cells.

Conclusions

Biocompatible scaffolds composed of silk-collagen inspired copolymer were produced in a fermentation process of genetically engineered yeasts. Incorporation of bioactive domains in recombinant way was successful. The obtained fibrillar hydrogel scaffolds were strong enough at 2% protein concentration to perform a cell culture study. An in vitro study conducted with MG 63 cells cultured on top of the hydrogels showed that cells survived on the scaffolds and attached to the surface. The study proved that biological properties of artificial proteins can be nicely tuned by incorporation of specific bioactive domain. Well- designed recombinant protein polymers are promising materials for use in regeneration medicine to induce desired cellular response.

References

[1] Kopecek J, Yang J. Smart self-assembled hybrid hydrogel biomaterials. Angew Chem Int Ed Engl 2012;51:7396-417.
[2] Sengupta D, Heilshorn SC. Protein-engineered biomaterials: Highly tunable tissue engineering scaffolds. Tissue Eng Part B Rev 2010;16:285-93.
[3] Bracalello A, Santopietro V, Vassalli M, Marletta G, Del Gaudio R, Bochicchio B, et al. Design and production of a chimeric resilin-, elastin-, and collagen-like engineered polypeptide. Biomacromolecules 2011;12:2957-65.
[4] MacEwan SR, Chilkoti A. Elastin-like polypeptides: Biomedical applications of tunable biopolymers. Biopolymers 2010;94:60-77.
[5] Rabotyagova OS, Cebe P, Kaplan DL. Self-assembly of genetically engineered spider silk block copolymers. Biomacromolecules 2009;10:229-36.
[6] Wlodarczyk-Biegun MK, Werten MWT, de Wolf FA, van den Beucken JJJP, Leeuwenburgh SCG, Kamperman M, et al. Genetically engineered silk-collagen-like copolymer for biomedical applications: Production, characterization and evaluation of cellular response. Acta Biomaterialia 2014;10:3620-9.

EFFECT OF INTERNAL ARCHITECTURE ON MECHANICAL PROPERTIES OF POLYCAPROLACTONE SCAFFOLDS FOR TISSUE REGENERATION

Barbara Ostrowska, Wojciech Święszkowski, Krzysztof J. Kurzydłowski

Division of Materials Design,
Faculty of Materials Science and Engineering,
Warsaw University of Technology,
02-507 Warsaw, Poland.

Abstract

The aim of the study was to investigate the influence of internal architecture of 3D printed scaffolds on their mechanical properties. The polycaprolactone scaffolds with six different internal architectures fabricated by rapid prototyping method were tested in this study. The scaffolds were plotted using a 330 μm dispensing needle, layer by layer with lay-down pattern of the fibers: 00/150/300; 00/300/600; 00/450/900, 00/600/1200, 00/750/1500 and 00/900/1800. Morphological analyses and mechanical properties examinations were performed. The obtained scaffolds had structures with high open porosity (50-60%) and interconnected pores ranging from 380 to 400 μm. The different lay-down pattern and the angle deposition of successive fiber layers resulted in different internal architecture and pore shape of the constructs, what was confirmed by scanning electron microscopy and microtomography analyzes. The geometries 00/900/1800 and 00/600/1200 were characterized with the most regular shape of pores between all analyzed architectures. The pores for 00/150/300 and 00/300/600 were not regular and arranged as a ladder-like helicoid structures. The lay-down pattern of the fibers affected significantly the mechanical properties of the scaffolds. The Young's modulus (E) of the scaffolds was increasing with increase of the angle deposition between successive layers. The scaffolds were also subjected to cyclic loading and again geometry and mechanical properties were under investigation. For all type of scaffolds the differences of mechanical properties after dynamic compression have been noticed. The geometries 00/900/1800 and 00/600/1200 exhibited the highest Young's Modulus after dynamic compression according to the rest of analyzed samples. According to the conducted research there is a clear correlation between internal architecture of polymeric scaffolds and their mechanical properties.

[Engineering of Biomaterials, 128-129, (2014), 8-9]

Introduction

The number of critical bone defects caused by injury, cancer or aging of the world population is increasing. Techniques currently used to repair these defects suffer from several disadvantages, such as a lack of mechanical and biological matching of bone characteristics, the requirement of second surgery and the risk of pathogen transmission. Scaffolds made of bioresorbable polymers are a promising alternative as they temporarily support regeneration of the damaged site and undergo complete degradation after new tissue is formed. Fabrication of bioresorbable polymers scaffolds for tissue engineering becomes a popular research topic in present days. Biodegradable and biocompatible scaffolds are required for 3D implants as a temporary support for cell growth and cell adhesion. There are several fabrication methods currently used for creating 3D porous structures with high porosity and interconnected pores. A rapid prototyping (RP) is one of the most interesting one. It allows for fabrication scaffolds with predesigned external geometry and internal architecture as well as required mechanical properties. For the cell culture survival on the scaffolds 3D constructs needs characterize with interconnecting porous to allow the culture media 3D flow in order to ensure continuous supply of nutrients and metabolites. Tissue formation is generated on porous scaffolds. Mechanical strength of the human body implant is directly connected with internal architecture of the scaffold and has to be tailored according to the different implant application. The goal of the present study was to determine the changes of the mechanical properties of fibrous PCL scaffolds with differnet internal architecture. Scaffolds with different lay-down pattern were investigated to select the optimal fiber lay-down orientation for bone tissue engineering.

Materials & methods

Cylindrical porous scaffolds (height: 4mm, diameter: 6mm) with three-dimensional orthogonal periodic porous architectures, were manufactured by Bioscaffolder® machine (SYSENG, Germany) from ε- polycaprolactone granulate (Sigma Aldrich PCL, average Mn ca. 70-90kDa), (FIG.1). The melted polymer was plotted with a 330μm dispensing needle layer by layer, with lay-down pattern of the fibers: 00/150/300; 00/300/600; 00/450/900, 00/600/1200, 00/750/1500 and 00/900/1800. The temperature of the fabrication process was between 900 and 1000C. After samples fabrication the internal architecture were investigated by

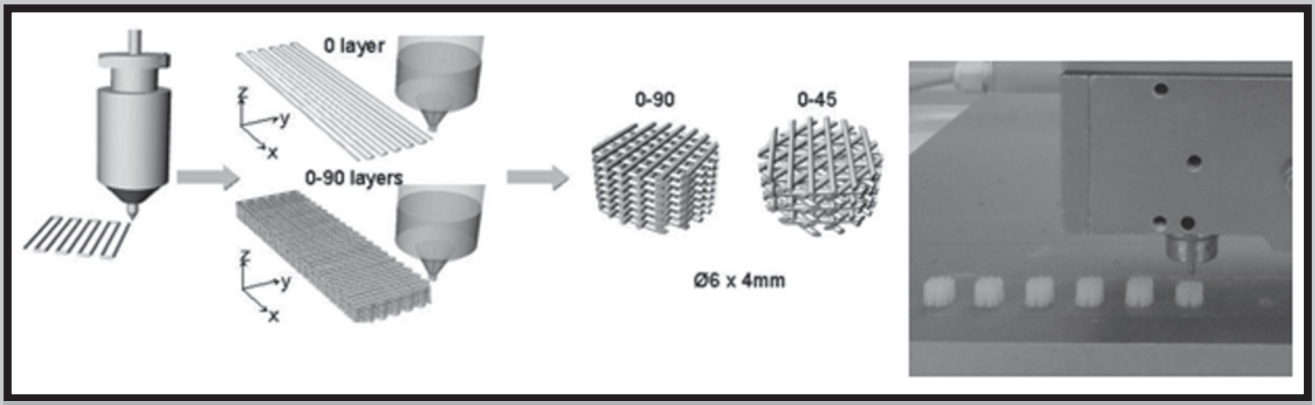

FIG. 1. Samples manufactured using Bioscaffolder® machine (SYSENG, Germany)

scanning electron microscope (HITACHI SU8000) and computed microtomography (SkyScan 1172). Static and dynamic compression tests were carried out using ElectroForce 5100 BioDynamic (BOCE, USA) at room temperature, at a crosshead speed of 1mm/min, up to 10% of compressive strain. At the beginning mechanical properties of the samples were studied in static compression tests. Then cyclic load (frequency 1Hz, 3600 cycle number) were applied to the scaffolds. After the dynamic tests, the same samples were tested in static compression conditions again.

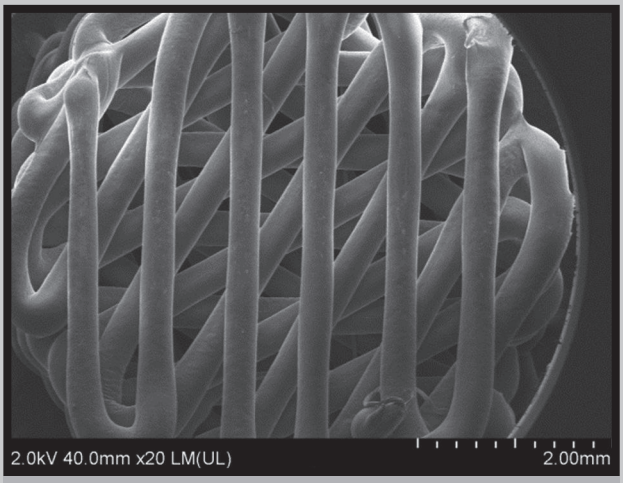

FIG. 2. Scanning Electron Microscopy (SEM) images of samples with internal architecture A) 00/150/300; B) 00/300/600; C) 00/450/900, D) 00/600/1200, E) 00/750/1500 and F) 00/900/1800.

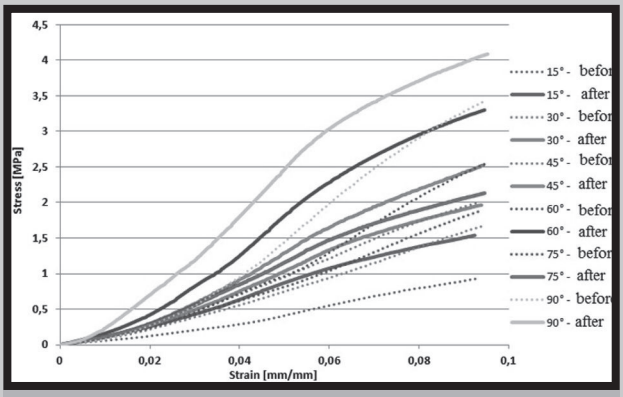

FIG. 3. Results of compression tests before and after cyclic load.

Results & discussion

The SEM and µCT observations of the microfibers scaffolds showed a well-defined internal geometry with regular interconnected pores ranging from 380 to 450µm with uniform distribution, as well as with high porosity (45-55%) (Fig. 2). The extruded filaments had a regular circular geometry with diameter of 300µm, corresponding to the used nozzle tip (330µm) (FIG.2). Delaminating of the layers wasn't noticed. The compression tests before and after cyclic loads were performed to show the influence of internal architecture on the mechanical properties of the scaffolds in dynamic conditions. Mechanical properties analysis showed big differences in elastic modulus between the tested scaffolds. The results indicate that the samples with lay-down pattern orientation 00/900/1800 and 00/600/1200 had the highest Yong's modulus before and after cyclic loading (FIG.3). Moreover, all analyzed samples had stiffened up after dynamic compression. The connections between layers remained consistent under compression in all tested constructions.

Conclusions

This study shows that scaffold architecture is relevant from a mechanical point view, since pore size and shape influence stiffness of the 3D constructs. The 3D plotter is able to fabricate structures with high reproducibility and flexibility, and it offers a wide variety of solutions in term of different architecture and geometrical configurations. The study demonstrates that PCL scaffolds with internal orientation 00/900/1800 and 00/600/1200 have the best mechanical properties among tested samples. This type of scaffold can be applied to produce highly functionalized 3D construct for bone tissue engineering aplications.

References

[1] R. Landers. U.Hübner. R. Schmelzeisen. R. Mülhaupt. "Rapid prototyping of scaffolds derived from thermoreversible hydrogels and tailored for applications in tissue engineering" Biomaterials 23 (2002) 4437-4447

[2] D.W. Hutmacher. M.A. Woodruff. Design. Fabrication and Characterization of Scaffolds via Solid Free-Form Fabrication Techniques. Biomaterials Fabrication and Processing Handbook. CRC Press; p.45-67. 2008

ANALIZA STRUKTURY CHEMICZNEJ HYDROKSY-APATYTU WZBOGACONEGO JONAMI M_N^{2+} WYGRZEWANEGO W WYSOKIEJ TEMPERATURZE

Joanna Kolmas, Mateusz Jabłoński, Anna Ślósarczyk, Waclaw Kolodziejski

[1]Warszawski Uniwersytet Medyczny,
Wydział Farmaceutyczny,
Katedra i Zakład Chemii Nieorganicznej i Analitycznej,
ul. Banacha 1, 02-097 Warszawa, Polska
[2] AGH Akademia Górniczo-Hutnicza,
Wydział Inżynierii Materiałowej i Ceramiki,
Al. Mickiewicza 30, 30-059 Kraków, Polska

Streszczenie

Syntetyczne hydroksyapatyty (HAs), ze względu na wysoką biokompatybilność z ludzkimi tkankami zmineralizowanymi, są szeroko stosowane jako biomateriały w ortopedii oraz stomatologii. Struktura hydroksyapatytu $Ca_{10}(PO_4)_6(OH)_2$ pozwala na szereg jonowych podstawień, które mogą zachodzić zarówno w pozycji kationów wapnia jak i ortofosforanów oraz strukturalnych grup hydroksylowych. Wprowadzenie dodatkowych jonów do struktury hydroksyapatytu może wpływać na jego właściwości biologiczne i fizykochemiczne.

Mangan jest śladowym pierwiastkiem wchodzącym w skład biologicznego apatytu (mineralnego składnika kości oraz zębów). Odgrywa on kluczową rolę w powstawaniu matrycy organicznej. Dodatkowo indukuje integryny, grupę receptorów umożliwiających adhezję komórek. Ostatnio przeprowadzone badania potwierdziły, że hydroksyapatyt wzbogacony jonami manganu Mn^{2+} wykazuje łatwiejszą osteointegrację niż czysty hydroksyapatyt, dlatego też może być z powodzeniem stosowany jako pokrycie implantów metalicznych.

W powyższej pracy wykorzystano standardową metodę mokrą do syntezy hydroksyapatytów zawierających niewielkie ilości jonów Mn^{2+}. Otrzymane próbki wygrzewano następnie w dwóch różnych temperaturach: 800 oraz 1250°C.

Głównym celem tej pracy było zbadanie wpływu procesu termicznego na strukturę chemiczną hydroksyapatytu wzbogaconego jonami manganowymi. Do badań fizykochemicznych wykorzystano: proszkową dyfraktometrię rentgenowską (PXRD), mikroskopię elektronową (SEM oraz TEM), spektroskopię w podczerwieni (FT-IR) oraz spektroskopię magnetycznego rezonansu jądrowego w ciele stałym (ssNMR).

Wprowadzenie jonów Mn^{2+} do struktury hydroksyapatytu zostało potwierdzone dzięki zastosowaniu metod PXRD oraz ssNMR. Wykazano także, że obecność manganu ułatwia termiczny rozkład hydroksyapatytu do oksyhydroksyapatytu. Próbki wygrzewane w wyższej temperaturze (1250°) okazały się niehomogeniczne. Zawierały, oprócz fazy hydroksyapatytu, dodatkowe fazy krystaliczne: oksyhydroksyapatyt, oksyapatyt, dziewięciotlenek dwufosforu i czterowapnia (TTCP) oraz α-ortofosforan wapnia (αTCP). Użyte metody fizykochemiczne pozwoliły stwierdzić, że w próbkach kalcynowanych (wygrzewanych w temperaturze 800°C) jony manganowe zajmują przede wszystkim pozycje wapnia Ca(I) w komórce elementarnej hydroksyapatytu. Podczas wygrzewania w wyższej temperaturze dochodzi do częściowego przemieszczenia jonów manganu w pozycje Ca(II).

[Engineering of Biomaterials, 128-129, (2014), 10-11]

STRUCTURAL CHARACTERIZATION OF THERMALLY PROCESSED HYDROXYAPATITE ENRICHED IN Mn_2^+ IONS

Joanna Kolmas, Mateusz Jabłoński, Anna Ślósarczyk, Waclaw Kolodziejski

[1]Medical University of Warsaw, Faculty of Pharmacy,
Department of Inorganic and Analytical Chemistry,
1 Banacha str., 02-097 Warsaw, Poland
[1] AGH University of Science and Technology,
Faculty of Materials Science and Ceramics,
30 Mickiewicz Ave, 30-059 Cracow, Poland

Abstract

Synthetic hydroxyapatites (HAs), due to their high compatibility with human mineralized tissues are widely used in implant materials for orthopaedic and dental applications. Hydroxyapatite structure $Ca_{10}(PO_4)_6(OH)_2$ is tolerant to several ionic substitutions. They can occur in HA for calcium cations, for orthophosphates and structural hydroxyl ions. The incorporation of additional ions into the apatite crystals may change their biological or physicochemical properties.

Manganese appears in biological apatite (bone and teeth) and plays a key role in the development of organic matrix. It also induces integrins, receptors mediating cellular interactions with extracellular matrix and cell surface ligands. Manganese-doped HA exhibits better osseointegration than pure HA, thus it may be used as a coating of metallic implants.

In this paper, hydroxyapatites enriched in small amounts of manganese ions Mn^{2+} were synthesized by standard wet method. The obtained samples were heated at two different temperatures: 800 and 1250ºC. The main aim of this study was to determine the influence of thermal processing of hydroxyapatite enriched in Mn^{2+} ions on its chemical structure. For profound physicochemical studies powder X-ray diffractometry (PXRD), electron microscopy (SEM and TEM), infrared spectroscopy (FT-IR) and solid-state nuclear magnetic resonance (ssNMR) were applied.

The incorporation of manganese ions was confirmed using PXRD and ssNMR methods. It was found that the presence of manganese facilitates hydroxyapatite dehydration and decomposition to oxyhydroxyapatite. The samples heated at 1250ºC are not homogenous and contain, apart from hydroxyapatite other crystalline phases: oxyhydroxyapatite, oxyapatite, tetracalcium phosphate (TTCP) and α-tricalcium phosphate (αTCP). In the calcined sample (heated at 800ºC), manganese ions preferentially occupy the Ca(I) position in the hydroxyapatite crystallographic unit cell. During heat treatment at the higher temperature, some Mn^{2+} ions move to the Ca(II) position.

[Engineering of Biomaterials, 128-129 (2014), 10-11]

Podziękowania

J.K. dziękuje Fundacji na rzecz Nauki Polskiej za wsparcie badań w ramach programu POMOST, współfinansowanego przez Unię Europejską (Fundusz Rozwoju Regionalnego).

Badania TEM zostały wykonane w Laboratorium Mikroskopii Elektronowej, w Instytucie Biologii Doświadczalnej im. M. Nenckiego. Do badań wykorzystano aparaturę zainstalowaną w ramach projektu współfinansowanego przez Unię Europejską (Fundusze Strukturalne): Centrum Zaawansowanych Technologii – wyposażenie Laboratorium Obrazowania Biologicznego i Medycznego.

Acknowledgements

J.K. thanks the Foundation for Polish Science for supporting her with the Parent-Bridge Programme that was co-financed by the EU European Regional Development Fund.

The TEM studies were performed in the Laboratory of Electron Microscopy, Nencki Institute of Experimental Biology, Warsaw, Poland. We used equipment installed within the project sponsored by the EU Structural Funds: Centre of Advanced Technology BIM – Equipment purchased for the Laboratory of Biological and Medical Imaging.containing selenite ions. The toxicity of the obtained materials were also studied.

OCENA TRWAŁOŚCI WŁÓKIEN PRZEZNACZONYCH NA PODŁOŻA DLA INŻYNIERII TKANKOWEJ W PŁYNACH FIZJOLOGICZNYCH

Izabella Rajzer[1]*, Ryszard Kwiatkowski[2]

ATH Akademia Techniczno-Humanistyczna w Bielsku-Białej, ul. Willowa 2, 43-309 Bielsko-Biała, Polska:
[1]Wydział Budowy Maszyn i Informatyki, Katedra Podstaw Budowy Maszyn, Zakład Inżynierii Materiałowej
[2]Wydział Nauk o Materiałach i Środowisku, Instytut Inżynierii Tekstyliów i Materiałów Polimerowych.
* e-mail: irajzer@ath.bielsko.pl

Streszczenie

Bardzo dużą rolę w procesie degradacji implantów odgrywa środowisko płynów fizjologicznych, których wpływ zależy od właściwości fizycznych i chemicznych materiału polimerowego oraz od jego reaktywności. W niniejszej pracy oceniono wpływ płynu PBS na trwałość kompozytowych włókien polikaprolakton / hydroksyapatyt w warunkach in vitro. Stopień degradacji włókien określano na podstawie zmian pH medium, stężenia jonów sodu i potasu w płynie po inkubacji próbek oraz zmian masy próbek podczas inkubacji. Ocenę zmian zachodzących we włóknach pod wpływem płynu PBS przeprowadzono wykorzystując skaningową mikroskopię elektronową (SEM) oraz rentgenowską analizę strukturalną (WAXD). Badania degradacji włókien przeprowadzone podczas inkubacji próbek w płynach fizjologicznych wykazały, że wytworzone włókna kompozytowe charakteryzuję się stabilnością w środowisku płynów ustrojowych przez długi okres czasu. Niewielkie zmiany na powierzchni włókien, zaobserwowane po 10 miesiącach inkubacji, w płynie fizjologicznym, wskazują na rozpoczęcie procesu degradacji, stąd też można przypuszczać, że czas całkowitej biodegradacji włókien może być skorelowany z czasem potrzebnym do kompletnego odtworzenia tkanki.

Słowa kluczowe: *włókna bioaktywne, podłoża, Inżynieria Tkankowa, degradacja, polikaprolakton*

[Inżynieria Biomateriałów, 128-129, (2014), 11-15]

ASSESSMENT OF THE STABILITY OF PCL-FIBRES INTENDED FOR USE AS SCAFFOLDS FOR TISSUE ENGINEERING IN PHYSIOLOGICAL FLUIDS

Izabella Rajzer[1]*, Ryszard Kwiatkowski[2]

ATH University of Bielsko-Biala,
1 Willowa street, 43-309 Bielsko-Biala, Poland:
[1]Faculty of Mechanical Engineering and Computer Science, Department of Mechanical Engineering Fundamentals, Division of Materials Science.
[2]Faculty of Materials and Environmental Sciences. Institute of Textile Engineering and Polymer Materials.
* e-mail: irajzer@ath.bielsko.pl

Abstract

Very important role in the process of implant degradation is played by the physiological fluid environment, the impact of which depends on the physical and chemical properties of the polymers and on its reactivity. This study evaluates the effect of PBS on the stability of composite polycaprolactone/hydroxyapatite fibres in vitro. The degree of degradation of the fibres was determined by the changes in pH of the fluid, the concentration of sodium and potassium ions in the fluid after incubation of the sample, and the changes in the weights of samples during incubation. Assessment of the changes in the fibres under the influence of PBS was carried out using scanning electron microscopy (SEM) and X-ray structural analysis (WAXD). The study of the degradation of fibres carried out during the incubation of samples in physiological fluids showed that the composite fibres produced are stable in the environment of physiological fluids over a long period of time. Minor changes on the surface of the fibres, observed after 10 months of incubation, in a body fluid, indicate the start of a process of degradation, hence it can be assumed that the time of total biodegradation of the fibres may be correlated with the time needed for a complete restoration of tissue.

Keywords: *Bioactive fibres, scaffold, tissue engineering, degradation, polycaprolactone*

[Engineering of Biomaterials, 128-129, (2014), 11-15]

Wprowadzenie

Polikaprolakton (PCL), jest biozgodnym polimerem o dłuższym czasie degradacji niż inne polimery z grupy poliestrów alifatycznych, dzięki temu biomateriały wykonane z tego polimeru mogą być wszczepiane w miejscach narażonych na szczególne obciążenia [1]. Zastosowanie PCL, cieszącego się lepszymi parametrami mechanicznymi, do wytwarzania włókien a z nich podłoży do leczenia ubytków tkanek, pozwala na utrzymanie odpowiedniej przestrzeni między komórkami wymaganej dla wzrostu komórek i formowania matrycy zewnątrzkomórkowej, nie tylko do momentu wytworzenia nowej tkanki, ale do momentu uzyskania przez nią odpowiednich parametrów mechanicznych [2].

Degradacja włókien z polikaprolaktonu w środowisku roztworów wodnych zależy od wielu czynników. Z jednej strony od budowy i własności samego polimeru takich jak budowa chemiczna, masa molowa, polidyspersja, temperatura zeszklenia (Tg), temperatura topnienia (Tm), krystaliczność, moduł elastyczności, pole powierzchni próbki i jej hydrofilowość czy hydrofobowość [3]. Obecność płynów powoduje hydrolizę nietrwałych wiązań w przypadku poliestrów oraz sprzyja wytwarzaniu rodników hydroksylowych lub innych reaktywnych grup, które mogą inicjować reakcje wolnorodnikowe. Ponadto istotnym czynnikiem mającym wpływ na sposób degradacji włókien są warunki panujące w otaczającym je środowisku (temperatura, pH itp.) [4].

PCL jest powszechnie stosowany do wytwarzania trójwymiarowych podłoży dla inżynierii tkankowej [5-6]. Jednakże słaba hydrofilowość podłoży z PCL wpływa na gorszą adhezje, proliferację i różnicowanie się komórek. Ponadto podłoża z PCL nie wykazują właściwości bioaktywnych, dlatego często modyfikowane są bioaktywnymi dodatkami [7]. W niniejszej pracy oceniono wpływ płynu PBS na trwałość kompozytowych włókien polikaprolakton/ hydroksyapatyt w warunkach in vitro. Włókna z czystego polikaprolaktonu jak również włókna kompozytowe modyfikowane hydroksyapatytem poddano ocenie trwałości, określając wpływ płynu PBS na zachowanie się próbek w środowisku in vitro. W organizmie człowieka polikaprolakton ulega powolnej, trwającej około 2 lata biodegradacji, która zachodzi na skutek hydrolizy wiązań estrowych. Przeprowadzone badania miały na celu określenie trwałości włókien w warunkach in vitro podczas inkubacji w płynie PBS

Materiały i metody

Do badań wykorzystano dwa rozdaje włókien wytworzonych metodą formowania za stopu: (1) włókna PCL niemodyfikowane oraz (2) włókna modyfikowane 5% dodatkiem hydroksyapatytu. Dokładny opis sposobu formowania włókien oraz wpływu dodatku hydroksyapatytu na strukturę i własności włókien opisano w poprzedniej publikacji [8]. Do wytwarzania włókien wykorzystano poli(ε-kaprolakton) firmy Sigma Aldrich (PCL) o masie cząsteczkowej 70000-90000 g/mol oraz nano-hydroksyapatyt syntetyczny (n-HAp) wytworzony w Katedrze Ceramiki i Materiałów Ogniotrwałych, Wydziału Inżynierii Materiałowej i Ceramiki, Akademii Górniczo-Hutniczej w Krakowie [9].

Ocenę trwałości włókien otrzymanych metodą formowania ze stopu przeprowadzono w płynie PBS przez okres 12 miesięcy. Płyn PBS jest wodnym roztworem soli fizjologicznej (0,9% NaCl) buforowanej fosforanami o pH 7,4 (ang. phosphate buffered saline). Próbki zanurzono w płynie PBS i inkubowano przez okres 12 miesięcy w polipropylenowych pojemnikach o pojemności 15 ml (firmy FALCON) w temperaturze 37°C. Stopień degradacji włókien określano na podstawie zmian pH medium, stężenia jonów

Introduction

Polycaprolactone (PCL) is a biocompatible polymer with longer degradation time than the other polymers from the group of aliphatic polyesters, thus biomaterials made using this polymer can be implanted in areas subjected to increased load [1]. The use of PCL, which has better mechanical parameters, to make fibres, from which scaffolds for the treatment of tissue defects are made, allows for maintaining sufficient space between the cells required for cell growth and extracellular matrix formation, not only until the moment of producing new tissue, but until it obtains the required mechanical parameters [2].

Degradation of polycaprolactone fibres in the environment of aqueous solutions depends on many factors. On the one hand, they include the structure and properties of the polymer itself, such as chemical structure, molecular weight, polydispersity, glass transition temperature (Tg), melting temperature (Tm), crystallinity, modulus of elasticity, the surface area of the sample and its hydrophilicity or hydrophobicity [3]. The presence of liquid causes the hydrolysis of labile bonds in the case of polyesters and promotes the formation of hydroxyl radicals or other reactive groups which can initiate free radical reactions. Another important factor affecting the way fibres are degraded are conditions in their surrounding environment (temperature, pH, etc.) [4].

PCL is commonly used to make three-dimensional scaffolds for tissue engineering [5-6]. However, poor hydrophilicity of PCL scaffolds results in a less successful adhesion, proliferation, and differentiation of cells. In addition, PCL scaffolds show no bioactive properties, which is why they often are modified with bioactive additives [7]. This study evaluates the effect of PBS on the stability of the composite polycaprolactone/hydroxyapatite fibres in vitro. Fibres made of pure polycaprolactone as well as composite fibres modified with hydroxyapatite were evaluated for stability, determining the effect of PBS on the behaviour of the samples in vitro. In the human body, polycaprolactone undergoes a slow biodegradation over the period of approximately two years, which occurs as a result of hydrolysis of

Materials and methods

In the study two types of fibres produced by melt spinning were used: (1) unmodified PCL fibres and (2) modified fibres containing 5% of hydroxyapatite. Detailed description of the method of the fibres production and the effect of the addition of hydroxyapatite on the structure and properties of fibres are described in a previous publication [8]. Poly(ε-caprolactone), with the molecular weight of 70000-90000 g/mol, made by Sigma Aldrich (PCL) was used for the fibres production, and synthetic nano-hydroxyapatite (n-HAp) was prepared in the Department of Ceramics and Refractories, Faculty of Materials Science and Ceramics, University of Science and Technology in Krakow [9].

Evaluation of the stability of fibres obtained by melt spinning was carried out in PBS fluid over a period of 12 months. PBS is a phosphate buffered saline (0.9% NaCl) with pH of 7.4. The samples were immersed in PBS and incubated for a period of 12 months in polypropylene containers with a capacity of 15 ml (made by FALCON) at 37°C. The degree of degradation of the fibres was determined by the changes in pH of the fluid, the concentration of sodium and potassium ions in the fluid sample after incubation, and the changes in the weight of the samples. Testing was performed using the ion analyser EasyLyte Ca/K/Na/pH made by Medica and the pH meter Cp-401 made by Elmetron. Percentage changes in the weight of the samples were calculated using the formula:

sodu i potasu w płynie po inkubacji próbek oraz zmian masy próbek. Badania wykonano przy użyciu analizatora jonów EasyLyte Ca/K/Na/pH firmy Medica oraz pH-metru Cp-401 firmy Elmetron. Procentowe zmiany masy próbek liczono według wzoru:

$\Delta m=(m_p-m_k)/m_k \cdot 100$ [%]

gdzie: m_p – masa próbki przed inkubacją; m_k – masa próbki po danym okresie inkubacji.

Ocenę zmian zachodzących w wytworzonych materiałach pod wpływem płynu PBS przeprowadzono wykorzystując skaningową mikroskopię elektronową (mikroskop JEOL 5500 JSM) oraz rentgenowską analizę strukturalną (WAXD). Badania rentgenowskie WAXD przeprowadzono przy użyciu dyfraktometru URD6 (Seifert, Niemcy) metodą krokową pomiaru rozpraszania rentgenowskiego (w zakresie kątów rozpraszania 2θ od 5° do 60°), przy użyciu lampy rentgenowskiej z anodą miedzianą (promieniowanie CuKα, λ = 1,542 Å) zasilanej z generatora rentgenowskiego ISO-DEBYEFLEX 3003.

Wyniki i dyskusja

Mikrostrukturę włókien PCL oraz PCL/n-HAp przedstawiono na RYS. 1. Włókna przedstawione na zdjęciach SEM różnią się obrazem powierzchni. Niemodyfikowane włókna PCL charakteryzują się gładką powierzchnią, przy większych powiększeniach można było zaobserwować charakterystyczne podłużne prążki. Na powierzchni włókien zawierających nanohydroksyapatyt (RYS.1c-d) zaobserwowano liczne nierówności (nieobecne w przypadku włókien niemodyfikowanych) potwierdzające obecność hydroksyapatytu w włóknach.

Na RYS. 2 przedstawiono procentowe zmiany masy włókien podczas inkubacji w płynie PBS przez okres 12 miesięcy. Brak zmian masy próbek podczas inkubacji w płynie PBS świadczy o stabilności włókien wytworzonych metodą formowania ze stopu. Nie zaobserwowano zmian w masie włókien kompozytowych wynikających z obecności proszku hydroksyapatytu. Wykres przedstawiający zależność stężenia jonów Na^+ i K^+ w płynie PBS podczas inkubacji próbek włókien przez okres 12 miesięcy przedstawiono na RYS. 3, natomiast zmiany pH płynu w którym inkubowane były próbki włókien przedstawiono na RYS. 4. Również w tym przypadku nie zaobserwowano zmian mogących świadczyć o rozpoczęciu procesu degradacji próbek.

$\Delta m=(m_p-m_k)/m_k \cdot 100$ [%]

where: m_p - weight of the sample before incubation; m_k - weight of the sample after incubation.

Assessment of the changes in the materials generated under the influence of PBS was carried out using scanning electron microscopy (JEOL 5500 JSM microscope) and wide angle X-ray diffraction analysis (WAXD). WAXD tests were conducted using the URD6 diffractometer (Seifert, Germany) by stepwise measurement of X-ray scattering (at a range of scattering angles 2θ from 5° to 60°), using an X-ray tube with a copper anode (CuKα radiation, λ = 1,542 Å) powered from a generator ISO-DEBYEFLEX 3003.

Results and Discussion

The microstructure of PCL and PCL/n-HAp fibres is shown in FIG. 1. The fibres shown in the SEM images differ in the appearance of their surface. Unmodified PCL fibres have a smooth surface and characteristic longitudinal striations can be seen at the higher magnifications. On the surface of fibres containing nano-hydroxyapatite (FIG.1 c-d), we observed numerous irregularities (absent in the case of unmodified fibres) confirming the presence of hydroxyapatite in the fibres.

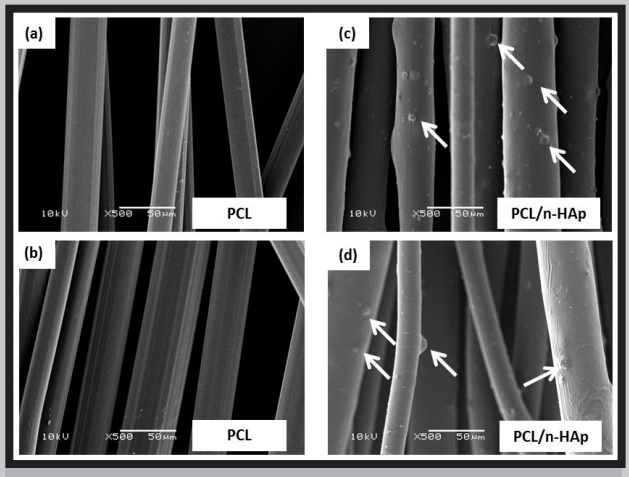

RYS. 1. Mikrostruktura włókien otrzymanych metodą formowania ze stopu: (a-b) włókna z polikaprolaktonu (PCL); (c-d) włókna z polikaprolaktonu modyfikowane hydroksyapatytem na etapie formowania (PCL/n-HAp).
FIG. 1. The microstructure of fibres obtained by melt moulding: (a-b) polycaprolactone fibres (PCL); (c-d) polycaprolactone fibres modified with hydroxyapatite at the stage of moulding (PCL/n-HAp).
PBS for a period of 12 months.

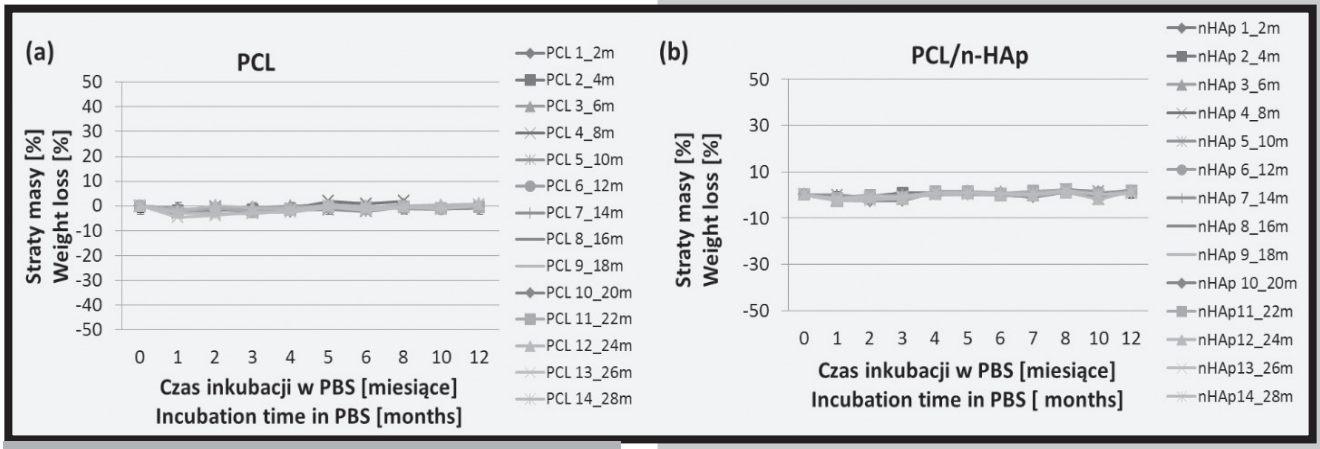

RYS. 2. Procentowe zmiany masy włókien podczas inkubacji włókien PCL i PCL/n-HAp w płynie PBS przez okres 12 miesięcy.
FIG. 2. Percentage changes in the weight of the fibre during incubation of PCL and PCL/n-HAp fibres in PBS for a period of 12 months.

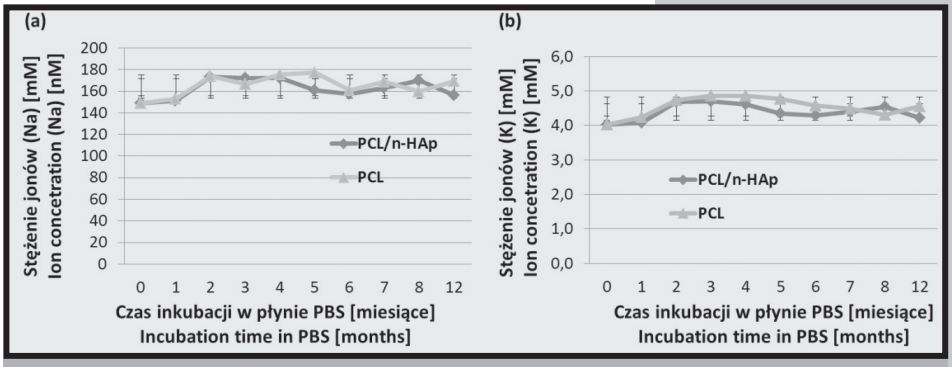

RYS. 3. Zmiany stężenia jonów Na+ i K+ w płynie PBS podczas inkubacji próbek włókien PCL i PCL/n-HAp przez okres 12 miesięcy.
FIG. 3. Changes in the concentration of Na+and K+ in PBS during the incubation of PCL and PCL/n-HAp fibre samples for a period of 12 months.

FIG. 2 shows the percentage changes in the weight of fibres during the incubation in PBS over the period of 12 months. Lack of changes in the weights of the samples incubated in PBS proves the stability of fibres produced by melt spinning. There were no changes in the weight of composite fibres resulting from the presence of hydroxyapatite powder. The graph showing the dependence of the concentration of Na^+ and K^+ ions in PBS during the incubation of fibre samples for a period of 12 months is shown in FIG. 3, and the changes in pH of the fluid in which the fibre samples were incubated are shown in FIG. 4.

Also, in this case, there were no changes that might indicate the start of the process of degradation of samples.

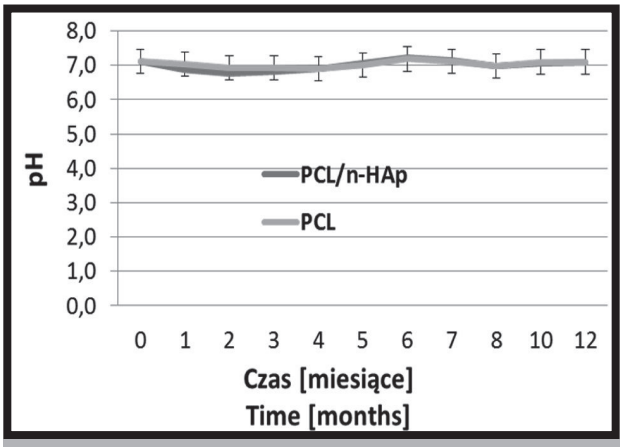

RYS. 4. Zmiany pH płynu PBS podczas inkubacji próbek włókien PCL i PCL/n-HAp przez okres 12 miesięcy.
FIG. 4. Changes in the pH of PBS during incubation of PCL and PCL/n-HAp fibre samples for a period of 12 months.

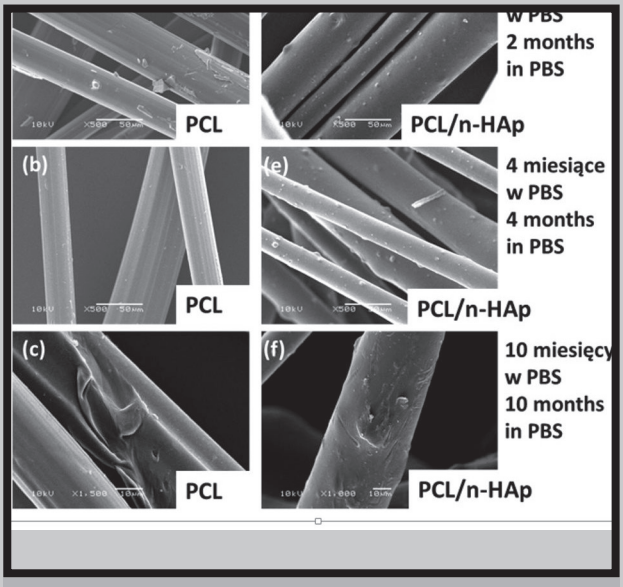

RYS. 5. Zmiany morfologii włókien podczas inkubacji próbek w płynie PBS przez okres 10 miesięcy.
FIG. 5. Changes in the morphology of fibres during the incubation of samples in PBS for a period of 10 months.

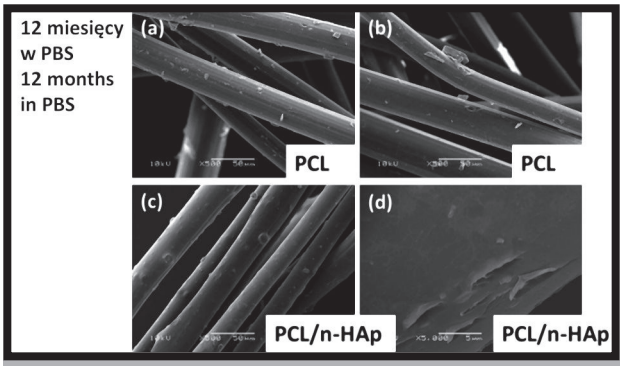

RYS. 6. Zmiany w morfologii włókien po inkubacji próbek w płynie PBS przez okres 12 miesięcy.
FIG. 6. Changes in the morphology of fibres after the incubation of samples in PBS for a period of 12 months.

FIGs 5 and 6 show the changes in the morphology of the fibres during the incubation of samples in PBS. The destruction of polymer due to the degradation in PBS probably takes place in several stages. First, the absorption of the fluid occurs, which results in softening the fibres, the appearance of a grid of fine cracks on their surface, the growth of the crack, and the destruction of the fibre in the final stage. Polycaprolactone is a semi-crystalline polymer. The more crystalline phases within the polymer structure the more resistant it is to physiological fluids. The hydrophobic character of PCL fibres and their semi-crystalline structure causes that the fibres are stable in PBS over a long period of time. The first changes on the surface of the fibres were observed after 10 months of incubating the fibres in PBS. Also, X-ray results (WAXD) confirm the stability of the samples incubated for a period of 8 months in PBS.

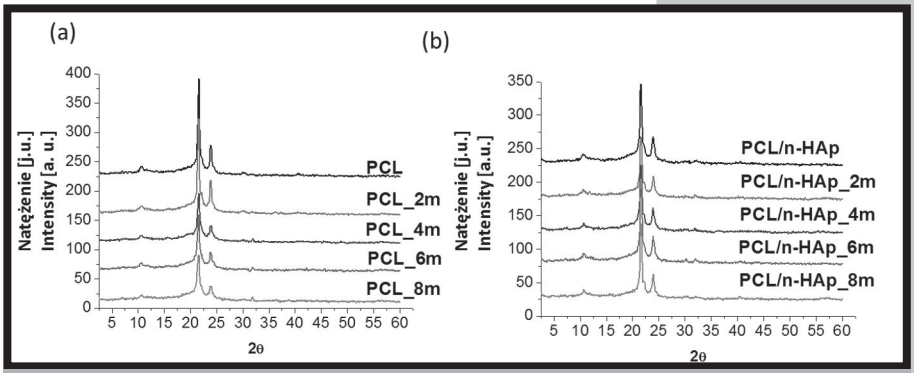

RYS. 7. Zestawienie krzywych dyfrakcyjnych dla włókien PCL i PCL/n-HAp inkubowanych w płynie PBS przez okres 8 miesięcy.
FIG. 7. Summary of diffraction curves for PCL and PCL/n-HAp fibres incubated in PBS for a period of 8 months.

Na RYS. 5 i 6 przedstawiono zmiany w morfologii włókien podczas inkubacji próbek w płynie PBS. Zniszczenie polimeru wskutek degradacji w płynie PBS prawdopodobnie przebiega w kilku etapach. Najpierw następuje absorpcja cieczy, czego następstwem jest zmiękczenie włókien, pojawienie się siatki drobnych pęknięć na ich powierzchni, wzrost szczeliny oraz w końcowym etapie zniszczenie włókna. Polikaprolakton jest polimerem semikrystalicznym. Im więcej fazy krystalicznej w strukturze polimeru tym jest on bardziej odporny na działanie płynów fizjologicznych. Hydrofobowy charakter włókien PCL oraz semikrystaliczna struktura sprawia, że włókna wykazują stabilność w płynie PBS przez długi okres czasu. Pierwsze zmiany na powierzchni włókien zaobserwowano po 10 miesiącach inkubacji włókien w płynie PBS. Również badania rentgenowskie (WAXD) potwierdzają stabilność próbek inkubowanych przez okres 8 miesięcy w płynie PBS. Na RYS. 7 przedstawiono zestawienie krzywych dyfrakcyjnych wykonanych po różnych okresach inkubacji próbek. Przeprowadzone badania potwierdzają niezmienny, semikrystaliczny charakter próbki podczas inkubacji.

Wnioski

Badania degradacji włókien przeprowadzone podczas inkubacji próbek w płynach fizjologicznych wykazały, że wytworzone włókna kompozytowe charakteryzuję się stabilnością w środowisku płynów ustrojowych przez długi okres czasu. Dzięki temu, w przyszłości, wytworzone z włókien kompozytowych podłoża tkankowe będą mogły przenosić obciążenia aż do momentu właściwego odtworzenia się tkanki. Niewielkie zmiany na powierzchni włókien, zaobserwowane po 10 miesiącach inkubacji, w płynie, wskazują na rozpoczęcie procesu degradacji, stąd też można przypuszczać, że czas całkowitej biodegradacji włókien może być skorelowany z czasem potrzebnym do kompletnego odtworzenia tkanki.

Podziękowania

Praca naukowa finansowana ze środków Narodowego Centrum Nauki (projekt numer: N N507550938, 2010-2013) oraz ze środków Ministerstwa Nauki i Szkolnictwa Wyższego (Iuventus Plus IP2012033372, 2013-2015). Autorzy składają serdeczne podziękowania pani dr Ewie Sarnie za pomoc w badaniach SEM.

FIG. 7 presents diffraction curves taken after various incubation periods of the samples. The study confirms the unchanging, semi-crystalline nature of the sample during incubation.in the specimen based on titanium alloy with regard to the sample based on titanium matrix with the same HAp content was caused by the lower size of Ti-6Al-4V power grains compared to the titanium powder.

Conclusions

The study of the degradation of fibres carried out during the incubation of samples in physiological fluids showed that the composite fibres produced are stable in the environment of physiological fluids over a long period of time. Thus, in the future, tissue scaffolds made from composite fibres will be able to carry the load until the proper reproduction of the tissue. Minor changes on the surface of the fibres, observed after 10 months of incubation, in a fluid, indicate the start of a process of degradation, hence it can be assumed that the time of total biodegradation of the fibres may be correlated with the time needed for a complete restoration of tissue.

Acknowledgements

This work was supported by Polish National Science Center (project number: N N507550938, 2010 - 2013) and by the Polish Ministry of Science and Higher Education (project Iuventu Plus III no. IP2013033372). The authors would like to thank Dr E. Sarna (ATH, University of Bielsko-Biała) for help in SEM study

Piśmiennictwo References

[1] Woodruff MA, Hutmacher DW. The return of a forgotten polymer-Polycaprolactone in the 21st century. Prog Polym Sci 2010;35 (10):1217-1256.
[2] Rajzer I. Evaluation of PCL and PCL/HAp scaffolds processed by electrospinning and porogen leaching techniques. Eng Biomater 2011;103: 4-7.
[3] Lei Y, Rai B, Ho KH, Teoh SH. In vitro degradation of novel bioactive polycaprolactone – 20% tricalcium phosphate composite scaffolds for bone engineering. Mater Sci Eng C 2007;27:293-298.
[4] Bosworth LA, Downes S. Physicochemical characterisation of degrading polycaprolactone scaffolds. Polymer Degradation and Stability 2010;95:2269-2276.
[5] Jang J-H, Castano O, Kim H-W. Electrospun materials as potential platforms for bone tissue engineering. Adv Drug Deliver Rev 2009;61:1065-1083.
[6] Plazas Bonilla CE, Trujillo S, Demirdögen B, Perilla JE, Elcin YM, Gómez Ribelles JL. New porous polycaprolactone–silica composites for bone regeneration. Mater Sci Eng C 2014;40(1):418-426
[7] Rajzer I. Fabrication of bioactive polycaprolactone/hydroxyapatite scaffolds with final bilayer nano-/micro- fibrous structures for tissue engineering application. J Mater Sci August 2014; 49(16):5799-5807.
[8] Rajzer I, Fabia J, Graczyk T, Piekarczyk W. Evaluation of PCL and PCL/n-HAp fibres processed by melt spinning. Eng Biomater 2013;118:2-4.
[9] Ślósarczyk A, Paszkiewicz Z, Zima A. The effect of phosphate source on the sintering of carbonate substituted hydroxyapatite. Ceram Int 2010;36(2):577-582.

OSADZANIE ELEKTROFORETYCZNE POLIMEROWYCH POWŁOK CHITOZANU NA BIOMATERIAŁACH METALOWYCH

Dawid Jugowiec[1]*, Agnieszka Radziszewska[1], Marcin Kot[2], Tomasz Moskalewicz[1]

AGH Akademia Górniczo-Hutnicza:
Al.A.Mickiewicza 30, 30-059 Kraków
[1] Wydział Inżynierii Metali i Informatyki Przemysłowej,
[2] Wydział Inżynierii Mechanicznej i Robotyki,
*e-mail: jugowiec@agh.edu.pl

Streszczenie

Powłokę chitozanu osadzono metodą elektroforezy na stopie tytanu Ti13Zr13Nb i stopie kobaltu Co28Cr-5Mo. W obecnej pracy skoncentrowano się głównie na doborze parametrów osadzania elektroforetycznego w celu otrzymania jednorodnych i ciągłych powłok chitozanu na biomateriałach metalowych. Stwierdzono, że jednorodność wytworzonych powłok istotnie zależała od rodzaju zastosowanego roztworu i parametrów osadzania. Mikrostrukturę materiałów podłoży oraz powłok zbadano za pomocą mikroskopii świetlnej oraz skaningowej- i transmisyjnej mikroskopii elektronowej. Zmierzono twardość i moduł Younga materiałów podłoży. Wykonano badania przyczepności powłok do podłoży stopu tytanu i stopu kobaltu.

***Słowa kluczowe**: powłoka chitozanu, elektroforeza, stop tytanu, stop kobaltu,*

[Inżynieria Biomateriałów, 128-129, (2014), 16-19]

Wprowadzenie

Tytan i jego stopy są najczęściej stosowanymi biomateriałami metalowymi w inżynierii biomedycznej [1,2]. Przykładem jest stop Ti13Zr13Nb, którego charakteryzuje wysoka odporność na korozję elektrochemiczną, dobra biokompatybilność oraz niski moduł Younga. Takie właściwości umożliwiają zastosowanie tego materiału w protetyce kości, stawów oraz zębów [3]. Stopy kobaltu, dzięki adekwatnej biozgodności, odporności na korozję oraz odpowiednich właściwości mechanicznych, są powszechnie stosowane w endoprotezoplastyce, urządzeniach stomatologicznych oraz konstrukcjach podtrzymujących zastawki serca [4,5]. Stopy kobaltu są szczególnie wykorzystywane na węzły tarcia

z uwagi na korzystniejsze, niż w przypadku stopów tytanu, właściwości tribologiczne [6]. W celu poprawy połączenia między sztywnymi implantami metalowymi oraz unaczynionej tkanki kostnej można zastosować biodegradowalne powłoki polimerowe. Jedną z metod umożliwiających wytwarzanie takich powłok jest osadzanie elektroforetyczne [7,8]. Podczas procesu elektroforezy, naładowane cząstki koloidalne przemieszczają się pod wpływem działania pola elektrycznego oraz osadzają się na przewodzącym podłożu o przeciwnym znaku [9]. Główną siłą napędową procesu jest ładunek i ruchliwość elektroforetyczna cząstek. Chitozan jest wyjątkowym polimerem, wykazującym właściwości biodegradowalne i bioaktywne, a także antybakteryjne. Dlatego jest chętnie używany w inżynierii biomedycznej do enkapsulacji leków, materiałów opatrunkowych oraz rusztowań komórkowych [10].

ELECTROPHORETIC DEPOSITION OF CHITOSAN COATINGS ON METTALIC BIOMATERIALS

Dawid Jugowiec[1]*, Agnieszka Radziszewska[1], Marcin Kot[2], Tomasz Moskalewicz[1]

AGH University of Science and Technology:
30 A.Mickiewicza 30 Ave, 30-059 Krakow, Poland
[1]Faculty of Metals Engineering and Industrial Computer Science, Mechanical Engineering and Robotics,
*e-mail: jugowiec@agh.edu.pl

Abstract

A chitosan coatings were electrophoretically deposited (EPD) on the Ti13Zr13Nb and Co28Cr5Mo alloys. The main aim of this work was to find optimal EPD parameters to obtain homogeneous and continuous coating on metallic biomaterials. It was found that the homogeneity of the as-deposited chitosan coatings on the substrate materials is highly dependent on chosen solution and EPD parameters. The microstructure of the substrate materials and coatings were investigated by light microscopy as well as scanning- and transmission electron microscopy. The hardness and Young's modulus of the alloys as well as adhesion of chitosan coatings to the substrate materials were investigated.

***Keywords:** chitosan coating, electrophoretic deposition, titanium alloy, cobalt alloy,*

[Engineering of Biomaterials, 128-129, (2014), 16-19]

Introduction

Titanium and its alloys are the most commonly used metallic biomaterials in biomedical engineering [1, 2]. Especially, Ti13Zr13Nb alloy is highly resistant to electrochemical corrosion, exhibits good biocompatibility and low value of the Young's modulus. Such properties makes it possible to use in the bone, joint and dental prosthetics [3]. CoCrMo alloys are widely used in numerous medical applications such as total hip and knee replacements, dental devices and support structures for heart valves given their adequate biocompatibility, wear and corrosion resistance as well good mechanical properties [4,5]. They are the preferred materials for articular applications with metal-on-metal contact since the tribological properties are superior in comparison with those of titanium alloys [6]. In order to further enhance connection between rigid metallic implants and vascularized bone tissue, the biodegradable polymers coatings can be applied. One of the prospective method to deposit such coatings is electrophoretic deposition (EPD) [7,8]. In the EPD process, the charged particles of material suspended in suspension are moved to and deposited onto an oppositely charged electrode under an applied electric field [9]. The main driving force of the EPD process is charge and electrophoretic mobility of particles. Chitosan is an unique polymer, which due to its biocompatibility, biodegradability and antibacterial properties has attracted much attention for a great variety of biomedical applications such as drug encapsulation, wound dressing materials and tissue engineering scaffolds [10].

The aim of this work was to investigate the deposition by EPD of chitosan coatings on Ti13Zr13Nb and Co28Cr5Mo alloys and to perform a preliminary microstructure and selected properties characterization of the coated materials.

Celem badań niniejszej pracy było wytworzenie powłok chitozanu na biomateriałach metalowych, stopie Ti13Zr13Nb i stopie Co28Cr5Mo, oraz wstępna analiza mikrostruktury i wybranych właściwości materiałów podłoży i powłok.

Materiał i metody

Na podłoża do osadzania powłok zastosowano stop kobaltu Co28Cr5Mo (Ergiloy 9.9135HL) i stop tytanu zbliżony do β Ti13Zr13Nb. Próbki miały kształt krążków o średnicy 20 mm i wysokości 2 mm. Powłoki osadzano metodą elektroforezy. Do osadzania stosowano dwa różne roztwory: rozcieńczony roztwór proszku chitozanu (Sigma-Aldrich) (0,5 g/l)

w wodzie destylowanej i 1%obj. roztworze kwasu octowego oraz roztwór proszku chitozanu (0,5 g/l) w wodzie destylowanej i 1%obj. roztworze kwasu octowego i 50% obj. alkoholu etylowego. Oba roztwory przygotowano za pomocą mieszania magnetycznego w czasie 24 godziny w temperaturze pokojowej. Jako przeciwelektrodę zastosowano płytkę ze stali austenitycznej. Proces elektroforezy przeprowadzono przy stałym napięciu z zakresu 8-30 V. Czas osadzania wynosił 4 minuty, a odległość między elektrodami wynosiła 10 mm. Do wstępnego doboru parametrów osadzania stosowano płytki stali austenitycznej X2CrNiMo18-14-3.

Badania mikrostruktury materiałów podłoży i powłoki wykonano za pomocą mikroskopii świetlnej, skaningowej- oraz transmisyjnej mikroskopii elektronowej (SEM, TEM). Identyfikację faz przeprowadzono metodą selektywnej dyfrakcji elektronów (SAED) oraz metodą dyfrakcji promieniowania rentgenowskiego (XRD). Do analizy składu chemicznego wykorzystano spektroskopię promieniowania rentgenowskiego z dyspersją energii (SEM-EDS). Zmierzono twardość oraz moduł Younga stopów za pomocą urządzenia Mikro-Combi-Tester, stosując obciążenie 1 N. Wykonano badania przyczepności powłok do podłoży za pomocą próby zarysowania.

Wyniki i dyskusja

Mikrostrukturę stopu Ti13Zr13Nb obserwowaną za pomocą SEM przedstawiono na RYS. 1a. Badania za pomocą TEM i XRD wykazały, że mikrostruktura stopu zbudowana była głównie z igieł fazy α' (o strukturze heksagonalnej zwartej, HZ) w ziarnach fazy β (o strukturze regularnej przestrzennie centrowanej, RPC). Sporadycznie stwierdzono występowanie również drobnych igieł fazy α'' (o strukturze rombowej, grupa przestrzenna Cmcm). Średnica ziarna wynosiła w zakresie od 20 μm do 60 μm. Szerokość igieł fazy α' mieściła się w zakresie 150 nm-280 nm. Mikroanaliza składu chemicznego wykonana za pomocą SEM-EDS wykazała następujący średni skład chemiczny stopu (w % masowych): 74,6 Ti, 13,4 Zr i 12 Nb. Twardość stopu wynosiła 3±0,2 GPa, zaś moduł Younga 89±2 GPa.

Mikrostruktura kutego na gorąco stopu Co28Cr5Mo składała się z jednorodnych, zrekrystalizowanych ziaren fazy α (o strukturze regularnej ściennie centrowanej, RSC). Średnica ziaren wyznaczona na podstawie obrazów mikrostruktury SEM zawierała się w zakresie 4μm-5μm (RYS. 1b). Podczas badań za pomocą TEM w mikrostrukturze stopu obserwowano liczne defekty struktury w postaci błędów ułożenia i bliźniaków. Stwierdzono, że twardość stopu kobaltu wynosiła 4,9±0,2 GPa, zaś moduł Younga 235±10 GPa.

Materials and methods

Titanium near - β alloy Ti13Zr13Nb and cobalt Co28Cr-5Mo (Ergiloy 9.9135HL) alloy were used as substrates for electrophoretic deposition of chitosan coatings. Samples were in the shape of discs with diameter of 20 mm and height of 2 mm. Dilute solution of chitosan (Sigma-Aldrich) (0.5 g/l) in a mixture of distilled water and 1 vol.% acetic acid and dilute solution of chitosan in a mixture of distilled water and 1 vol.% acetic acid and 50 vol.% ethanol were prepared by magnetic stirring at room temperature for 24 hours and later used for EPD. The counter electrode was an austenitic steel plate. The EPD was carried out in a two-electrode cell, under constant voltage conditions in the range of 8-30 V. Deposition time was 4 minutes and the distance between electrodes in the EPD cells was 10 mm. Austenitic X2CrNi-Mo18-14-3 steel plates were used for preliminary selection of deposition parameters.

The microstructure of the metallic substrates and chitosan coatings were characterized by light microscopy (LM) as well as scanning- and transmission electron microscopy (SEM, TEM). Phase identification was performed by means of selected area electron diffraction (SAED) and by X-ray diffractometry (XRD). The chemical composition was analyzed via energy dispersive X-ray spectroscopy (SEM-EDS).The hardness and Young modulus of metallic alloys were investigated by Micro-Combi-Tester device (CSM Instruments) with Vicker's indenter and load value of 1 N. The adhesion of coatings to the substrates was analyzed by scratch-test.

Results and discussions

Microstructure of the Ti13Zr13Nb alloy observed by SEM is shown in FIG. 1a. The TEM and XRD investigation exhibited that the microstructure of the alloy was composed mainly of α' (hexagonal close-packed; hcp) laths in β (body-centered cubic; bcc) grains. Sporadically, a fine α'' laths (orthorhombic, Cmcm space group) also could be observed. The grain size ranged from 20 μm to 60 μm. Width of α' laths was in the range from 150 nm to 280 nm. The mean chemical composition of the alloy investigated by SEM-EDS microanalysis was (in wt.%): 74.6 Ti, 13.4 Zr and 12 Nb. Hardness and Young's modulus of the alloy were measured as 3±0.2 GPa and 89±2 GPa, respectively.

The microstructure of the Co28Cr5Mo alloy consisted of homogenous, recrystallized grains of α (face-centered cubic; fcc) phase. The grains diameter was measured on SEM images to be in range of 4μm-15μm (FIG.1b). The TEM investigation revealed occurrence of numerous stacking fault defects and twins in alloy microstructure. Hardness and Young's modulus values of the alloy were 4.9±0.2 GPa and 235±10 GPa, respectively.

Selection of appropriate solution and process parameters for electrophoretic deposition of chitosan on metallic biomaterials was the main focus of our work. In order to facilitate this task, austenitic steel plates were used as model substrate material. Two different solutions were prepared and used for EPD. It was found that the composition of solution has a significant influence on the uniformity of the coatings. Chitosan was positively charged under acidic conditions. During the deposition of the coatings from solution of chitosan (0.5 g/l) in a mixture of distilled water and 1 vol.% acetic acid the formation of many H_2 bubbles was observed, whose presence significantly affected the uniformity of the coatings deposited. Much lower amount of bubbles and thus better homogeneity of the coatings could be obtained while using solution of chitosan (0.5 g/l) in a mixture of distilled water and 1%vol. of acetic acid and 50% vol. of ethanol.

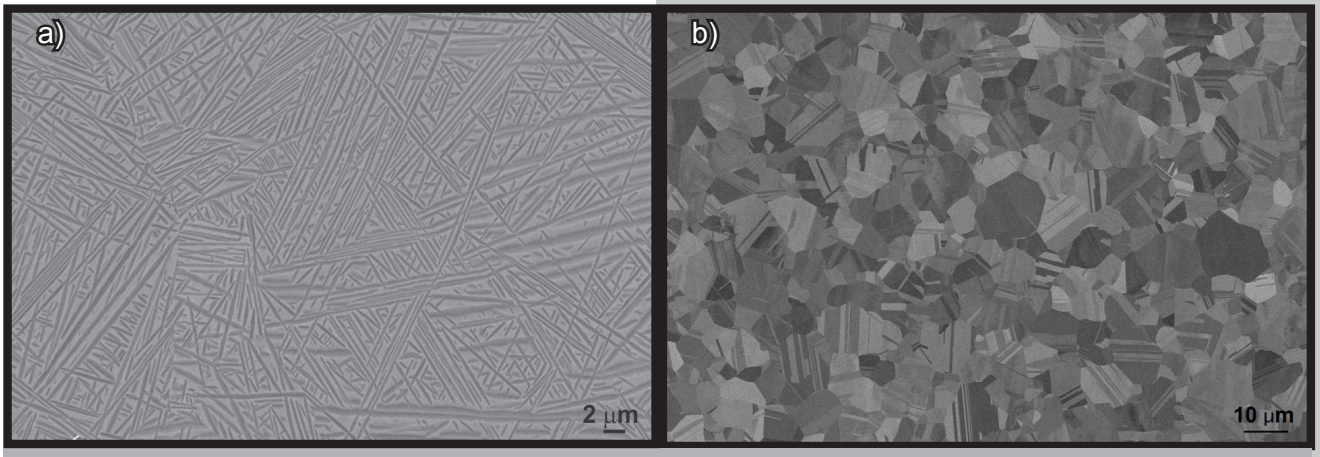

RYS. 1. Mikrostruktura stopu Ti13Zr13Nb (a) i stopu Co28Cr5Mo (b), SEM.
FIG. 1. The microstructure of Ti13Zr13Nb (a) and Co28Cr5Mo (b) alloys, SEM.

Dużą część pracy poświęcono na dobór roztworu i parametrów osadzania elektroforetycznego. Badania takie, ze względu na ułatwienie eksperymentu, przeprowadzono na modelowym podłożu ze stali austenitycznej X2CrNiMo18-14-3. Stosowano dwa różne roztwory. Stwierdzono, że skład roztworu ma istotny wpływ na jednorodność powłok. Podczas osadzania powłok z roztworu proszku chitozanu (Sigma-Aldrich) (0,5 g/l) w mieszaninie wody destylowanej i 1 %obj. kwasu octowego obserwowano tworzenie się licznych pęcherzyków H_2, co istotnie pogarszało jednorodność wytwarzanych powłok. Znacznie mniej pęcherzyków, a tym samym lepszą jednorodność powłok otrzymano podczas osadzania z roztworu proszku chitozanu (0,5 g/l) w mieszaninie wody destylowanej i 1 % obj. roztworze kwasu octowego oraz 50 % obj. alkoholu etylowego. Wynika to ze znacznego zmniejszenia zawartości wody w roztworze, a tym samym ograniczenia wydzielania się gazów.

Podobny wpływ na tworzenie się pęcherzyków miało napięcie podczas osadzania elektroforetycznego. Najbardziej jednorodne i ciągłe powłoki otrzymano przy napięciu wynoszącym 10 V (RYS.2).

Wraz ze wzrostem napięcia obserwowano coraz intensywniejsze tworzenie się pęcherzyków. Stwierdzono, że powłoka na stopie tytanu jest bardziej jednorodna od powłoki na stopie kobaltu. Na RYS. 3 przedstawiono powierzchnię powłoki chitozanu na stopie Ti13Zr13Nb obserwowaną za pomocą SEM. Podczas badań SEM, nawet przy małym napięciu przyspieszającym, obserwowano tworzenie się pęcherzyków w powłoce na skutek oddziaływania wiązki elektronów ze stosunkowo cienką, delikatną powłoką polimerową. Dalsze szczegółowe badania kinetyki osadzania chitozanu na biomateriałach metalowych i analiza mikrostruktury powłok są w toku.

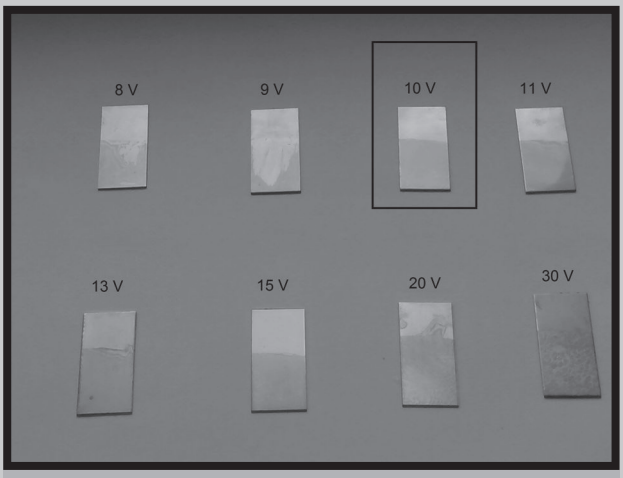

RYS. 2. Płytki stali austenitycznej pokryte powłoką chitozanu przy stosowaniu różnych wartości napięć w czasie 4 minut.
FIG. 2. Austenitic steel plates coated with chitosan using different voltage values during 4 minutes.

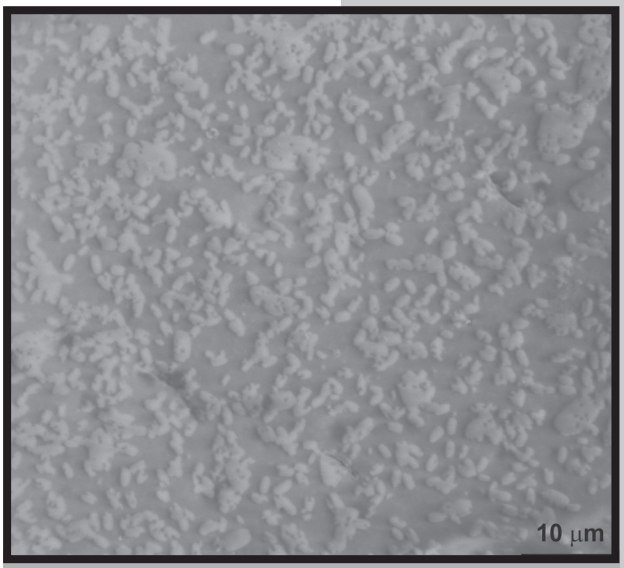

RYS. 3. Powierzchnia powłoki chitozanu osadzonej elektroforetycznie na stopie Ti13Zr13Nb, SEM.
FIG. 3. Surface of the chitosan coating electrophoretically deposited on Ti-13Zr-13Nb alloy, SEM.

This is due to a significant reduction in water content in the suspension, thereby reducing gas evolution. Similar effect on the formation of bubbles during the deposition had electrophoretic voltage. The most homogeneous and continuous coatings were deposited at the voltage of 10 V (FIG.2).

More intense formation of bubbles could be observed with the increase in the voltage for electrophoretic process. It was found that the coating on the titanium alloy is more homogeneous than coating on the cobalt alloy. The surface of the chitosan coating on Ti13Zr13Nb alloy observed by SEM is shown in FIG. 3. During SEM observations it was found, that formation of bubbles is caused by reaction between electron beam with relatively thin, soft polymeric coating. Further detailed studies of the EPD kinetics of chitosan and coatings microstructure are in progress.

Zgodnie z oczekiwaniami wynikającymi z charakteru powłoki stwierdzono stosunkowo słabą jej przyczepność do podłoży stopu Ti13Zr13Nb i stopu Co28Cr5Mo. Próby zarysowania wykazały, że obciążenie krytyczne wynosiło odpowiednio 2N i 3N. Przy tym obciążeniu pojawiały się pierwsze wykruszenia powłok na bokach rysy. Wzrost obciążenia do 5 N prowadził do znacznej intensyfikacji tego procesu i powłoki były usuwane ze znacznych obszarów wokół toru zarysowania.

Podsumowanie

W mikrostrukturze stopu Ti13Zr13Nb stwierdzono występowanie głównie fazy α' i fazy β oraz sporadycznie fazy α''. Twardość stopu wynosiła 3±0,2 GPa, zaś moduł Younga 89±2 GPa. Mikrostruktura stopu Co28Cr5Mo zbudowana była z jednorodnych, zrekrystalizowanych ziaren fazy α. W ziarnach występowały liczne błędy ułożenia i bliźniaki. Twardość stopu kobaltu wynosiła 4,9±0,2 GPa, zaś moduł Younga 235±10 GPa.

Dobrano skład chemiczny roztworu i parametry osadzania elektroforetycznego powłok chitozanu na stopie tytanu Ti13Zr13Nb i stopie kobaltu Co28Cr5Mo. Zauważono ścisłą zależność pomiędzy jednorodnością osadzanych powłok, a składem roztworu i wartością napięcia podczas osadzania elektroforetycznego. Największą skuteczność osadzania chitozanu obserwowano na powierzchni stopu tytanu. Dalsze szczegółowe badania kinetyki osadzania chitozanu na biomateriałach metalowych z uwzględnieniem potencjału elektrokinetycznego i pH roztworu, jak również charakterystyka ich mikrostruktury są w toku.

Podziękowania

Praca naukowa finansowana ze środków Narodowego Centrum Nauki przyznanych na podstawie decyzji numer DEC-2013/09/B/ST8/00145.

Autorzy dziękują dr inż.S.Kącowi i mgr inż. A.Gruszczyńskiemu za pomoc w wykonaniu badań SEM.

As expected, tested coatings were characterized by relatively poor adhesion to the Ti13Zr13Nb and Co28Cr5Mo substrates. Scratch tests showed that the critical load was 2 N and 3 N, respectively. At this load first delamination of coatings appeared on the sides of scratch tracks. The rise of load up to 5N led to a significant intensification of this process and large area of coatings removal around scratches.

Summary

The microstructure of the Ti13Zr13Nb alloy consisted mainly of α' and β phases. Sporadically α'' laths were also found. Hardness and Young modulus values of the alloy were measured as 3±0.2 GPa and 89±2 GPa, respectively. The microstructure of the Co28Cr5Mo alloy consisted of homogenous, recrystallised grains of α phase. The grains contained numerous stacking faults defects and twins. Hardness and Young modulus values of the alloy were 4.9±0.2 GPa and 235±10 GPa, respectively.

The adequate solution composition and process parameters were selected for electrophoretic deposition of chitosan coatings on Ti13Zr13Nb and Co28Cr5Mo alloys. It was found that the uniformity of the deposited chitosan coating on the substrate materials is highly dependent on chosen solution and EPD voltage. The greatest efficiency of the coating deposition was observed on titanium alloy surfaces. Further detailed studies of the deposition kinetics of chitosan on metallic biomaterials with regard to zeta potential and pH, as well as coatings microstructure characterization, are in progress.

Acknowledgments

This work was supported by the Polish National Science Centre (decision no. DEC-2013/09/B/ST8/00145).

The authors appreciate a valuable contribution of Dr S.Kąc and A.Gruszczyński, MSc (AGH University of Science and Technology) to the SEM investigation.

Piśmiennictwo

[1] I Cvijović-Alagić , Z. Cvijović, S. Mitrović, V. Panić, M. Rakin, Corrosion Science 53 (2011) 796-808
[2] L.T. Duarte, S.R. Biaggio, R.C. Rocha-Filho, N. Bocchi, Corrosion Science 72 (2013) 35-40
[3] W. Simka, M. Mosiałek, G. Nawrat, P. Nowak, J. Żak, J. Szade, A. Winiarski, A. Maciej, L. Szyk-Warszyńska, Surface & Coatings Technology 213 (2012) 239-246
[4] A.S. Mukasyan, Material Research Innovations 7 (2003) 245-252
[5] J.V. Giacchi, O. Fornaro, H. Palacio, Materials Characterisation 68 (2012) 49-57

References

[6] W.C. Rodrigues, L.R. Broilo, L. Schaeffer, G. Knörnschild, F.R.M. Espinoza, Powder Technology 206 (2011) 233-238
[7] N.S. Raddaha, L. Cordero-Arias, S. Cabanas-Polo, S. Virtanen, J.A. Roether, A.R. Boccaccini, Materials 7 (2014) 1814-1829
[8] A.R. Boccaccini, S. Keim, R. Ma, Y. Li, I. Zhitomirsky, Journal of the Royal Society Interface 7 (2010) 581-613
[9] O. Van der Biest, S. Put, G. Anné, J. Vlugels, Journal of Material Science 39 (2004) 779-785
[10] F. Gebhardt, S. Seuss, M.C. Turhan, H. Hornberger, S. Virtanen, A.R. Boccaccini, Materials Letters 66 (2012) 302-304

MODYFIKACJA RUSZTOWANIA KOSTNEGO CHITOSAN/HA ZA POMOCĄ β-1,3-GLUKANU ZNACZĄCO POPRAWIA JEGO BIOKOMPATYBILNOŚĆ IN VITRO

Agata Przekora*, Grażyna Ginalska

Uniwersytet Medyczny w Lublinie,
Katedra i Zakład Biochemii i Biotechnologii,
ul. W.Chodźki 1, 20-093 Lublin
*e-mail: agata.przekora@umlub.pl

Streszczenie

Inżynieria tkankowa kości kładzie nacisk na produkcje trójwymiarowego, porowatego rusztowania, które posiadałoby zdolność stymulowania adhezji, proliferacji i różnicowania osteoblastów. Takie rusztowanie wspierałoby proces regeneracji i tworzenia funkcjonalnej tkanki kostnej [1-3].

Celem niniejszej pracy było udowodnienie za pomocą 2 linii osteoblastycznych, że dodatek β-1,3-glukanu do rusztowania na bazie chitosanu i hydroksyapatytu (chit/HA) skutkuje wytworzeniem nowego, trójskładnikowego kompozytu chitosan/β-1,3-glukan/hydroksyapatyt (chit/glu/HA), który posiada lepszą biokompatybilność w porównaniu do dwuskładnikowego materiału chit/HA.

Trójskładnikowe rusztowanie wyprodukowano poprzez modyfikację kompozytu chit/HA za pomocą bakteryjnego β-1,3-glukanu jak to zostało opisane wcześniej [2,3]. Eksperymenty in vitro przeprowadzono z zastosowaniem linii komórkowej prawidłowych ludzkich płodowych osteoblastów (hFOB 1.19) oraz linii komórkowej mysich preosteoblastów (MC3T3-E1 Subclone 4). Cytotoksyczność materiałów oznaczono metodą kontaktu bezpośredniego za pomocą podwójnego barwienia fluorescencyjnego „żywe/martwe komórki". Kalceina-AM barwi na zielono jedynie żywe komórki, natomiast jodek propidyny barwi kwasy nukleinowe martwych komórek emitując czerwoną fluorescencję jader komórkowych. Wybarwione komórki obserwowano w mikroskopie konfokalnym. Liczbę osteoblastów przyklejonych do powierzchni rusztowań kostnych określono ilościowo po lizie komórek za pomocą testu LDH total. Wzrost i proliferację komórek na powierzchni biokompozytów oceniono poprzez obserwację w mikroskopie konfokalnym stosując podwójne barwienie fluorescencyjne cytoszkieltu i jąder komórkowych. Komórki linii hFOB 1.19 i MC3T3-E1 hodowano bezpośrednio na powierzchni biomateriałów przez 9 dni. Co trzeci dzień komórki barwiono za pomocą barwników fluorescencyjnych AlexaFluor635phalloidin i Hoechst 33342 w celu oceny ich morfologii oraz wzrostu ich liczby w czasie. Barwnik AlexaFluor635phalloidin zapewnia czerwoną fluorescencję filamentów cytoszkieletu, natomiast Hoechst 33342 barwi jadra komórkowe na niebiesko.

Barwienie „żywe/martwe komórki" wykazało zgrupowania żywych, emitujących zieloną fluorescencje komórek na powierzchni obydwu biokompozytów (chit/HA i chit/glu/HA). Jednakże, komórki hFOB 1.19 porastające powierzchnię rusztowania chit/HA były okrągłe i nie wykazywały typowego dla ich morfologii podłużnego kształtu, co sugeruje, że nie przykleiły się do powierzchni chit/HA (RYS.1). Ponadto, na powierzchni materiału chit/HA zaobserwowano dość dużą liczbę martwych, czerwonych komórek linii hFOB 1.19. Komórki hFOB 1.19 hodowane na powierzchni chit/glu/HA były rozpłaszczone i miały podłużny kształt, co świadczy o ich dobrej adhezji do powierzchni tego materiału.

MODIFICATION OF BONE CHITOSAN/HA SCAFFOLD WITH β-1,3-GLUCAN SIGNIFICANTLY IMPROVES ITS BIOCOMPATIBILITY IN VITRO

Agata Przekora*, Grażyna Ginalska

Medical University of Lublin,
Department of Biochemistry and Biotechnology,
1 W.Chodźki str., 20-093 Lublin
*e-mail: agata.przekora@umlub.pl

Abstract

Bone tissue engineering put emphasis on fabrication three-dimensional porous scaffolds that possess ability to enhance adhesion, proliferation and differentiation of osteoblast cells, therefore supporting bone regeneration and functional bone tissue formation [1-3].

The aim of this work was to prove using 2 osteoblastic cell lines that addition of β-1,3-glucan to chitosan/hydroxyapatite (chit/HA) scaffold results in fabrication of novel tri-component chitosan/β-1,3-glucan/hydroxyapatite (chit/glu/HA) composite that possesses better biocompatibility compared to bi-component chit/HA material.

Tri-component scaffold was fabricated by modification of chit/HA composite with bacterial β-1,3-glucan as was described previously [2,3]. In vitro experiments were carried out using human foetal osteoblast cell line (hFOB 1.19) and mouse calvarial preosteoblast cell line (MC3T3-E1 Subclone 4). Cytotoxicity of the scaffolds was evaluated by direct-contact method using live/dead double fluorescent staining. The calcein-AM dye stains only viable cells giving green fluorescence and propidium iodide dye stains nucleic acids of only dead cells emitting red fluorescence. Stained cells were observed under confocal microscope. Cell adhesion to the scaffold surfaces was determined quantitatively after cell lysis by LDH total test. Cell growth and proliferation on the biocomposite surfaces were evaluated by confocal microscope observation using double fluorescent staining of osteoblast cytoskeleton and nuclei. HFOB 1.19 and MC3T3-E1 cells were cultured directly on the scaffold surfaces for 9 days and every third day cells were stained with AlexaFluor635phalloidin and Hoechst 33342 fluorescent dyes in order to assess cell morphology and increase in cell number. AlexaFluor635phalloidin dye provides red fluorescence of cytoskeletal filaments, while Hoechst 33342 gives blue fluorescence of nuclei.

Live/dead double staining showed clusters of viable green fluorescent osteoblast cells on the surface of both biocomposite samples (chit/HA and chit/glu/HA). However, hFOB 1.19 cells growing on the chit/HA surface were spherical and did not reveal their typical lengthened shape what indicates that hFOB 1.19 cells were not attached to the chit/HA surface (FIG.1). Moreover, there were quite a lot of dead, red fluorescent hFOB 1.19 cells on the chit/HA material. HFOB 1.19 cells cultured on the chit/glu/HA sample were flattened and had lengthened shape what proves their good adhesion to the composite surface. MC3T3-E1 cells growing on both materials were flattened and revealed typical stellar shape. Only occasional dead red fluorescent cells were observed. However, there were meaningfully less MC3T3-E1 cells on the surface of chit/HA composite compared to chit/glu/HA sample.

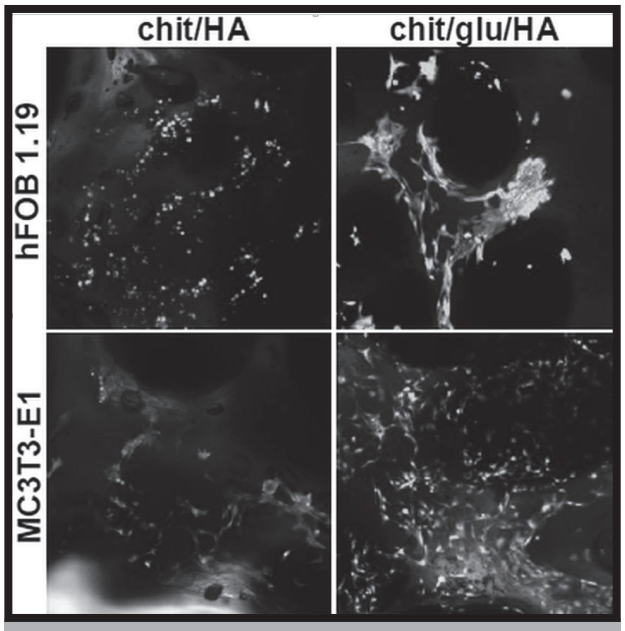

RYS. 1. Podwójne barwienie fluorescencyjne „żywe/martwe komórki" 24 h po inokulacji materiałów, pow. 100x.
FIG. 1. Live/dead double fluorescent staining 24 after cell seeding, magn. 100x.

Komórki linii MC3T3-E1 porastające powierzchnię obydwu materiałów były rozpłaszczone i miały typowy dla nich gwiazdkowaty kształt. Jedynie pojedyncze martwe, czerwone komórki MC3T3-E1 zaobserwowano na powierzchni tych kompozytów. Jednakże w porównaniu do rusztowania chit/glu/HA, zdecydowanie mniej komórek MC3T3-E1 było na powierzchni kompozytu chit/HA.

LDH total test wykazał znacząco lepszą adhezję komórek hFOB 1.19 i MC3T3-E1 do powierzchni materiału chit/glu/HA (RYS. 2). Trzy godziny od momentu inokulacji rusztowań, do powierzchni kompozytu chit/HA przykleiło się 30% (1.6 x 10^4) komórek linii hFOB 1.19, natomiast do materiału chit/glu/HA 50% (2.6x10^4) komórek. W przypadku komórek linii MC3T3-E1, do materiału chit/HA przykleiło się 20% (1.9x10^4) komórek, a do kompozytu chit/glu/HA aż 70% (7x10^4) komórek.

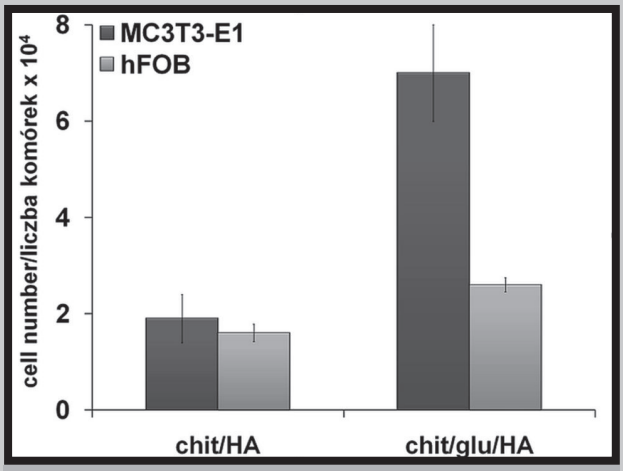

RYS. 2. Całkowita liczba komórek przyklejonych do powierzchni chit/HA i chit/glu/HA po 3 h od inokulacji.
FIG. 2. Total cell number attached to the chit/HA and chit/glu/HA surfaces 3 h after cell seeding.

LDH total assay demonstrated significantly higher number of hFOB 1.19 and MC3T3-E1 cells attached to the chit/glu/HA compared to the chit/HA sample (FIG. 2). Three hours after cell inoculation there were 30% (1.6x10^4 cells) and 50% (2.6x10^4 cells) of hFOB 1.19 cells attached to the chit/HA and chit/glu/HA composites, respectively and 20% (1.9x10^4 cells) and 70% (7x10^4 cells) of MC3T3-E1 cells attached to the chit/HA and chit/glu/HA scaffolds, respectively.

Microscopic observation showed good osteoblast growth and proliferation only on chit/glu/HA scaffold (FIG.3). The number of hFOB 1.19 and MC3T3-E1 cells growing on the chit/glu/HA increased with time during the in vitro culture. Osteoblasts revealed their typical morphology and had well extensive cytoskeleton. There were also well visible blue fluorescent nuclei. After 9-day culture, chit/glu/HA surface was covered by multilayer of hFOB 1.19 and MC3T3-E1 cells, which revealed extensive network of cytoskeletal filaments and numerous filopodia. Osteoblast cells cultured on the chit/glu/HA were well spread, flattened and generated large filamentous structure of the cytoskeleton what indicates that this scaffold is very favourable to cell

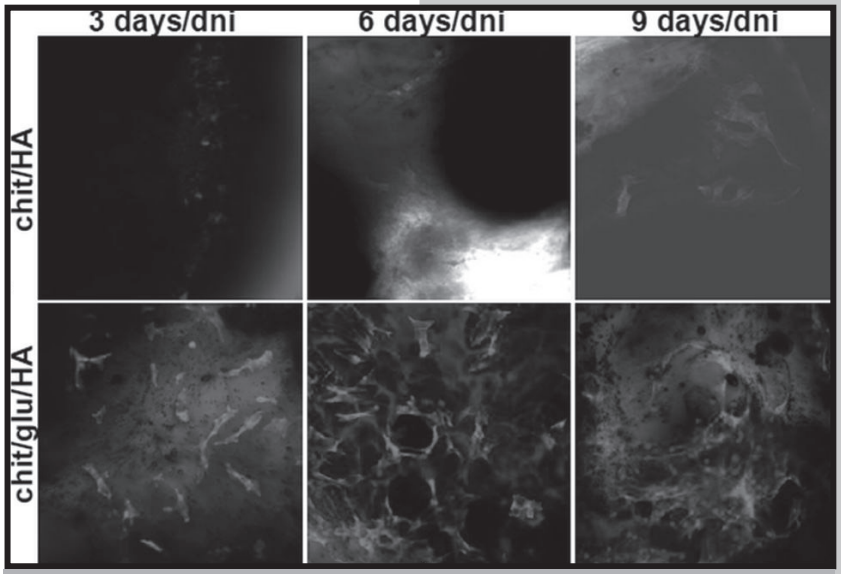

RYS. 3. Ocena proliferacji. Komórki linii MC3T3-E1 hodowane na powierzchni rusztowania chit/HA i chit/glu/HA, pow. 200x.
FIG. 3. Proliferation evaluation. MC3T3-E1 cells cultured on the surface of chit/HA and chit/glu/HA scaffold, magn. 200x.

Obserwacja mikroskopowa wykazała dobry wzrost i proliferację osteoblastów linii hFOB 1.19 i MC3T3-E1 jedynie na rusztowaniu chit/glu/HA (RYS. 3). Liczba komórek porastających powierzchnię chit/glu/HA wzrastała wraz z wydłużającym się czasem hodowli in vitro. Osteoblasty miały typową dla danej linii komórkowej morfologię i dobrze rozbudowany cytoszkielet. Fluoryzujące na niebiesko jądra komórkowe były również bardzo dobrze widoczne. Po 9 dniach prowadzenia hodowli, powierzchnia rusztowania chit/glu/HA była pokryta wielowarstwą komórek linii hFOB 1.19 i MC3T3-E1, które posiadały dobrze rozwiniętą sieć filamentów cytoszkieletu i liczne wypustki cytoplazmatyczne. Osteoblasty hodowane na materiale chit/glu/HA były rozpłaszczone i posiadały dobrze rozbudowaną strukturę cytoszkieletu, co sugeruje, że ten materiał sprzyja adhezji i proliferacji komórek. Udowodniono, że materiał chit/HA całkowicie nie sprzyja adhezji, wzrostowi i proliferacji komórek hFOB 1.19. Przez cały czas trwania eksperymentu na powierzchni chit/HA zaobserwowano jedynie pojedyncze, okrągłe komórki hFOB 1.19. Co więcej, ich liczba nie wzrastała w czasie, a komórki były drobne i okrągłe, co może świadczyć o tym, że były martwe. W przypadku komórek linii MC3T3-E1, 3 dni po inokulacji materiału chit/HA zaobserwowano jedynie pojedyncze komórki na powierzchni próbki (RYS. 3). Ponadto, komórki MC3T3-E1 były okrągłe i nie miały typowego gwiazdkowego kształtu, co świadczy o ich słabej adhezji do powierzchni chit/HA. Jednakże, liczba komórek MC3T3-E1 wzrastała w czasie i po 9 dniach prowadzenia hodowli na powierzchni materiału chit/HA zaobserwowano obszary o małej gęstości komórek MC3T3-E1, które miały gwiazdkowaty kształt, widoczny cytoszkielet i wypustki cytoplazmatyczne.

Przeprowadzone eksperymenty in vitro oraz uzyskane zdjęcia z mikroskopu konfokalnego wyraźnie udowadniają, że dodatek β-1,3-glukanu do rusztowania chit/HA stymuluje adhezję, wzrost i proliferację komórek linii hFOB 1.19 i MC3T3-E1. Oba testowane biomateriały były nietoksyczne i pozwalały na wstępną adhezję komórek. Jednakże na powierzchni rusztowania zawierającego β-1,3-glukan zaobserwowano znacząco lepsze rozpłaszczanie się komórek, ich szybszy wzrost i proliferację. Analizując uzyskane wyniki można wysnuć wniosek, że nowy trójskładnikowy kompozyt jest obiecującym materiałem do stosowania w inżynierii tkankowej kości jako rusztowanie komórek mające za zadanie przyspieszenie procesów regeneracyjnych oraz tworzenie nowej, funkcjonalnej tkanki kostnej.

[Inżynieria Biomateriałów, 128-129, (2014), 20-22]

Podziękowania

Praca finansowana w ramach DS MNd 2. Badania przeprowadzono z wykorzystaniem sprzętu zakupionego w projekcie realizowanym zgodnie z umową nr POPW.01.03.00-06-010/09-00 w ramach Programu Operacyjnego Rozwój Polski Wschodniej 2007-2013, Osi Priorytetowej I, Nowoczesna Gospodarka, Działanie 1.3. Wspieranie Innowacji.

adhesion and proliferation. The chit/HA biomaterial was proved to be completely unfavourable to adhesion, growth, and proliferation of hFOB 1.19 cells. Only single spherical hFOB 1.19 cells were observed on the chit/HA sample throughout the full length of the experiment. Moreover, the hFOB 1.19 cell number did not increase with time, cells were tiny and spherical what may indicate that were already dead. In the case of MC3T3-E1 cells, 3 days after cell seeding there were only individual MC3T3-E1 cells on the chit/HA surface (Fig. 3). Furthermore, visualized MC3T3-E1 cells were spherical and did not reveal typical stellar shape what indicates that cells were not well attached. However, the number of MC3T3-E1 cells increased with time and 9 days after cell inoculation there was low density culture of stellar shape MC3T3-E1 cells with visible cytoskeleton and filopodia on the chit/HA material.

Conducted in vitro experiments and obtained confocal microscopy images clearly prove that addition of β-1,3-glucan to the chit/HA scaffold enhances adhesion, growth, and proliferation of hFOB 1.19 and MC3T3-E1 cells. Both investigated biomaterials were non-toxic and allowed for initial cell attachment. However, significantly better cell spreading, growth, and proliferation were observed on the scaffold containing β-1,3-glucan. Based on the obtained results, it may be inferred that novel tri-component composite is promising material for bone tissue engineering applications as cell scaffold to accelerate bone regeneration and new bone formation process.

[Engineering of Biomaterials, 128-129, (2014), 20-22]

Acknowledgements

Financial assistance was provided by DS MNd 2 project. The paper was developed using the equipment purchased within the agreement No. POPW.01.03.00-06-010/09-00 Operational Program Development of Eastern Poland 2007-2013, Priority Axis I, Modern Economy, Operations 1.3. Innovations Promotion.

Piśmiennictwo References

[1] Chun, J.H., Kim, W.-G., Kim, H.-C., 2008. Fabrication of porous chitosan scaffold in order to improve biocompatibility. J. Phys. Chem. Solids. 69, 1573-1576.

[2] Przekora, A., Ginalska, G., 2014. Biological properties of novel chitosan-based composites for medical application as bone substitute. Cent. Eur. J. Biol., 9(6), 634-641.

[3] Przekora, A., Palka, K., Ginalska, G., 2014. Chitosan/β-1,3-glucan/calcium phosphate ceramics composites – Novel cell scaffolds for bone tissue engineering application. J. Biotechnol. 182-183(182), 46-53.

SYNTEZA I ANALIZA ELEMENTARNA HYDROKSYAPATYTÓW DOMIESZKOWANYCH KRZEMEM

Lukasz Pajchel*, Alicja Zawialow, Joanna Kolmas*, Waclaw Kolodziejski

Warszawski Uniwersytet Medyczny,
Katedra i Zakład Chemii Nieorganicznej i Analitycznej,
ul. Banacha 1, 02-091 Warszawa, Polska

[Inżynieria Biomateriałów, 128-129, (2014), 23-25]

Wprowadzenie

Hydroksyapatyty (HA; o wzorze chemicznym $Ca_{10}(PO_4)_6(OH)_2$) należą do szerokiej grupy minerałów nazywanej apatytami. Apatyty występują w przyrodzie jako minerały geologiczne oraz biologiczne [1]. Hydroksyapatyty biologiczne stanowią składnik nieorganiczny zębów i kości [1].

Krzem jest mikroelementem niezbędnym dla prawidłowego funkcjonowania organizmu człowieka. Dzienna zalecana przez FDA dawka krzemu dla kobiet i mężczyzn wynosi odpowiednio 19 i 40 mg. Krzem jest niezbędny do prawidłowego funkcjonowania skóry, włosów i paznokci. Zaleca się jego suplementację w przypadku podwyższonego ryzyka miażdżycy oraz osteoporozy. Pierwsze badania na temat roli krzemu w organizmie człowieka prowadzono już w latach siedemdziesiątych XX w. Wskazują one na dużą rolę krzemu w mineralizacji kości. Jest on również niezbędnym składnikiem w procesach syntezy kolagenu oraz stymulacji podziału komórek kostnych [2,3].

Syntetyczne hydroksyapatyty są wykorzystywane w medycynie i stomatologii jako materiał wypełniający lub pokrywający implanty [1]. Prowadzone badania zmierzają do ciągłego poszukiwania nowych materiałów na bazie hydroksyapatytów, gdyż, szczególnie hydroksyapatyty krzemowe, dają duże nadzieje na podwyższenie bioaktywności i biozgodności takich materiałów [4].

Celem prowadzonych badań była synteza serii hydroksyapatytów krzemowych o różnej zawartości krzemu a następnie opracowanie metody oznaczenia zawartości tego pierwiastka w tych związkach metodą fluorescencji rentgenowskiej z dyspersją długości fali (WD-XRF).

Materiały i metody

W trakcie syntezy poprzez wytrącenie z roztworu wodnego uzyskano serię próbek hydroksyapatytów krzemowych o różnej zawartości krzemu. Jeżeli przyjmiemy wzór ogólny otrzymanych związków jako $Ca_{10}(PO_4)_6$-$x(SiO_4)x(OH)_{2-x}$, to zaplanowano, że x = 0; 0.4; 0.6; 0.8; 1.0; 1.2; 1.4 oraz 1.8. Jony SiO_4^{3-} zastępują jony PO_4^{3-} oraz grupy OH^-.

Następnie otrzymane próbki poddano badaniom w celu oceny ich podobieństwa do stechiometrycznego hydroksyapatytu oraz zakupionego hydroksyapatytu krzemowego o deklarowanej zawartości krzemu (Sigma -Aldrich). Badania strukturalne przeprowadzono metodą dyfraktometrii proszkowej (XRD), spektroskopii w podczerwieni (IR) oraz metodą magnetycznego rezonansu jądrowego w ciele stałym (NMR). Natomiast badania zawartości krzemu wykonano metodą fluorescencji rentgenowskiej z dyspersją długości fali (WD-XRF), a jako metodę porównawczą zastosowano atomową spektrometrię emisyjną z wzbudzaniem plazmowym (ICP-AES).

SYNTHESIS END ELEMENTAL ANALYSIS OF SILICON-SUBSTITUTED HYDROXYAPATITES

Lukasz Pajchel*, Alicja Zawialow, Joanna Kolmas*, Waclaw Kolodziejski

Medical University of Warsaw,
Department of Inorganic and Analytical Chemistry,
1 Banacha str., 02-091 Warsaw, Poland

[Engineering of Biomaterials, 128-129, (2014), 23-25]

Introduction

Hydroxyapatites (HA; chemical formula - $Ca_{10}(PO_4)_6(OH)_2$) belong to the group of minerals named apatites. Apatites exist naturally as geological and biological minerals. Biological hydroxyapatites are inorganic components of teeth and bones [1].

Silicon (Si) is a chemical element essential for humans. Daily Si intakes of 40 and 19 mg are recommended by FDA for men and women, respectively. Si is beneficial in the case of arteriosclerosis and osteoporosis, for aging of skin, hair and nails. First studies on the function of Si in higher organisms were carried out in the early 1970s. They showed that Si plays an important role in the calcification of bones. It is also required for the synthesis of collagen and stimulates bone cells division [2,3].

Synthetic HAs are used in medicine and dentistry as materials for bioceramics and implant coatings [1]. Researchers are still looking for better biomaterials based on modified HAs. Silicon-substituted hydroxyapatites (Si-HA) seem to be promising as far their bioactivity and biocompatibility are concerned [4].

The aim of our study was to synthesize various Si-HA materials and determine their Si concentrations using wavelength–dispersive x-ray fluorescence spectroscopy (WD-XRF).

Materials and methods

The Si-HA samples with various concentrations of Si were synthesized by precipitation in aqueous solutions. Chemical formulas of those samples were $Ca_{10}(PO_4)_6$-$x(SiO_4)x(OH)_{2-x}$, with x = 0; 0.4; 0.6; 0.8; 1.0; 1.2; 1.4 and 1.8. The SiO_4^{3-} ions were introduced instead of PO_4^{3-} and OH^- groups ($0 \leq x < 2$). The Si-HA samples were compared with stechiometric HA and commercial Si-HA (Sigma-Aldrich). Structural differences were analyzed using powder X-ray diffraction (XRD), infrared spectroscopy (IR) and nuclear magnetic resonance (NMR). The Si concentrations were measured using WD–XRF and compared to those obtained using inductively coupled plasma atomic emission spectroscopy (ICP – AES). Crystals were visualized using transmission electron microscopy (TEM).

Procedure

Wavelength dispersive X-ray fluorescence spectroscopy

The Si content was determined using a Thermo Advant'x WD–XRF spectrometer and the Si Kα line. Calibration curve were prepared on 9 points in the range from 0 to 5.5 wt.%.

W celu oceny kształtu kryształów wykonano zdjęcia metodą transmisyjnej mikroskopii elektronowej (TEM).

Wykonanie badań

Fluorescencja rentgenowska z dyspersją długości fali

Oznaczenie zwartości krzemu wykonano na aparacie WD-XRF firmy Thermo model Advant'x wykorzystując linię emisyjną krzemu Kα. Wykorzystano linię kalibracyjną opartą na 9 punktach w zakresie od 0 do 5.5% krzemu. Tabletki uformowano przy użyciu prasy hydraulicznej firmy Specac używając matrycy o średnicy 13 mm przy nacisku 10 ton przez 10 minut. Do wykonania krzywej wzorcowej użyto talku jako źródła krzemu, mieszaniny kwasu borowego jako lepiszcza oraz hydroksyapatytu. Tabletki z próbek badanych przygotowano w identyczny sposób mieszając kwas borowy i badane hydroksyapatyty domieszkowane krzemem.

Atomowa spektrometria emisyjna z wzbudzaniem plazmowym

Badane próbki były również oznaczane z użyciem aparatu ICP-AES Perkin Elmer OPTIMAL 3100 XL. Roztwory wzorcowe przygotowano rozcieńczając roztwór wzorcowy krzemu (1000 mg/ml ± 4mg/l, Sigma-Aldrich, wzorzec krzemu dla AAS, c(NaOH)=2%) w zakresie od 10 do 50 ppm. Badane próbki zostały rozpuszczone w stężonym kwasie azotowym i rozcieńczone wodą.

Transmisyjna mikroskopia elektronowa

W celu oceny kryształów hydroksyapatytów krzemowych wykonano zdjęcia TEM z użyciem mikroskopu Jeol JEM 1400. Kropla próbki zawieszonej w etanolu została naniesiona na niklową siatkę pokrytą błoną z formvaru. Po wyschnięciu siatki były oglądane przy napięciu 80kV.

The measurements were done on tablets formed with a hydraulic Specac press (a 13 mm pellet die, pressure of 10 tons applied during 10 min). The tablets used for the calibration were made of talc as a source of Si and a mixture of boric acid with HA. The boric acid was used as a binder. The tablets containing samples were prepared in a similar way – they included boric acid and Si-HA. Each analysis was repeated 6 times.

Inductively coupled plasma atomic emission spectroscopy

The Si content was also measured using a Perkin Elmer OPTIMAL 3100 XL apparatus. For the calibration, solutions containing from 10 to 50 ppm of Si were prepared by dilution of a standard Si solution (1000 mg/ml ± 4mg/l, Sigma-Aldrich, Si standard for AAS, c(NaOH)=2% w/w). The studied samples were dissolved in concentrated nitric acid and diluted with water.

Transmission electron microscopy

The studied Si-HA crystals were observed using a Jeol JEM 1400 microscope. A drop of sample suspension in ethanol was placed on a Ni grid covered with a formvar film, allowed to dry and analyzed under the accelerating voltage of 80kV.

Results and discussion

The recorded XRD, NMR and IR spectra were typical for hydroxyapatites [7]. This proves that the synthesis was correct and successful.

The Si concentrations determined using WD–XRF and ICP-AES are presented in the TABLE 1. The results for the commercial material (WD–XRF 2.33 wt.%; ICP-AES 2.16 wt.%) were similar to that declared by the producer (2.33 wt.%). Generally, the Si concentrations determined using ICP-AES were lower than those from the WD-XRF method.

The HA and Si-HA crystals were observed on the TEM images. The images were of very good quality and clearly showed that the HA crystals were much larger than the Si-HA crystals.

TABELA 1. Zawartość procentowa krzemu w komercyjnym SI-HA oraz zsyntetyzowanych Si-HA
TABLE 1. Concentration of Si in the commercial Si-HA and synthesized Si-HA.

x	Zawartość % krzemu wyliczona na podstawie reagentów syntezy Concentration of Si expected from synthesis (% wt.)	Zawartość % krzemu oznaczona metodą XRF Concentration of Si determinated using XRF	Zawartość % krzemu oznaczona metodą ICP Concentration of Si determinated using ICP
		% Si	% Si
0,4	1,12	0,03	0,07
0,6	1,69	0,66	0,65
0,8	2,27	0,60	0,47
1,0	2,85	2,25	1,46
1,2	3,43	2,70	1,86
1,4	4,02	2,29	2,42
1,8	5,21	4,38	2,67
Komercjalny commercial Si-HA	2,33	2,33	2,16

Dyskusja wyników

Widma otrzymane metodami XRD, NMR i IR są zgodne z doniesieniami literaturowymi i potwierdzają otrzymanie hydroksyapatytów domieszkowanych krzemem [7]. W TABELI 1 zaprezentowano procentowe zawartości krzemu oznaczone metodami WD-XRF oraz ICP-AES. Dla zakupionego hydroksyapatytu domieszkowanego krzemem uzyskano wartości bardzo zbliżone do deklarowanej przez producenta. Zaobserwowano również zależność, iż wyniki otrzymane metodą ICP-AES są nisze niż wyniki otrzymane metodą WD-XRF.

Analizując zdjęcia wykonane metodą TEM zauważono, że kryształy hydroksyapatytów domieszkowanych krzemem są znacznie mniejsze niż kryształy hydroksyapatytu stechiometrycznego.

Wnioski

1. Udało się uzyskać serię hydroksyapatytów krzemowych o różnej zawartości krzemu. Ich strukturę potwierdzono metodami spektroskopowymi (IR i NMR)
2. Potwierdzono możliwość wykorzystania metody WD -XRF do oznaczania zawartości krzemu w hydroksyapatytach domieszkowanych tym pierwiastkiem.
3. Zaobserwowano, że wielkość kryształów hydroksyapatytów krzemowych maleje wraz ze zwiększaniem się zawartości krzemu w próbce.

Podziękowania

Autorzy składają serdeczne podziękowanie dr Marzenie Kuras (WUM) za pomoc w analizie zawartości krzemu metodą ICP-AES. Przedstawione w pracy badania zostały sfinansowane ze środków Warszawskiego Uniwersytetu Medycznego: grant Młodego Naukowca FW23/PM32/13. Badania TEM zostały przeprowadzone w Laboratorium Mikroskopii Elektronowej IBD PAN w Warszawie. Mikroskop TEM JEM 1400 (Jeol Co., Japan, 2008) został zakupiony z funduszy strukturalnych UE w ramach projektu CZT BIM - Wyposażenie Laboratorium Obrazowania Biologicznego i Medycznego.

Conclusions

1. We have successfully synthesized hydroxyapatites (Si-HA) containing various concentrations of Si. Their structure was confirmed using MAS NMR and IR spectroscopies.
2. We have proved that the WD-XRF spectroscopy can be used to estimate the Si content in the Si-HA samples.
3. It has been shown that the Si-HA crystals become smaller with increasing Si content.

Acknowledgments

The authors are grateful to dr Marzena Kuras (WUM) for their help in the ICP-AES analyses, respectively. This work was supported Medical University of Warsaw: Young Scientist grant number FW23/PM32/13. The TEM studies were performed in the Laboratory of Electron Microscopy, Nencki Institute of Experimental Biology, Warsaw, Poland Electron microscope JEM 1400 (JEOL Co., Japan, 2008) equipped with energy-dispersive full range X-ray microanalysis system (EDS INCA Energy TEM, Oxford Instruments, Great Britain), tomographic holder and high resolution digital camera (CCD MORADA, SiS-Olympus, Germany). The above mentioned equipment was installed within the project sponsored by the EU Structural Funds: Centre of Advanced Technology BIM - Equipment purchase for the Laboratory of Biological and Medical Imaging.

Piśmiennictwo References

[1] E. Bogya, R. Barabás, A. Csavdári, V. Dejeu, I. Bâldea. Hydroxyapatite modified with silica used for sorption of copper(II). Chemical Papers 63 (5) (2009) 568–573.
[2] J.D. Kirschmann, Ed., Nutrition Almanac, McGrow-Hill, New York, 2007.
[3] E. Carlisle, Silicon: An Essential Element for the Chick, Science 178 (1972) 619-621.
[4] E. S. Thian, J. Huang, S. M. Best, Z. H. Barber, W. Bonfield. A new way of incorporating silicon in hydroxyapatite (Si-HA) as thin films. Journal Of Materials Science: Materials In Medicine 16 (2005) 411– 415.
[5] E. O. Stejskal, J. D. Memory, High-Resolution NMR in the Solid State. Fundamentals of CP/MAS, Oxford University Press, Oxford, 1994.
[6] W. Kolodziejski, J. Klinowski, "Kinetics of Cross-Polarization in Solid-State NMR: A Guide for Chemists" Chemical Reviews, 102 (2002) 613.
[7] J. Kolmas, A. Jaklewicz, A. Zima, M. Budko, Z. Paszkiewicz, J. Lis, A. Ślósarczyk, W. Kolodziejski, Incorporation of carbonate and magnesium ions into synthetic hydroxyapatite: The effect on physicochemical properties, Journal of Molecular Structure 987 (2011) 40-50

PODŁOŻA WŁÓKNISTE Z POCHODNEJ KWASU HIALURONOWEGO OTRZYMANE METODĄ ELEKTROPRZĘDZENIA

Paulina Król, Ewelina Pabjańczyk-Wlazło, Michał Chrznowski, Izabella Krucińska, Grzegorz Szparaga, Maciej Boguń

Katedra Materiałoznawstwa, Towaroznawstwa i Metrologii Włókienniczej, Wydział Technologii Materiałowych i Wzornictwa Tekstyliów, Politechnika Łódzka, ul. Żeromskiego 116, 90-924 Łódź, Polska

Abstract

Celem realizowanej pracy badawczej jest dobranie układu: polimer – rozpuszczalnik - substancja pomocnicza, aby uzyskać metodą elektroprzędzenia biozgodne włókniste podłoża z kwasu hialuronowego o nano- i mikro- metrycznych rozmiarach włókien. W przeprowadzonych badaniach skupiono się nad doborem stężenia roztworu oraz rodzajem i ilością substancji pomocniczych. W dalszej części badań objętych projektem 2012/07/B/ST8/03378 zrealizowane zostaną badania nad wpływem rodzaju i ilości wprowadzonych aktywnych dodatków: antybiotyków z rodziny cefalosporyn oraz cynku. Określony zostanie także wpływ typowych rozpuszczalników, a także obecność środków powierzchniowo czynnych na odpowiedź komórkową i cytotoksyczność takich struktur.

[Inżynieria Biomateriałów, 128-129, (2014), 26-28]

Wstęp

Bardzo istotnym i znaczącym problemem w przypadku otrzymywania nanowłókien metodą elektroprzędzenia oraz włóknistych podłoży z biopolimerów takich jak: alginian czy kwas hialuronowy jest dobór parametrów roztworów przędzalniczych w celu uzyskania odpowiednich jego właściwości, umożliwiających dobrą przerobowość. W przypadku otrzymywania włókien z kwasu hialuronowego oraz jego pochodnych głównym problemem jest bowiem przygotowanie roztworu przędzalniczego, o optymalnych właściwościach, takich jak: stężenie i napięcie powierzchniowe, które zapewniałyby odpowiedni przebieg i stabilność procesu przędzenia włókien oraz otrzymanie materiału włóknistego o założonych parametrach. Roztwory kwasu hialuronowego w wodzie cechują się bowiem wysoką wartością napięcia powierzchniowego oraz lepkością dynamiczną pozorną [1-3]. Najlepszym rozpuszczalnikiem kwasu hialuronowego jest woda, która posiada jednak dość wysoką wartość napięcia powierzchniowego, w porównaniu do innych powszechnie stosowanych rozpuszczalników, rzędu 72,75 mN/m. W celu poprawy właściwości płynu przędzalniczego, umożliwiając jego przerobowość metodą elektroprzędzenia, stosuje się dodatki zmniejszające napięcie powierzchniowe. Jako substancje powierzchniowo-czynne stosuję się najczęściej: alkohol etylowy [4,5], kwas mrówkowy, dimetyloformamid (DMF) [4,6], wodorotlenek sodu [3,7] oraz mieszaniny powyższych.

HYALURONIC ACID-DERIVED FIBROUS MATERIALS PREPARED BY ELECTROSPINNING

Paulina Król, Ewelina Pabjańczyk-Wlazło, Michał Chrznowski, Izabella Krucińska, Grzegorz Szparaga, Maciej Boguń

Department of Material and Commodity Sciences and Textile Metrology, Faculty of Material Technologies and Textile Design, Lodz University of Technology, 116 Żeromskiego Street, 90-924 Lodz,Poland

Abstract

The objective of the project will be to select the polymer/solvent/additive system to prepare fibres and fibrous matrices enriched with active substances from the hyaluronic acid matrix by electrospinning with nano- and micro- metric sizes of fibers. The aim of this study was to select a concentration and composition of spinning solutions as well as the type and amount auxiliary substances. In the next part of the research, included in the project 2012/07/B/ST8/03378, the studies on the influence of the type and amount entered active additives: cephalosporin family of antibiotics and zinc will be implemented. Simultaneously, the effect of typical solvents used in electrospinning and the presence of surfactants in polymer solutions on cellular cytotoxicity response of such structures will be defined.

[Engineering of Biomaterials, 128-129, (2014), 26-28]

Introduction

The selection of an appropriate composition of spinning solutions to yield suitable parameters which ensure good processing is a vital and significant issue in the preparation of nanofibres by electrospinning and fibrous matrices from biopolymers, such as alginate or hyaluronic acid. The major problem when preparing fibres from hyaluronic acid and its derivatives is the preparation of a spinning solution with optimum properties, such as concentration and surface tension, which ensure the appropriate course and stability of the fibre spinning process and yield a fibrous material with defined parameters. For aqueous hyaluronic acid solutions have very high surface tension values and apparent dynamic viscosity [1-3]. The best hyaluronic acid solvent is water, which, however, has a fairly high surface tension compared to other commonly used solvents, of 72,75 mN/m. In order to improve the spinning properties of the fluid, allowing its processability by electrospinning, extra components are used to reduce the surface tension. As those components the most common surfactants are being used: ethanol [4,5], formic acid, dimethylformamide (DMF) [4,6], sodium hydroxide [3,7], and mixtures thereof

Materials, methods and results

In the studies wide range of polymers, differing molar mass, has been used: 2.0–2.2 MDa; 1.8–2.0 MDa; 100-150 kDa and 80-130 kDa. As a polymer sodium hyalutonate (HA) purchased in Contripo Biotech with cosmetic purity has been used. The solutions has been prepared with the distilled water as a solvent.

TABELA 1. Właściwości płynów przędzalniczych użytych do elektroprzędzenia włóknistych podłoży.
TABLE 1. Properties of the spinning solutions used for electrospinning of fibrous substrates.

Symbol próbki Sample	Masa molowa Molar mass [kDa]	Stężenie polimeru Polymer concentration [%]	Skład płynu przędzalniczego Spinning solution composition	Lepkość dynamiczna pozorna Dynamic viscosity[Pa·s]	Napięcie powierzchniowe Surface tension [mN/m]
1	2000 – 2200	1	HA / woda (water)/ alkohol (ethanol / NaCl	11,62	57,55
2	1800 - 2000	0,5	HA / woda (water) /DMF	2,16	54,73
3	100 - 150	12	HA / WA / DMF	-	-
4			HA / WA / NMP	-	-

Materiały, metodyka, wyniki

W badaniach wykorzystana została szeroka gama polimerów znacząco różniących się masą molową: 2,0-2,2 MDa; 1,8-2,0 MDa; 100-150 kDa oraz 80 - 130 kDa. Użytym polimerem był hialuronian sodu (HA), o czystości kosmetycznej, zakupiony w Contripo Biotech. Jako rozpuszczalnik zastosowana była woda destylowana.

Jako substancje pomocnicze do sporządzenia roztworów przędzalniczych wykorzystano: dimetylosulfotlenek (DMSO), dimetyloformamid (DMF), alkohol etylowy, aceton, N-metylo-pirolidon (NMP), wodny roztwór chlorku sodu, wodny roztwór chlorku potasu, wodę amoniakalną (WA) oraz mieszaniny powyższych.

Podłoża włókniste formowano metodą elektroprzędzenia przy zastosowaniu płynów przędzalniczych charakteryzujących się stężeniem z zakresu: 0,5-12%.

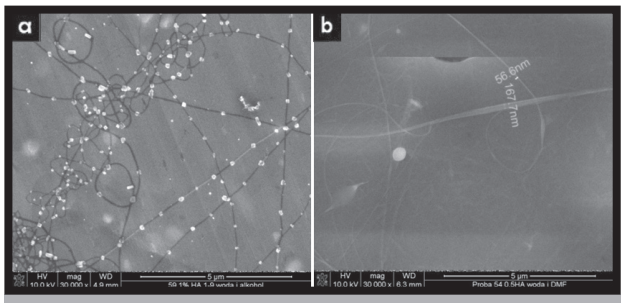

RYS. 1. Zdjęcia SEM włókien uzyskanych z płynu przędzalniczego o składzie: a) 1% HA/woda/alkohol/0,5M NaCl (próbka 1); b) 0,5% HA/woda/DMF (próbka 2).
FIG. 1. SEM image of fibres obtained from the spinning liquid with the composition: a) 1% HA/water/ethanol/0,5M NaCl (sample 1); b) 0,5% HA/water/DMF (sample 2).

Wnioski

We wstępnych próbach udało się uzyskać optymalny skład i stężenie płynu przędzalniczego umożliwiający jego przerób metodą elektroprzędzenia. Jednocześnie do dalszych prac wytypowano polimer o właściwej, z uwagi na metodę przetwórstwa, masie molowej. Uzyskane podłoża charakteryzują się włóknami o rozmiarach manometrycznych zawierających się w przedziale 32-216 nm.

Podziękowanie

Badania realizowane są dzięki finansowaniu Narodowego Centrum Nauki nr projektu 2012/07/B/ST8/03378.

As auxiliary substances to prepare spinning solutions following solvents were used: dimethyl sulfoxide (DMSO), dimethylformamide (DMF), ethyl alcohol, acetone, N-methylpyrrolidone (NMP), aqueous solution of sodium chloride, potassium chloride aqueous solution, ammonia water (WA), and mixtures thereof.

Fibrous materials has been prepared by electrospinning by applying spinning solutions with the concentration at range of 0.5-12%.

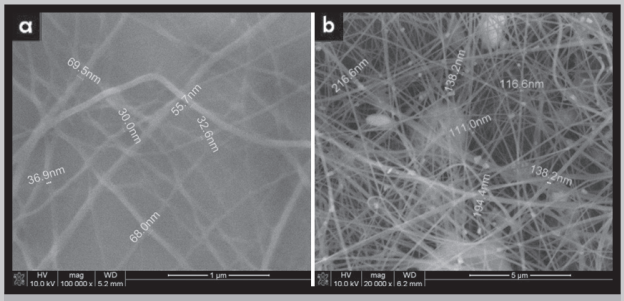

RYS. 2. Zdjęcia SEM włókien uzyskanych z płynu przędzalniczego o składzie: a) 12% HA/WA/DMF (próbka 3); 12% HA/WA/NMP (próbka 4).
FIG. 2. SEM image of fibres obtained from the spinning liquid with the composition: a) 12% HA/WA/DMF (sample 3); 12% HA/WA/NMP (sample 4).

Conclusions

The preliminary trials succeeded in obtaining the optimal composition and concentration of the spinning liquid which allows its processing through electrospinning. Simultaneously, polymer with proper molar mass, according to the processing method, has been selected for further work. Obtained fibers are characterized by a nanometric size comprised within the range of 32-216 nm.

Acknowledgement

The research was financed by National Science Centre project 2012/07/B/ST8/03378.

Piśmiennictwo

[1] Nanotechnologies for the Life Sciences Vol. 9 Tissue, Cell and Organ Engineering, Edited by C.S.S.R. Kumar, 2006, WILEY-VCH, ISBN: 3-527-31389-3
[2] X. Wanga, I.C. Uma, D. Fangb, A. Okamotoc, B.S. Hsiao, Formation of water-resistant hyaluronic acid nanofibers by blowing -assisted electro-spinning and non-toxic post treatments, Polymer, 46, (2005), pp. 4853–4867
[3] E.K. Brenner, J.D. Schiffman, E.A. Thompson, L.J. Toth, C.L. Schauer, Electrospinning of hyaluronic acid nanofibers from aqueous ammonium solutions, Carbohydrate Polymers, 87, (2012), pp. 926– 929
[4] L. Junxing, H. Aihua , C.C. Han, D. Fang,2 B.S. Hsiao, B. Chu, Electrospinning of Hyaluronic Acid (HA) and HA/Gelatin Blends, Macromol. Rapid Commun., 2006, 27, pp. 114–120

References

[5] K. Kyu-Oh, A. Yaeko, K. Wei, K. Byoung-Suhk, K. Ick-Soo, Cells Attachment Property of PVA Hydrogel Nanofibers Incorporating Hyaluronic Acid for Tissue Engineering, Journal of Biomaterials and Nanobiotechnology, 2, 2011, pp. 353-360
[6] L. Yang, M. Guiping, F. Dawei, X. Juan, Z. Hongwen, N. Jun, Effects of solution properties and electric field on the electrospinning of hyaluronic acid, Carbohydrate Polymers, Vol.83, Issue 2, 2011, pp. 1011–1015
[7] R.L. Fischer, M.G. McCoy, S.A. Grant, Electrospinning collagen and hyaluronic acid nanofiber meshes, Journal of Materials Science: Materials in Medicine, 23, 2012, pp. 1645–1654

IZOLOWANE ZŁAMANIE TRZPIENIA ENDOPROTEZY STAWU BIODROWEGO – OPIS DWÓCH PRZYPADKÓW

Żaneta Anna Mierzejewska*, Zbigniew Oksiuta

Politechnika Białostocka,
Ul. Wiejska 45c, 15-351 Białystok, Polska
* e-mail: a.mierzejewska@doktoranci.pb.edu.pl

Streszczenie

Staw biodrowy zbudowany jest z panewki biodrowej, anatomicznie uformowanej z kości miednicy oraz głowy kości udowej. Oba te elementy pokryte są chrząstką i otoczone torebką stawową, wypełnioną płynem synowialnym, którego zadaniem jest odżywianie chrząstki oraz amortyzowanie sił działających na staw. Jakiekolwiek zmiany w tym układzie mogą prowadzić do uszkodzenia i deformacji stawu, co skutkuje utratą funkcjonalności oraz bólem. Terapią, która przywraca pacjentowi możliwość bezbolesnego funkcjonowania jest endoprotezoplastyka, polegająca na chirurgicznym wycięciu zmienionych chorobowo powierzchni stawowych i zastąpieniu ich sztucznymi elementami. Jednakże, jak każda chirurgiczna interwencja, endoprotezoplastyka niesie ze sobą ryzyko powikłań. Jednym z nich jest izolowane złamanie trzpienia stawu biodrowego – trzpień ulega złamaniu w kanale szpikowym przy czym tkanki otaczające implant nie zostają uszkodzone.

W pracy przedstawione i porównane zostały dwa przypadki izolowanego złamania trzpienia endoprotezy stawu biodrowego, rozpoznane ok. 3 lata po wszczepieniu implantów. Celem pracy było zbadanie cech i mikrostruktury reimplantowanych trzpieni, zdefiniowanie relacji pomiędzy strukturą a wielkością ziaren i zidentyfikowanie ognisk pękania. W tym celu zbadane zostały mikrostruktura, wielkość ziaren, skład chemiczny oraz twardość obu trzpieni.

ISOLATED FRACTURE OF THE HIP STEM PROSTHESIS - REPORT OF TWO CASES

Żaneta Anna Mierzejewska*, Zbigniew Oksiuta

Bialystok University of Technology,
45c Wiejska Street, 15-351 Białystok, Poland
* e-mail: a.mierzejewska@doktoranci.pb.edu.pl

Abstract

The hip joint is composed of acetabular, anatomical surface of pelvis and the femoral head. Both of these elements are covered with cartilage and enclosed in a capsule, filled with synovium, which aim is to nourish the cartilage and depreciate forces acting on the hip joint. Any lesions in this system can lead to damage and deformation of the joint, which results in loss of function and pain. The treatment that restores the patient's ability to functioning is the total hip replacement, which consists of surgical excision of the damaged joint surface and implanted in place of artificial elements. However, like any surgical intervention, this procedure carried the risk of complications. One of them is isolated stem fracture, which consisting of the stem break inside the medullary canal without damaging surrounding tissue.

The work presents and compares two cases of isolated fracture of hip stems, which were recognized three years after the operation. The aim of the study was to investigate the properties and microstructure of reimplanted stems, made of austenitic, to define the relationship between the structure and the size of the grains and to identify outbreaks of cracking. Microstructure, grain size, chemical composition and hardness of both stems have been investigated.

Badania mikroskopowe ujawniły defekty materiału. Obserwacje przełomu za pomocą skaningowego mikroskopu elektronowego (SEM) ujawniły obecność prążków zmęczeniowych, co wskazuje na zmęczeniowy charakter przełomu. Liniowy pomiar twardości ujawnił znaczną niejednorodność materiału.

Uzyskane wyniki stanowią podstawę do dalszych badań tego zjawiska.

Słowa kluczowe: *endoprotezoplastyka, złamanie izolowane, powikłania po całkowitej artroplastyce, reimplantacja*

[Inżynieria Biomateriałów, 128-129, (2014), 28-31]

Wprowadzenie

Endoprotezoplastyka stawu biodrowego jest jedną z najbardziej udanych technik operacyjnych w chirurgii ortopedycznej. Jest to popularna metoda stosowana w celu przywrócenia normalnego funkcjonowania stawu biodrowego, uszkodzonego przez złamania lub choroby [1]. Niestety, proteza stawu biodrowego nie jest ostatecznym rozwiązaniem problemów zdrowotnych. Podczas eksploatacji, implanty chirurgiczne są wystawione na agresywne środowisko korozyjne, zużycie i obciążenia. Ten szeroki zakres zmiennych powoduje wiele różnych mechanizmów uszkodzeń [1].

Złamanie trzpienia stawu biodrowego stanowi trudne w leczeniu powikłanie. Częstość występowania tej komplikacji zależy od wielu czynników: zastosowanego przez chirurga sprzętu operacyjnego, materiału, z którego wykonany został implant, masy ciała pacjenta i populacji [2,3]. Złamania izolowane były często odnotowywane w przypadku protez wytwarzanych w latach sześćdziesiątych i siedemdziesiątych. Wynikało to z niskich właściwości wytrzymałościowych stosowanych wówczas materiałów [4,5]. Najczęściej trzpienie pękały w wyniku zmęczenia materiału, spowodowanego niekorzystnymi warunkami biomechanicznymi, obluzowaniem w kanale szpikowym lub nieprawidłową geometrią [2].

Zastosowanie materiałów o wysokiej wytrzymałości, a także intensywne prace nad konstrukcją implantów spowodowały zmniejszenie częstotliwości występowania tej komplikacji, w związku z tym złamania izolowane trzpienia endoprotezy stawu biodrowego stały się rzadkim powikłaniem [6-10].

Materiały i metody

Trzpienie wykonane były z austenitycznej stali nierdzewnej REX 734. Złamania zdiagnozowane zostały po około trzech latach od implantacji. Dla porównania składów chemicznych obu trzpieni z normą ASTM F1586 wykonano iskrową spektroskopię elektronową (Thermo ARL Quantris, Switzerland). Szczegółowe badanie mikrostruktury, po odpowiednim przygotowaniu próbek, przeprowadzone zostało za pomocą mikroskopu optycznego (OM) Nikon Eclipse LV1000. Powierzchnię przełomu zbadano przy użyciu skaningowego mikroskopu elektronowego (SEM) Hitachi S-3000N, wyposażonego w analizator spektroskopowy (Energy Dispersive Spectroscopy EDS). Badania twardości wykonano za pomocą uniwersalnego wgłębnika Vickersa z obciążeniem 5 kg.

Microscopic examination revealed defects in material. A breakthrough observation, carried out by scanning electron microscopy (SEM) revealed the presence of fatigue striations, which clearly indicated the nature of the fatigue fracture. Linear hardness measurements revealed significant heterogeneity of the material.

The results obtained in this work will be used for further research on this topic.

Keywords: *endoprosthesoplasty, isolated stem fracture, complications of total hip arthroplasty, reimplantation*

[Engineering of Biomaterials, 128-129, (2014), 28-31]

Introduction

Primary hip arthroplasty has become one of the most successful operation techniques in orthopedic surgery, which is popular strategy used for restore the normal function of the hip joint damaged by fracture or disease [1]. Unfortunately, the hip prosthesis is not the ultimate solution to health problems. During service life, surgical implants are exposed to an aggressive environment in terms of corrosion, wear and loading. This wide range of variables has resulted in a wide range of failure mechanisms [1].

Fracture of the femoral stem constitutes a dramatic long – term complication of total hip surgery. The incidence of this complication varies with many factors, including the device used, the material from which the prosthesis was made, the surgeon, patient body mass index and population [2,3]. Relatively high rates of fracture of the femoral stem of total hip arthroplasties were seen with early designs manufactured in the 1960s and 1970s because of the material's low fatigue strength and the presence of metallurgical defects [4,5]. The stems generally failed via a fatigue mechanism because of unfavorable biomechanics such as varus positioning, loosening, loss of proximal support, geometry of the stem or surface damage of the implant [2].

Fractures have been reported in a variety of prosthetic designs and materials. The use of high-strength materials including forged cobalt chrome, titanium alloy and high-nitrogen stainless steel, as well as further development of stem design and stem geometry, have led to a reduction in the incidence of this complication, and the occurrence of fracture with modern femoral stems is a now a very rare event [6-10].

Materials and methods

The stems were forged using high nitrogen stainless steel. The failure occurred after only 3 years service. To compare the chemical composition of fractured stems with ASTM F1586 standard spark emission spectroscopy (Thermo ARL Quantris, Switzerland) was used. Detailed microscopic examinations of the microstructure after etching polished samples were carried out by a Nikon Eclipse LV1000 optical microscope (OM). The fracture surfaces of stems were examined by means of a Hitachi S-3000N Scanning Electron Microscopy (SEM) equipped with Energy Dispersive Spectroscopy (EDS) detector. Hardness measurements were performed using Vickers universal indenter with load of 5 kg.

Wyniki i dyskusja

Skład chemiczny obu trzpieni przedstawiono w TABELI 1. Dla porównania zamieszczono również skład chemiczny austenitycznej stali nierdzewnej REX 734, zgodny z normą ISO 5832-9. Wyniki przeprowadzonych analiz wskazały, że materiał zastosowany do wytworzenia obu implantów był zgodny z wytyczonymi normami, jednakże zauważalne są niewielkie różnice w składzie chemicznym obu próbek.

Results and discussions

The chemical composition of tested stems is shown in TABLE 1. For comparison the chemical composition of the high nitrogen austenitic stainless steel according to ISO 5832-9 standard (REX 734 grade) is also presented. The results of chemical analysis of the tested steel revealed, that the material of stem, in general, fulfils the ISO requirements, however, there are some differences in chemical composition of the tested stems in comparison with the standard.

TABELA 1.
TABLE 1.

	C	Si	Mn	P	S	Cr	Mo	Cu	Ni	N	Nb
Rex 734 (ISO 5832-9)	0.08[a]	0.75[a]	2-4.25	0.025[a]	0.01[a]	19.5-22	2-3	0.25[a]	9-11	0.25-0.5	0.25-0.8
Trzpień I Stem I	0.037	0.39	4.54	0.021	0.017	21.36	2.17	0.19	9.83	0.36	0.26
Trzpień II Stem II	0.036	0.27	4.1	0.002	0.015	21.14	2.33	0.036	7.05	-	0.39
[a] – zawartość maksymalna / maximum content											

Badania mikroskopowe ujawniły znaczną ilość defektów materiałowych w obu trzpieniach. Wyróżnić można tutaj pory i pustki, zlokalizowane na obrzeżach próbek, a także nieciągłości i rozwarstwienia materiału, prawdopodobnie wynikające z przeciążenia materiału. Nie wykryto natomiast obecności ani też żadnych zmian spowodowanych korozją. Obserwacje prowadzone za pomocą skaningowego mikroskopu elektronowego potwierdziły, że złamanie implantu było wynikiem zmęczenia materiału. W obu próbkach zauważono świadczące o takim charakterze zniszczenia prążki zmęczeniowe. Duża powierzchnia obszaru pękania zmęczeniowego w porównaniu z obszarem pękania doraźnego w obu przypadkach, wskazuje na działanie niewielkich obciążeń i niewielkiej prędkości propagacji pęknięć. Twardość obu trzpieni zbadana została powyżej i poniżej przełomu, w bezpośredniej odległości. Dla pierwszego trzpienia średnia twardość badanego materiału wyniosła ~ 335 HV/5 i była zgodna z normą ASTM. Jednakże zauważono, że twardość materiału jest niejednorodna – powyżej przełomu twardość wynosiła 342±2 HV/5, natomiast poniżej – 325±5 HV/5. Twardość drugiego trzpienia wyniosła 342 HV/5±6 powyżej złamania i 340 HV/5±4 poniżej. Ta niejednorodność twardości mogła być spowodowana nieprawidłowo przeprowadzonym procesem obróbki cieplno – plastycznej.

Microscopic examination revealed numerous defects in both stems. Among them are pores and emptiness, located on the outskirts of the tested samples and a plurality of recesses and delamination of the material, probably due to the overloading of a fatigue character. There were no changes caused by corrosion. Observations of the material by using scanning electron microscopy (SEM), clearly proved that the destruction was caused by material fatigue, however in the second stem the pattern wave of propagation of the fracture was not visible because the fracture surfaces were polished as a result of walking after the fracture had occurred. Large surface of the fatigue crack zone area indicated for small stresses and small crack propagation velocities. For the first stem an average hardness of tested material is ~ 335 HV/5 and fulfils ASTM requirements. However, an interesting effect was observed – hardness of stem material above the breakthrough was 342±2 HV/5 and below – 325±5 HV/5. For the second stem hardness of stem material was measured at 342 HV/5±6 above the fracture and 340 HV/5±4 below the fracture. This may be caused by uneven distribution of forces during plastic forming and shaping the implant or underlying reasons for this heterogeneity can be improperly carried out heat treatment.

Wnioski

Celem pracy było przeanalizowanie i opisanie dwóch przypadków złamania cementowych trzpieni endoprotezy stawu biodrowego, wykonanych ze stali austenitycznej REX 734.Na krótki czas eksploatacji implantów mogło mieć wpływ wiele czynników, m.in.: niezgodny z normami skład chemiczny, nieprawidłowo przeprowadzona obróbka cieplno – plastyczna skutkująca niejednorodną twardością materiału, obecność wtrąceń niemetalicznych i wad materiałowych.

Badania mikrostruktury, zarówno poniżej jak i powyżej przełomu ujawniły strukturę homogeniczną, jednorodną z małymi ziarnami, typowymi dla materiałów kutych. Badania twardości wykazały znaczną niejednorodność materiału zastosowanego do wytworzenia obu implantów. Nie odnotowano zmian spowodowanych obecnością korozji, co może wskazywać na równomierne rozłożenie głównych składników stopowych, takich jak chrom i nikiel.

Conclusions

The main goal of this work was to analyse and describe a failure mechanism of cemented hip stem made of austenitic stainless steel, REX 734 grade. There are some factors such as: chemical composition, higher hardness measured in the inner part of the stem and secondary cracks initiated at the non – metallic inclusions, that can explain early fracture of the hip endoprosthesis after 3 years of implantation.

The microstructure in remote areas and close to the fracture surfaces were homogeneous and possessed a relatively small, refined grain size, typical of forged components. There were no changes caused by intergranular corrosion or pitting, which may indicate an even distribution of the major alloy components such as chromium and nickel.

Zaobserwowano natomiast obecność porów oraz węglików, zlokalizowanych zarówno w bezpośredniej jak i dalszej odległości od przełomu, a także rozwarstwienia i nieciągłości materiału. Obserwacje powierzchni przełomu, za pomocą skaningowej mikroskopii elektronowej, wyraźnie pokazuje, że zniszczenie materiału nastąpiło w wyniku zmęczenia. W tym przypadku, połączenie prążków zmęczeniowych i brak wad metalurgicznych trzpienia wskazuje, że pękanie spowodowane było przeciążeniem trzpienia.

Podziękowania

Praca zrealizowana została przy wsparciu Wydziału Mechanicznego Politechniki Białostockiej, projekt numer MB/WM/14/2014.

Metallurgical defects such as porosity and gross carbides inclusions close to the fracture sites and in remote areas were observed. The results of the hardness revealed heterogeneity of the material. Pictures taken by means of a scanning electron microscope revealed the presence of pores and a plurality of recesses and delamination of the material resulting from the overload of an endurance. Observations of fracture surface, using scanning electron microscopy, clearly proves that the destruction of materials occurred as a result of fatigue. In this case, the combination of the fatigue striation and the absence of any defects of the stem indicate that the fracture may be due simply to overloading of the stem.

Acknowledgments

This scientific work was supported by the Faculty od Mechanical Engineering, Bialystok University of Technology, project No MB/WM/14/2014.

Piśmiennictwo

[1] Nunley R. M., Ruh E. L., Zhang Q., Della Valle C. J., Engh C. A,. Berend M. E, Parvizi J., Clohisy J. C., Barrack R. L.: Do Patients Return To Work After Hip Arthroplasty Surgery, J Arthroplasty, 2011 Sep, 26(6 suppl):92-98.e1-3
[2] Kamachi M. U., Sridhar T.M., Eliaz N., Baldev R. A..: Failures Of Stainless Seel Orthopaedic Devices: Causes And Remedies, Corros Rev, 2003, 21:231-67.
[3] Martens M., Aernoudt E., De Meester P., Ducheyne P., Muller J.C., Delangh R., Kestelijn P.: Factors In The Mechanical Failure Of The Femoral Component In Total Hip Prosthesis, Acta Orthop Scandinavica 1974, 45(5):693-710
[4] Kotela A., Ambroziak P., Deszczyński M.J.: Złamanie Trzpienia Endoprotezy Stawu Biodrowego – Opis Przypadku, Ostry Dyżur, 2012, Tom 5, Numer 1-2
[5] Carlsson A. S., Gentz C. F., Stenport J.: Fracture Of The Femoral Prosthesis In Total Hip Replacement According To Charnley, Acta Orthop Scand 1977, 48(6):650-5

References

[6] Wróblewski B.M.: Fractured Stem In Total Hip Replacement – A Clinical Review Of 120 Cases, Acta Orthop Scand 1982 Apr, 53(2):279-84
[7] Akinola B., Mahmud T., Deroeck N.: Fracture Of An Exeter Stem-A Case Report, The Internet Journal Of Orthopedic Surgery 2009, Vol.16 Number 1
[8] Jarvi K., Kerry R.M.: Case Report Segmental Stem Fracture Of A Cemented Femoral Prosthesis, The Journal Of Arthroplasty, 2007, Vol. 22 No. 4 Jun 1 2007
[9] Roffey P.: Case Study: Failure Of A High Nitrogen Stainless Steel Femoral Stem, Engineering Failure Analysis 2012 Mar; Vol. 20
[10] Sen R.K., Mootha A.K., Saini R., Kumar V.: Segmental Fracture Of A Cemented Femoral Stem - A Case Report And Review Of Litrature. The Internet Journal Of Orthopedic Surgery 2009; Vol. 13 No. 1

PRZEMIANY FAZOWE I TEKSTURA W WYCISKANYM NA GORĄCO STOPIE NiTi Z PAMIĘCIĄ KSZTAŁTU PRZEZNACZONYM DO ZASTOSOWAŃ MEDYCZNYCH

Z.Lekston*, M.Zubko, T.Goryczka, J.Lelątko, D.Stróż, K.Prusik

Instytut Nauki o Materiałach, Uniwersytet Śląski,
41-500 Chorzów, 75 Pułku Piechoty 1A
zlekston@us.edu.pl

Streszczenie

W pracy przedstawiono badania przemian fazowych oraz badania tekstury w próbkach pręta uzyskanego po wyciskaniu współbieżnym na gorąco z wlewka NiTi odlanego w procesie wytapiania i odlewania w indukcyjnym piecu próżniowym. Proces wyciskania na gorąco przeprowadzono przy użyciu oprzyrządowania własnej konstrukcji na prasie laboratoryjnej o maksymalnej sile nacisku 1000 kN. Próbki do badań wycięto poprzecznie i wzdłuż osi ze strefy głowy i stopy pręta. Badania przebiegu przemian fazowych przeprowadzono metodami DSC i rentgenografii temperaturowej. Stwierdzono, że w próbkach po wyciskaniu i po zastosowanej obróbce cieplnej przemiany zachodziły dwustopniowo, odwracalnie wg sekwencji B2↔R↔B19'. Również metodą rentgenograficzną stwierdzono obecność tekstury osiowej <110>. Uzyskany pręt przeznaczono do dalszego wyciskania na gorąco w celu redukcji średnicy i uzyskania półwyrobu do wykonania prototypowych wyrobów medycznych w postaci klamer do zespoleń złamań kości.

[Inżynieria Biomateriałów, 128-129, (2014), 32-35]

Wprowadzenie

Stopy NiTi wykazujące efekty pamięci kształtu jako materiały inteligentne są coraz szerzej stosowane w technice i medycynie [1-3]. Dobre własności mechaniczne, odporność na korozję i efekty pamięci kształtu zależą od ich składu chemicznego, czystości stopów, zastosowanych sposobów procesu technologicznego, wytapiania, odlewania i przeróbki plastycznej oraz procesów obróbki cieplnej i cieplno-mechanicznej [4]. Z uwagi na znaczną skalę trudności technologicznych i duże koszty wytwarzania tych stopów i wyrobów tylko wysoko rozwinięte kraje podejmują masową, komercyjną produkcję do zastosowań w przemyśle i medycynie. W kraju, po wieloletnich badaniach w zakresie opracowania technologii wytwarzania tych stopów w skali laboratoryjnej, badaniach struktury i właściwości oraz badaniach klinicznych sprawdzenia możliwości ich zastosowania w chirurgii kostnej podjęto próby wytwarzania tych stopów w skali półprzemysłowej. Aktualnie w ramach programu INNOTECH realizowany jest projekt wdrożenia produkcji stopów i wyrobów medycznych NiTi z pamięcią kształtu. W przeróbce plastycznej na gorąco wlewków NiTi w skali laboratoryjnej oprócz stosowanych wcześniej sposobów kucia swobodnego, kucia rotacyjnego i walcowania zastosowano współbieżne wyciskanie na gorąco [5].

PHASE TRANSFORMATIONS AND TEXTURE IN A HOT EXTRUDED NiTi SHAPE MEMORY ALLOY INTENDED FOR MEDICAL APPLICATIONS

Z.Lekston*, M.Zubko, T.Goryczka, J.Lelątko, D.Stróż, K.Prusik

Institute of Materials Science, University of Silesia,
41-500 Chorzów, 75 Pułku Piechoty 1A]
zlekston@us.edu.pl

Abstract

The paper presents results of study of phase transitions and the texture of the samples cut from a rod obtained after hot direct extrusion of an NiTi ingot. The alloy was cast in the process of melting and casting in a vacuum induction furnace. Hot extrusion process was carried out using self-constructed instruments on a laboratory press with a maximum pressing force of 1000 kN. Test samples were cut transversely and along the axis of the head and foot of the rod. The study of phase transformations was performed using differential scanning calorimetry (DSC) and temperature X-ray diffraction (TXRD). It was found that in the hot-extruded samples and after heat processing, two stages of the reversible transformation took place according to the B2→R→B19' sequence. Weak axial texture <110> was also confirmed by the performed X-ray measurements. The resulting rod was intended for further hot extrusion in order to reduce the diameter and to obtain a semi-finished product for further manufacture of the prototype medical devices in the form of staples for the fixation of bone fractures.

[Engineering of Biomaterials, 128-129, (2014), 32-35]

Introduction

Shape memory NiTi alloys as smart materials are more and more often used in engineering and medicine [1,2]. Good mechanical properties, corrosion resistance and memory effects depend on their chemical composition, on the purity of the alloys, on the applied technological process, on smelting, casting and plastic processing, as well as on the heat treatment and thermo-mechanical processes [3,4]. Due to considerable technological difficulties and high production costs of these alloys, only highly developed countries deal with the mass commercial production intended for industrial and medical uses. In Poland, after many years of research into the production technology of manufacturing these alloys on a laboratory scale, testing of the structure and properties as well as clinical studies aimed at examination the possibilities of their application in bone surgery an attempt has been made to produce these alloys on a semi-industrial scale. Currently, the project to produce the NiTi shape memory alloys and medical devices is being implemented under the INNOTECH programme. Hot plastic processing of NiTi ingots on a laboratory scale uses direct hot extrusion [5] along with previously used methods such as open die forging, rotary forging and rolling.

Jest to skuteczny i szybki sposób przeróbki plastycznej na gorąco, w którym uzyskane półwyroby wykazują znacznie mniejszy stopień utlenienia powierzchni i w związku z tym mniejsze straty materiału. W pracy przedstawiono badania przemian fazowych oraz badania tekstury w próbkach pręta uzyskanego w procesie współbieżnego wyciskania pręta z wlewka NiTi o składzie namiarowym Ti-50,8% at. Ni. Materiał ten poddano dalszej przeróbce na druty o różnych średnicach do wytworzenia prototypowych wyrobów medycznych w postaci klamer z pamięcią kształtu do zespoleń złamań kości.

Celem podjętej pracy było zbadanie przebiegu przemian fazowych podczas chłodzenia i nagrzewania, wyznaczenie temperatur charakterystycznych oraz zbadanie tekstury w stopie NiTi po wyciskaniu współbieżnym na gorąco i po obróbce cieplnej.

Materiał i metody

W badaniach użyto stop NiTi o namiarowym składzie chemicznym Ti-50,8 at.% Ni uzyskany metodą wytapiania i odlewania w indukcyjnym piecu próżniowym Balzers VSG 10. Wytop o masie 900 g wykonano w Laboratorium Materiałów dla Przemysłu Lotniczego Politechniki Rzeszowskiej. Wlewek homogenizowano w oporowym, rurowym piecu próżniowym w temperaturze 900°C w czasie 48 godzin przy ciśnieniu $5x10^{-5}$ Pa. Fragment wlewka o średnicy 25 mm i wysokości 68 mm przeciśnięto współbieżnie na gorąco przy użyciu oprzyrządowania własnej konstrukcji na prasie laboratoryjnej MT 100 uzyskując pręt o średnicy 15 mm i długości 145 mm. Proces wyciskania realizowano po nagrzaniu wlewka do temperatury około 1000°C [5]. Temperatury charakterystyczne przemian fazowych po różnej obróbce cieplnej wyznaczono z krzywych DSC uzyskanych przy użyciu kalorymetru DSC 1 firmy METTLER TOLEDO podczas chłodzenia i nagrzewania próbek w zakresie temperatur -100 - 60°C z szybkością zmian temperatury 10°/min. Przemiany fazowe podczas chłodzenia i nagrzewania próbek w zakresie temperatur -180 do +100°C z szybkością 1°C/min. rejestrowano metodą rentgenografii temperaturowej przy użyciu dyfraktometru rentgenowskiego PANalytical Empyrean z kamerą temperaturową Anton Paar TTK450. Badania tekstury próbek po wyciskaniu i po obróbce cieplnej wykonano przy użyciu przystawki do badań tekstury na dyfraktometrze Philips PW1040.

Wyniki badań i dyskusja

Przebieg przemian fazowych w próbkach badanego stopu NiTi po wyciskaniu na gorąco i po wyżarzaniu w temperaturach 400 i 500°C w czasie 30 minut pokazano na krzywych uzyskanych z pomiarów przeprowadzonych przy użyciu różnicowego kalorymetru skaningowego (RYS.1).

Na krzywych zarejestrowanych podczas chłodzenia próbki po wyciskaniu na gorąco wyraźnie widać dwustopniowy przebieg przemian B2→R→B19'. Natomiast po wyżarzaniu w temperaturze 400 i 500°C obserwowano pojedyncze, poszerzone piki. Może to sugerować, że przemiany B2→R oraz R→B19' następują po sobie w wąskim zakresie temperatur. Podczas nagrzewania wszystkich badanych próbek na krzywych DSC obserwowano dwa efekty cieplne świadczące o dwustopniowym przebiegu przemian wg sekwencji B19'→R→B2.

Badania rentgenograficzne potwierdziły, że we wszystkich badanych próbkach przemiany fazowe podczas chłodzenia i nagrzewania zachodziły odwracalnie z udziałem pośredniej fazy R wg sekwencji B2↔R↔B19'.

It is an effective and fast way of hot plastic processing during which the obtained semi-products have a much lower degree of surface oxidation and therefore less material is wasted. This paper presents the study of phase transitions and the tests of the texture of the samples cut from the rod obtained as a result of direct extrusion of the NiTi ingot with a nominal chemical composition of Ti-50.8 at. % Ni. The material was further processed into the wires with different diameters in the production of prototype medical devices such as shape memory staples for the fixation of bone fractures.

The aim of the study was to investigate phase transition during cooling and heating, to determine the characteristic temperatures and to investigate the texture of the NiTi alloy after hot direct extrusion and after heat treatment.

Material and methods

The NiTi alloy with a chemical composition of Ti-50.8 at.% Ni obtained by melting and casting in a Balzers VSG 10 vacuum induction furnace was used. The melt of 900 g was obtained in the Laboratory for Aerospace Materials at the Rzeszów University of Technology. The ingot was homogenized in the vacuum resistance tube furnace at 900°C for 48 hours under the pressure of $5x10^{-5}$ Pa. A part of an ingot with the diameter of 25 mm and the height of 68 mm was subjected to direct hot extrusion with the use of self-designed tools on the MT 100 laboratory press. In result a 145 mm long rod with the studies aimed at examination the possibilities of their application in bone surgery an attempt has been made to produce these alloys on a semi-industrial scale. Currently, the project to produce the NiTi shape memory alloys and medical devices is being implemented under the INNOTECH programme. Hot plastic processing of NiTi ingots on a laboratory scale uses direct hot extrusion [5] along with previously used methods such as open die forging, rotary forging and rolling. It is an effective and fast way of hot plastic processing during which the obtained semi-products have a much lower degree of surface oxidation and therefore less material is wasted. This paper presents the study of phase transitions and the tests of the texture of the samples cut from the rod obtained as a result of direct extrusion of the NiTi ingot with a nominal chemical composition of Ti-50.8 at.% Ni. The material was further processed into the wires with different diameters in the production of prototype medical devices such as shape memory staples for the fixation of bone fractures.

The aim of the study was to investigate phase transition during cooling and heating, to determine the characteristic temperatures and to investigate the texture of the NiTi alloy after hot direct extrusion and after heat treatment.

Research results and discussion

The NiTi alloy with a chemical composition of Ti-50.8 at.The curves obtained from the measurements carried out using a differential scanning calorimeterpresent phase transitions in the samples of the tested NiTi alloy after hot extrusion and annealing at 400 and 500°C for 30 minutes (FIG.1).

On the curves recorded during cooling the sample after hot extrusion, a clear two-stage B2→R→B19' transitions can be observed. However, after annealing at 400 and 500°C broadened single peaks were observed. It may suggest that the B2→R and R→B19' transitions follow each other in a narrow temperature range. While all the tested samples were heated, two thermal effects were observed on the DSC curves, which proves a two-stage course of transitions according to the B19'→R→B2 sequence.

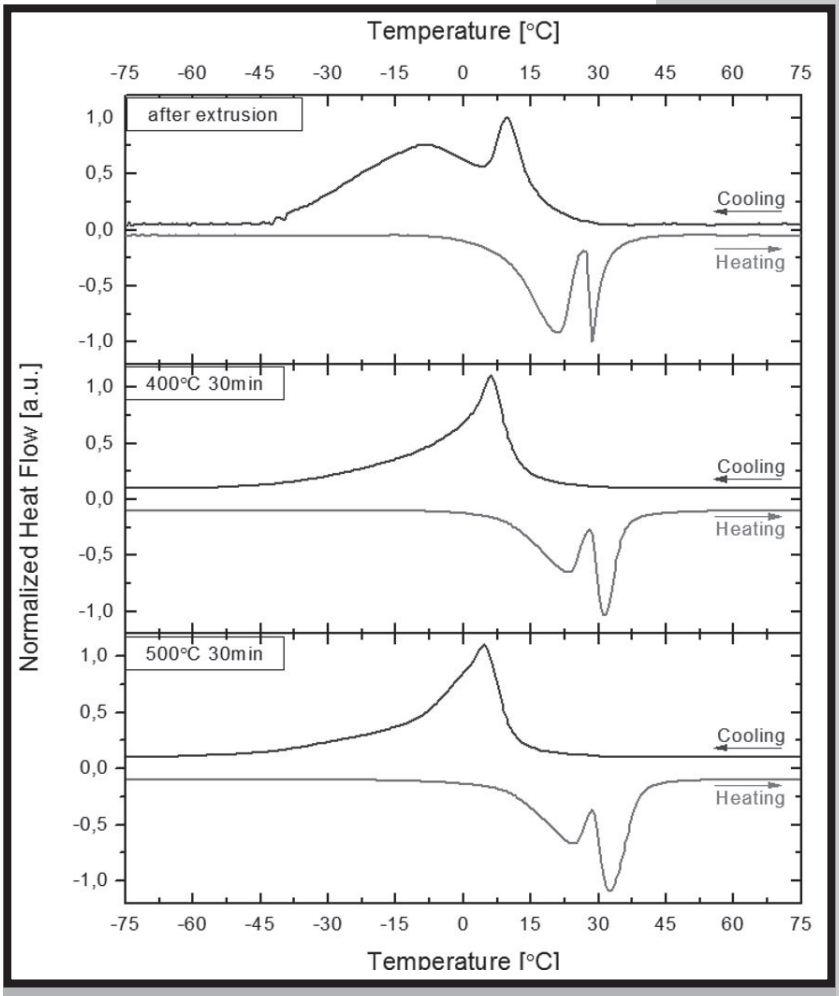

RYS. 1. Krzywe DSC próbek po wyciskaniu na gorąco i po obróbce cieplnej.
FIG. 1. DSC curves of the samples after hot extrusion and heat treatment.

Przykładowe dyfraktogramy zarejestrowane podczas chłodzenia próbek po wyciskaniu na gorąco oraz po wyżarzaniu w 400 i 500°C przez 30 minut pokazano na RYS. 2. Przemiana fazy macierzystej w fazę romboedryczną B2→R obserwowana jest jako rozszczepienie refleksu braggowskiego 110B2 na dwa refleksy 011R oraz 01R. Kolejna przemiana fazy R w fazę martenzytyczną R→B19' obserwowana jest jako pojawienie refleksów fazy B19' o wskaźnikach 110B19', 002B19', 11 B19', 020B19', 111B19'.

X-ray diffraction measurements confirmed that in all studied samples that were tested phase transitions during cooling and heating occurred reversibly with the presence of the intermediate rhombohedral R phase according to the B2↔R↔B19' sequence. Examples of diffraction patterns recorded with a diffractometer with an Anton Paar temperature camera during cooling of the samples after their hot extrusion and after annealing at 400 and 500°C for 30 minutes are shown in Figure 2. The transition of the parent phase into the B2→R rhombohedral phase is observed as the splitting of the 110B2 Bragg diffraction peak into two diffraction peaks: 011R and 01R. Another transition of the R phase into martensite phase (R→B19') is observed as the appearance of diffraction peaks the B19' phase with the following indices: 110B19', 002B19', 11 B19', 020B19', 111B19'.

X-ray studies of the texture of the samples cut transversely and along the axis of the extruded NiTi rod were also performed. The samples were cut from the head and foot of the ingot. The pole figures were measured for planes (001)B2 and (011)B2. FIG. 3 shows pole figures of the longitudinal cross-sections of the samples cut from the head and foot of the rod. Density distribution of the poles on pole figures (110)B2 shows their distribution around the theoretical position of the texture axis <110>. Densities of the poles form an extended ring around the theoretical position of the axial texture <110> also on the pole figure (100)B2. Both figures show low density values of the poles, and their distribution. It suggests that a relatively week texture has been formed. The direction distribution function was calculated form the pole figures. Based on it, the share of grains directed in accordance with the identified texture was calculated. The calculations assumed that the texture was composed of the grains deviated by ±15° form the theoretical position of the texture <110>.

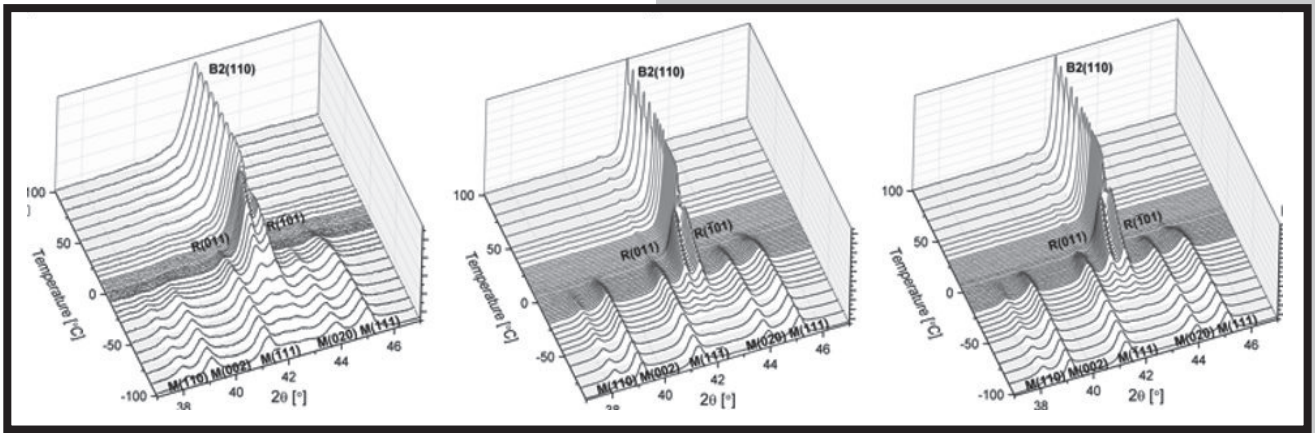

RYS. 2. Dyfraktogramy zarejestrowane podczas chłodzenia próbek: po wyciskaniu na gorąco (a) oraz po wyżarzaniu w temperaturze 400°C (b) i 500°C (c) przez 30 minut.
FIG. 2. Diffraction patterns recorded while cooling of the samples, after hot extrusion (a) and after annealing at 400°C (b) and 500°C (c) for 30 minutes.

Wykonano również rentgenograficzne badania tekstury próbek wyciętych poprzecznie i wzdłuż osi wyciskanego pręta NiTi. Próbki wycięto ze strefy głowy i stopy wlewka. Figury biegunowe zmierzono dla płaszczyzn (001)B2 oraz (011)B2. Na RYS.3 pokazano figury biegunowe dla przekrojów wzdłużnych próbek wyciętych ze strefy głowy i stopy pręta. Rozłożenie gęstości biegunów na figurach biegunowych (110)B2 wskazuje na ich rozkład wokół teoretycznego położenia tekstury osiowej <110>. Również na figurze biegunowej (100)B2 gęstości biegunów formują poszerzony pierścień wokół teoretycznego położenia tekstury osiowej <110>. Obie figury wykazują niskie wartości gęstości biegunów oraz ich rozproszenie. Świadczy to o powstaniu relatywnie słabej tekstury. Z figur biegunowych wyliczono funkcję rozkładu orientacji, na podstawie której wyliczono udział ziaren zorientowanych zgodnie ze zidentyfikowaną teksturą. W obliczeniach przyjęto, że teksturę tworzą ziarna odchylone o ±15° od teoretycznego położenia tekstury <110>. Ilość ziaren zorientowana zgodnie ze zidentyfikowaną teksturą nie przekracza 20%.

Podsumowanie

Na krzywych DSC zarejestrowanych podczas chłodzenia próbek wyżarzanych obserwowano pojedynczy rozmyty efekt cieplny co sugeruje, że przemiany fazowe od fazy macierzystej B2 do martenzytu B19' w tych próbkach zachodzą w bardzo wąskim zakresie temperatur. Przedstawione wyniki pomiarów rentgenowskich potwierdziły przebieg przemian w tych próbkach z udziałem fazy romboedrycznej R wg sekwencji B2→R→B19'. Na podstawie wykonanych badań stwierdzono, że we wszystkich badanych próbkach przemiany fazowe podczas chłodzenia i nagrzewania zachodziły odwracalnie z udziałem pośredniej fazy romboedrycznej R wg sekwencji B2↔R↔B19'. W próbce po wyciskaniu, bez obróbki cieplnej, przemiany podczas nagrzewania zachodzą w pożądanym zakresie temperatur poniżej 37oC, co umożliwi przygotowanie implantów z pamięcią kształtu działających pod wpływem ciepła ciała pacjenta. Zastosowanie wyciskania na gorąco, zamiast kucia swobodnego lub walcowania, skróci czas przeróbki zgrubnej wlewków i kęsów, obniży koszty i poprawi jakość półproduktów wytwarzanych w skali półprzemysłowej.

Na podstawie badań tekstury stwierdzono, że po zastosowanym wyciskaniu współbieżnym na gorąco nie nastąpiło wyraźne steksturowanie osiowe. Około 20% ziaren było zorientowanych zgodnie z teksturą osiową <110>, natomiast pozostałe ziarna były zorientowane przypadkowo. Prawdopodobnie przy dalszej redukcji średnic przy użyciu tej metody przeróbki plastycznej zwiększy się steksturowanie osiowe, co może wpłynąć na poprawę własności mechanicznych i efektywność zjawisk pamięci kształtu uzyskanych półwyrobów.

Podziękowania

W pracy wykorzystano wyniki badań finansowanych ze środków Narodowego Centrum Badań i Rozwoju w ramach projektu nr INNOTECH-K1/IN1/46/157239/NCBR/12.

Piśmiennictwo

[1] T.Yoneyama, S.Miyazaki Ed., Shape memory alloys for biomedical applications, Woodhead Publishing Limited, Cambridge, England (2009)
[2] L.G.Machado, M. A. Savi., Medical applications of shape memory alloys. Brazilian Journal of Medical and Biological Research 36 (2003) 683-691

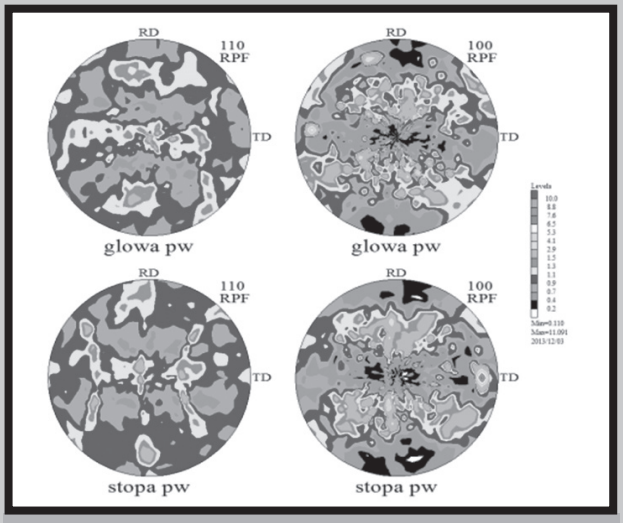

RYS.3. Figury biegunowe (001)B2 oraz (011)B2 dla przekrojów wzdłużnych próbek wyciętych z głowy i stopy wyciskanego na gorąco pręta NiTi.
FIG.3 Pole figures (001)B2 and (011)B2 for the longitudinal sections of the samples cut form the head and feet of the hot-extruded NiTi rod.

Summary

A single broadened peak was observed on the DSC curves recorded during the cooling of the annealed samples. It suggested that the phase in these samples occur in a very narrow range of temperatures. Presented results of the X-ray analysis confirmed the existence of phase transformations in these samples. Based on the performed measurements it was found that in all tested samples phase transitions during cooling and heating occurred with the presence of an intermediate rhombohedral R phase in accordance with the B2↔R↔B19' sequence. After extrusion, without any heat treatment, there are transitions in the sample which occur during heating in the desired temperature range below 37°C. This is promising from the point of view of applications for shape memory implants activated by the patient's body heat. The use of hot extrusion, instead of open die forging or rolling, will reduce the time of rough processing of ingots and billets and thus will reduce the costs and improve the quality of semi-products manufactured on a semi-industrial scale.

On the basis on the texture analysis, it was found that using hot direct extrusion did not result in clear axial texture. About 20% of the grains were oriented in accordance with the axial texture <110>, while the remaining grains were randomly oriented. It is possible that further reduction of the diameter while using this method of plastic processing will increase axial texture which can improve mechanical properties and efficiency of the shape memory effects of the obtained semi-products.

Acknowledgements

The study uses the results of the research funded by the National Centre for Research and Development under the project No. INNOTECH-K1/IN1/46/157239/NCBR/12.

References

[3] H.Morawiec, Z.Lekston., Implanty medyczne z pamięcią kształtu. Wyd. Pol. Śl. Gliwice (2010)
[4] A.R.Pelton, J.DiCello, and S.Miyazaki, Optimization of Processing and Properties of Medical Grade Nitinol Wire, Min. Invas. Ther. Allied Technol., 9 (1), (2000) 107–118
[5] Z.Lekston, M.Zubko, K.Prusik, D.Stróż Microstructure, Phase Transformations, and Properties of Hot- Extruded Ni-Rich NiTi Shape Memory Alloy. JMEP (2014) DOI: 10.1007/s11665-014

WSTĘPNE BADANIA NAD SYNTEZĄ I CHARAKTERYSTYKĄ WIELKOCZĄSTECZKOWYCH KONIUGATÓW KAMPTOTECYNY

Marcin Sobczak[1]*, Ewa Oledzka[1], Andrzej Plichta[2], Joanna Kolmas[1], Urszula Piotrowska[1]

[1] Warszawski Uniwersytety Medyczny,
Wydział Farmaceutyczny,
Katedra i Zakład Chemii Nieorganicznej i Analitycznej,
Banacha 1, 02-097 Warszawa, Polska
[2]Politechnika Warszawska, Wydział Chemiczny,
Katedra Chemii i Technologii Polimerów,
Noakowskiego 3, 00-664 Warszawa, Polska
* e-mail: marcin.sobczak@wum.edu.pl

Streszczenie

Otrzymano nowe wielkocząsteczkowe koniugaty kamptotecyny. Matryce polimerowe zostały otrzymane w wyniku polimeryzacji z otwarciem pierścienia ε-kaprolaktonu, glikolidu, rac-laktydu oraz węglanu trimetylenu. Zsyntezowane matryce i kamptotecynę połączono za pomocą 1,6-diizocyjanianu heksametylenu. Otrzymane koniugaty wielkocząsteczkowe scharakteryzowano za pomocą spektroskopii 1H i 13C NMR oraz FTIR. Toksyczność otrzymanych produktów polimerycznych oceniono na podstawie testów przeprowadzonych przy użyciu bakterii luminescencyjnych oraz pierwotniaków. Ponadto, przeprowadzono badania kinetyki uwalniania kamptotecyny w warunkach in vitro.

Słowa kluczowe: *kamptotecyna, koniugaty wielkocząsteczkowe, uwalnianie w warunkach in vitro, polimery biodegradowalne, polimery bioresorbowalne*

[Inżynieria Biomateriałów, 128-129, (2014), 36-39]

Wprowadzenie

20(S)-kamptotecyna ((S)-4-etylo-4-hydroksy-1H-pirano[3',4':6,7]indolizino[1,2-b]chinolino-3,14-(4H,12H)-dionu, CAMPT) jest pentacyklicznym alkaloidem, który został po raz pierwszy wyizolowany przez Wall`a i współpracowników w 1966 roku z chińskiego drzewa Camptotheca acuminate [1]. Szeroki zakres aktywności przeciwnowotworowej CAMPT zweryfikowano na modelach zwierzęcych w odniesieniu do raka płuc, prostaty, piersi, jelita grubego, żołądka, pęcherza moczowego, czerniaka oraz jajnika [1-2]. Jednakże, zastosowanie terapeutyczne CAMPT jest utrudnione ze względu na jej niską rozpuszczalność w wodzie, wysoką toksyczność i szybką dezaktywację pierścienia laktonowego w wyniku hydrolizy w fizjologicznym pH [1-2].

Polimery biodegradowalne i bioresorbowalne są szeroko cenione w opracowywaniu systemów kontrolowanego uwalniania substancji leczniczych. Takie systemy dostarczania substancji czynnych są bardzo efektywne i charakteryzują się zdolnością precyzyjnego transportu substancji leczniczej do określonych tkanek lub komórek [3-5]. Z tego punktu widzenia, wady CAMPT można ograniczyć poprzez jej przyłączenie do matrycy wielkocząsteczkowej. Polimerowe koniugaty CAMPT mogą polepszać jej biodystrybucję.

PRELIMINARY STUDY UNDER SYNTHESIS AND CHARACTERIZATION OF MACROMOLECULAR CONJUGATES OF CAMPTOTHECIN

Marcin Sobczak[1]*, Ewa Oledzka[1], Andrzej Plichta[2], Joanna Kolmas[1], Urszula Piotrowska[1]

[1] Medical University of Warsaw, Faculty of Pharmacy,
Department of Inorganic And Analytical Chemistry,
1.Banacha str., 02-097 Warsaw, Poland
[2] Warsaw University of Technology, Faculty of Chemistry,
Chair of Polymer Chemistry And Technology,
3 Noakowskiego str., 00-664 Warsaw, Poland
* e-mail: marcin.sobczak@wum.edu.pl

Abstract

New macromolecular conjugates of camptothecin were prepared. The polymeric matrixes were obtained by the ring-opening polymerization of ε-caprolactone, glycolide, rac-lactide or trimethylene carbonate. The synthesized polymers and camptothecin were coupled via 1,6-hexamethylene diisocyanate. The synthesized macromolecular conjugates of camptothecin were characterized by 1H and 13C NMR or FTIR spectroscopy. Toxicity of the obtained polymeric products were evaluated with bacterial luminescence test and two protozoan assays. Furthermore, the in vitro release of camptothecin from the obtained conjugates was investigated.

Keywords*: camptothecin, macromolecular conjugates, in vitro release, biodegradable polymers, bioresorbable polymers*

[Engineering of Biomaterials, 128-129, (2014), 36-39]

Introduction

20(S)-Camptothecin ((S)-4-ethyl-4-hydroxy-1H-pyrano[3',4':6,7]indolizino[1,2-b]quinoline-3,14-(4H,12H)-dione, CAMPT), a pentacyclic alkaloid was first isolated by Wall and co-workers in 1966 from the Chinese tree Camptotheca acuminate [1]. CAMPT has been verified as a broad range of anti-cancer activity in animal models including lung, prostate, breast, colon, stomach, bladder, ovarian and melanoma cancers [1-2]. However, its therapeutic application is hindered by a low solubility, high toxicity and rapid inactivation through lactone ring hydrolysis at a physiological pH [1-2].

The biodegradable or bioresorbable polymers are very desirable for the controlled drug delivery systems. Such delivery systems are not toxic and can transport the drug molecule to the specific tissue or cell more efficiently and more specifically [3-5]. From this point of view, the disadvantage of CAMPT might be overcome by its attaching to the macromolecular matrix. The polymeric conjugates of CAMPT could act as a transport form for this drug and enhance its biodistribution.

W ciągu ostatnich kilku lat, koniugaty CAMPT na bazie rozpuszczalnych w wodzie polimerów, takich jak glikol polioksyetylenowy [6-8], poli(kwas L-glutaminowy) [9-10], polimerów opartych na β-cyklodekstrynie [11], poli[N-(2-hydroksypropylo)metakrylamidzie] [12] poli[(N-karboksybutylo)-L-aspartamidzie] [13-14] i poli(amidoaminach) [15-16] zostały zsyntezowane i scharakteryzowane.

Głównym celem niniejszej pracy było otrzymanie poliestrowych i poli(estro-węglanowych) koniugatów kamptotecyny. Przeprowadzono wstępne badania nad wpływem struktury łańcucha polimeru na proces uwalniania CAMPT. Toksyczność otrzymanych produktów polimerycznych oceniono na podstawie testów przeprowadzonych przy użyciu bakterii luminescencyjnych oraz pierwotniaków.

Materiały i metody

Uwalnianie substancji leczniczej w warunkach in vitro

Otrzymane wielkocząsteczkowe koniugaty kamptotecyny (10 mg) zostały umieszczone w 10 mL PBS (0.01 M, pH 7.4) w 37°C. Stężenie uwalnianej substancji leczniczej oznaczano przy użyciu spektrofotometru UV-Vis. W określonych odstępach czasu, 10 mL mieszaniny usuwano z układu, zastępując ją świeżą porcją buforu (10 mL). Procent uwolnionej CAMPT obliczano na podstawie krzywej kalibracji otrzymanej uprzednio w tych samych warunkach w jakich prowadzono proces uwalniania. Pomiar absorbancji prowadzono przy długości fali 355 nm (postać laktonowa) lub 368 nm (postać karboksylowa). Wszystkie eksperymenty powtórzono trzykrotnie.

Koniugaty: CON-CAMPT-1 (został otrzymany z kopolimeru CL/GL), CON-CAMPT-2 (CL/rac-LA), CON-CAMPT-3 (CL/TMC), CON-CAMPT-4 (GL/rac-LA), CON-CAMPT-5 (GL/TMC), CON-CAMPT-6 (rac-LA/TMC).

Charakterystyka spektroskopowa

Otrzymane poliestry, poli(estro-węglany) oraz wielkocząsteczkowe koniugaty CAMPT scharakteryzowano za pomocą spektroskopii 1H i 13C NMR (Varian 300 MHz) oraz FTIR (Perkin-Elmer).

Widma NMR rejestrowano w CDCl3 i DMSO-d6. Próbki do analizy FTIR przygotowano w postaci tabletek z KBr.

Wyniki i dyskusja

Głównym celem niniejszej pracy była synteza nowych wielkocząsteczkowych koniugatów CAMPT. Jako matryce polimerowe użyto biodegradowlane i bioresorbowalne poliestry i poli(estro-węglany). Matryce wielkocząsteczkowe otrzymano w wyniku polimeryzacji z otwarciem pierścienia cyklicznych estrów (ε-kaprolaktonu (CL), glikolidu (GL), rac-laktydu (rac-LA)) oraz cyklicznego węglanu (węglan trimetylenu (TMC)). Proces prowadzono w obecności glikolu polioksyetylenowego (PEG 200) jako makroinicjatora oraz oktanianiu cyny (II) (SnOct2) jako katalizatora.

Dokonano oceny cytotoksyczności otrzymanych polimerów stosując w tym celu bakterie luminescencyjne V. Fischeri oraz pierwotniaki S. Ambiguum i T. Thermophila. Stwierdzono, że wszystkie otrzymane poliestry i poli(estro -węglany) są nietoksyczne, zarówno względem bakterii jak i pierwotniaków.

In the past few years, the covalent conjugates of CAMPT with water-soluble polymers, such as polyethylene glycol [6-8], poly(L-glutamic acid) [9-10], β-cyclodextrin based polymers [11], poly[N-(2-hydroxypropyl)methacrylamide] [12], poly[(N-carboxybutyl)-L-aspartamide] [13-14], poly(amido amine) [15-16] have been developed and characterized.

The aim of this study was to prepare polyesters or poly(ester-carbonate)s conjugates containing CAMPT. The preliminary studies of the influence of polymeric chain structure on the release process of CAMPT were described. The toxicity test of the obtained polymeric matrixes were evaluated with bacterial luminescence test and two protozoan assays.

Materials and methods

In vitro Evaluation of Drug Release

The obtained macromolecular conjugates of CAMPT (10 mg) were put into 10 mL of PBS (0.01 M, pH 7.4) at 37°C, and the initial UV measurement was carried out. The mixture was stirred and a 10 mL sample was removed at selected intervals followed by 10 mL of a fresh buffer replacing. The quantity of the released CAMPT was determined from the calibration curve previously obtained under the same conditions and analyzed by means of UV-Vis spectrophotometer. The percentage of the drug released was calculated based on a peak area of UV absorbance at 355 (lactone form) or 368 nm (carboxyl form). Each experiment was carried out in triplicate.

The conjugates: CON-CAMPT-1 (was obtained from CL/GL copolymer), CON-CAMPT-2 (CL/rac-LA), CON-CAMPT-3 (CL/TMC), CON-CAMPT-4 (GL/rac-LA), CON-CAMPT-5 (GL/TMC), CON-CAMPT-6 (rac-LA/TMC).

Characterizations

The polyesters, poly(ester-carbonate)s and polymeric conjugates of CAMPT were characterized by means of 1H and 13C NMR (Varian 300 MHz), and FTIR spectroscopy (Perkin-Elmer). The NMR spectra were recorded in CDCl3 and DMSO-d6. The IR spectra were measured from KBr pellets.

Results and Discussions

The main aim of this study was to obtain new macromolecular conjugates of CAMPT. As polymeric matrixes biodegradable and bioresorbable polyesters or poly(ester-carbonate)s were used. The macromolecular matrixes were obtained by the ring-opening polymerization (ROP) of cyclic esters (ε-caprolactone (CL), glycolide (GL) and rac-lactide (rac-LA)) and cyclic carbonate (trimethylene carbonate (TMC)). The ring-opening polymerization (ROP) process was carried out in the presence of poly(ethylene glycol) (PEG-200) as macro-co-initiators and tin (II) 2-ethylhexanoate (SnOct2) as a catalyst.

The cytotoxicity evaluation of the received polymers was studied using the luminescent bacteria V. Fischeri and two ciliated protozoans S. Ambiguum and T. Thermophila. It was found that the obtained polyesters or poly(ester-carbonate)s are not toxic to all test bionts, both bacteria and protozoa because of the sample is considered toxic when the percent of a toxic effect (PE) is higher than 20.

W następnym etapie pracy, otrzymano wielkocząsteczkowe koniugaty CAMPT. Matryce polimerowe i substancja lecznicza zostały połączone za pomocą 1,6-diizocyjanianu heksametylenu. Strukturę zsyntezowanych koniugatów wielkocząsteczkowych potwierdzono techniką NMR. Na widmach NMR widoczne były charakterystyczne sygnały pochodzące od CAMPT (bez grupy hydroksylowej, która przereagowała z grupą izocyjanianową), tym samym potwierdzając obecność wiązania kowalencyjnego pomiędzy cząsteczką substancji czynnej a makrocząsteczką.

Uwalnianie CAMPT z otrzymanych koniugatów polimerowych w warunkach in vitro przeprowadzono w buforze PBS w temperaturze 37°C w ciągu 1-12 tygodni. Procent uwolnionej substancji leczniczej w pH 7.4 przedstawiono na RYS. 1. Stwierdzono, że struktura zsyntezowanych kopolimerów, zawartość jednostek komonomeru w łańcuchu polimeru oraz Mn PEG stosowanego jako makroinicjator, mają istotny wpływ na szybkość uwalniania CAMPT z otrzymanych koniugatów wielkocząsteczkowych.

In the next step of this study, the macromolecular conjugates of CAMPT were obtained. The polymers and CAMPT were coupled via 1,6-diisocyanatohexane (HDI). The chemical structures of the prepared polymeric conjugates of CAMPT was confirmed by NMR studies. All the conjugate spectra have revealed the characteristic signals originated from CAMPT (without hydroxyl group which has reacted with isocyanate group) indicating successful preparation of the macromolecular conjugates of CAMPT.

In vitro CAMPT release from the macromolecular conjugates was carried out in PBS buffer at 37°C for 1-12 weeks. The kinetic rates of CAMPT released from polymer conjugates at pH 7.4 were shown in FIG. 1. It has been found that many factors are influencing the release of CAMPT from the obtained macromolecular conjugates, namely the copolymers structure, co-monomer unit content in the polymer chain and Mn of PEG used as macro-coinitiator.

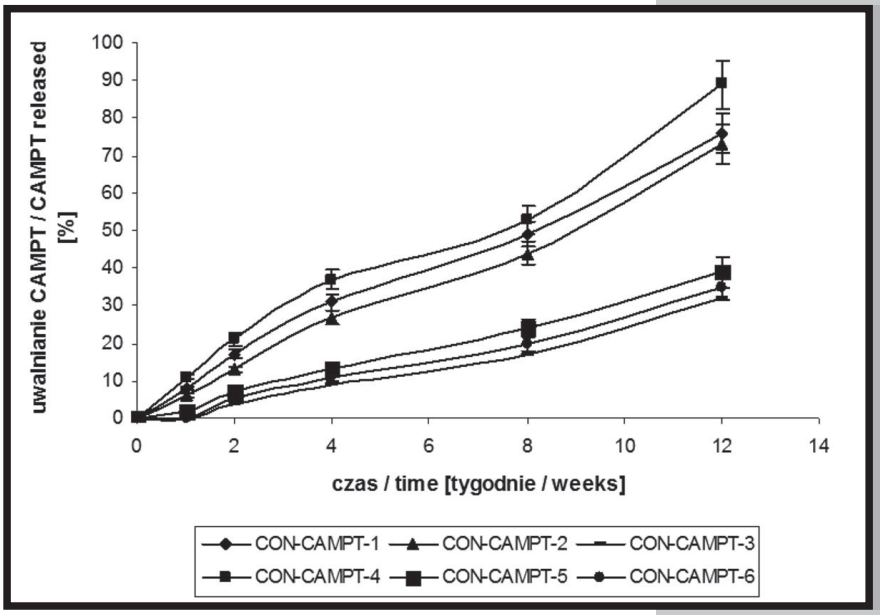

RYS. 1. Uwalnianie CAMPT z otrzymanych koniugatów wielkocząsteczkowych.
FIG. 1. Release of CAMPT from the obtained macromolecular conjugates.

Wnioski

W pracy przedstawiono wstępne wyniki badań nad syntezą nowych wielkocząsteczkowych koniugatów CAMPT. Substancja lecznicza została kowalencyjnie związana z łańcuchem kopolimerów (CL, GL, rac-LA, TMC i PEG) poprzez wiązanie uretanowe. Otrzymane poliestry lub poli(estro-węglany) okazały się być nietoksyczne. Na podstawie przeprowadzonych badań wykazano, że szybkość uwalniania CAMPT jest bezpośrednio zależna od struktury otrzymanych kopolimerów. Szybkość uwalniania CAMPT była większa dla koniugatów otrzymanych z kopolimerów CL, rac-LA i GL, w porównaniu do kopolimerów zawierających segmenty TMC. Uzyskane wyniki wskazują, że zsyntezowane matryce poliestrowe i poli(estro-węglanowe) są obiecujące w technologii systemów kontrolowanego uwalniania CAMPT.

Podziękowania

Praca została sfinansowana przez Ministerstwo Nauki i Szkolnictwa Wyższego w ramach projektu badawczego (MNiSzW OPUS-5 2013/09/B/ST5/03480: „Opracowanie implantacyjnych systemów dozowania leku o działaniu antynowotworowym immobilizowanego na matrycy polimerowej").

Conclusions

The synthesis of novel macromolecular conjugates of CAMPT is reported in this study. The drug was covalently attached to the copolymers of CL, GL, rac-LA, TMC or PEG chain ends of via urethane linkage. The obtained polyesters or poly(ester-carbonate)s matrixes are not toxic. The rates of CAMPT release were shown to be directly dependent on the nature of the received copolymers. The kinetic rates of CAMPT released was seen to be faster for the polymeric conjugates contained CL, rac-LA or GL units as compared to those with TMC units. The obtained results demonstrate that the polyesters or poly(ester-carbonate)s are interesting and promising materials for the controlled release of CAMPT.

Acknowledgements

This work was supported by the research programme (Project MNiSzW OPUS-5 2013/09/B/ST5/03480: "Elaboration of anti-cancer drug implantational delivery system immobilized on polymer matrix") of the Ministry of Science and Higher Education in Poland.

Piśmiennictwo

[1] Li Q.-Y., Zu Y.-G., Shi R.-Z., Yao L.-P.: Review Camptothecin: Current Perspectives. Curr. Med. Chem. 13(17) (2006) 2021-2039.
[2] Liew S.T., Yang L.-X.: Design, synthesis and development of novel camptothecin drugs. Curr. Pharm. Design. 14(11) (2008) 1078-1097.
[3] Hoste K., De Winne K., Schacht E.: Polymeric prodrugs. Int. J. Pharm. 277 (2004) 119-131.
[4] Uhrich K.E., Cannizzaro S.M., Langer R.S., Shakesheff K.M.: Polymeric systems for controlled drug release. Chem. Rev. 99 (1999) 3181-3198.
[5] Ouchi T., Ohya Y.: Macromolecular prodrugs. Prog. Polym. Sci. 20 (1995) 211-257.
[6] Fleming A.B., Haverstick K., Saltzman W.M.: In vitro cytotoxicity and in vivo distribution after direct delivery of PEG-camptothecin conjugates to the rat brain. Bioconjugate Chem. 15(6) (2004) 1364-1375.
[7] Warnecke A., Kratz F.: Maleimide-oligo(ethylene glycol) derivatives of camptothecin as albumin-binding prodrugs: Synthesis and antitumor efficacy. Bioconjugate Chem. 14 (2003) 377-387.
[8] Greenwald R.B., Zhao H., Xia J.: Tripartate poly(ethylene glycol) prodrugs of the open lactone form of camptothecin. Bioorg. Med. Chem. Lett. 11(12) (2003) 2635-2639.
[10] Singer J.W., Bhatt R., Tulinsky J., Buhler K.R., Heasley E., Klein P., De Vries P.:Water-soluble poly-(L-glutamic acid)-Gly-camptothecin conjugates enhance camptothecin stability and efficacy in vivo. J. Control. Release 74 (2001) 243-247.
[9] De Vries P., Tulinsky J., Bellamy G., Baker B., Singer J.W., Klein P.: Synthesis and in vivo antitumor activity of poly(L-glutamic acid) conjugates of 20(S)-camptothecin. J. Med. Chem. 46(1) (2003) 190-193.

References

[11] Cheng J.J., Khin K.T., Jensen G.S., Liu A., Davis M.E.: Synthesis of linear, β-cyclodextrin-based polymers and their camptothecin conjugates. Bioconjugate Chem. 14(5) (2003) 1007-1017.
[12] Caiolfa V.R., Zamai M., Fiorino A., Frigerio E., Pellizzoni C., D'Argy R., Ghiglieri A., Castelli M.G., Farao M., Pesenti E., Gigli M., Angelucci F., Suarato, A.: Polymer-bound camptothecin: Initial biodistribution and antitumour activity studies. J. Control. Release 65(1-2) (2000) 105-119.
[13] Fan N., Duan K., Wang C., Liu S., Luo S., Yu J., Huang J., Li Y., Wang, D.: Fabrication of nanomicelle with enhanced solubility and stability of camptothecin based on α,β-poly[(N-carboxybutyl)-l-aspartamide]-camptothecin conjugate. Colloids and Surf. B Biointerfaces 75 (2010) 543-549.
[14] Zhang W., Huang J., Fan N., Yu J., Liu Y., Liu S., Wang D., Li, Y.: Nanomicelle with long-term circulation and enhanced stability of camptothecin based on mPEGylated α,β-poly (l-aspartic acid)-camptothecin conjugate. Colloids and Surf. B Biointerfaces 81(1) (2010) 297-303.
[15] Chun C., Kuh H.-J., Song S.-C.: Injectable poly(organophosphazene)-camptothecin conjugate hydrogels: Synthesis, characterization, and antitumor activities. Eur. J. Pharm. Biopharm. 81(3) (2012) 582-590.
[16] Fan H., Huang J., Li Y., Yu J., Chen, J.: Fabrication of reduction-degradable micelle based on disulfide-linked graft copolymer-camptothecin conjugate for enhancing solubility and stability of camptothecin. Polymer 51(22) (2010) 5107-5114.

CHARAKTERYSTYKA STRUKTURALNA SPIEKANEGO POROWATEGO TYTANU

Magdalena Klimas[1]*, Agata Dudek[2]

Politechnika Częstochowska,
Wydział Inżynierii Produkcji i Technologii Materiałów,
Instytut Inżynierii Materiałowej,
al.Armii Krajowej 19, 42-200 Częstochowa
*e-mail: magdaklimas@wip.pcz.pl

Streszczenie

Celem niniejszej pracy było otrzymanie porowatych próbek tytanowych metodą metalurgii proszków. Podczas spiekania zastosowano dwie temperatury spiekania (1000 i 1100°C) i następujące atmosfery ochronne: argon, próżnia. Otrzymane materiały poddano badaniom mikrostrukturalnym. Celem określenia gęstości, porowatości oraz nasiąkliwości otrzymanych materiałów dokonano ważenia hydrostatycznego w wodzie zdejonizowanej zgodnie z normą PN EN ISO 2738: 2001. Określono również topografię powierzchni wytworzonych materiałów.

Słowa kluczowe: *porowaty tytan, spiekanie, metalurgia proszków*

[Inżynieria Biomateriałów, 128-129, (2014), 40-42]

Wstęp

Spośród biomateriałów metalicznych, ze względu na bardzo dobre parametry mechaniczne, stosunkowo niską gęstość, bardzo dobrą odporność korozyjną oraz najlepszą wśród biomateriałów metalicznych biozgodność, najczęściej stosowany jest tytan oraz jego stopy [1,2]. Celem poprawy procesów osteointegracji stosuje się porowate warstwy wierzchnie lub materiały spiekane. Zastosowanie materiałów porowatych zapewnia również dopasowanie własności mechanicznych do wartości zbliżonych do kości, co pozwala uniknąć zjawiska niekorzystnego umocnienia kości znanego jako stress shielding [3,4].

Jedną z metod otrzymywania porowatych materiałów tytanowych jest metoda metalurgii proszków, która pozwala na uzyskanie jednorodnej drobnoziarnistej struktury o polepszonych właściwościach funkcjonalnych w porównaniu z materiałem otrzymanym za pomocą innych metod [5].

Materiały i metody

Materiałem do badań były próbki wykonane metodą metalurgii proszków. Celem otrzymania materiałów metalicznych użyto proszku tytanu o nieregularnym kształcie zakupionym komercyjnie (HDH Ti 99,10%, rozmiar cząstek 0-45 μm). Proszek był prasowany pod ciśnieniem 270 MPa a następnie otrzymane wypraski suszono w suszarce laboratoryjnej. Dwie serie wyprasek były spiekane w atmosferze ochronnej argonu w temperaturach 1000°C i 1100°C odpowiednio przez czas jednej godziny, seria trzecia wyprasek była spiekana w próżni w temperaturze 1000°C przez czas 1 godziny (TABELA 1).

Wyniki i dyskusja

Materiały otrzymane metodą metalurgii proszków poddano badaniom mikrostrukturalnym używając do tego celu mikroskopu skaningowego JEOL JSM-6610LV. Otrzymane mikrostruktury przedstawiono na RYS. 1.

MICROSTRUCTURAL CHARACTERISATION OF SINTERED POROUS TITANIUM

Magdalena Klimas[1]*, Agata Dudek[2]

Czestochowa University of Technology
Faculty of Production Engineering
and Materials Technology
19 Armii Krajowej Ave., 42-200 Czestochowa, Poland
*e-mail: magdaklimas@wip.pcz.pl

Abstract

The aim of this work was to obtain porous titanium specimens using a powder metallurgy process. During sintering, two sintering temperatures (1000 and 1100°C) and two shielding gases (argon, vacuum) were used. The materials obtained were subjected to microstructural analysis. Furthermore, hydrostatic weighing in deionized water according to the PN EN ISO 2738: 2001 standard was used to evaluate density, porosity and water absorption capacity. Topology of the surface of the materials was also determined.

Keywords: *porous titanium, sintering, powder metallurgy*

[Engineering of Biomaterials, 128-129, (2014), 40-42]

Introduction

Due to good mechanical parameters, relatively low density, very good corrosion resistance and best biocompatibility among metallic biomaterials, titanium and its alloys are the most popular materials among metallic biomaterials [1,2]. In order to improve osseointegration processes, porous surface layers and sintered materials are used in practice. The use of bulk porous materials also enables to adjust the mechanical properties to the values closer to the bone to prevent “stress shielding” [3,4].

One of the methods to obtain porous titanium materials is powder metallurgy, which ensures a homogeneous fine-grain structure with improved functional properties compared to the materials obtained using other methods [5].

Materials and methods

The materials used in the study were specimens obtained by means of powder metallurgy. In order to obtain metallic material, the authors used Ti powder with an irregular shape of particles purchased commercially (HDH Ti 99.10%, particle size 0-45 μm). The powder was axially compressed at the load of 270 MPa and dried in a laboratory drier. Two sets of moulded pieces were sintered in argon atmosphere at the temperature 1000°C and 1100°C for 1 hour, whereas the third set of moulded piece was sintered in vacuum, also at temperature of 1000°C for 1 hour (TABLE 1).

Results and discussion

The materials obtained by means of powder metallurgy were used for microstructural examinations using JEOL JSM-6610LV scanning microscope. The microstructures obtained are presented in FIG.1.

TABELA 1. Próbki użyte do badań.
TABLE 1. The specimens used in the study.

Numer serii próbek Specimen series number	Rodzaj próbki Specimen Type	
	Temperatura spiekania Sintering temperature	Atmosfera ochronna Shielding gas medium
1	1000ºC	argon
2	1100ºC	argon
3	1000ºC	Próżnia/vacuum

Microstuructural analysis revealed presence of substantial number of pores in the materials obtained. The greatest porosity was found for titanium sintered at the temperature of 1000°C with argon used as a shielding gas. Increasing the sintering temperature to 1100°C resulted in decreasing porosity of the material obtained, which has also been documented in other studies [6]. Sintering in vacuum yielded materials with the lowest porosity.

The density, porosity and water absorption capacity in the obtained materials were measured using hydrostatic weighing in deionized water according to standard PN EN ISO 2738:2001P. The specimens were afterwards washed and dried. The measurements were carried out with an accuracy of 0.01g for 3 specimens of each specimen.

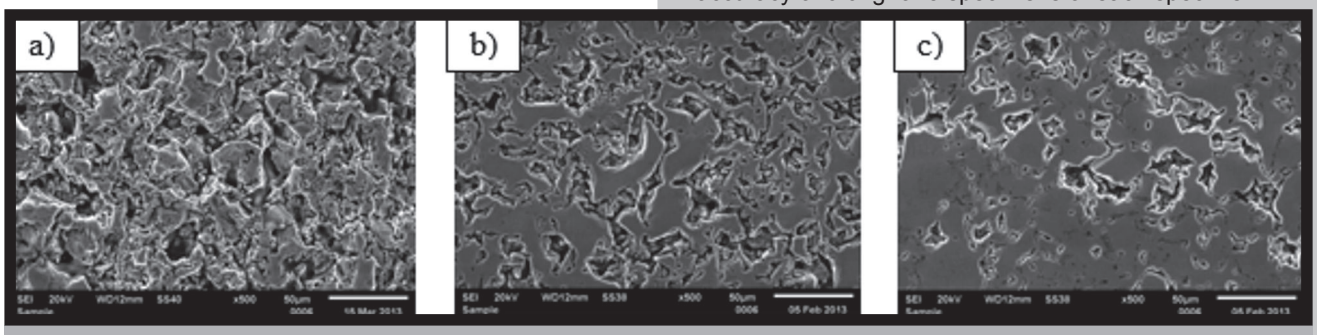

RYS. 1. Mikrostruktury z serii próbek: a) numer 1, b) numer 2, c) numer 3 otrzymanych metodą metalurgii proszków.
FIG. 1. Microstructure from specimen series: a) number 1, b) number 2, c) number 3 obtained by metallurgy powder method.

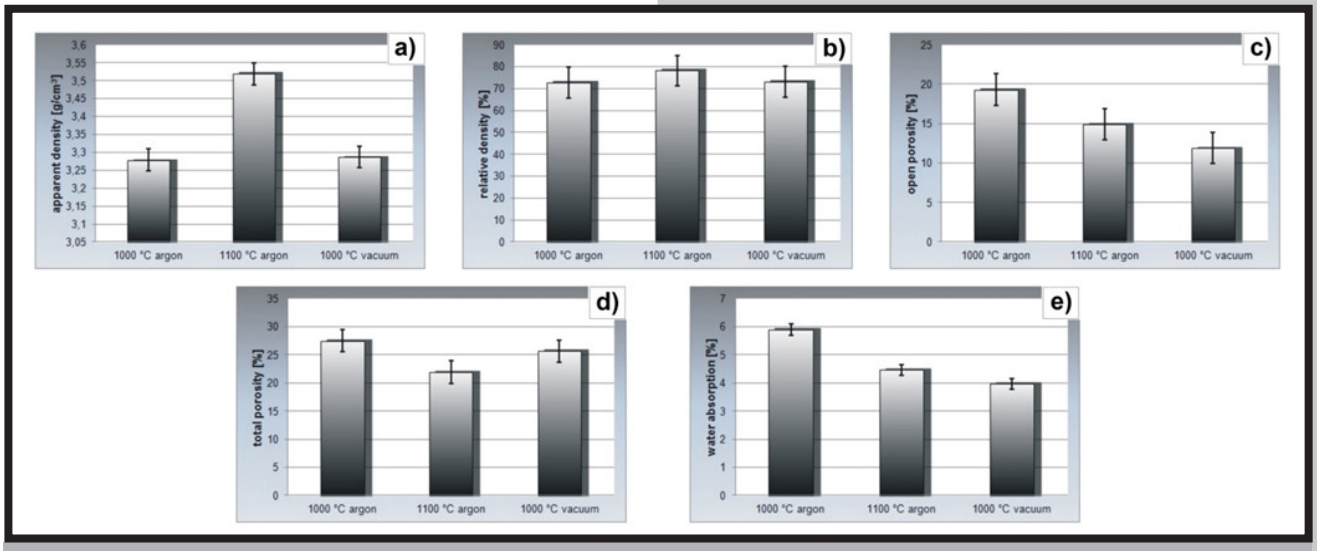

RYS. 2. Wykresy: a) gęstości pozornej, b) gęstości względnej, c) porowatości otwartej, d) porowatości całkowitej, e) nasiąkliwości spieków metalicznych.
FIG. 2. Graph of: a) apparent density, b) relative density, c) open porosity, d) total porosity, e) water absorption of metallic sinters.

Analiza mikrostrukturalna ujawniła obecność znacznej ilości porów w wytworzonych materiałach. Największą porowatością charakteryzował się tytan spiekany w temperaturze 1000°C w atmosferze ochronnej argonu. Podwyższenie temperatury spiekania do 1100°C skutkowało zmniejszeniem porowatości wytworzonego materiału, co potwierdzają m.in. badania [6]. Spiekanie w próżni skutkowało otrzymaniem materiału o najmniejszej porowatości.

Gęstość, porowatość i nasiąkliwość otrzymanych materiałów zmierzono za pomocą metody ważenia hydrostatycznego w wodzie zdejonizowanej zgodnie z normą PN EN ISO 2738:2001P. Próbki wcześniej oczyszczono i wysuszono. Pomiary dokonano z dokładnością do 0.01g dla 5 próbek z każdego rodzaju.

The density, porosity and water absorption capacity of the obtained materials are presented in FIGs.2a-e, respectively.

The highest apparent and relative density among the materials obtained was found for the specimen sintered with argon used as a shielding gas at the temperature of 1100°C. Using the shielding atmosphere of argon and increased sintering temperature leads to obtaining materials with lower apparent density. The conclusions drawn during microstructural examinations concerning porosity of the materials obtained are supported by the examinations using hydrostatic weighing. Among other factors, material water absorption capacity depends first and foremost on open porosity.

TABELA 2. Parametry chropowatości badanych próbek.
TABLE 2. Roughness parameters measured on specimen surface.

Numer serii próbek Specimen series number	R_t, µm	R_{max}, µm	R_z, µm	R_a, µm	R_p, µm	R_{Sm}, mm
1	56,02	52,74	35,55	6,43	37,92	0,0976
2	40,61	40,61	23,88	4,14	14,16	0,0667
3	33,20	29,73	18,13	2,96	11,32	0,0618

Gęstość, porowatość i nasiąkliwość próbek zaprezentowano na RYS. 2a-e, odpowiednio.

Największą gęstość pozorną i względną wśród wytworzonych materiałów posiadała próbka spiekana

w argonie w temperaturze 1100ºC. Zastosowanie atmosfery ochronnej argonu, jak również podniesienie temperatury spiekania powoduje otrzymanie materiału o coraz mniejszej gęstości pozornej. Wnioski wyciągnięte podczas badań mikrostrukturalnych, dotyczące porowatości wytworzonych materiałów, potwierdziły się podczas badań przy użyciu ważenia hydrostatycznego. Nasiąkliwość materiałów zależy, oprócz innych czynników, przede wszystkim od porowatości otwartej.

Celem określenia parametrów chropowatości powierzchni autorzy zastosowali profilometr Hommel T1000. Pomiary wykonano z dokładnością do 0,01 µm. Wyznaczenie parametrów chropowatości powierzchni wykonano w kontakcie z badaną powierzchnią poprzez sprzężenie igły różnicowym układem pomiarowym.

Otrzymane wyniki będące średnią arytmetyczną trzech pomiarów dla każdej próbki prezentuje TABELA 2.

Najwyższą wartość średniego arytmetycznego odchylenia rzędnych profilu od linii średniej, określane jako parametr Ra zaobserwowano dla serii próbek, które były spiekane w atmosferze ochronnej argonu w temperaturze 1000°C przez czas 1 godziny. Podwyższenie temperatury spiekania do 11000C wpłynęło na spadek parametrów chropowatości. Rodzaj zastosowanej atmosfery podczas spiekania (argon, próżnia) przy stałej temperaturze (1100ºC) przyczynia się do spadku parametrów chropowatości w porównaniu do próbki spiekanej w atmosferze argonu. Fakt ten jest bardzo ważny, ponieważ zmiana chropowatości powierzchni biomateriału wpływa na absorpcję białek, co ma znaczenie przy przerastaniu tkanki kostnej na wszczepionej protezie [7,8].

Wnioski

Stopień porowatości otrzymanych metodą metalurgii proszków materiałów zależy od temperatury jak również atmosfery ochronnej stosowanej podczas spiekania. Przeprowadzone badania pozwalają stwierdzić, że zarówno temperatura jaki i atmosfera spiekania mają wpływ na stopień porowatości wytworzonego materiału,
Stopień porowatości otwartej wytworzonych materiałów bezpośrednio przekłada się na parametry chropowatości tych materiałów.

To determine the parameters of the surface profile, the authors used a Hommel T1000 roughness tester. The measurements were performed with an accuracy of 0.01 µm using an electromagnetic profilometer with a differential system equipped with a stylus moving on the measured surface.

The results of the roughness parameter represented by arithmetic means from three measurements for each specimen are presented in TABLE 2.

The highest value of mean arithmetic vertical deviations of the roughness profile from the mean line, denoted as Ra parameter, was observed for the specimens which were sintered in the shielding atmosphere of argon at the temperature of 1000°C for 1 hour. Increasing sintering temperature to 1100°C caused a decline in roughness parameters. The type of shielding atmosphere used during sintering (argon, vacuum) at the constant temperature (1100°C) contributes to the decline in roughness parameters compared to the specimen sintered in the argon atmosphere. This fact is very important since the change in roughness of biomaterial causes protein absorption, which is essential for osseointegration of bone tissue in the prosthesis implanted [7,8].

Conclusions

Porosity degree of the materials obtained using powder metallurgy depends on the temperate as well as shielding gas used during sintering. The present study demonstrated that both temperature and type of sintering gas affect porosity degree of the material obtained. Open porosity degree of the materials directly affects the roughness parameter for these materials.

Piśmiennictwo References

[1] Rack H.J., Quazi J.I., Titanium alloys for biomedical applications, Materials Science and Engineering C 2006, 26, 1269-1277.
[2] Niinomii M., Mechanical properties of biomedical titanium alloys, Materials Science and Engineering A 1998, 243, 231-236.
[3] Szaraniec B., Ziąbka M., Chłopek J., Papargyri S., Tsipas D.: Obtaining of porous titanium for medical implants. Engineering of Biomaterials 11 81-84 (2008) 49-52
[4] Sobieszczyk S.: Rozwój bioaktywnych implantów porowatych na osnowie stopów tytanu, Wydawnictwo Politechniki Gdańskiej, Gdańsk 2013.
[5] Król M., Dobrzański L.A., Reimann Ł., Czaja I., Surface quality in selective laser melting of metal powders, Archives of Materials Science and Engineering 2013, 60/2, 87-92
[6] Esen Z., Tarhan Bor E., Bor S.: Characterization of loose powder sintered porous titanium and
Ti6Al4V alloy, Turkish J. Eng. Env. Sci.33 (2009) , 207 – 219.
[7] Tang F., Fudouzi H., Uchikoshi T., Sakka Y., Preparation of porous materials with controlled pore size and porosity, Journal of the European Ceramic Society 2004, 24, 341.
[8] De Aza P.N., Luklinska Z.B., Guitian F., De Aza F., Mechanism of bonelike formation on a bioactive implant in vivo, Biomaterials 2003, 24, 1437

BADANIA NAD NOWYMI BIODEGRADOWALNYMI KOMPOZYTOWYMI SYSTEMAMI DOSTARCZANIA BISFOSFONIANÓW

Marcin Sobczak[1]*, Joanna Kolmas[1], Ewa Olędzka[1], Cezary Dębek[2]

[1] Warszawski Uniwersytety Medyczny,
Wydział Farmaceutyczny,
Katedra i Zakład Chemii Nieorganicznej i Analitycznej,
Banacha 1, 02-097 Warszawa, Polska
[2] Instytut Inżynierii Materiałowej Polimerów i Barwników,
ul. Marii Skłodowskiej-Curie 55, 87-100 Toruń, Polska
*e-mail: marcin.sobczak@wum.edu.pl

Streszczenie

Nowe kompozytowe systemy dostarczania bisfosfonianów otrzymano z poliuretanów biodegradowalnych (PU) i nanokrystalicznego hydroksyapatytu (HAP). W pierwszym etapie, zsyntezowano PU z poli(ε-kaprolaktono) dioli (PCL), glikolu polioksyetylenowego, 1,6-diizocyjanianiu heksametylenu i butano-1,4-diolu. PCL zostały otrzymane w procesie polimeryzacji z otwarciem pierścienia katalizowanym enzymami. Następnie, otrzymano kompozytowe systemy dostarczania klodronianu. Przeprowadzono badania fizykochemiczne przygotowanych biomateriałów. Wykonano również badania cytotoksyczności zsyntezowanych polimerów. Wstępne wyniki badań wskazują, że otrzymane kompozyty stanowią perspektywiczną grupę biomateriałów, które mogą potencjalnie zostać wykorzystane w technologii implantacyjnych systemów dostarczania leków.

***Słowa kluczowe**: biomateriały, bisfosfoniany, klodronian, poliuretany, hydroksyapatyt*

[Inżynieria Biomateriałów, 128-129, (2014), 43-45]

Wprowadzenie

W ostatnich latach, wielkocząsteczkowe systemy dostarczania leków (DDS) budzą ogromne zainteresowanie [1-3]. Polimerowe DDS cechują się unikalną farmakokinetyką, dystrybucją i farmakologiczną efektywnością. Do chwili obecnej otrzymano kilka bisfosfonianowych (BP) systemów dostarczania leków (BPDDS) [4-12]. Obejmują one dendrymery, hydrożele, liposomy, nanokapsułki, nanosfery i koniugaty wielkocząsteczkowe. Szczególne zainteresowanie wzbudzają biomateriały BPDDS stosowane jako implanty ortopedyczne [4,5].

Alifatyczne i cykloalifatyczne poliuretany (PU) charakteryzują się wysoką zdolnością do biodegradacji i biokompatybilnością w stosunku do tkanek ludzkich. Atrybuty te czynią ich korzystnymi i nadzwyczajnie użytecznymi w technologii systemów DDS [3,13].

Głównym celem niniejszej pracy było otrzymanie kompozytowych systemów dostarczania klodronianu na bazie biodegradowalnych PU i nanokrystalicznego HAP. Omówiono wyniki badań strukturalnych i chemicznych nowych biomateriałów.

DEVELOPMENT OF NEW BIODEGRADABLE COMPOSITE DELIVERY SYSTEMS OF BISPHOSPHONATES

Marcin Sobczak[1]*, Joanna Kolmas[1], Ewa Olędzka[1], Cezary Dębek[2]

[1] Medical University of Warsaw,
Faculty of Pharmacy, Department of Inorganic
and Analytical Chemistry,
1 Banacha Street, 02-097 Warsaw, Poland
[2] Institute for Engineering of Polymer Materials and Dyes,
55 Marii Skłodowskiej-Curie 55, Street
87-100 Toruń, Poland
*e-mail: marcin.sobczak@wum.edu.pl 4

Abstract

New composite bisphosphonate delivery systems were prepared from biodegradable polyurethanes (PU) and nanocrystalline hydroxyapatite (HAP). In the first step, the PU were synthesized from poly(ε-caprolactone) diols (PCL), poly(ethylene adipate) diol, 1,6-hexamethylene diisocyanate and 1,4-butanediol. The PCL were obtained by the ring-opening polymerization catalyzed by the enzyme. Next, composite drug delivery systems for clodronate were prepared. The physico-chemical properties of the obtained biomaterials were determined. The cytotoxicity of the synthesized polymers was tested. The preliminary results show that the prepared composites are perspective biomaterials and they can be potentially applied in the technology of implantation drug delivery systems.

***Keywords:** biomaterials, bisphosphonates, clodronate, polyurethanes; hydroxyapatite*

[Engineering of Biomaterials, 128-129, (2014), 43-45]

Introduction

In recent years, macromolecular drug delivery systems (DDS) have became the focus of interest [1-3]. Polymeric DDS exhibit unique pharmacokinetics, distribution and pharmacological efficacy. Numerous bisphosphonates (BP) delivery systems (BPDDS) have been investigated [4-12]. They include dendrimeric polymers, hydrogels, liposomes, nanocapsules, nanospheres and macromolecular conjugates. One particularly interesting kind of BPDDS comprises biomaterials used as orthopaedic implants [4,5].

Aliphatic or cycloaliphatic polyurethanes (PU) demonstrate good biodegradability and biocompatibility in human tissues. These attributes make them advantageous and extremely useful for the technology of controlled DDS [3,13].

The main aim of this study has been to prepare composite clodronate (CLO) DDS using biodegradable PU hydroxyapatite (HAP) as components. The structures and chemical compositions of the new biomaterials were investigated and discussed based on the results obtained.

Materiały i metody

Wcześniej otrzymane PU rozpuszczano w DMSO uzyskując stężenie polimeru na poziomie 10-20% (w/v). Następnie, roztwory PU mieszano z HAP. Strukturę porowatą materiału uzyskiwano poprzez mieszanie PU i HAP z NaCl (w stosunku masowym 0.5 g NaCl do 1,5 g PU). Mieszaninę PU/HAP/sól umieszczano w formie. Następnie, formy utrzymywano w warunkach próżniowych w temp. 50°C przez 48 h. Przygotowane próbki przemywano wodą destylowaną przez 24h w celu całkowitego usunięcia NaCl. Otrzymane kompozyty suszono pod zmniejszonym ciśnieniem w temp. pokojowej przez około tydzień.

CLO (w odpowiednim stężeniu) wprowadzano do otrzymanego kompozytu metodą zanurzeniową. W celu umieszczenia substancji leczniczej w porach materiału wykonano pięciokrotny cykl próżnia/argon. Następnie, kompozyty suszono pod zmniejszonym ciśnieniem w temp. pokojowej aż do uzyskania stałej masy. Ilość związanego CLO oszacowano na podstawie różnicy masy kompozytów przed i po operacji inkorporowania.

Proces uwalniania CLO z otrzymanych kompozytów BPDDS prowadzony był w temp. 37°C w buforze fosforanowym (PBS) (pH 7.4) przygotowanym w stosunku 15 mg kompozytu do 1 ml buforu. Uwalniany z biomateriału CLO oznaczano metodą HPLC CAD.

Wyniki i dyskusja

Celem pierwszej części badań było otrzymanie poli(ε-kaprolaktono) dioli (PCL), które następnie wykorzystano jako prekursory w syntezie poliuretanów (PU). Polimeryzację z otwarciem pierścienia ε-kaprolaktonu (CL) w obecności glikolu dietylenowego (DEG) i lipazy Candida antarctica (CA) prowadzono w temp. 70°C przez 14 dni. Stosunek molowy CL do DEG był następujący: 20 : 1 (PCL-1), 30 : 1 (PCL-2) i 40 : 1 (PCL-3). Wartości Mn dla poszczególnych makrodioli (wyznaczone metodą GPC) wynosiły 1800 (PCL-1), 2400 (PCL-2) i 3200 g/mol (PCL-3).

PU zostały otrzymane z PCL, glikolu polioksyetylenowego jako segmentów miękkich oraz 1,6-diizocyjanianiu heksametylenu (HMDI) i butano-1,4-diolu (BD) jako komponentów segmentów sztywnych. 1,4-diazabicyklo[2.2.2] oktan (DABCO) został użyty jako katalizator procesu poliaddycji. PU otrzymano metodą prepolimerową w masie. Indeks izocyjanianowy (stosunek grup izocyjanianowych do hydroksylowych) wynosił 1.05.

Kompozyty poliuretanowo-hydroksyapatytowe (PU-HAP) zostały otrzymane z wcześniej zsyntezowanych PU-1, PU-2 i PU-3. Biomateriały otrzymano w wyniku zmieszania PU, HAP i nanokrystalicznego NaCl. Gęstość kompozytów wynosiła od 0.21 do 0.27 g/cm^3. Z kolei, porowatość (P) kompozytów PU-HAP wynosiła od 55% do 65%.

Wykonano również testy cytotoksyczności otrzymanych PU wykorzystując w tym celu bakterie luminescencyjne V. Fischeri oraz pierwotniaki S. Ambiguum i T. Thermophila. Stwierdzono, że wszystkie otrzymane PU były nietoksyczne, zarówno względem bakterii jak i pierwotniaków.

Zawartość substancji leczniczej w otrzymanych kompozytach wynosiła około 1% wag. Badania kinetyki uwalniania CLO z otrzymanych kompozytów PU-HAP prowadzone były w roztworze PBS w temp. 37°C przez 1-8 tygodni. Profile uwalniania CLO z biomateriałów w pH 7.4 przedstawiono na RYS. 1.

Materials and methods

The previously synthesized PU were first dissolved in DMSO at a concentration of 10-20% (w/v). Next, the PU solution were mixed with HAP. Pores were created by mixing the mixture of PU and HAP with 0.5 g of NaCl crystals per 1.5 g of PU. The PU/HAP/salt mixtures were poured into a mould. Next, the mould were dried in vacuo at 50°C for 48 h. The samples were washed for 24 h in distilled water to remove NaCl. The composite samples were later dried in vacuo at room temperature for about one week.

CLO was incorporated into the PU composites by immersing the material into an aqueous drug solution of known concentration. The solution was pulled into the pores of the biomaterials by repeated five-cycles of vacuum/argon. PU composites were dried in vacuo at room temperature until the weight of the impregnated materials remained unchanged. The gain in weight of the PU composites following impregnation was taken as the weight of the CLO incorporated into the biomaterials.

The composite BPDDS were incubated in a phosphate buffer solution (PBS) (pH 7.4) at a ratio of 15 mg of composite to 1 ml of buffer at 37°C. The quantity of the released CLO was determined from the calibration curve previously obtained under the same conditions and analyzed by means of the HPLC CAD method.

Results and discussions

The aim of the first part of this study was to obtain poly(ε-caprolactone) diols (PCL) which could be applied as precursor of further polyurethanes (PU) synthesis. The ring opening polymerization of ε-caprolactone (CL) in the presence of diethylene glycol (DEG) and the lipase from Candida antarctica (CA) were conducted at 70°C for 14 days. The molar ratio of CL/DEG was either 20 : 1 (PCL-1), 30 : 1 (PCL-2) or 40 : 1 (PCL-3). The Mn values of the PCL diols determined by the GPC method were 1800 (PCL-1), 2400 (PCL-2) and 3200 Da (PCL-3).

The PU were obtained using PCL, dihydroxy(polyethylene adipate) (OEAD) as the soft segments, and 1,6-hexamethylene diisocyanate (HMDI) and 1,4-butanediol (BD) as components of the hard segments. 1,4-diazabicyclo[2.2.2] octane (DABCO) was used as the polyaddition catalyst. A two-step melt polymerization procedure was engaged to this process. The isocyanate index (isocyanate to hydroxyl equivalent ratio) was 1.05.

The polyurethane/hydroxyapatite composites (PU-HAP) were obtained from previously synthesized PU-1, PU-2 and PU-3. The composites were formed by mixing the mixture of PU and nanocrystalline HAP with NaCl. The density (d) of composites values were ranged from 0.21 to 0.27 g/cm^3. The porosity (P) of the PU-HAP composites was 55% and 65%.

Cytotoxic tests of the obtained PU were carried using the luminescent bacteria V. fischeri and two ciliated protozoa S. ambiguum and T. termophila. All the tested samples were not toxic to any of the tested bionts, whether bacteria or protozoa.

The drug content in the PU-HAP composites was 1% wt. In vitro CLO release from the PU-HAP composites was conducted in a PBS buffer at 37°C for 1-8 weeks. The kinetic rates of CLO released from the obtained biomaterials at pH 7.4 are shown in FIG. 1.

Stwierdzono, że kinetyka uwalniania CLO wzrastała ze wzrostem P kompozytów oraz zmniejszała się ze wzrostem wartości Mn PCL zastosowanych w syntezie PU. Zaobserwowano również, że P kompozytów PU-HAP zmniejszała się ze wzrostem zawartości HAP.

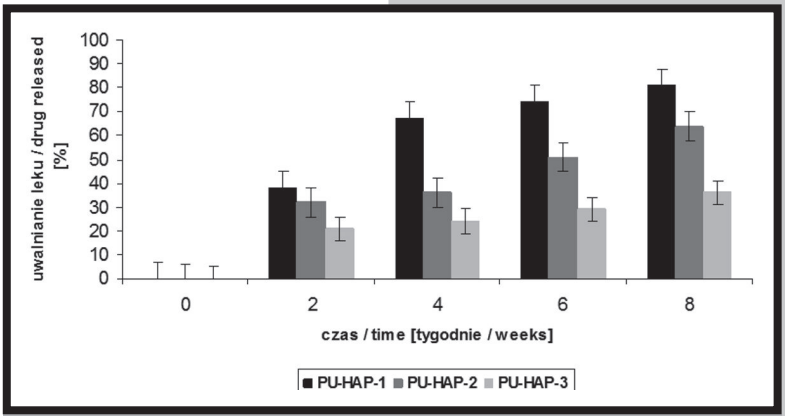

RYS. 1. Uwalnianie CLO z otrzymanych kompozytów.
FIG. 1. Release of CLO from the obtained composites.

Wnioski

Nowe kompozytowe systemy dostarczania bisfosfonianów zostały otrzymane z poliuretanów biodegradowalnych i nanokrystalicznego hydroksyapatytu. Otrzymane wielkocząsteczkowe matryce nie wykazywały cytotoksyczności. Kinetyka uwalniania klodronianu zależała generalnie od rodzaju zastosowanego poliuretanu oraz porowatości kompozytu. Uzyskane wyniki wskazują, że otrzymane kompozyty poliuretanowo-hydroksyapatytowe umożliwiają kontrolowane uwalnianie klodronianiu i mogą potencjalnie stanowić efektywne implantacyjne systemy terapeutyczne.

Podziękowania

Praca została sfinansowana przez Ministerstwo Nauki i Szkolnictwa Wyższego w ramach projektu badawczego (MNiSzW MNiSzW-2011/03/D/ST5/05793: „Opracowanie oraz badanie właściwości kompozytu polimerowo-apatytowego zawierającego selen oraz bisfosfoniany").

It was found that the rate of CLO release increases with increasing the P and decreasing the Mn of PCL used in PU synthesis. The P of the PU-HAP composites decreases with increasing HAP content.

Conclusions

New composite bisphosphonate delivery systems were prepared from biodegradable polyurethanes and nanocrystalline hydroxyapatite. The obtained macromolecular matrices were non-cytotoxic. The rates of clodronate release were shown to be directly dependent upon the nature of the obtained polyurethanes and the porosity of the composites. The results demonstrate that the polyurethane/hydroxyapatite composites are promising materials for the controlled release of clodronate and they can find practical applications as effective implantation drug delivery systems.

Acknowledgments

This work was supported by the research programme (Project MNiSzW-2011/03/D/ST5/05793: "Development and characterization of polymer-apatite composite containing selenium and bisphosphonates") of the Ministry of Science and Higher Education in Poland.

Piśmiennictwo

[1] Uhrich K.E., Cannizzaro S.M., Langer, R.S., Shakesheff K.: Polymeric systems for controlled drug release. Chem. Rev. 99 (1999) 3181-3198.
[2] Ouchi T., Ohya Y.: Macromolecular prodrugs. Prog. Polym. Sci. 20 (1995) 211-257.
[3] Sobczak M., Olędzka E., Kołodziejski W., Kuźmicz, R.: Pharmaceutical application of polymers. Polimery 52 (2007) 411-420.
[4] Giger E.V., Castagner B., Leroux J.-Ch.: Biomedical applications of bisphosphonates. J. Control. Release 167 (2013) 175-188.
[5] Karrholm J., Borssen B., Lowenhielm G., Snorrason F.: Does early micromotion of femoral stem prostheses matter? 4-7-Year stereoradiographic follow-up of 84 cemented prostheses. J. Bone Joint Surg. Br. 76(6) (1994) 912-917.
[6] Cremers S., Papapoulos S.: Pharmacology of bisphosphonates. Bone 49 (2011) 42-49.
[7] Katsumi H., Takashima M., Sano J.-I., Nishiyama K., Kitamura N., Sakane T., Hibi T., Yamamoto A.: Development of polyethylene glycol-conjugated alendronate, a novel nitrogen-containing bisphosphonate derivative: evaluation of absorption, safety, and effects after intrapulmonary administration in rats. J. Pharm. Sci. 100 (2011) 3783-3792.

References

[8] Bellido T., Plotkin L.I.: Novel actions of bisphosphonates in bone: preservation of osteoblast and osteocyte viability. Bone 49 (2011) 50-55.
[9] Gutman D., Golomb G.: Liposomal alendronate for the treatment of restenosis. J. Control. Release 161 (2012) 619-627.
[10] Zeisberger S.M., Odermatt B., Marty C., Zehnder-Fjallman A.H.M., Ballmer-Hofer K., Schwendener R.A.: Clodronate-liposome-mediated depletion of tumour associated macrophages: a new and highly effective antiangiogenic therapy approach. Br. J. Cancer 95 (2006) 272-281.
[11] Salzano G., Marra M., Porru M., Zappavigna S., Abbruzzese A., La Rotonda M.I., Leonetti C., Caraglia M., De Rosa G.: Self-assembly nanoparticles for the delivery of bisphosphonates into tumors. Int. J. Pharm. 403 (2011) 292-297.
[12] Wang G., Mostafa N.Z., Incani V., Kucharski C., Uludag H.: Bisphosphonate decorated lipid nanoparticles designed as drug carriers for bone diseases. J. Biomed. Mater. Res. A 100(3) (2012) 684-693.
[13] Cherng J.Y., Houa T.Y., Shih M.F., Talsma H., Hennink W.E.: Polyurethane-based drug delivery systems. Int. J. Pharm. 450 (2013) 145-162.

FOTO-BIODEGRADOWALNE KOMPOZYTY POLI (KWASU L-MLEKOWEGO) I TiO_2

Anna Sobczyk-Guzenda[1]*, Sławomir Owczarek[1], Rafał Kaczorowski[2], Maciej Gazicki-Lipman[1], Hieronim Szymanowski[1]

[1]Politechnika Łódzka, Instytut Inżynierii Materiałowej, ul.Stefanowskiego 1/15, 90-924 Łódź,
[2]Politechnika Łódzka,
Katedra Technologii Materiałowych i Systemów Produkcji, ul. Stefanowskiego 1/15, 90-924 Łódź
*e-mail: anna.sobczyk-guzenda@p.lodz.pl

Streszczenie

Wielofunkcyjne kompozyty składające się z polimerów oraz nieorganicznych nanododatków zmieniające pierwotne właściwości polimeru są uznawane za nowoczesne materiały, które można wykorzystać w wielu dziedzinach przemysłu oraz życia codziennego. Wpływ nanonapełniacza na modyfikację właściwości matrycy polimerowej zależy w dużym stopniu od kształtu i wielkości jego cząstek, cech powierzchniowych oraz co za tym idzie stopnia jego dyspersji.

W przedstawionej pracy wytworzono kompozyty składające się ditlenku tytanu (IV) TiO_2 oraz poli(kwasu mlekowego) (PLA). Użyto zarówno niemodyfikowany TiO_2 oraz modyfikowany metodą RF PECVD (Radio Frequency Plasma Enhanced Chemical Vapour Deposition). Proces ten przeprowadzono przy dwóch przepływach metanu 15 i 30 sccm. W celu sprawdzenia efektywności modyfikacji wykonano badanie FTIR (Fourier Transform Infrared Spectroscopy). Badanie to potwierdziło obecność na powierzchni ziaren TiO_2 grup $-CH_2$ i $-CH_3$. Gotowe kompozyty poddano badaniom właściwości mechanicznych takich jak statyczna próba na rozciąganie oraz pomiar udarności. Otrzymane wyniki dowiodły, że dodatek TiO_2 zarówno modyfikowanego jak i niemodyfikowanego nie zmienia wytrzymałości na rozciąganie natomiast poprawia jego udarność. Obecność niemodyfikowanego TiO_2 w matrycy PLA obniża nieco wartość kąta zwilżania gotowego kompozytu, a modyfikacja powierzchni TiO_2 w plazmie metanowej prowadzi do zmniejszenia zwilżalności produktu końcowego.

Słowa kluczowe: *kompozyt, polilaktyd, TiO_2, metoda RF PECVD, biodegradacja*

[Inżynieria Biomateriałów, 128-129, (2014), 46-49]

Wprowadzenie

Obecnie popyt na polimery biodegradowalne rośnie w szybkich tempie. W tym obszarze polilaktyd (PLA) odgrywa znaczącą rolę, zaczyna powoli wypierać konwencjonalne polimery syntetyczne w szczególności w zastosowaniach biomedycznych. Spowodowane jest to topniejącymi zasobami ropy naftowej i dbaniem o ochronę środowiska. Postęp technologiczny oraz opracowywanie nowych metod wytwarzania tego polimeru przyczyniły się do wzrostu jego masowej produkcji. PLA wykazuje wiele zalet, głównie takich jak: łatwość przetwarzania, biodegradowalność oraz szerokie możliwości aplikacyjne. Jego wadami są natomiast sztywność, kruchość oraz łatwość sorpcji wilgoci [1,2].

PHOTO-BIODEGRADABLE POLY(L-LACTIC ACID)/TiO_2 NANOCOMPOSITES

Anna Sobczyk-Guzenda[1]*, Sławomir Owczarek[1], Rafał Kaczorowski[2], Maciej Gazicki-Lipman[1], Hieronim Szymanowski[1]

[1]Lodz University of Technology,
Institute of Materials Science and Engineering,
1/15 Stefanowskiego Str, 90-924 Lodz, Poland
[2]Lodz University of Technology,
Department of Materials Engineering and Production Systems,
1/15 Stefanowskiego Str, 90-924 Lodz, Poland
*e-mail: anna.sobczyk-guzenda@p.lodz.pl

Abstarct

Multifunctional composites consisting of polymers or inorganic nanoadditions, which change the original properties of a polymer are considered to be modern materials for many industrial and daily life applications. An influence of a nanofiller on modification process of polymer matrix properties is strongly dependent on its particles shape and size, surface characteristics and in consequence its dispersion grade.

In the present work composites consisting of titanium dioxide (IV) TiO_2 and polylactic acid (PLA) were prepared. Unmodified TiO_2 as well as modified one by RF PECVD (Radio Frequency Plasma Enhanced Chemical Vapour Deposition) technique were used. Two different methane flow rates (15 and 30 sccm) were used during processes. In order to check the efficiency of modification process FTiR (Fourier Transform Infrared Spectroscopy) research was conducted. The results show that there are $-CH_2$ and $-CH_3$ groups present at the TiO_2 grains surface. Mechanical properties like tensile testing and impact resistance of the composites were measured. The results prove that an addition of TiO_2 (modified and unmodified) does not influence the tensile strength but improves impact resistance value. A presence of unmodified TiO_2 in PLA matrix slightly reduces the water contact angle value for a composite. Methane plasma surface treatment leads to wetting properties reduction of a final product.

Keywords: *composite, polylactic acid, TiO_2, RF PECVD technique, biodegradation*

[Engineering of Biomaterials, 128-129, (2014), 46-49]

Introduction

Nowadays demand on biodegradable polymers is growing very rapidly. Polylactic acid (PLA) plays a significant role in this area - it starts to displace conventional synthetic polymers, especially in biomedical applications. The reason of this tendency is that the world's reserves of petroleum are decreasing and that people care about environmental protection. Technical progress and working out of new production methods of this polymer contributed to an increase of its mass production. PLA exhibits many advantages, mainly: recycling facility, biodegradation and broad application scope. Its disadvantages are: inflexibility, brittleness and an ease of moisture sorption [1,2].

Badacze z wielu ośrodków zajmują się modyfikacją właściwości fizycznych, mechanicznych jak i przyśpieszeniem bądź zwolnieniem tempa degradacji. W tym celu dodaję się do matrycy PLA m.in. nieorganiczne nanonapełniacze. Dodaje się zarówno anizotropowe (krzemiany, nanorurki węglowe, hydroksyapatyt) [1,3] jak i izotropowe nanocząstki (SiO_2, $CaCO_3$ i TiO_2) [4,5]. Spośród tych powszechnie znanych napełniaczy najczęściej wykorzystywanym tego typu materiałem jest ditlenek tytanu (IV) TiO_2. Głównie używa się go do otrzymania mieszanek z polichlorkiem winylu, polistyrenem, polietylenem oraz polipropylenem [1,5,6]. Dodatek TiO_2 do matrycy polimerowej powoduje wzrost stopnia krystaliczności, wpływa także na zmianę położenia punktu płynięcia oraz zmienia wartość temperatury zeszklenia. Wprowadzenie TiO_2 do PLA ogranicza jego przepuszczalność dla gazów. Ponadto taki kompozyt może wykazywać właściwości bakteriobójcze, grzybobójcze oraz samoczyszczące po wzbudzeniu go światłem o odpowiednim zakresie spektralnym [7].

W pracy przedstawiono wpływ niemodyfikowanego i modyfikowanego TiO_2 metodą RF PECVD (Radio Frequency Plasma Enhanced Chemical Vapour Deposition) na właściwości mechaniczne i fizyczne PLA.

Materiały i metody

Jako matrycę polimerową wykorzystano PLA o nazwie handlowej PolyLactic Acid, Ingeo™ 3052D wyprodukowany przez NatureWorks LLC. Jako napełniacz zastosowano TiO_2 w postaci sypkiej, o nazwie handlowej Aeroxide P25 (78% anatazu, 14% rutylu I 8% fazy amorficznej).

Proces modyfikacji napełniacza (TiO_2) przeprowadzano w obrotowym reaktorze RF PECVD. Aparatura składa się z czterech układów: obrotowej komory reaktora w.cz, układu zasilania polem elektrycznym w.cz., układu zasilającego reaktor w gaz roboczy, układu próżniowego wraz z systemem rejestracji ciśnienia. Jako gaz roboczy wykorzystano metan. Zastosowano dwa przepływy tego gazu 15 i 30 sccm. Moc wyładowania jarzeniowego była stała i wynosiła 100 W. Optymalny czas trwania procesu modyfikacji plazmowej ustalony został na poziomie 4 minut plus 2 minuty dodatkowej aktywacji proszku metanem już bez udziału plazmy.

Analizę FTIR (Fourier Transform Infrared Spectroscopy) na zmodyfikowanym proszku wykonano w zakresie pomiarowym od 4000 do 400 cm^{-1}, przy rozdzielczości 4 cm^{-1} z użyciem spektrometru FTIR model Nicolet iS50. Pomiar przeprowadzono z wykorzystaniem przystawki odbiciowej typy DRIFT firmy Harrick.

Mieszanki TiO_2/PLA wykonane były metodą wtrysku na hydraulicznej wtryskarce ślimakowej ArburgAllrounder 320C.

Próbki do badań przygotowywano w postaci kształtek typu A1 zgodnie z normą PN-EN ISO 527-1:2012 i PN-EN ISO 527-2:2012. Zostały poddane statycznej próbie rozciągania przy wykorzystaniu maszyny wytrzymałościowej firmy Luis Schopper o zakresie siły 0÷5000 N i prędkości badania 32 mm/min. Badanie udarności przeprowadzano na aparacie typu Dynstat na znormalizowanych próbkach bez karbu, które wycinano z części pomiarowej kształtki A1.

Kąt zwilżania mierzony był za pomocą urządzenia firmy Kruss GmbH Germany, model FM40 EasyDrop. Objętość kropli pomiarowej wynosiła 0,8 µl.

Scientists from different research centers deal with modification of physical and mechanical properties as well as accelerating or slowing down the degradation time. To do that inorganic nanofillers can be added to PLA matrix. Anisotropic (silicates, carbon nanotubes, hydroxyapatite) [1,3] or isotropic (SiO_2, $CaCO_3$ i TiO_2) [4,5] nanoparticles can be used. Among these widely known fillers titanium dioxide (IV) TiO_2 is most frequently used. Usually it serves to achieve mixtures with polyvinyl chloride, polystyrene, polyethylene and polypropylene [1,5,6]. An addition of TiO_2 in the polymer matrix causes an increase of crystallinity degree, influences the flow point position and changes the glass transition value. An addition of TiO_2 to PLA reduces its permeability to gases. Additionally such a composite may exhibit bactericidal, antifungal and self-cleaning properties after radiating it by light of adequate spectral range [7].

In present work an influence of unmodified and modified TiO_2 by RF PECVD (Radio Frequency Plasma Enhanced Chemical Vapour Deposition) technique on PLA mechanical and physical properties is presented..

Materials and methods

As a polymer matrix poly(L-lactic acid) was used, known under a trade name PolyLactic Acid, Ingeo™ 3052D prodeced by NAtureWorks LLC. TiO_2 powder known under a trade name Aeroxide P25 (78% of anatase, 14% of rutile and 8% of amorphous phase) was used as a filler.

Modification process of the filler (TiO_2) was performed in a rotary RF PECVD reactor. The apparatus consists of four main parts: high frequency rotary reactor chamber, an electric field of a high frequency power supply system, operating gases supply system, vacuum system with pressure recording. Methane was used as an operating gas.

Two flow rates of this gas were used: 15 and 30 sccm. 100 W of glow discharge power was a constant parameter. The optimal process duration of 4 minutes was established plus 2 minutes of an additional powder activation by methane (without plasma presence).

FTiR (Fourier Transform Infrared Spectroscopy) analysis at a modified powder was made in a range from 4000 to 400 cm^{-1}, with the resolution of 4 cm^{-1}. The Nicolet iS50 spectrometer was used. The analysis was made with use of DRIFT type of diffuse reflection accessory produced by Harrick company. TiO_2/PLA mixtures were prepared by injection molding technique at ArburgAllrounder 320C hydraulic injection molding machine.

According to PN-EN ISO standard 527-1:2012 and PN-EN ISO standard 527-2:2012, the samples were prepared in A1 type forms. Tensile strength examinations were performed with a use of Luis Schopper tensile testing machine in a force range of 0÷5000 N and 32 mm/min speed. Impact resistance studies were made at Dynstat type apparatus at unnothed speciments, which were cut out of a measurement part of A1 form.

Contact angle value studies were performed by an apparatus of Kruss GmbH Germany company, FM40 EasyDrop model. Drop volume was set to 0,8 µl.

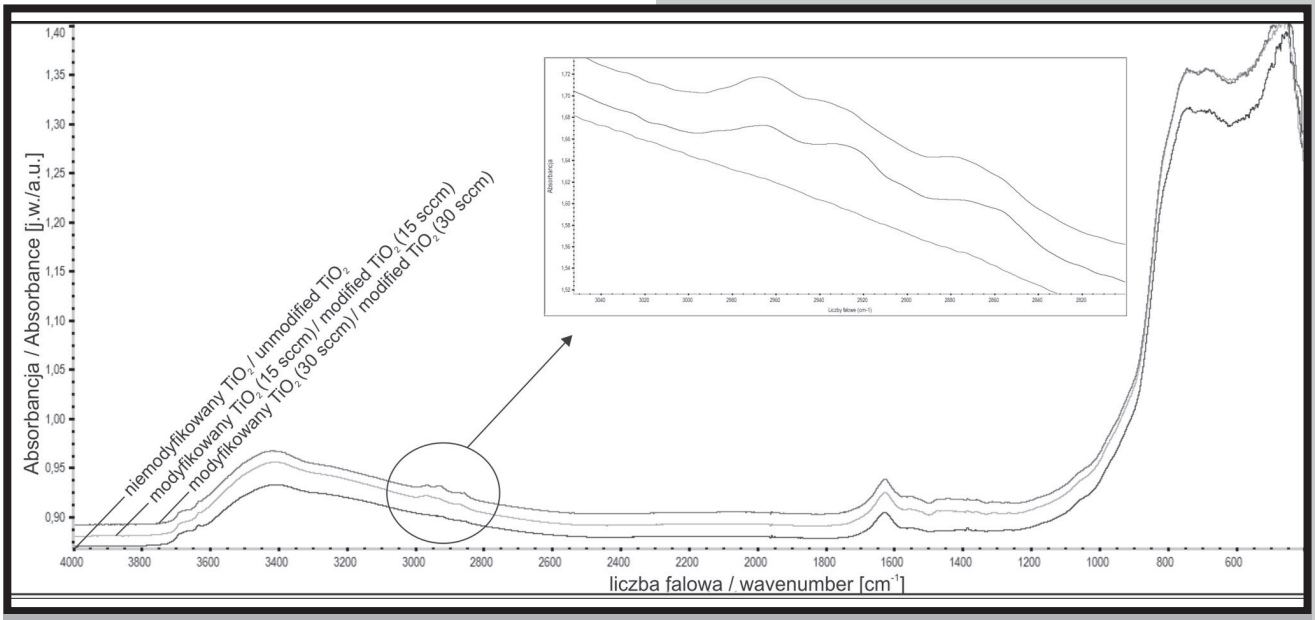

RYS. 1. Widmo FTIR dla proszku TiO_2 niemodyfikowanego i modyfikowanego przy przepływie metanu 15 i 30 sccm.
FIG. 1. FTiR spectrum for unmodified and modified TiO_2 powder at 15 and 300 sccm of methane flow rate.

Wyniki i dyskusja

Na RYS. 1 przedstawiono widmo FTIR dla niemodyfikowanego TiO_2 oraz poddanego modyfikacji w plazmie niskotemperaturowej przy przepływie metanu 15 i 30 sccm. We wszystkich widmach występują charakterystyczne piki dla anatazu oraz rutylu przy liczbach falowych 400-500 cm^{-1} oraz 600-700 cm^{-1}, które związane są z występowaniem wiązania Ti-O-Ti. Ponadto stwierdzono obecność szerokiego pasma w zakresie 3700 a 3200 cm^{-1} pochodzącego od drgań rozciągających grupy hydroksylowej -OH. W przypadku proszku modyfikowanego piki znajdujące się przy liczbach falowych 1545, 1452 i 1415 cm^{-1} świadczą o obecności wiązania M-O-C oraz grup $–CH_2$ i $-CH_3$. Z kolei szerokie maksimum leżące w zakresie od 3000 do 2800 cm^{-1} potwierdza obecność drgań rozciągających grup alifatycznych $-CH_x$. Pasma posiadające maksimum przy liczbie falowej 2964 i 2872 cm^{-1} należą do grypy metylowej. Z kolei pasma leżące przy 2926 i 2850 cm^{-1} związane są z obecnością grupy metylenowej pochodzących też odpowiednio od jej drgań antysymetrycznych i symetrycznych.

Wyniki z pomiarów wytrzymałości na rozerwanie oraz udarności przedstawiono w TABELI 1. Przybliżona literaturowa wartość wytrzymałości na rozerwanie dla czystego PLA wynosi ok. 55 MPa [1]. Badany PLA posiada przybliżoną wartość do danych literaturowych. Dodatek niemodyfikowanego TiO_2 powoduje niewielki wzrost tej wartości. Przy czym nieco większy wzrost wartości wytrzymałości zaobserwowano dla modyfikowanego napełniacza. Należy tutaj jednak podkreślić, że rozrzut pomiędzy otrzymanymi wynikami jest jednak nieduży. Z kolei zastosowany nanododatek poprawia wyraźnie udarność próbek. Wzrost jej wartości następuję nie tylko wraz ze zwiększaniem się zawartości TiO_2 ale i także po zastosowaniu wcześniejszej modyfikacji jego powierzchni. Jest to dowód na obecność na powierzchni TiO_2 zaszczepionych grup –CHX przez które wprowadzone cząsteczki napełniacza wiążą się ze strukturą matrycy polimerowej.

Results and discussions

FIG. 1. shows FTiR spectrum for unmodified and low temperature plasma modified TiO_2 (at methane flow rate of 15 and 30 sccm). All spectra contain typical peaks for anatase and rutile at 400-500 cm^{-1} and 600-700 cm^{-1} wavenumbers, which are related to Ti-O-Ti bonding. Additionally in the range from 3700 to 3200 cm^{-1} a wide band coming from stretching vibrations of -OH hydroxyl group is present. In case of the modified powder, peaks at 1545, 1452 and 1415 cm^{-1} wavenumbers indicate a presence of M-O-C bonding and $-CH_2$ as well as $-CH_3$ groups. Wide maximum in the range from 3000 to 2800 cm^{-1} proves a presence of stretching vibrations of $-CH_x$ aliphatic groups. Bands with a maximum by 2964 and 2872 cm^{-1} wavenumbers belong to methyl group. Bands with a maximum by 2926 i 2850 cm^{-1} wavenumbers come from methylene group and correspond to its antisymmetric and symmetric vibrations respectively.

TABLE 1. shows tensile strength and impact resistance studies results. According to the literature the tensile strength for pure PLA equals ca. 55 MPa [1]. Measured PLA exhibits a very similar value of this parameter. An addition of unmodified TiO_2 causes a slight increase of this value. A bit larger increase of tensile strength is observed for the modified filler. Though, the differences in results are very small. Then nanoaddition significantly improves the impact resistance value. It grows not only according to an increase of an amount of TiO_2, but also after its surface modification. It proves that there are -CHx groups at the surface of TiO_2, which bond inserted filler particles with the structure of the polymer matrix.

Water contact angle values for the pure PLA amount to ca. 80 deg. An insert of unmodified TiO_2 to its structure causes multistage loss of water contact angle value - this tendency is decreasing together with an increase of filler concentration. An insert of the modified TiO_2 leads to an increase of the water contact angle value toward the value for the pure PLA.

TABELA 1. Zestawienie właściwości mechanicznych dla czystego PLA oraz kompozytów TiO_2/PLA.
TABLE 1. Mechanical properties of pure PLA and TiO_2/PLA composites.

próbka sample	wytrzymałość na rozerwanie tensile strength [MPa]	udarność impact resistance [kJ/m^2]
PLA	53,7	7,6
1%TiO_2/PLA	54,1	8,3
2%TiO_2/PLA	53,5	8,8
4%TiO_2/PLA	50,8	7,7
1% TiO_2/PLA [15 sccm]	55,1	9,0
2% TiO_2/PLA [15 sccm]	54,4	9,2
4% TiO_2/PLA [15 sccm]	50,3	8,6
1% TiO_2/PLA [30 sccm]	55,0	9,6
2% TiO_2/PLA [30 sccm]	54,4	9,3
4% TiO_2/PLA [30 sccm]	52,1	8,0

Otrzymane wartości kątów zwilżania wodą czystego PLA wynoszą ok. 80 deg. Wprowadzenie niemodyfikowanego TiO_2 do jego struktury powoduje kilkustopniowy spadek jego wartości, zmniejszający się wraz ze zwiększaniem stężenia napełniacza. Z kolei dodatek modyfikowanego TiO_2 prowadzi do podniesienia wartości kąta zwilżania do wartości odpowiadającej czystemu PLA.

Wnioski

Z przedstawionych w niniejszej pracy wyników można sformułować następujące wnioski:

- możliwa jest skuteczna modyfikacja proszku TiO_2 metodą RF PECVD o czym świadczą zaszczepione grupy $-CH_2$ oraz $-CH_3$,
- zarówno dodatek niemodyfikowanego jak i modyfikowanego TiO_2 do matrycy polimery PLA nie powoduje znaczących zmian w wytrzymałości na rozerwanie otrzymanego kompozytu,
- dodatek modyfikowanego TiO_2 do PLA znacznie poprawia udarność uzyskanego materiału,
- modyfikacja TiO_2 prowadzi do zmniejszenia zwilżalności powierzchni kompozytu TiO_2/PLA

Podziękowania

Praca finansowana jest z Własnego Funduszu Stypendialnego PŁ nr um. RNB/WFS/11/2013

TABELA 2. Wyniki pomiarów kątów zwilżania wodą dla czystego PLA i kompozytów TiO_2/PLA.
TABLE 2. Water contact angle values for pure PLA and TiO_2/PLA composites

próbka/sample	Kąt zwilżania water contact angle [deg]
PLA	79,1
1%TiO_2/PLA	76,0
2%TiO_2/PLA	73,1
4%TiO_2/PLA	72,5
1%TiO_2/PLA [15 sccm]	80,5
2%TiO_2/PLA [15 sccm]	77,4
4%TiO_2/PLA [15 sccm]	76,7
1%TiO_2/PLA [30 sccm]	82,7
2%TiO_2/PLA [30 sccm]	77,8
4%TiO_2/PLA [30 sccm]	75,8

Conclusions

On the basis of the results presented in this work the following conclusions can be drawn:

- an effective modification of TiO_2 powder by RF PECVD technique is possible - it is indicated by a presence of $-CH_2$ and $-CH_3$ groups,
- an insert of unmodified as well as modified TiO_2 to the PLA polymer lattice does not influence much tensile strength of the composite,
- an insert of modified TiO_2 to PLA significantly improves the impact resistance of prepared material,
- modification of TiO_2 leads to reduction of wetting properties of TiO_2/PLA composite surface.

Acknowledgements

The work is supported by the TUL Internal Scholarship Foundation contract No RNB/WFS/11/2013

Piśmiennictwo

[1] Luo Y.-B., Li W.-D.,. Wang X.-L, Xu D.-Y., Wang Y.-Z.: Preparation and properties of nanocomposites based on poly(lactic acid) and functionalized TiO2. Acta Materialia 57 (2009) 3182–3191.
[2] Malinowski R., Łubkowski D. Badania wpływu temperatury i czasu suszenia na wybrane właściwości polilaktydu (PLA), Inżynieria i Aparatura Chemiczna 5 (2010) 77-78.
[3] Ray SS, Bousmina M.Biodegradable polymers and their layered silicate nanocmoposites: in greening the 21 st century materials world. Prog Mater Sci. 50 (2005) 962-1079.
[4] Reijnders L. The release of TiO_2 and SiO_2 nanoparticles from nanocomposites. Polymer Degradation and Stability 94 (2009) 73–876.

References

[5] Ramakrishna S, Mayer J, Wintermantel E, Leong KW. Biomedical applications of polymer-composite materials: a review. Compos Sci Technol. 61 (2001) 1189–1224.
[6] Zhao X, Li Z, Chen Y, Shi L and Zhu Y. Solid-phase photocatalytic degradation of polyethylene plastic under UV and solar light irradiation. Journal of Molecular Catalysis A: Chemical. 268 (2007)101-106.
[7] Ali N.A., Noori F.T.M. Gas Barrier Properties of Biodegradable Polymer Nanocomposites Films Chemistry in Materials Science 6 (2014) 44-51

OCENA CYTOTOKSYCZNOŚCI I N VITRO NANOKOMPOZYTU PCL/HAp JAKO RUSZTOWANIA DLA INŻYNIERII TKANKOWEJ

Katarzyna Klimek[1], Małgorzata Świętek[2], Marta Błażewicz[2], Grażyna Ginalska[1]

[1]Uniwersytet Medyczny w Lublinie, Katedra Biochemii i Biotechnologii, W.Chodźki 1, 20-093 Lublin, Polska
[2]AGH Akademia Górniczo-Hutnicza, Wydział Inżynierii Materiałowej i Ceramiki, Katedra Biomateriałów, A.Mickiewicza 30, 30-059, Kraków

[Inżynieria Biomateriałów, 128-129, (2014), 50-53]

Wstęp

Inżynieria tkankowa (BTE) stała się jednym z najbardziej obiecujących obszarów badań, zajmujących się wykorzystaniem tworzyw bioceramicznych oraz polimerów w celu stworzenia idealnych biomateriałów syntetycznych [1]. Hydroksyapatyt (HAp) jest tworzywem bioceramicznym, który ze względu na wysoką biokompatybiilność i właściwości osteoindukcyjne używany jest jako substytut kostny [2]. W inżynierii tkankowej wykorzystywane są także polimery, takie jak poli(ε-kaprolakton) (PCL), które wykazują dobre właściwości mechaniczne lecz niewielką aktywność biologiczną. Z tego powodu, jednym z rozwiązań jest tworzenie skafoldów kompozytowych, które łączą w sobie zalety obu typów biomateriałów [3]. Obecne prace coraz częściej dotyczą kompozytów na bazie PCL, ze względu na ich unikatowe właściwości. Liczne badania potwierdzają, że kompozyty na bazie PCL wykazują większą zdolność do pobudzania procesów zasiedlania, proliferacji oraz różnicowania komórek niż sam PCL [2,4,5].

Celem pracy było stworzenie skafoldu nanokompozytowego PCL/HAp zmodyfikowaną metodą odlewania z roztworu/wypłukiwania soli oraz ocena właściwości biologicznych otrzymanego materiału w stosunku do ludzkich płodowych osteoblastów (h-FOB 1.19).

Materiały i metody

Przygotowanie skafoldów.

Poli(ε-kaprolakton) (M_n 45000) oraz hydroksyapatyt (<200 nm) został zakupiony w Sigma-Aldrich. Zastosowanym rozpuszczalnikiem był dichlorometan pozyskany z Avantor Performance Materials Poland S.A. Jako porogen wykorzystano chlorek sodu o dwóch wielkościach ziaren: 300 µm i 200 µm. Do rozdziału porogenu na frakcje zastosowano wytrząsarkę ultradźwiękową. Do wytworzenia gąbek zastosowano metodę odlewania z roztworu/wymywania porogenu (solvent casting/porogen leaching). Przygotowano 20% (wt/wt) roztwór poli(ε-kaprolaktonu) w dichlorometanie, który następnie homogenizowano przez 24 godziny na mieszadle magnetycznym. Osobno przygotowano mieszaninę cząstek stałych: zawierającą: 20 g chlorku sodu o rozmiarze ziaren 300 µm, 10 g chlorku sodu o rozmiarze ziaren 200 µm oraz hydroksyapatytu. Roztwór polimeru zmieszano z mieszaniną porogenu i hydroksyapatytu, umieszczono w formie i pozostawiono na 7 dni w celu powolnego odparowania rozpuszczalnika. Następnie wymyto cząstki porogenu poprzez powolne wypłukiwanie w wodzie destylowanej, aż do osiągnięcia przewodnictwa wody destylowanej. Następnie gąbki suszono przez 24 godziny w suszarce, w temp. 40°C.

IN VITRO CYTOTOXICITY ASSESSMENT OF PCL/HAp NANOCOMPOSITE SCAFFOLD FOR BONE TISSUE ENGINEERING

Katarzyna Klimek[1], Małgorzata Świętek[2], Marta Błażewicz[2], Grażyna Ginalska[1]

[1]Medical University of Lublin, Department of Biochemistry and Biotechnology, 1 Chodzki Street, 20-093 Lublin, Poland
[2]AGH University of Science and technology, Faculty of Materials Science and Ceramics, Department of Biomaterials, 30 A.Mickiewicza Ave, 30-059 Krakow, Poland

[Engineering of Biomaterials, 128-129, (2014), 50-53]

Introduction

Bone tissue engineering (BTE) became one of the most promising areas of research, focusing on bioceramics and polymers to reach ideal synthetic biomaterials [1]. The hydroxyapatite (HAp) is a bioceramics that has been investigated as a biocompatible and osteoinductive biomaterial for use as bone substitute [2]. On the other hand, the polymers used in BTE such as poly(ε-caprolactone) (PCL), exhibit good mechanical properties, but low intrinsic bioactivity. For this reason, one of the main strategies are designing of composite scaffold which combine the advantages of two biomaterials classes [3]. The present studies focus on development of PCL composites, because of their unique properties. It is known that the PCL composites show higher seeding efficiency, proliferation rates and differentiation effect than PCL alone [2,4,5].

The aim of this study was to fabricate a novel PCL/HAp nanocomposite scaffold by solvent casting/salt leaching modified method, and to assess biological properties of this composite using human fetal osteoblasts (h-FOB 1.19).

Materials and methods

Preparation of scaffold.

Poly(ε-caprolactone) (M_n 45000) and hydroxyapatite (<200nm particle size) were purchased from Sigma Aldrich Co. The solvent used to prepare polymer solution was dichloromethane obtained from Avantor Performance Materials Poland S.A. As a porogen two grain size fractions 200 µm and 300 µm of sodium chloride were used. To obtain individual fractions of porogen an ultrasonic sieving processor was applied. For fabrication PCL/HAp scaffold solvent casting/salt leaching method was applied. Poly(ε-caprolactone) was dissolved in dichloromethane in order to prepare 20% (wt/wt) solution of polymer which was later homogenized continuously on magnetic stirrer for 24 hours. Separately the mixture of solid particles was prepared. It contained: 20 g of 300 µm grain fraction of porogen, 10 g of 200 µm grain fraction of porogen and hydroxyapatite. The solution of polymer was mixed with compound of sodium chloride and nanoaddition. The mixture was put into template and left for 7 days to allow the slow evaporation of dissolvent. Afterwards, porogen particles were removing by dissolving in distillate water and leaching until the conductivity of the distillate water was achieved. At the end, composite scaffolds were dried in 40°C for 24 hours.

Obrazowanie mikrostruktury

W celu zobrazowania i optymalizacji morfologii włókien nanokompozytu PCL/HAp, wykorzystano elektronowy mikroskop skaningowy (SEM). Bezpośrednio przez obserwacją próbki zostały napylone warstwą węgla.

Badania z wykorzystaniem hodowli komórkowych

W badaniach in vitro wykorzystano ludzkie, prawidłowe preosteoblasty linii h-FOB 1.19, pochodzące z Amerykańskiej Kolekcji Hodowli Komórkowych (ATCC). Hodowlę prowadzono w temperaturze 34°C i atmosferze 5% CO_2. Bezpośrednio przez eksperymentami, krążki nanokompozytu zostały wysterylizowany w 75% roztworze etanolu przez 4 godziny. Po tym czasie, materiały dodatkowo sterylizowano promieniowaniem ultrafioletowym przez 2 godziny. W celu wypłukania resztek etanolu, wysterylizowane materiały inkubowano przez 24 godziny w roztworze PBS.

Ocena aktywności cytotoksycznej w teście pośrednim

W badaniu aktywności cytotoksycznej kompozytu PCL/HAP wykorzystano metodę pośrednią z wykorzystaniem ekstraktu z badanego materiału, zgodnie z normą ISO 10993-5. Stosunek masy materiału do objętości płynu hodowlanego wynosił 0,1 g/ml. Kontrolę negatywną stanowiło podłoże hodowlane bez dodatku kompozytu, natomiast kontrolę pozytywną stanowił 10% DMSO. Na początku zawiesinę komórek h-FOB 1.19 w pełnym podłożu hodowlanym doprowadzono do gęstości $1{,}5x10^5$ kom./ml i rozlewano po 100 µl do dołków płytki 96-dołkowej. Po całonocnej inkubacji w temperaturze 34°C, ściągano płyn hodowlany i dodawano po 100 µl/dołek odpowiednich ekstraktów. Po 24- i 48- godzinnej inkubacji w standardowych warunkach, żywotność komórek została oznaczona metodami MTT oraz NRU. W celu wykonania testu MTT, do dołków dodawano po 25 µl roztworu MTT w PBS o stężeniu 5mg/ml, inkubowano przez 3 godziny w temperaturze 34°C, a następnie dodawano po 100 µl na dołek roztworu SDS-HCL. Po 12-godzinnej inkubacji mierzono absorbancję roztworu przy długości fali 570 nm za pomocą automatycznego czytnika płytek (Biotek ELx50). W celu wykonania testu NRU, komórki przemyto roztworem PBS i dodawano 100µl roztworu NRU (50 µl/ml DMEM/F12). Po 3 godzinnej inkubacji w 34°C komórki przemywano roztworem PBS i dodawano po 100µl/dołek roztworu rozpuszczalnika (1% lodowaty kwas octowy/ 49% woda destylowana/ 50% etanol). Następnie płytkę wytrząsano przez 20 min i mierzono absorbancję przy długości fali 540 nm za pomocą automatycznego czytnika płytek (Biotek ELx50).

Badania wpływu biomateriału na proliferację komórek.

W badaniu stopnia proliferacji komórek użyto test z Sulforodaminą B (SRB). Zawiesinę komórek h-FOB 1.19 w pełnym podłożu doprowadzono do gęstości $3x10^4$ kom./ml i rozlewano po 700µl bezpośrednio na materiał umieszczony w płytce 24-dołkowej. Jako kontrolę użyto nietoksycznych krążków polistyrenowych (13 mm średnicy). Po 96- godzinnej inkubacji w temperaturze 34°C, usunięto podłoże hodowlane, a krążki przeniesiono do sąsiadujących dołków w nowej płytce 24-dołkowej. Następnie dodano 700 µl pełnego podłoża hodowlanego, komórki utrwalono 175 µl 50% kwasu trójchlorooctowego (TCA) i umieszczono przez godzinę w temperaturze 4°C. Po zakończeniu inkubacji, krążki przemyto wodą i pozostawiono do wyschnięcia. Po tym czasie, komórki barwiono przez 20 min dodając 700 µl 0,4% SRB rozpuszczonej w 1% kwasie octowym, a następnie przemywano 5 razy 1% kwasem octowym w celu wypłukania niezwiązanych cząstek. W celu uwolnienia związanych białek komórkowych dodawano po 700 µl 10mM roztworu Tris i wytrząsano płytkę przez 20 min.

Microstructure visualization

Scanning Electron Microscopy (SEM) (Zeiss ULTRA plus) was used for determining and optimizing the fiber morphology of PCL/HAp nanocomposite scaffold. The samples were sputtered with carbon before observation.

Cell culture

The in vitro assessment was carried out using human fetal osteoblasts (h-FOB 1.19) purchased from American Type Culture Collection (ATCC). The cells were cultured at 34°C in a humidified atmosphere of 5% CO_2. For cell culture studies the biomaterial was cut into small circular discs (3 mm thick, 13mm diameter) and sterilized with 75% (v/v) ethanol solution for 4 hours. The samples were additionally sterilized with ultrafiolet light for 2 hours. The sterilized pieces were preincubated in PBS solution for 24 hours to replace the ethanol remaining in the samples.

Cytotoxicity evaluation by indirect test.

The cytotoxic activity of PCL/HAp nanocomposite scaffold was evaluated by indirect test using extracts prepared according to ISO 10993-5. The ratio between biomaterial weight and the volume of culture medium was 0.1 g/ml. Culture medium without sample and 10% DMSO was served as a negative control and positive control, respectively. Firstly, the h-FOB 1.19 cells were seeded in 96-well plates in 100 µl of complete medium at concentration of $1.5x10^5$ cells/ml. After overnight incubation at 34°C, the culture medium was removed and 100 µl of extracts or 10% DMSO were added. After 24- and 48-hour incubation, in order to evaluate cell viability, the MTT and NRU assays were performed. For the MTT assay, 25 µl of the MTT solution (5mg/ml in the PBS) per well were added and the plate was incubated at 34°C for 3 hours. Next, 100 µl of SDS-HCL solution per well was added. After 12-hour incubation the absorbance was measured with a microplate reader (Biotek ELx50) at 570 nm. For the NRU assay, cells were rinsed with the PSB and 100 µl of NRU solution (50 µl/ml DMEM/F12) in culture medium per well were added and the plate was incubated at 34°C for 3 hours. After incubation, the cells were rinsed with PBS, and 100 µl of solvent (1% glacial acetic acid, 49% distilled water, 50% ethanol) per well was added. Then, the plate was agitated for 20 minutes and the absorbance was measured at 540nm using microplate reader (Biotek ELx50).

Cell proliferation assessment.

To evaluate cell proliferation, the Sulforhodamine B (SRB) In Vitro Toxicology Assay was used. The h-FOB 1.19 cells were seeded directly on the nanocomposite discs in 24-well plates in 700 µl of complete medium at concentration of $3x10^4$ cells/disc. As a control, non-toxic polystyrene discs (13 mm diameter) were used. After 96 hours incubation at 34°C, the culture medium was removed and discs were transferred to the corresponding wells in a new 24-well plate. Next, 700 µl of complete medium were added and the cells were fixed with 175 µl of 50% trichloroacetic acid (TCA) at 4°C for 1 hour. After incubation, the discs were washed with tap water and the plate was air-dried. After that time, the cells were stained for 20 minutes with 700 µl of 0.4% SRB dissolved in 1% acetic acid and washed five times with 1% acetic acid to remove unbound stain. Then, the bound protein stain was solubilised with 700 µl of 10mM Tris base. The plate was agitated for 20 minutes. The absorbance was measured at 492 nm and subtracting the background was measured at 620 nm using a microplate reader (Biotek Synergy H4). Since the discs absorb some SRB, additional controls containing discs and cell-free medium were run.

Absorbancję mierzono przy długości fali 492 nm za pomocą automatycznego czytnika płytek (Biotek Synergy H4). Absorbancję tła mierzono przy długości fali 650 nm i odejmowano od pierwotnego pomiaru. Ponieważ biomateriał chłonie SRB, dodatkowo wykonano kontrolę zawierającą same biomateriały oraz kontrolę z podłożem hodowlanym.

Ocena zdolności adhezyjnej komórek do biomateriału.

Zdolność adhezyjną komórek h-FOB 1.19 do kompozytu PCL/HAp oceniano metodą bezpośrednią z wykorzystaniem fioletu krystalicznego (CV). W celu oznaczenia stopnia adhezji komórek do biomateriału, zawiesinę komórek h-FOB 1.19 w pełnym podłożu doprowadzono do gęstości $5x10^4$ kom./ml i rozlewano po 700 µl bezpośrednio na materiał umieszczony w płytce 24-dołkowej. Jako kontrolę użyto nietoksycznych krążków polistyrenowych (13mm średnicy). Po 3-godzinnej inkubacji w temperaturze 34°C, usunięto podłoże hodowlane, a krążki przeniesiono do sąsiadujących dołków w nowej płytce 24-dołkowej. Następnie, komórki utrwalono dodając 700 µl 2% paraformaldehydu (pH 7.4) przez godzinę. Po tym czasie zlano paraformaldehyd, a komórki wybarwiono przez 5 min 0,5% roztworem fioletu krystalicznego w 20% etanolu. Następnie krążki 5-cio krotnie przemyto wodą i pozostawiono do wyschnięcia. Po wyschnięciu, zaabsorbowany barwnik wyekstrahowano dodając 1000µl 96% etanolu. Płytkę wytrząsano przez 15 minut i mierzono absorbancję przy długości fali 570 nm za pomocą automatycznego czytnika płytek (Biotek Synergy H4). Ponieważ biomateriał chłonie fiolet krystaliczny, dodatkowo wykonano kontrolę zawierającą same biomateriały oraz kontrolę z podłożem hodowlanym.

Wyniki

Obserwacje przeprowadzone za pomocą skaningowej mikroskopii elektronowej wykazały kompleksową porowatość wytworzonego nanokompozytu. Obecne są pory o zróżnicowanych rozmiarach i kształtach. Kształty dużych porów (300, 200 µm) odzwierciedlają kształty ziaren porogenu. Hydroksyapatyt obecny jest w postaci małych, charakterystycznych granulek (analiza EDX potwierdziła zarówno obecność fosforu jak i wapnia). Hydroksyapatyt prawdopodobnie zlokalizowany jest zarówno przy powierzchni porów jak i w głębi kompozytowej gąbki. Obecność pików węgla i tlenu w analizie EDX pochodzą od polimeru.

W celu oceny aktywności cytotoksycznej nanokompozytu PCL/HAp w stosunku do linii komórkowej h-FOB 1.19, wykonano testy MTT i NRU. W obu przeprowadzonych testach nie otrzymaliśmy wyników istotnych statystycznie. Po 24-godzinnej inkubacji, w teście MTT wykazano, że aktywność metaboliczna komórek traktowanych ekstraktem z PCL/HAp spadła do 90,3% w porównaniu do kontroli. Wydłużenie czasu inkubacji (48 godz.) spowodowało dalszy spadek żywotności do 85,3% w porównaniu z kontrolą. Warto podkreślić, że wyniki testu MTT zostały częściowo potwierdzone w teście NRU. Zarówno po 24- jak i 48- godzinnej inkubacji, ilość pochłoniętej przez komórki czerwieni obojętnej była stosunkowo wysoka, a żywotność komórek nieznacznie spadła do odpowiednio 93,7% oraz 92,3%, w porównaniu do kontroli.

Dodatkowo, oceniano zdolność komórek do adhezji i proliferacji. Główną rolę w procesach adhezji i proliferacji komórek odgrywają wzajemne interakcje między komórkami a biomateriałem. W naszych badaniach ocenialiśmy stopień proliferacji osteoblastów za pomocą testu z sulforodaminą B.

Cell adherence assessment.

The ability of the h-FOB 1.19 cells to adhere to PCL/HAp nanocomposite scaffold was evaluated by direct test using crystal violet assay (CV). In order to determine the cells adherence, the h-FOB 1.19 cells were seeded directly on the composite discs in 24-well plates in 700 µl of complete medium at concentration of $5x10^4$ cells/disc. As a control, non-toxic polystyrene discs (13 mm diameter) were used. After 3- hour incubation at 34°C, the culture medium was removed and discs were transferred to corresponding wells in a new 24-well plate. Next, the cells adhered to the discs were fixed with 700 µl of 2% paraformaldehyde (pH 7.4) for 1 hour. Then, paraformadehyde was removed and the cells on the discs were stained with 0,5% crystal violet in 20% ethanol for 5 minutes. After that, the discs were washed five times with water and the plate was air-dried. After drying, the absorbed dye was solubilised with 1000 µl of 96% ethanol. The plate were agitated for 15 minutes. The absorbance was measured with a microplate reader (Biotek Synergy H4) at 570 nm. Since the discs absorb some CV, additional controls containing discs and cell-free medium were run.

Results

Studies carried out using scanning electron microscope demonstrated the complex porosity of fabricated nanocomposites. Pores with different shapes and sizes were present. The shapes of huge pores (300, 200 µm) reflected the shape of particle. Hydroxyapatite is observed in the form of granules (EDX analysis confirmed the presence of phosphorus and calcium). Hydroxyapatite was probably localized both on the surface and inside the nanocomposite scaffold. Peaks of carbon and oxygen in EDX analysis were associated with polymer.

In our study, MTT and NRU assays were performed in order to determine the cytotoxic activity of PCL/HAp nanocomposite scaffold on h-FOB 1.19 cell line. We observed that both MTT and NRU assays did not give statistically significant results. After 24-hour incubation, the MTT test showed that h-FOB cells metabolic activity exposed to the PCL/HAp nanocomposite extract were decreased to 90.3%, compared to the control. In addition, we observed that cell metabolic activity was slightly reduced in time-dependent manner. After 48-hour exposure, the cell metabolic activity was decreased to 85.3%, compared to the control. Furthermore, it was noted that the NRU test partially confirmed the MTT test results. After both 24- and 48- hour incubation, the amount of incorporated neutral red was relatively high, and the cell viability was slightly decreased to 93.7% and 92.3%, respectively, compared to the control.

Moreover, the cell adhesion and proliferation were also tested. The interactions between the cells and the biomaterial scaffolds play main role in cell adhesion and proliferation. In our study, we evaluated the osteoblasts proliferation rates, using Sulforhodamine B assay. After 96-hour incubation, the cell numbers on the PCL/HAp nanocomposite scaffolds were increased remarkably. The study demonstrated, that the amount of incorporated Sulforhodamine B increased approximately three-fold, compared to the control. Furthermore, in order to determine cell adherence ability, the CV test was performed. The CV test results clearly confirmed the Sulforhodamine test results. After 3-hour incubation, we observed greater cell adhesion to the PCL/HAp nanocomposite scaffold than to the polystyrene (control).

Po 96-godzinnej inkubacji, liczba komórek na nanokompozycie PCL/HAp znacząco wzrosła. Ilość związanej przez komórki sulforodaminy B wzrosła prawie 3-krotnie w porównaniu z kontrolą. Ponadto, w celu określenia zdolności adhezyjnej komórek do biomateriału, wykonano CV test. Otrzymane w teście CV wyniki potwierdzają wyniki otrzymane w teście z sulforodaminą B. Po 3-godzinnej inkubacji, obserwowano większą adhezję komórek do nanokompozytu PCL/HAp niż do polistyrenu (kontrola).

Wnioski

W naszej pracy badaliśmy strukturę i biokompatybilność skafoldu nanokompozytowego PCL/HAp orzymanego zmodyfikowaną metodą odlewania z roztworu/wypłukiwania soli. Warto podkreślić, że skafold nanokompozytowy PCL/HAp jest wysoce porowaty, nie toksyczny i pobudza komórki do procesów adhezji i proliferacji. Dlatego też, mamy nadzieję, że nasz biomateriał znajdzie w przyszłości zastosowanie w inżynierii tkankowej jako substytut kostny.

Podziękowania

Badania zostały sfinansowane w ramach projektu DS2 (Uniwersytet Medyczny w Lublinie, Polska). Praca powstała z wykorzystaniem sprzętu zakupionego projekcie realizowanym zgodnie z umową nr PORPW.01.03.00-06-010/09-00 w ramach Projektu Operacyjnego Rozwój Polski Wschodniej 2007-2013, Osi Priorytetowej I, Nowoczesna Gospodarka, Działanie 1.3 Wspieranie Innowacji.

Conclusion

In this work, we studied the morphologies and biocompatibility of the PCL/HAp nanocomposite scaffold fabricated by solvent casting/salt leaching modified method. It was noted that PCL/HAp nanocomposite scaffold was high porous, non-toxic and induced cell adhesion and proliferation. Therefore, we hope that our biomaterial will find some application as bone substitute for bone tissue engineering.

Acknowledgments

This study was supported by a DS2 grant (Medical University in Lublin, Poland). The paper was developed using the equipment purchased within agreement No. PORPW.01.03.00-06-010/09-00 Operational Program Development of Eastern Poland 2007-2013, Priority Axis I, Modern Economy, Operations 1.3. Innovations Promotion.

Piśmiennictwo References

[1] Stevens M.M.: Biomaterials for bone tissue engineering. Mater Today 11 (2008) 18-25.
[2] Park S.A., Lee S.H., Kim W.D.: Fabrication of porous polycaprolactone/hydroxyapatite (PCL/HA) blend scaffolds using a 3D plotting system for bone tissue engineering. Bioprocess Biosyst. Eng. 34 (2011) 505-513.
[3] Zhao J., Guo L.Y., Yang X.B., Weng J.: Preparation of bioactive porous HA/PCL composite scaffolds. Appl. Surface Sci. 255 (2008) 2942-2946.
[4] Rodenas-Rochina J., Luis Gomez Ribelles J., Lebourg M.: Comparative study of PCL-HAp and PCL-bioglass composite scaffolds for bone tissue engineering. J. Mater. Sci.: Mater. Med. 24 (2013) 1293-1308.
[5] Mei N., Chen G., Zhou P., Chen X., Shao Z.-Z. :Biocompatibility of Poly(ε-caprolactone) Scaffold Modified by Chitosan-The Fibroblasts Proliferation in vitro. J. Biomater. Appl. 19 (2005) 323-329.

ZASTOSOWOWANIE FOSFORANÓW WAPNIA W STOMATOLOGII

Zofia Kula , Anna Laska , Hieronim Szymanowski*

Politechnika Łódzka, Instytut Inżynierii Materiałowej,
ul. Stefanowskiego 1/15, 90-924 Łódź
*e-mail: hieronim.szymanowski@p.lodz.pl

Streszczenie

Fosforany wapnia zaliczane są do biomateriałów ceramicznych, resorbowalnych. Kości i zęby kręgowców zbudowane są z fosforanu wapnia, głównie z hydroksyapatytu. Zajmuje on szczególne miejsce pośród fosforanów wapnia, ze względu na wyjątkowe właściwości fizykochemiczne i biologiczne.

Zarówno hydroksyapatyt (HAp), jak i ortofosforan (V) wapnia (TCP) są solami trójzasadowego kwasu ortofosforowego – H_3PO_4. Dzięki właściwościom użytkowym znalazły szerokie zastosowanie w medycynie i stomatologii. Amorficzny fosforan wapnia dodawany jest do preparatów wybielających, stosowanych do metody nakładkowej oraz metody z wykorzystaniem lampy UV. Badania kliniczne dowodzą, że amorficzny fosforan wapnia (ACP) ma następujące właściwości: odbudowuje szkliwo poprzez wytworzenie nowej powłoki hydroksyapatytowej na powierzchni zębów, zmniejsza nadwrażliwość zębów, przywraca zębom połysk i wygładza ich powierzchnię oraz zmniejsza ryzyko nawrotu przebarwień.

Słowa kluczowe: *hydroksyapatyt, fosforany wapnia, szkliwo*

[Inżynieria Biomateriałów, 128-129, (2014), 54-56]

Wprowadzenie

Resorbowalne fosforany wapnia (głównie hydroksyapatyt HAp) jako biomateriały ceramiczne już od dawna znalazły swoje miejsce w medycynie i weterynarii. Obecnie coraz częściej pojawiają się także publikacje naukowe dotyczące stosowania HAp w stomatologii. Dotychczas stosowane kompozyty do wypełnień bezpośrednich zawierają napełniacze poprawiające właściwości mechaniczne kompozytów stomatologicznych. Zęby są głownie zbudowane z hydroksyapatytu dlatego bada się kompozyty zawierające ten biomateriał. Uważa się, że mogą one niwelować nadwrażliwość w przypadku głębokich ubytków, zapobiegać próchnicy wtórnej oraz zwiększać estetykę. Prowadzona badania wykazują, że fosforany wapnia posiadają właściwości osteokondukcyjne. Materiały tego typu można podzielić na materiały alloplastyczne i heterogenne pochodzenia zwierzęcego. Najbardziej popularnymi wśród materiałów alloplastycznych są materiały ceramiczne i dzielą się na biozgodne, które nie wywołują szkodliwych reakcji w organizmie (np. tlenek glinu) oraz materiały bioaktywne (wspomagające biologiczne procesy odbudowy kości). O zdolnościach osteokonduktywnych decyduje w głównej mierze struktura powierzchni materiału [9]. Fosforany wapnia są materiałami dobrze tolerowanymi przez organizm. Mają działanie stymulujące procesy odbudowy kości i szybko ulegają osteointegracji.

Fosforany wapnia, które mogą być pochodzenia syntetycznego (HAp, TCP oraz dwufazowe materiały implantacyjne BCP zawierające hydroksyapatyt i ortofosforan (V) wapnia, α i β TCP) i naturalnego (naturalna kość, szkielety koralowców) [7].

THE APPLICATIONS OF CALCIUM PHOSPHATES IN DENTISTRY

Zofia Kula , Anna Laska , Hieronim Szymanowski*

Lodz University of Technologuy,
Institute of Materials Science and Engineering
1/15 Stefanowskiego Street, 90-924 Lodz, Poland
*e-mail: hieronim.szymanowski@p.lodz.pl

Abstract

Calcium phosphates are among the ceramic biomaterials, resorbable. Bones and teeth of vertebrates are composed of calcium phosphate, mainly hydroxyapatite, which occupies a special place among the calcium phosphates, due to the unique physical, chemical and biological properties.

Both the hydroxyapatite (HAp), as well as orthophosphate (V) phosphate (TCP) are salts of tribasic phosphoric acid - H_3PO_4. Excellent utility properties found wide application in medicine and dentistry. The amorphous calcium phosphate is added to the bleaching preparations used for the overlay method and the method using a UV lamp. Clinical studies show that the amorphous calcium phosphate (ACP) has the following characteristics: recovering, by creating a new enamel hydroxyapatite coating on the surface of the teeth, reduce hypersensitivity of the teeth, the teeth restores the gloss and smooth the surface and reduce the risk of recurrence of discoloration.

Keywords: *hydroxyapatite, calcium phosphates, enamel*

[Engineering of Biomaterials, 128-129, (2014), 54-56]

Introduction

Resorbable calcium phosphates (mainly hydroxyapatite HAp) as ceramic biomaterials are commonly used in medicine and veterinary for some time. Recently, scientific publications about HAp usage in dentistry appear more frequently. Composites currently used in direct dental fillings contain fillers which improve mechanical properties of dental composites. Teeth consist mainly of hydroxyapatite, therefore composites containing it are under investigation. It is thought that such composites may eliminate hypersensitivity in case of deep cavity, prevent secondary caries and improve aesthetics. According to carried out tests calcium phosphates possess osteoconductive properties. Among that type materials can be distinguished two categories – alloplastic materials and heterogenous animal origin materials. The most popular of alloplastic materials are ceramics that are divided into groups – biocompatible materials that present non-toxic reaction in human organism (e.g. aluminium oxide) and bioactive materials (they support biological processes in bone regeneration). Osteoconductivity of material depends mostly on material surface structure [9]. Calcium phosphates are well-tolerated materials in living organisms. They stimulate bone regeneration processes and integrate fast with tissue (fast osteointegration).

Calcium phosphates can be either synthetic (HAp, TCP and two-phased implanted materials BCP which contain hydroxyapatite and calcium orthophosphate, α- and β-TCP) or natural (natural bone, skeletons of corals) [7].

Hydroksyapatyt

Oznaczany jest w literaturze symbolami HAp, HAP, HA lub OHAp [3,4].W strukturze HAp jony wapniowe i fosforanowe układają się na płaszczyźnie sześciokąta, wokół położonej w środku grupy hydroksylowej OH^-. W obrazie trójwymiarowym kolumna jonów hydroksylowych wyznacza długą oś (oś c) powstającego kryształu. Ca^{1-} oznacza jony wapnia leżące bliżej, Ca^{2-} jony wapnia leżące dalej od osi c [1]. Opisana struktura jest schematycznie przedstawiona na RYS. 1.

Wprowadzenie jonów fluoru przyspiesza powstawanie kryształów hydroksyapatytu oraz zwiększa ich stabilność poprzez zmniejszenie ich rozpuszczalności w środowisku kwasowym. Hydroksyapayt jest związkiem nieorganicznym wchodzącym w skład naszych zębów. TABELA 1 przedstawia skład szkliwa i zębiny.

Syntetyczny hydroksyapayt znalazł szerokie zastosowanie w leczeniu schorzeń tkanki kostnej. W stomatologii wykorzystuje się go do znoszenia nadwrażliwości zębiny w okolicach obnażonych szyjek zębowych, do leczenia biologicznego miazgi zębowej oraz ubytków hipoplastycznych szkliwa. Dodawany jest również do cementów dentystycznych i past do zębów jako środek oczyszczający i polerujący zęby. Cementy stomatologiczne są stostowane do rekonstrukcji i odbudowy twardych tkanek zęba jako wypełnienia czasowe lub ostateczne ich ubytków. Proszek w cementach fosforanowo wapniowych składa się zwykle z amorficznego fosforanu wapnia (ACP), α-trójfosforanu wapnia (α-TCP), difosforanu wapnia (DCP) dziewięciotlenku difosforu (V) tetrawapnia (TTCP), jednowodnego fosforanu jednowapniowego (MCPM) i węglanu wapnia (CC).

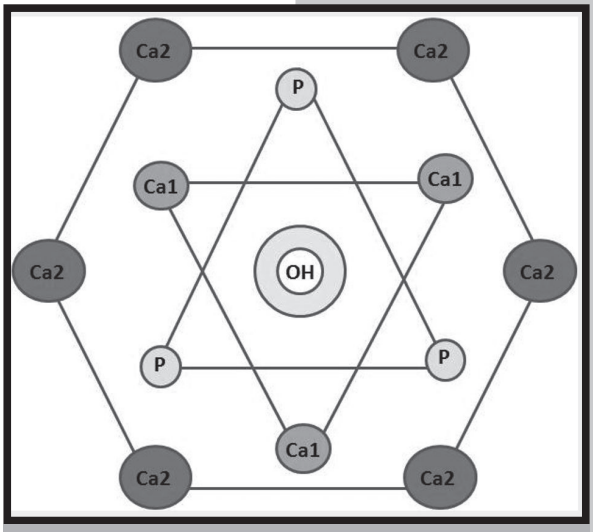

RYS. 1. Element struktury kryształu HAp.
FIG. 1. Element of crystal structure of HAp.

Hydroxyapatite

In the literature it is abbreviated HAp, HAP, HA or OHAp [3,4]. In the structure of HAp calcium and phosphate ions are arranged on hexagon plane, where hydroxyl group OH^- is in the centre. In three-dimensional image column of hydroxyl ions outlines long axis (axis c) of created crystal. Ca^{1-} means calcium ions that are closer to axis c, Ca^{2-} –calcium ions located further away from that axis [1].

Insertion of fluorine ions accelerates formation of hydroxyapatite crystals and increases their stability by decrease of solubility in acid environment. Hydroxyapatite is inorganic compound occurring in human teeth composition (in the TABLE 1 composition of enamel and dentin is presented). Synthetic hydroxyapatite has found a wide range of application in the treatment of bone tissue diseases. In dentistry it is used to reduce the sensitivity of exposed tooth necks, in biological healing of dental pulp and hypoplastic loss of enamel. It is also added to dental cements and toothpaste as tooth cleaning and polishing agent. Dental cements are applied in reconstruction and reconstruction of hard tissue of teeth as temporary fillings or final fillings of cavities. Powder in calcium phosphate cements consists of amorphous calcium phosphate (ACP), α- tricalcium phosphate (TCP), dicalcium phosphate (DCP), tetracalcium diphosphate 10-oxide (TTCP), monohydrate calcium phosphate (MCPM) and calcium carbonate (CC).

Amorphous calcium phosphate is added to tooth whitening agents used in the overlay method or the method with UV lamps. Clinical research indicates that amorphous calcium phosphate (ACP) has such properties as: it rebuilds and reinforces tooth enamel by creating new layer of hydroxyapatite on tooth surface, it restores tooth gloss, smoothes tooth surface and reduces the risk of relapses of tooth discolouration.

TABELA 1. / TABLE 1.

Skład Composition	Szkliwo Enamel		Zębina Dentin	
	Masa Mass	Objętość Volume	Masa Mass	Objętość Volume
Związki nieorganiczne Inorganic Compounds	96%	89%	70%	47%
Związki organiczne Organic Compounds	1%	2%	20%	32%
Woda /Water	3%	9%	10%	21%
Składniki organiczne Organic Compounds	Enameliny Enamelins		Kolagen typ I, fosfoproteiny glikoproteiny, proteoglikany, fosforaza zasadowa, metaloproteinazy białka surowicy krwi, fosfolipidy, kwas cytrynowy Type I collagen, phosphoproteins and another acidic glycoproteins, proteoglycans, grothw factors, alkaline phosphatase, protein metalloproteinases of blood serum, phospholipids, citric acid	
Składniki nieorganiczne Inorganic Compounds	Fosforan wapnia (duże kryształy hydroksyapatytu, węglan wapnia, magnez, potas, sód , fluor Calcium phosphate (large crystals of HAp), calcium carbonate, magnesium, potassium, sodium, fluorine)		Fosforan wapnia (małe kryształy hydroksyapatytu) śladowe ilości jonów fluorowych i węglanowych Calcium phosphate (small crystals of HAp), trace quantities of fluorine and sodium ions	

Amorficzny fosforan wapnia dodawany jest do preparatów wybielających, stosowanych do metody nakładkowej oraz metody z wykorzystaniem lampy UV. Badania kliniczne dowodzą, że amorficzny fosforan wapnia (ACP) ma następujące właściwości: odbudowuje szkliwo poprzez wytworzenie nowej powłoki hydroksyapatytowej na powierzchni zębów, przywraca zębom połysk i wygładza ich powierzchnię oraz zmniejsza ryzyko nawrotu przebarwień.

Hydroksyapayt jest stosowany do uzupełniania ubytków kostnych po hemisekcji, radektomii czy amputacji korzenia zębowego, a także w chirurgii szczękowo-twarzaowej, aby wypełnić ubytki po usuniętych torbielach lub guzach. Hydroksyapayt jest dielektrykiem, co ma ogromne znaczenie w przypadku produkcji z niego implantów. Nie nagrzewają się w czasie wykonywanych zabiegów fizykoterapeutycznych i nie zaburzają w organizmie sygnałów elektrycznych za pośrednictwem systemu nerwowego [8].

Po zabiegu ekstrakcji wprowadzony do zębodołu, powoduje zmniejszenie krwawienia i objętości skrzepu, przez co przyspiesza regenerację i zapobiega powikłaniom zapalnym. W przypadku implantologii zwiększa zdolność tolerancji ciała obcego i przyspiesza gojenie po wymieszaniu z krwią pacjenta, szpikiem kostnym i solą fizjologiczną.

Fosforan (V) wapnia – TCP

TCP jest syntetycznym dwuortofosforanem trójwapnia. Charakteryzuje się barwą białą i występuje w dwóch odminach polimorficznych wysokotemperaturowej α i niskotemperaturowej β. Odmiana wysokotemperaturowa α TCP odznacza się lepszą rozpuszczalnością i większą szybkością rozpuszczania w stosunku do niskotemperaturowej β TCP, co przyczyniło się do szerszego zastosowania w medycynie i stomatologii w porównaniu z wysokotemperaturową [7].

Chemiczne i mineralogiczne podobieństwo do tkanki kostnej sprawia, że jest on biozgodny i posiada właściwości osteokondukcyjne. Cechuje się dobrą tolerancją, brakiem odczynów zapalnych ze strony tkanek gospodarza i co naj¬ważniejsze brakiem ryzyka związanego z infekcją wirusem HIV, żółtaczką oraz prionami. [6] Stosowany jest głownie do odbudowy ubytków kostnych, przed zabiegiem zakładania implantu zębowego.

Wnioski

Hydroksyapatyt i fosforan (V) wapnia – TCP ze względu na korzystne właściwości biomechaniczne, bardzo dobre właściwości fizyko-chemiczne, wysoką biozgodność z tkanką kostną oraz osteokondukcyjność są materiałami budzącymi duże zainteresowanie inżynierów pracujących nad nowymi biomateriałami, które można zastosować w stomatologii. Obecnie jest prowadzony szereg różnych badań nad fosforanami wapnia, w celu poszukiwania nowych zastosowań, które przyczynią się do dalszego rozwoju dziedzin medycznych.

Hydroxyapatite is used in filling bone cavities after hemisection, radectomy or root amputation, but also in maxillofacial surgery in order to fill loss after removed cysts and tumours. Hydroxyapatite is a dielectric, which plays a crucial role in production process of HAp-containing implants. The implants do not heat during physiotherapy treatments and do not influence electric signals via nervous system [8].

After extraction procedure hydroxyapatite can be inserted in the alveolus (tooth socket) in order to alleviate bleeding and reduce the volume of clot, which accelerates the regeneration and prevents inflammatory complications. In the case of implantology, HAp improves tolerance of foreign object in human body and promotes the healing after mixing with patient blood, bone marrow and physiological saline.

Tricalcium Phosphate – TCP

TCP is synthetic tricalcium diortophosphate. TCP has white colour and exists in two polymorths – high-temperature α and low-temperature β. High-temperature form α-TCP is characterised by better solubility and higher dissolution rate in comparison to low-temperature β-TCP, which contributed to wider range of application in medicine and dentistry [7].

Close chemical and mineralogical (crystal) resemblance to bone tissue causes that TCP is biocompatible and possesses osteoconductive properties. It presents good tolerance, the lack of inflammatory response from host tissues and, most importantly, the lack of risk related to HIV infection, jaundice and prions [6]. TCP is mainly used in bone tissue regeneration before insertion of dental implant.

Conclusion

Hydroxyapatite and tricalcium phosphate TCP are particularly attractive as new biomaterials used in dental applications due to their favourable biomechanical properties, very good physical-chemical properties, high biocompatibility with bone tissue and osteoconduction. Currently, a series of studies under calcium phosphates are conducted to find new applications and contribute to the further development in medical sciences.

Piśmiennictwo

[1] Kmieć Z. „Histologia i Cytofizjologia Zęba i Jamy Ustnej" 2007
[2] Wiglusz R. „Nano-hydroksyapatyty w zastosowaniach biomedycznych" Postępy Farmacji 1-2/2012
[3] Ślósarczyk A „Bioceramika hydroksyapaytowa" Biuletyn Ceramiczny nr13, Ceramika 51, Polskie Towarzystwo Ceramiczne, Kraków 1997
[4] http://geology.com/minerals/apatite.shtml
[5] Zima A. „Wpływ dodatków modyfikujących na właściwości hydroksyapatytowych wielofunkcyjnych tworzyw implantacyjnych przeznaczonych na nośniki leków" Akademia Górniczo-Hutnicza Kraków 2007

References

[6] Puchała P. „Przegląd biomateriałów na podstawie piśmiennictwa" Elamed TPS 10/2008
[7] Sobczak-Kupiec A. „Właściwości fizyko-chemiczne ortofosforanów wapnia istotnych dla medycyny TCP i HAp" Kraków Technical Chemistry 1/2010
[8] Błażewicz S „Biocybernetyka i inżynieria biomedyczna 2000" Tom 4, EXIT Warszawa 2003
[9] Szyszkowska A. „Materiały stosowane do odbudowy ubytków kostnych w stomatologii – praca poglądowa" Implantoprotetyka, Kraków 4/2008

MODYFIKACJA POWIERZCHNI KLAMER KOSTNYCH NiTi Z PAMIĘCIĄ KSZTAŁTU PORZEZ NISKOTEMPERATUROWE JARZENIOWE AZOTOWANIE I TLENOAZOTOWANIE

Z.Lekston[1*], T.Wierzchoń[2], J.Lelątko[1], D.Stróż[1], J.Cieplak[3], J.Dybich[4]

[1]Instytut Nauki o Materiałach, Uniwersytet Śląski,
41-500 Chorzów, 75 Pułku Piechoty 1A
[2]Wydział Inżynierii Materiałowej, Politechnika Warszawska,
02-507 Warszawa, ul. Wołoska 141
[3]BHH Mikromed Sp. z o.o.,
42-530 Dąbrowa Górnicza, ul. Katowicka 11
[4]BHH Mikrohuta Sp. z o.o.,
42-530 Dąbrowa Górnicza, ul. Katowicka 11
zlekston@us.edu.pl

Streszczenie

W pracy przedstawiono opis technologii niskotemperaturowego azotowania i tlenoazotowania jarzeniowego stopów NiTi z pamięcią kształtu. Opisano azotowanie jarzeniowe z wykorzystaniem zjawiska rozpylania katodowego, oraz warunki azotowania i utleniania jarzeniowego detali NiTi w jednym procesie technologicznym. Badania topografii powierzchni przed i po procesach jarzeniowej obróbki przeprowadzono metodą mikroskopii sił atomowych przy użyciu mikroskopu AMF firmy Veeco. Opracowane sposoby modyfikacji powierzchni zastosowano do azotowania i tlenoazotowania klamer NiTi do zespoleń złamań kości. Uzyskano klamry z jednorodnymi barwnymi warstwami. Stwierdzono podwyższenie temperatur odzysku kształtu klamer po obróbce jarzeniowej.

[Inżynieria Biomateriałów, 128-129, (2014), 57-60]

Wprowadzenie

Stopy NiTi wykazujące efekty pamięci kształtu uznane jako biomateriały metaliczne są coraz szerzej stosowane w medycynie [1,2]. Łuki ortodontyczne, klamry kostne, stenty, filtry Simona, korki Amplatzera , dystraktory dla chirurgii plastycznej, klipsy CAC dla chirurgii jamy brzusznej oraz inne wyroby dla chirurgii małoinwazyjnej to przykłady najczęściej stosowanych wyrobów medycznych NiTi [3]. Końcowa obróbka powierzchni implantów NiTi decyduje o ich przydatności do zastosowania [4]. Istotne jest takie przygotowanie powierzchni aby zachować własności funkcjonalne, wytworzyć biokompatybilną warstwę zewnętrzną TiO_2 w postaci rutylu i nie spowodować wytworzenia podwarstwy wzbogaconej w nikiel. Poprawę właściwości korozyjnych, trybologicznych i biokompatybilności uzyskano poprzez zastosowanie nowatorskiej technologii azotowania lub tlenoazotowania jarzeniowego [5,6].

Celem tej pracy było przedstawienie opracowanej technologii obróbki jarzeniowej stopów NiTi, wytworzenie biokompatybilnych warstw azotku tytanu TiN i dwutlenku tytanu TiO_2 w postaci rutylu na klamrach NiTi do zespoleń złamań kości oraz sprawdzenie wpływu zastosowanej obróbki powierzchni na temperaturę odzysku kształtu. Wytworzone klamry z warstwami wierzchnimi przeznaczone są do dalszych badań „in vitro" w celu potwierdzenia ich przydatności do zastosowań w ortopedii i chirurgii twarzoczaszki oraz w medycynie weterynaryjnej.

SURFACE MODIFICATION OF NiTi SHAPE MEMORY BONE STAPLES BY LOW-TEMPERATURE GLOW DISCHARGE OXIDATION AND NITRIDING

Z.Lekston[1*], T.Wierzchoń[2], J.Lelątko[1], D.Stróż[1], J.Cieplak[3], J.Dybich[4]

[1]Institute of Materials Science, University of Silesia,
1A 75 Pułku Piechoty Street, 41-500 Chorzów
[2]Faculty of Materials Engineering, Warsaw University of Technology, 141 Wołoska Street, 02-507 Warszawa
[3]BHH Mikromed Sp. z o.o.,
11 Katowicka Street, 42-530 Dąbrowa Górnicza
[4]BHH Mikrohuta Sp. z o.o.,
11 Katowicka Street, 42-530 Dąbrowa Górnicza
zlekston@us.edu.pl

Abstract

The paper presents a description of the technology of low -temperature glow discharge nitriding and oxynitriding of NiTi shape memory alloys. Glow discharge nitriding that uses cathode sputtering and the conditions of the glow discharge nitriding and oxidation of the NiTi details in one process have been described. The studies of surface topography of NiTi samples before and after the process of the glow discharge nitriding and oxynitriding were conducted using a Veeco atomic force microscope (AFM). The developed methods have been used for nitriding and oxynitriding the surface of the NiTi staples for the fixation of bone fractures. In this way we obtained staples with uniform colored layers. The shape recovery temperature of the NiTi shape memory staples was increased after the glow-discharge treatment.

[Engineering of Biomaterials, 128-129, (2014), 57-60]

Introduction

Shape memory NiTi alloys recognized as metallic biomaterials are more and more often used in medicine [1,2]. Orthodontic archwires, bone staples, stents, Simon's filters, Amplatzer's plugs, plastic surgery distractors, compression anastomosis clips for abdominal surgery and other products for minimally invasive surgery are examples of the most commonly used NiTi medical devices [3]. The final surface treatment of NiTi implants decides on their suitability for use [4]. It is important that the surface is prepared in such a way so as to retain functional properties, create a biocompatible TiO_2 outer layer in the form of rutile, and not to produce a nickel-enriched sublayer. The improvement of the corrosion, tribology and biocompatibility properties was obtained through the use of an innovative low-temperature glow discharge nitriding and oxynitriding [5,6].

The aim of the study was to present the glow-discharge treatment of the NiTi alloys that has been developed, formation of the bio-compatible layers of TiN titanium nitride and TiO_2 titanium dioxide in the form of rutile on NiTi clamps for the fixation of bone fractures and examination of the influence of the surface treatment that was applied on the shape recovery temperature. The manufactured clamps with surface layers are to undergo further "in vitro" testing in order to confirm their suitability for orthopaedics, craniofacial surgery and veterinary medicine.

Materiał i metodyka badań

Badania wykonano na próbkach stopu NiTi o zawartości 50,8%at. uzyskanego w ramach projektu INNOTECH. Azotowanie i tlenoazotowanie prototypowych klamer NiTi z pamięcią kształtu wytworzonych przez współwykonawców projektu (BHH Mikrohuta, BHH Mikromed) przeprowadzono wg technologii opracowanej na Wydziale Inżynierii Materiałowej Politechniki Warszawskiej. Wytworzone na powierzchni warstwy badano przy użyciu mikroskopu sił atomowych AFM firmy Vecco. Temperatury odzysku kształtu klamer po azotowaniu i tlenoazotowaniu wyznaczono z krzywych odzysku kształtu zarejestrowanych wg standardu ASTM 2082-06.

Wyniki badań i dyskusja

Technologia azotowania jarzeniowego stopów NiTi

W oparciu o przeprowadzone wcześniej badania procesu azotowania jarzeniowego stopu NiTi firmy AMT (Belgia) stwierdzono, że temperatura obróbki nie powinna przekraczać 350°C [5]. Zatem w celu uzyskania warstw azotkowych zastosowano odpowiednie warunki technologiczne procesu: temperatura - T=300°C, czas procesu azotowania - t=30 min., ciśnienie w komorze roboczej - p=1,6 hPa (atmosfera reaktywna – N_2 o czystości 99,99%). Przeprowadzono badania wpływu zjawiska rozpylania katodowego na tworzenie się warstwy azotku tytanu, w których wykazano, że z uwagi na jednorodność strukturalną warstwy (widoczną m.in. poprzez jednakową barwę na całej obrabianej powierzchni) korzystna jest, przed etapem azotowania jarzeniowego na potencjale katody, dodatkowa obróbka powierzchni stopu NiTi przy ciśnieniu rzędu 1,0 hPa przez 10 min., w temperaturze 250°C w atmosferze Ar+20% H_2. Wykorzystując zjawisko rozpylania katodowego można wpływać na aktywację warstwy wierzchniej obrabianego stopu NiTi. Badania korozyjne wykazały wpływ sposobu przygotowania powierzchni stopu NiTi (szlifowanie, polerowanie) na odporność korozyjną warstw TiN [6]. Opracowany proces technologiczny azotowania jarzeniowego umożliwiający wytworzenie warstwy azotku tytanu o wymaganej grubości należy prowadzić w kilku kolejnych etapach:

• Przygotowanie detali ze stopu NiTi do azotowania jarzeniowego – czyszczenie i odtłuszczanie w acetonie w płuczce ultradźwiękowej

• Przygotowanie urządzenia do procesu azotowania - umieszczenie detali w specjalnych uchwytach na katodzie w komorze roboczej, wytworzenie próżni w komorze roboczej rzędu $1x10^{-1}$ hPa, „płukanie" komory roboczej argonem o czystości 99,99% w tzw. próżni dynamicznej rzędu 2-3 hPa przy ciągłym przepływie argonu przez komorę roboczą

• Nagrzewanie wsadu do temperatury procesu ok. 250°C po włączeniu zasilacza napięciowo - impulsowego przy ciśnieniu 2 hPa i wprowadzeniu atmosfery azotu o czystości 99,99%

• Aktywacja powierzchni obrabianego stopu NiTi polegająca na wprowadzeniu atmosfery Ar/N_2 (1/1) i wygrzewaniu w temperaturze 250°C przez 10 minut i osiągnięcie temperatury 300°C

• Realizacja procesu azotowania jarzeniowego: temperatura - T=300°C, ciśnienie - p=1,6 hPa (N_2), czas - t=15-45 min (w zależności od wymaganej grubości warstwy TiN)

• Chłodzenie wsadu poprzez stopniowe obniżanie parametrów prądowo-napięciowych zasilacza w celu osiągnięcia temperatury wsadu ok. 150°C i chłodzenie bez wyładowania jarzeniowego w próżni dynamicznej rzędu 3 hPa w atmosferze N_2 do temperatury około 50°C

Material and methods

The tests were performed on the samples of the NiTi alloy containing 50.8at% Ni obtained under the INNOTECH project. Nitriding and oxynitriding of the prototype NiTi shape memory staples co-produced under the project (BHH Mikrohuta, BHH Mikromed) were performed according to the technology described in the survey results. The layers formed on the surface were observed with the a Vecco atomic force microscope AFM. Shape recovery temperatures of the staples before and after nitriding and oxynitriding were determined based on the shape recovery curves recorded according to the ASTM 2082-06 standard.

Results and discussion

Glow-discharge nitriding of NiTi alloys

Based on the prior research into the glow-discharge nitriding of NiTi by AMT (Belgium) it was found that the treatment temperature should not exceed 350°C [5]. Thus, in order to obtain the nitride layers, the following technological process conditions were met: temperature - T=300°C, nitriding time - t=30 min, pressure in the working chamber - p=1,6 hPa (reactive atmosphere - N2 purity 99,99%). The effects of cathode sputtering on the formation of the titanium nitride layer were studied. As a result it was shown that due to the structural homogeneity of the layer (visible inter alia thanks to a uniform color over the entire surface that was under treatment) additional treatment of the surface of the NiTi alloy at the pressure of 1.0 hPa for 10 minutes, at 250°C and in the atmosphere of Ar+20% H_2, prior to the glow-discharge nitriding on the cathode potential is beneficial. The use of cathode sputtering we can influence the activation of the surface layer of the NiTi alloy. Corrosion tests show that the way in which the surface of the NiTi alloy is prepared (grinding, polishing) influences the corrosion resistance of TiN layers [6].

The process of glow-discharge nitriding that has been developed and which allows to produce a titanium nitride layer of the required thickness must be carried out in several successive stages:

• Preparation of the NiTi alloy details for nitriding - cleaning and degreasing in acetone in an ultrasound bath

• Preparation of the device for a nitriding by placing the parts/elements in loops on the cathode in the working chamber, creation of a $1x10^{-1}$ hPa vacuum in the working chamber, "washing" of the working chamber with continuous flow of argon with purity of 99.99%.

• Heating of the batch to the process temperature of approx. 250°C after turning on the switching power and voltage supply at the pressure of 2 hPa, and the introduction of the nitrogen atmosphere with the purity of 99.99%

• Activation of the surface of the NiTi alloy by using the Ar/N_2 (1/1) atmosphere and annealing at 250°C for 10 minutes and reaching the temperature of 300°C

• Implementation of the glow-discharge nitriding: temperature - T=300°C, pressure - p=1.6 hPa (N_2), time - t=15-45 min (depending on the required thickness of the TiN layer)

• Cooling the batch by gradual reduction of the parameters of the power-voltage supply in order to achieve a batch temperature of approx. 150°C and cooling without a glow discharge in the dynamic vacuum of 3 hPa in the N_2 atmosphere to about 50°C

Zmieniając czas procesu azotowania jarzeniowego można uzyskać warstwy azotku tytanu o grubościach w zakresie 20÷70 nm, natomiast poprzez odpowiednie przygotowanie powierzchni obrabianego stopu NiTi (szlifowanie, względnie polerowanie) można kształtować topografię i morfologię wytwarzanej warstwy azotku tytanu.

Azotowanie i utlenianie jarzeniowe próbek NiTi w jednym procesie technologicznym

W wyniku przeprowadzonych badań wpływu składu mieszaniny reaktywnej składającej się z mieszaniny azotu i powietrza (od 5% do 20% objętości) względnie N_2 z tlenem (do 10% objętości) na utlenianie powierzchni z wytworzonym azotkiem tytanu opracowano warunki procesu tlenoazotowania jarzeniowego, składającego się w pierwszym etapie z procesu – azotowania jarzeniowego oraz w drugim etapie z procesu – utleniania jarzeniowego przy następujących parametrach: temperatura procesu: T=300°C, czas procesu: t =15 min. (dla atmosfery N_2+O_2 –10% obj.) lub 30 min. (dla atmosfery reaktywnej N_2+powietrze – 20%obj.), ciśnienie w komorze roboczej: 1,5 hPa.

Proces tlenoazotowania jarzeniowego realizowany jest w jednym cyklu technologicznym, tj. bezpośrednio po procesie azotowania zmienia się atmosferę reaktywną wprowadzając powietrze w ilości 20% objętościowych w mieszaninie z azotem lub tlen w ilości 10% objętości w mieszaninie z azotem. Zastosowanie tlenu, czy też powietrza w mieszaninie z azotem oraz czas procesu wpływa istotnie na morfologię wytwarzanych warstw dwutlenku tytanu – TiO_2 (rutylu) i azotku tytanu oraz pozwala zmieniać ich strukturę, grubość oraz topografię powierzchni (RYS. 1).

By varying the nitriding process time it is possible to get a titanium nitride layer with a thickness from 20 to 70 nm, and through adequate preparation of the surfaces of the processed NiTi alloy (grinding, or polishing) it is possible to shape the topography and morphology of the produced titanium nitride layer.

Glow-discharge nitriding and oxidation of NiTi samples in a single technological process

As a result of the research into the influence of the reactive a mixture of nitrogen and air (5% to 20% of the volume) or N_2 or with oxygen (up to 10% of the volume) on the oxidation of the surface with the produced titanium nitride the conditions of the glow discharge oxynitriding were developed. Its first stage consists in glow-discharge nitriding, and its second stage in the glow-discharge oxidation with the following parameters: process temperature: T=300°C, the process time t=15 min. (for the atmosphere of N_2+O_2 – 10%vol.) or 30 mins (for the reactive atmosphere of N_2+air - 20%vol.) pressure in the working chamber: 1.5 hPa.

The glow discharge oxynitriding is performed in a single technological cycle, ie. immediately after nitriding it changes into a reactive atmosphere introducing 20% of air (by volume) in the mixture of nitrogen and oxygen in an amount of 10% by volume in the mixture with nitrogen. The use of oxygen, or air, in the mixture with nitrogen and the process time significantly affects the morphology of the titanium dioxide layers that are produced titanium nitride - TiN and titanium dioxide - TiO_2 (rutile), and can change their structure, thickness and topography of the surface (FIG. 1).

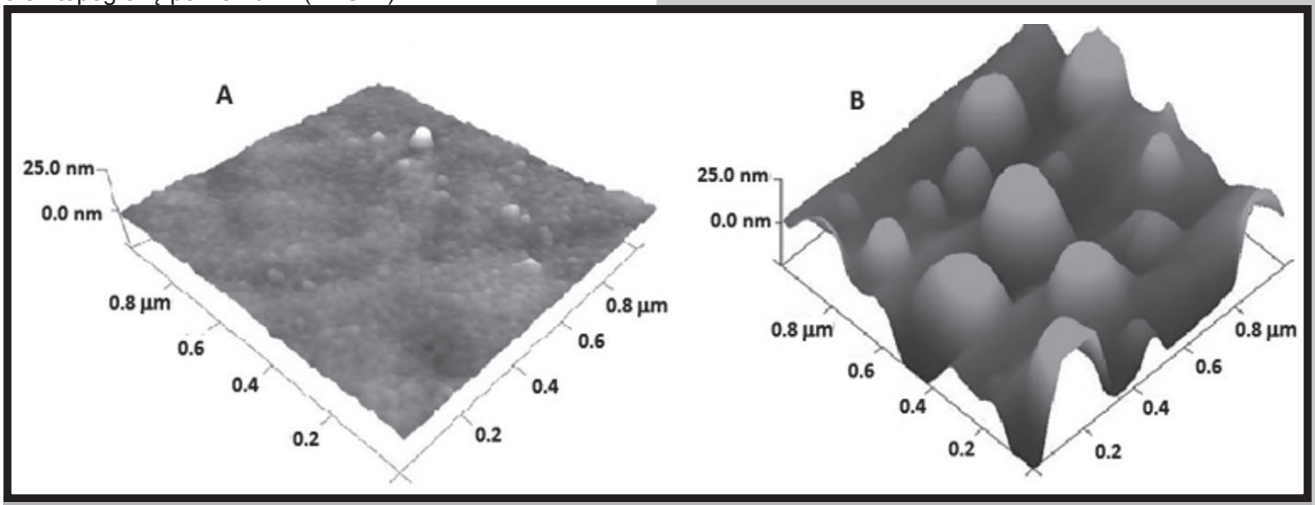

RYS. 1. Obrazy AFM warstw wytworzonych na powierzchni stopu Ni50,8 Ti49,2 w procesach jarzeniowych w atmosferze N_2+O_2 (10% obj.): A – warstwa azotowana i B – warstwa tlenoazotowana. Powiększenie –1 µm x 1 µm.
FIG. 1. AFM images of the nitride (A) and oxynitride (B) layers formed through glow discharge treatment on the surface of the Ni50,8 Ti49,2 alloy in the N_2+O_2 atmosphere (10 vol.%). Zoom - 1 µm x 1 µm.

Klamry z pamięcią kształtu po azotowaniu jarzeniowym uzyskały równomierną jasno-żółtą barwę, natomiast klamry po tlenoazotowaniu jarzeniowym barwę niebiesko-fioletową (RYS. 2).

Po azotowaniu i tlenoazotowaniu nastąpiło wyraźne podwyższenie temperatur odzysku kształtu klamer w porównaniu do temperatur odzysku kształtu klamer w stanie wyjściowym, po pasywacji w autoklawie w parze wodnej, o temperaturze 134°C, w czasie 30 minut (RYS. 3).

The staples after glow discharge nitriding obtained light yellow color while the staples after oxynitriding were blue (FIG. 2).

After nitriding and oxynitriding a distinct increase in temperature the shape recovery of staples as compared to the shape recovery temperature of staples in the initial state after passivation in steam autoclave, at a temperature of 134°C, for 30 minutes (FIG. 3).

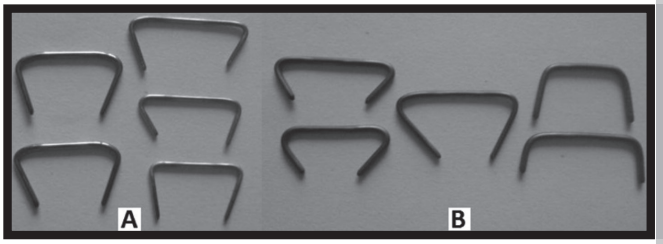

RYS. 2. Klamry NiTi z pamięcią kształtu do zespoleń złamań kości: A - po azotowaniu jarzeniowym, B - po tlenoazotowaniu jarzeniowym.
FIG. 2. NiTi shape memory staples for bone fracture fixation: A - after glow discharge nitriding, B - after glow discharge oxynitriding.

Podsumowanie

Przeprowadzone badania wpływu warunków technologicznych procesów azotowania i tlenoazotowania jarzeniowego (tj. temperatury, ciśnienia w komorze roboczej, składu mieszaniny gazowej, czasu obróbki) zarówno na potencjalne katody, jak i w plazmie, wykazały, że jednorodne warstwy azotku tytanu TiN, jak też warstwy TiO_2+TiN o grubości powyżej 20÷30nm oraz warstwy TiO_2 otrzymuje się prowadząc procesy na potencjale katody [6]. Wykorzystanie zjawiska rozpylania katodowego do podwyższenia aktywacji warstwy wierzchniej obrabianego stopu NiTi umożliwia wytwarzanie warstw azotku tytanu już w temperaturach około 300°C oraz przebieg reakcji utleniania w kontakcie z aktywną chemicznie niskotemperaturową plazmą. Topografię powierzchni warstw TiO_2+TiN można kształtować zarówno sposobem przygotowania powierzchni stopu NiTi (szlifowanie lub polerowanie), jak też poprzez wykorzystanie zjawiska rozpylania katodowego, a także odpowiedni dobór mieszaniny reaktywnej. Opracowane sposoby azotowania i tlenoazotowania wykorzystano do modyfikacji powierzchni klamer NiTi z pamięcią kształtu do zespoleń złamań kostnych. Klamry azotowane uzyskały jasnożółtą barwę natomiast klamry tlenoazotowane jednorodną barwę niebieską. Stwierdzono, że po obróbce jarzeniowej nastąpiło korzystne podwyższenie temperatury odzysku kształtu klamer w porównaniu z temperaturą odzysku kształtu klamer po pasywacji w autoklawie. Jest to związane z obniżeniem zawartości niklu w osnowie stopu z powodu procesu wydzielania cząstek Ni_4Ti_3 podczas obróbki jarzeniowej w temperaturze powyżej 300°C.

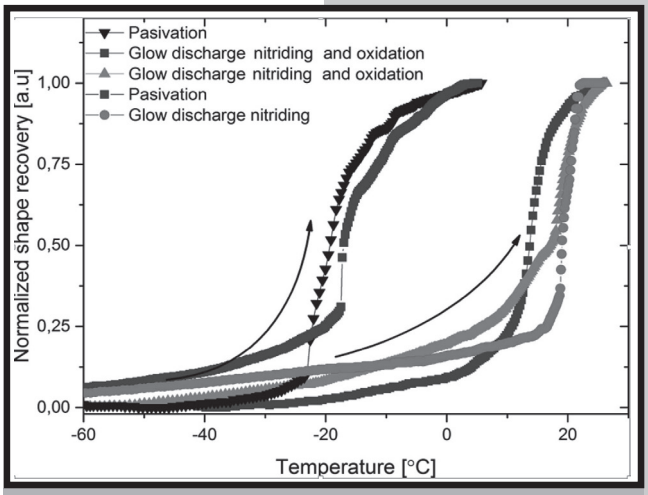

RYS. 3. Krzywe odzysku kształtu klamer NiTi po pasywacji w autoklawie oraz po azotowaniu i tlenoazotowaniu jarzeniowym.
FIG. 3. Shape recovery curves of pasivated staples and staples after nitriding and oxynitriding.

Podziękowania

W pracy wykorzystano wyniki badań finansowanych ze środków Narodowego Centrum Badań i Rozwoju w ramach projektu nr INNOTECH-K1/IN1/46/157239/NCBR/12.

Piśmiennictwo

[1] L.G. Machado, M.A.Savi., Medical applications of shape memory alloys. Brazilian Journal of Medical and Biological Research 36 (2003) 683-691
[2] T.Yoneyama, S.Miyazaki., Shape memory alloys for biomedical applications, Woodhead Publishing Limited, Cambridge, England (2009)
[3] H.Morawiec, Z.Lekston., Implanty medyczne z pamięcią kształtu. Wyd. Pol. Śl. Gliwice (2010)nanocomposites. Polymer Degradation
[4] J.Lelątko, T.Goryczka., Modyfikacja powierzchni stopów NiTi wykazujących pamięć kształtu. Wyd. Uniwersytet Śląski, Katowice (2013)

Summary

The research into the effects of technological processes of the glow discharge nitriding and oxynitriding (i.e. temperature, pressure in the working chamber, composition of the gas mixture, treatment time) on both the potential cathodes and in plasma, showed that a uniform layers of the TiN titanium nitride, as well as the TiO_2+TiN layers with the thickness of more than 20÷30 nm and TiO_2 layers are obtained by carrying out the processes on the potential of the cathode [6]. The use of cathode sputtering to increase the activation of the surface layer of the processed NiTi layer enables the manufacture the layers of titanium nitride at about 300°C, and oxidation in contact with a chemically reactive low temperature plasma. Surface topography of TiO_2+TiN layers can be formed both by the preparation of the NiTi alloy surface (grinding or polishing), and also by using cathode sputtering as well as an appropriate choice of a reactive mixture. The developed nitriding and oxynitriding methods are used to modify the surface of the NiTi shape memory clamps for the fixation of bone fractures. The staples that were nitrided were light yellow while the staples after oxynitriding were blue. It was found that the shape recovery temperature of the staples after the glow-discharge treatment is increase with comparisson to the shape recovery temperature of the passivation staples. It is related to the reduction of nickel in the matrix of the alloy due to precipitation process of Ni_4Ti_3 particles during glow-discharge treatment at about 300°C.

Acnowledgements

The study uses the results of the research funded by the National Centre for Research and Development under the project No. Innotech-K1/IN1 /46/157239/NRDC/12.

References

[5] J. Lelątko, Z. Lekston, T. Wierzchoń, T. Goryczka., Influence of Low Temperature Glow Discharge Nitriding and/or Oxiding Process on Structure and Shape Memory Effect in NiTi Alloy., Materials Science Forum 738-739 (2013) 344-347
[6] J.Kamiński, T. Borowski, M.Tarnowski, M.Ossowski, K.Rożniatowski, Z.Lekston, T. Wierzchoń., The influence of low temperature glow discharge assisted nitriding on corrosion resistance of NiTi shape memory alloy. Inżynieria Materiałowa 4 (2013) 1-4

CHARAKTERYSTYKA ANIZOTROPOWYCH WŁAŚCIWOŚCI MECHANICZNYCH SKÓRY ŚWINI

Sylwia Łagan*, Aneta Liber-Kneć

Politechnika Krakowska, Instytut Mechaniki Stosowanej,
Zakład Mechaniki Doświadczalnej i Biomechaniki,
ul.Warszawska 24, 31-155 Kraków
*e-mail: slagan@mech.pk.edu.pl

***Słowa kluczowe**: tkanka skórna, próbki zwierzęce, test rozciągania, linie Langer'a*
[Inżynieria Biomateriałów, 128-129, (2014), 61-63]

Wprowadzenie

Ludzka skóra stanowi kompleksową tkankę składającą się z kilku heterogenicznych warstw, epidermy, dermy i hipodermy, z których każda posiada unikalną strukturę i funkcję [1]. Skóra poddana działaniu naprężenia zachowuje się jak niehomogeniczny, anizotropowy, nieliniowy lepko-sprężysty materiał [2]. Właściwości mechaniczne skóry silnie zależą od topografii, czynników ryzyka, wieku, gatunku, środowiskowych czynników fizyko-chemicznych, tj. temperatura, ciśnienie osmotyczne, pH i szybkości odkształcenia [3,4].

Anizotropia skóry została rozpoznana w 19-stym wiku przez Karla Langera, który oznaczył naturalne linie napięcia, które pojawiają się w obrębie skóry [5]. Linie te pojawiają się, kiedy skóra zostanie punktowo naciśnięta przez okrągłe urządzenie. W tym przypadku włókna kolagenowe stają się równoległe do kierunku najmniejszego napięcia skóry, w końcu prowadząc do powstania eliptycznych szczelin. Kierunek tych szczelin odpowiada liniom Langera. Włókna elastyny i kolagenowe wzdłuż linii Langera są bardziej rozciągliwe niż prostopadłe do tych linii. Dlatego, rozciągliwość skóry jest niższa (i stąd wyższa sztywność) w kierunku tych linii [2,6].

Celem badań była ocena podstawowych właściwości mechanicznych skóry świni domowej, w zależności od kierunku pobrania próbek. Analiza literatury pokazuje, że w większości badań in vitro skóry wykorzystuje się substytuty w postaci skóry świni, która charakteryzuje się podobnymi właściwościami mechanicznymi do skóry ludzkiej lub substytuty syntetyczne, tj. silikon lub poliuretan [2,4,7].

Materiały i metody

Próbki do badań skóry zostały pobrane z grzbietu świni domowej (wiek 6 miesięcy) w trzech kierunkach (po 5 sztuk): wzdłużnym, poprzecznym i skośnym w stosunku do obwodu ciała. Wszystkie próbki miały wymiary: 100 mm długości i 10 mm szerokości, natomiast różniły się grubością, średnia jej wartość wyniosła 1,89±0,10 mm. Przed testami próbki były przechowywane (nie dłużej niz 12 godzin) w 0,9% roztworze soli fizjologicznej w temperaturze 4ºC. Dla próbek skóry oznaczono właściwości mechaniczne przy statycznym rozciąganiu z prędkością 5 mm/min na maszynie wytrzymałościowej MTS Insight 50. Baza pomiarowa próbki wynosiła 40 mm.

A CHARACTERISTIC OF ANISOTROPIC MECHANICAL PROPERTIEC OF A PIG'S SKIN

Sylwia Łagan*, Aneta Liber-Kneć

Krakow University of Technology,
Division of Applied Mechanics, Division of Experimental Mechanics and Biomechanics,
24 Warszawska Street24, 31-155 Krakow
*e-mail: slagan@mech.pk.edu.pl

***Keywords:** skin, animal specimens, mechanical properties, anisotropy, Langer's lines*
[Engineering of Biomaterials, 128-129, (2014), 61-63]

Introduction

The human skin is a complex tissue which consists of several heterogeneous layers: the epidermis, the dermis, and the hypodermis. Each layer has a unique structure and function [1]. The skin subjected to stress behaves like a non-homogeneous, anisotropic, and non-linear viscoelastic material [2]. The mechanical properties of the skin strongly depend on the topography, risk factors, age, species, physical and chemical environmental factors such as temperature, osmotic pressure, pH, and on the strain rate [3,4].

The anisotropy of the human skin was identified in the 19th century by Karl Langer who mapped the natural lines of tension which occur within the skin [5]. These lines appear when the skin is punctured by a round instrument. In this case, the collagen fibers of the mesh become aligned parallel to the direction of the least extensibility, eventually leading to elliptical clefts. The direction of these clefts corresponds to Langer's lines. The elastin and collagen fibers along Langer's lines are more stretched than those perpendicular to these lines. Therefore, the extensibility of skin is lower (thus its higher stiffness) in the direction of these lines [2,6].

The aim of the research was an evaluation of the basic mechanical properties of a pig's skin depending on the direction of sample taking. A professional literature analysis shows that substitutes like a pig's skin (which has similar mechanical properties to the human skin) or synthetic substitutes , e.g. silicon or polyurethane are used in the majority of in vitro skin tests [2,4,7].

Materials and methods

The samples for skin examinations were taken from the back of a 6-month old domesticated pig in three directions: parallel, perpendicular, and oblique (45°) in the reference to the short axis of the body (minimum 5 samples). All samples had the same dimensions: the length 100 mm and the width 10 mm, but different thicknesses. The average thickness was equal to 1.89± 0.10 mm. Until time of examination (no longer than 12 hours) samples were stored at 4ºC in 0,9% normal saline. The mechanical properties under static tension were determined with the use of the MTS Insight 50 testing machine extended samples at the speed of 5 mm/minute. The measurement base of the sample was 40 mm.

Na podstawie zarejestrowanych krzywych siła–wydłużenie oznaczono podstawowe właściwości mechaniczne skóry, tj.: wytrzymałość na rozciąganie (σmax), moduł Younga (E) oraz odkształcenie dla siły maksymalnej (ε). Wartość modułu Young'a została obliczona dla dwóch zakresów krzywej rozciągania: początkowego o niskim nachyleniu (E_1), w którym obciążenia są przenoszone przez włókna elastyczne [9] oraz środkowego prostoliniowego (E_2), dla którego za przenoszenie obciążeń odpowiadają włókna kolagenowe [9].

Wyniki i dyskusja

Skóra pobrana w trzech kierunkach wykazuje różne wartości wytrzymałości na rozciąganie, wartość naprężenia dla kierunku pobrania wzdłużnego wyniosła 15,72±0,54 MPa, poprzecznego 7,92±2,23 MPa i skośnego 3,01±0,93 MPa (RYS. 1). Wartość modułu Young'a, analogicznie jak wartość wytrzymałości na rozciąganie jest najwyższa dla próbek wzdłużnych, dla początkowego zakresu próby rozciągania wartość modułu (E_1) wyniosła 3,97±0,48 MPa, a dla liniowego odcinka krzywej rozciągania (E_2) 62,76±0,99 MPa. Dla kierunku pobrania próbek skośnego i porzecznego wartości modułów są na porównywalnym poziomie (RYS. 2).

Przegląd literatury wskazuje, że właściwości biomechaniczne skóry oznaczane są zarówno w badaniach in vivo jak i in vitro [2]. Porównując wyniki badań, zarówno z wynikami dla skóry świńskiej, jak i ludzkiej można zauważyć duże różnice w oznaczonych wartościach parametrów wytrzymałościowych [2,4,7]. Wynika to z czynników opisanych we wstępie.

On the basis of the recorded curves of the force–extension, basic skin mechanical properties, i.e. the tensile strength (σmax), Young's modulus (E), and the strain for a maximum force (ε) were determined. For the calculations, a rectangular cross section of the sample was taken. The value of Young's modulus was calculated for two ranges of the tension curve: the initial one with a low slope (E_1) in which loads are carried by elastic fibers [9], and the middle-rectilinear (E_2) in which loads are transported by collagen fibers [9].

Results and discussion

The skin taken in three directions reveals various values of tensile strength. The value of the stress for the parallel direction of taking (in the reference to the short axis of the body) equalled 15.72 ± 0.54 MPa, perpendicular 7.92±2.23 MPa, and oblique 3.01±0.93 MPa (FIG.1).

The value of Young's modulus, analogically to the value of tensile strength, is the highest for the parallel samples. For the initial stage of the tensile test, Young's modulus (E1) equalled 3.97 ± 0.48 MPa, and for the linear segment of the tensile curve (E2) it was 62.76 ± 0.99 MPa. For the oblique and perpendicular directions of sample taking, the values of the determined moduli are comparable (FIG. 2).

The literature review shows that the biomechanical properties of skin have been measured by both in vivo and in vitro tests [2]. No standard exist, thus study comparisons are difficult. While comparing the obtained test results to both the results for a pig's skin and for the human skin, great differences in the determined values of the strength parameters can be noticed [2,4,7]. This is due to the factors described in the introduction.

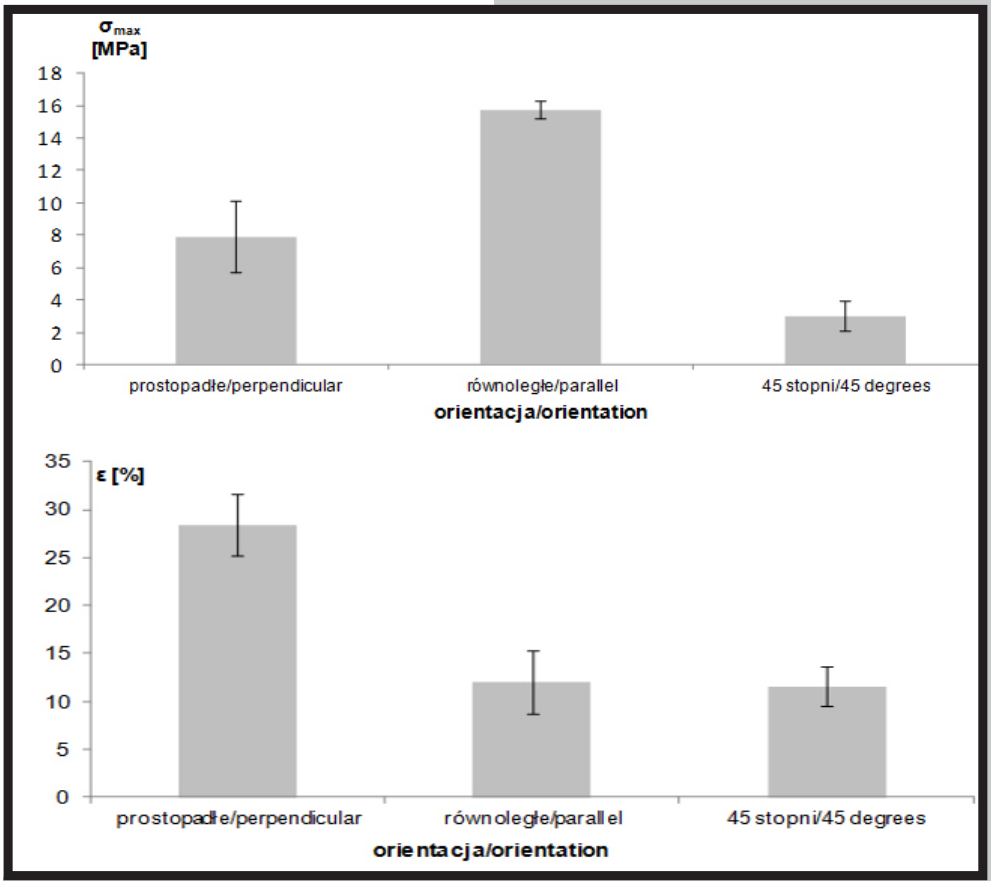

RYS. 1. Średnie wartości wytrzymałości na rozciąganie (σmax) i odkształcenia (ε) w zależności od kierunku pobrania.
FIG. 1. The average tensile strength values (σmax) and strain (ε) depending on the direction of sample taking.

Otrzymane wartości wytrzymałości i modułu sprężystości dla próbek skóry pobranych wzdłuż kręgosłupa świni różnią się znacznie od otrzymanych dla skóry świni przez Żak i wsp. [4], natomiast w pewnym zakresie wartości wytrzymałości na rozciąganie pokrywają się z otrzymanymi przez Lim, Hong i wsp. [7]. Przebieg jednoosiowego rozciągania próbek skóry świni zgadza się dobrze z próbkami skóry ludzkiej. Jednocześnie otrzymane zakresy wartości parametrów wytrzymałościowych skóry świńskiej korespondują z wartościami wytrzymałości skóry ludzkiej oznaczonej przez Ni Annaidh i wsp. [2] oraz Silver i wsp. [10].

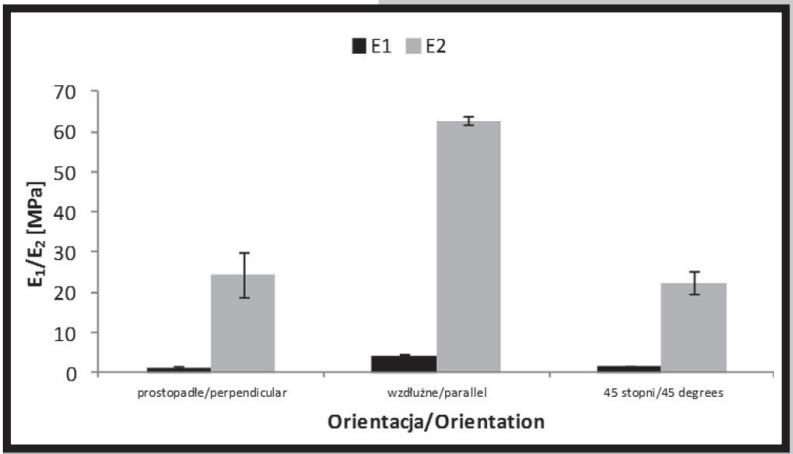

RYS. 2. Średnie wartości modułu Younga (E_1 i E_2) w zależności od kierunku pobrania próbki.
FIG. 2. The average Young's modulus (E_1 and E_2) depending on the direction of sample taking.

Wnioski

Odpowiedź skóry na obciążenia mechaniczne wykazuje wyraźnie jej lepko-sprężysty charakter. Energia dyssypacji, energia pochłaniania, energia zniszczenia, korelacja pomiędzy czynnikami reologicznymi, jak również poznanie parametrów mechanicznych skóry jest kluczowym dla oceny bezpieczeństwa organów i tkanek wewnętrznych, które skóra chroni przed urazami [10]. Obecnie opracowuje się matematyczne modele procesu wzrostu tkanek [11], czy ich regeneracji. Badania parametrów mechanicznych skóry pokazały, że wyniki znacząco zależą od orientacji włókien kolagenowych. Również sposoby, miejsca pobrania i przygotowania materiału badawczego wpływają na otrzymywane rezultaty [9,11]. Dane uzyskane w niniejszych badaniach dostarczają podstawowych informacji dla sformułowania strukturalnego modelu konstytutywnego skóry.

The obtained values of strength and modulus of elasticity for the skin samples taken along the pig's spine differ significantly from the values obtained for the pig's skin by Żak et al. who tested skin samples excised from different regions of the body [4]. However, the tensile strength values are equal in a certain range with the values obtained by Lim, Hong et al. [7].

The uniaxial tensile behavior of pig's skin obtained in this study agrees well with that of human skin. The stress versus strain curve up to maximal force is J-shaped, although slope of the curve may differ from species to species. The obtained ranges of strength parameter values of a pig's skin correspond with the strength value of the human skin determined by Ni Annaidh et al. [2] and Silver et al. [10].

Conclusions

The response of the skin to the mechanical loads clearly reveals its viscoelastic character. Dissipation energy, absorption energy, destruction energy, correlation between rheological factors, as well as researching skin mechanical parameters are crucial for the evaluation of the safety of the internal organs and tissues which are protected against injury by the skin [10]. From the point of view of an analogy between the human skin and a pig's skin mathematical models of a tissue growth process [11] or tissue regeneration are worked out in mechanics. In order to achieve this goal both quantitative and qualitative experimental research is necessary.

The methods, the spots from where the skin was taken, and the preparation of the researched material influence the obtained results [9,11]. The data obtained in this study will provide essential information for model the skin using a structural constitutive model.

Piśmiennictwo

[1] Pailler-Mattei C., Beca S., Zahouani H., In vivo measurements of the elastic mechanical properties of human skin by indentation tests, Medical Engineering & Physics, 2008, 30, 599-606.
[2] Ni Annaidh A., Bruyere K., Destrade M., Gilchrist M. D., Ottenio M., Characterizing the anisotropic mechanical properties of excised human skin, Journal of the Mechanical Behavior of Biomedical Materials, 2012, 5(1), 139-148.
[3] Lemaitre J., Handbook of Material Behavior. Non linear Models and Properties, 10.11. Biomechanics of soft tissue, Academic Press, USA, 2001, 1057-1070.
[4] Żak M., Kuropka P., Kobielarz M., Dudek A., Kaleta-Kuratewicz K., Szotek S., Determination of the mechanical properties of the skin of pig fetuses with respect to its structure, Acta of Bioengineering and Biomechanics, 2011, 13 (2), 37-43.
[5] Langer K., On the anatomy and physiology of the skin, British Journal of Plastic Surgery, 1978, 17(31), 93-106.

References

[6] Hendriks F.M., Mechanical behavior of human skin in vivo – a literature review, Nat. Lab. Unclassified report 820, Philips Research Laboratories, 2001, p. 52. 7] Lim J., Hong J., Chen W.W., Weerasooriya T., Mechanical response of pig skin under dynamic tensile loading, International Journal of Impact Engineering, 2011, 38, 130-135.
[8] Neligan P. C., Gurtner G. C., Plastic surgery. Principles, vol. 1, Elsevier, 2013, p. 306.
[9] Corr D., Hart D., Biomechanics of scar tissue and uninjured skin, Advances in Wound Care, 2013, 2, 2, 37-43.
[10] Silver F.H., Freeman J.W., DeVore D., Viscoelstic properties of human skin and processed dermis, Skin Research and Technology, 2001, 7, 18-23.
[11] Corr D.T., Gallant-Behm C.L., Shrive N.G., Hart D.A., Biomechanical behavior of scar tissue and uninjured skin in a porcine model, Wound Repair and Regeneration, 2009, 17, 250-259.

AKTYWNOŚĆ ANTYBAKTERYJNA DOMIESZKOWANYCH SREBREM POWŁOK TiO_2 WYTWARZANYCH METODĄ RF PECVD

Sławomir Owczarek[1], Anna Sobczyk-Guzenda[1], Hieronim Szymanowski[1]*, Lukas Volesky[2], Witold Jakubowski[1], Maciej Gazicki-Lipman[1]

[1]Politechnika Łódzka, Instytut Inżynierii Materiałowej, ul Stefanowskiego 1/15, 90-924 Łódź
[2]Uniwersytet Techniczny w Libercu, Instytut Nauki o Materiałach, ul. Studencka 2, 461-17 Liberec
*e-mail: Hieronim.szymanowski@p.lodz.pl

Streszczenie

W ramach pracy wykorzystano metodę RF PECVD (Radio Frequency Plasma Enhanced Chemical Vapour Deposition) do wytworzenia powłok TiO_2-Ag. Domieszkowanie ditlenku tytanu srebrem miało na celu intensyfikację właściwości fotokatalitycznych i bakteriobójczych wykazywanych przez ten materiał. Związkiem wyjściowym jonów srebra był acetyloacetonian srebra. Kontrola jego temperatury umożliwiła wytworzenie na podłożach krzemowych powłok o różnej zawartości srebra. Ze względu na to, że korzystny wpływ jonów srebra na powłokę TiO_2 występuje przy ich niskim stężeniu, sterowano temperaturą sublimatora w taki sposób aby zawartość Ag w powłoce nie przekraczała kilku procent. Tak wytworzone powłoki zbadano na spektrometrze EDX (Energy Dispersive X-Ray) pod kątem składu chemicznego. Analiza wyników dostarcza informacji o wprost proporcjonalnym wzroście udziału atomów Ag do wzrostu temperatury ich związku wyjściowego. Po naświetleniu powłok światłem z zakresu UV określono wartość fotozwilżalności przez wodę oraz przeżywalności bakterii E. coli na ich powierzchni. Z badań kąta zwilżania wynika, że zaledwie kilkuminutowe naświetlanie promieniowaniem UV może wystarczyć do uzyskania przez powłokę właściwości superhydrofilowych. Najsilniejszą zwilżalność powierzchni wykazuje powłoka o najmniejszej zawartości srebra (0,03%). W przypadku badań bakteriobójczych czas naświetlania (2 lub 4 min.) promieniowaniem UV nie wpływa w sposób istotny na wartość przeżywalności bakterii. Bardziej istotnym czynnikiem jest zawartość srebra w powłoce - zbyt duża ilość powoduje obniżenie właściwości bakteriobójczych.

Słowa kluczowe: *ditlenek tytanu, srebro, bakteriobójczość, RF PECVD*

[Inżynieria Biomateriałów, 128-129, (2014), 64-66]

Wprowadzenie

Powłoki antybakteryjne posiadają wiele zastosowań wpływających istotnie na poprawę warunków higienicznych a tym samym zdrowie ludzkie. Są one stosowane m. in. do pokrywania narzędzi medycznych, podłóg, armatury łazienkowej czy tkanin. Jednymi z najpopularniejszych czynników bakteriobójczych są: TiO_2, Ag, SiO_2, ZnO oraz nanorurki węglowe [1].

Srebro jest znane jako materiał bakteriobójczy od ok. 6000 lat. W przeszłości srebrne naczynia służyły do przechowywania wody czy wina, wykonywano z niego również sztućce.

ANTIBACTERIAL ACTIVITY OF Ag DOPED TiO_2 FILMS DEPOSITED BY RF PECVD METHOD

Sławomir Owczarek[1], Anna Sobczyk-Guzenda[1], Hieronim Szymanowski[1]*, Lukas Volesky[2], Witold Jakubowski[1], Maciej Gazicki-Lipman[1]

[1]Lodz University of Technology,
Institute of Materials Science and Engineering,
1/15 Stefanowskiego Str., 90-924 Lodz, Poland
[2]Technical University of Liberec,
Faculty of Mechanical Engineering,
2 Studentska Str. 461-17 Liberec, Czech Republic
*e-mail: hieronim.szymanowski@p.lodz.pl

Abstract

In present work RF PECVD (Radio Frequency Chemical Vapour Deposition) technique was used to prepare TiO_2-Ag coatings. The purpose of preparing silver doped titanium dioxide coatings was to step up photocatalytic and antibacterial properties of this substance. Silver acetylacetonate was the precursor of silver ions. Thanks to temperature control it was possible to prepare coatings of different Ag contain at silicon substrates. The temperature was controlled so that not to exceed a few percentage amount of silver in the coating, because its favourable influence on TiO_2 coatings exists when concentration of silver ions is low. Coatings were examined under EDX (Energy Dispersive X-Ray) spectrometer to check atomic contain of elements. The results show that the percentage of Ag atoms increases directly proportionally to the temperature increase of its precursor. After exposition to UV radiation the water photo hydrophillic and bactericidal properties of coatings were measured. The water contact angle measurements have shown that super hydrophillic properties were obtained just after few minutes of UV radiation exposition. The coating of lowest silver contain (0,03%) exhibit the lowest water contact angle. In case of bactericidal studies the time of UV radiation (2 or 4 minutes) does not influence much the bacteria survival rate. Silver content is a more important factor - to big amount causes decreasing of antibacterial properties of the coating.

Keywords: *titanium dioxide, silver, antibacterial properties, RF PECVD technique*

[Engineering of Biomaterials, 128-129, (2014), 64-66]

Introduction

There are many applications for antibacterial coatings that significantly improve hygienic conditions, what is important to human life. Such coatings ate used in covering medical instruments, floors, bathroom fittings or fabrics. One of the mostly used bactericidal agents are: TiO_2, Ag, SiO_2, ZnO and carbon nanotubes [1].

Antibacterial properties of silver have been known for about 6000 years. In the past silver vessels were used to store water and wine, cutlery was also made of silver. Hippocrates used silver to heal wounds [2]. In a contact with bacteria silver acts as catalyst which suppress the act of enzymes that are in charge of cellular respiration [3].

Titanium dioxide (TiO_2) exists in three polymorphic forms of which anatase is the one that exhibits very strong bactericidal properties. Under UV radiation a pair of electron and

Hipokrates stosował srebro do opatrywania ran [2]. Pierwiastek ten w kontakcie z bakterią działa jak katalizator hamujący działanie enzymów umożliwiających jej oddychanie [3].

Ditlenek tytanu (TiO_2) występuje w trzech odmianach polimorficznych, z których anataz prezentuje wyjątkowo silne działanie antybakteryjne. Pod wpływem promieniowania UV tworzy się para elektron – dziura elektronowa. Ich reakcja z wodą lub tlenem skutkuje powstaniem na powierzchni wolnych rodników, które mogą przerwać łańcuch DNA komórki bakteryjnej i tym samym doprowadzić do jej śmierci [4].

Domieszkowanie srebrem ditlenku tytanu prowadzi do zwiększenia jego aktywności fotokatalitycznej poprzez tworzenie pułapek elektronowych spowalniających proces rekombinacji pary elektron – dziura elektronowa [5]. Niniejsza praca obejmuje wytworzenie powłok TiO_2 domieszkowanych srebrem z wykorzystaniem techniki RF PECVD, a następnie ich zbadanie pod kątem składu atomowego, fotozwilżalności oraz bakteriobójczości.

Materiały i metody

Powłoki TiO_2-Ag naniesione zostały na podłoża krzemowe z wykorzystaniem metody RF PECVD przy mocy wyładowania jarzeniowego równej 300 W i czasie procesu 60min. Źródłem tytanu był ciekły czterochlorek tytanu ($TiCl_4$) znajdujący się w temperaturze 0ºC. Jako gazu nośnego dla tego związku użyto argonu w ilości 1,5 sccm. Tlen wprowadzony został do komory w postaci gazu w ilości 70 sccm. Jako źródło srebra użyto związku stałego acetyloacetonianu srebra, którego temperatura dla poszczególnych procesów wynosiła 40, 60, 80, 100 lub 120ºC. Ciśnienie w komorze w trakcie procesów wynosiło 0,24 Torr.

Pomiar atomowej zawartości poszczególnych pierwiastków w powłokach TiO_2-Ag, w zależności od temperatury acetyloacetonianu srebra), wykonano za pomocą spektrometru EDX.

Pomiar kąta zwilżania dla powłok o różnej zawartości srebra wykonany został na próbkach nienaświetlanych. Następnie pomiaru dokonywano co 5 minut na próbkach naświetlanych lampą UV o natężeniu 16 mW/cm^2. Cieczą zwilżającą była woda destylowana.

Badania przeżywalności bakterii przeprowadzono na bakterii Escherichia coli ze szczepu DH5α. Zawiesinę bakteryjną w ilości 20 µl naniesiono na powłoki, które naświetlone zostały następnie promieniowaniem UV o natężeniu 16 mW/cm^2. Dla każdego stężenia srebra w powłoce naświetlanie trwało 2 oraz 4 minuty.

Wyniki i dyskusja

W pomiarze składu elementarnego wykryto obecność takich pierwiastków jak srebro, tytan, tlen, węgiel i chlor. Na podstawie tych danych ustalono stosunek atomowej zawartości tlenu do tytanu, który wyniósł od 1,62 dla temperatury sublimatora 40ºC do 2,74 dla 120ºC. Z badań wynika, że zawartość tlenu i chloru w powłoce jest stała niezależnie od procesu i wynosi odpowiednio ok. 58% i 2 %. Zgodnie z oczekiwaniami wraz ze wzrostem temperatury sublimatora rośnie zawartość srebra w powłoce i wynosi 0,03; 0,67; 1,1; 3,8 oraz 7,56%. Tą samą zależność wykazują atomy węgla (wartości od 4,7 do 10,2%). Zmiana zawartości srebra i węgla w powłoce jest niwelowany przez zawartość atomów tytanu.

Zmiany kąta zwilżania w czasie naświetlania światłem UV dla powłok TiO_2-Ag przy trzech różnych stężeniach srebra przedstawiono na RYS. 1.

electron hole is created. Their reaction with water or oxygen creates free radicals, which are able to kill the bacteria by breaking its DNA structure [4].

Silver doping of titanium dioxide increases its photocatalytic activity by creating electron traps which increase recombination time of the electron - electron hole pair [5]. In current work silver doped TiO_2 coatings were prepared by RF PECVD technique. Their atomic content, photo hydrophillicity and bactericidal properties were measured.

Materials and methods

TiO_2-Ag coatings were deposited on silicon substrates by RF PECVD (Radio Frequency Chemical Vapour Deposition) technique at 300 W of glow discharge power and process duration of 60 minutes. Liquid titanium tetrachloride ($TiCl_4$) at the temperature of 0ºC was the source of titanium. As a carrier of this compound, argon in the amount of 1,5 sccm was used. The oxygen flow rate was 70 sccm. A constant state silver acetylacetonate was used as a source of silver. Its temperature was 40, 60, 80, 100 or 120ºC depending on the process. The pressure in the reactor chamber during processes was 0,24 Torr.

Atomic content of elements in the TiO_2-Ag coatings, prepared in processes of different silver acetylacetonate temperature, was measured by EDX (Energy Dispersive X-Ray) spectrometer.

For coatings of different silver amount which were kept in the dark, water contact angle was measured. The next measurements were made every 5 minutes of UV radiation of the intensity of 16 mW/cm^2. As a damping liquid a dehydrated water was used.

The bactericidal studies were conducted with the use of Escherichia coli bacteria, strain DH5α. A suspension of bacteria in the amount of 20 µl was put on the coatings, which were later radiated by UV light of the intensity of 16 mW/cm^2. The radiation took 2 and 4 minutes for each coating of different silver content.

Results and discussions

Atomic content studies have shown that such elements as: silver, titanium, oxygen, carbon and chloride are present in the coatings. On the basis of the results, an atomic content of oxygen to titanium was determined. It equals from 1.62 for 40ºC to 2.74 for 120ºC sublimator temperature. The content of oxygen and chloride in the coating is constant for every process and equals ca. 58% and 2% respectively. As expected, an increase of sublimator temperature causes an increase of atomic content of silver in the coating, which equals: 0.03; 0.67; 1.1; 3.8 and 7.56%. The same dependency is observed in case of atomic content of carbon (values from 4.7 to 10.2%). Changes in silver and carbon atoms content is equalized by the content of titanium atoms.

Water contact angle values, for TiO2-Ag coatings of different silver content, in function of UV radiation time are shown on FIG. 1.

The water contact angle of not radiated coatings varies from 90 to 100 deg depending on the process. The highest increase of photo hydrophillicity in case of all coatings was obtained during first 5 minutes of radiation. After 35 minutes of radiation the coating of the lowest silver content became super hydrophilic. For the other coatings the water contact angle decreased under 20 deg after 30 minutes.

Values of an average survival rate of bacteria after radiation for coatings of three different silver content is shown on FIG. 2.

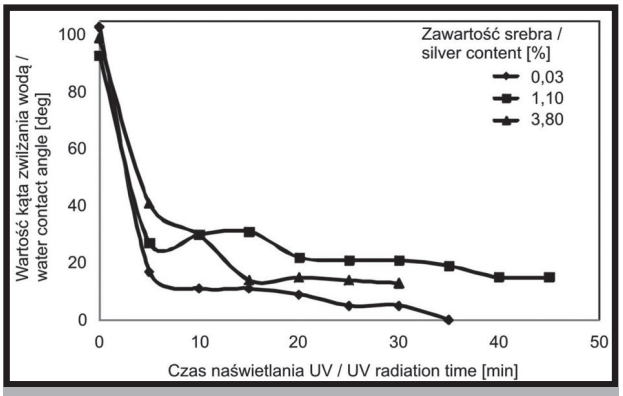

RYS. 1. Wpływ czasu naświetlania UV na wartość kąta zwilżania dla różnych stężeń srebra w powłoce TiO_2-Ag.
FIG. 1. An effect of UV radiation on water contact angle for different silver content in TiO_2-Ag coating.

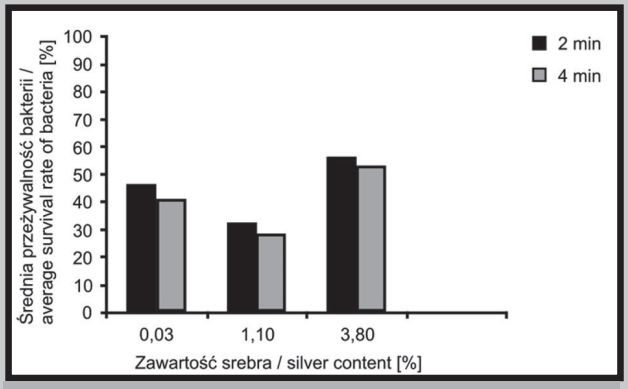

RYS. 2. Przeżywalność bakterii E. coli po 2 i 4 minutach naświetlania UV na powłokach TiO_2 o różnej zawartości srebra.
FIG. 2. An average survival rate of E. coli bacteria after 2 and 4 minutes of UV radiation on silver doped TiO_2 coatings of different Ag content.

Kąt zwilżania powłok nienaświetlanych wynosi od 90 do 100 deg w zależności od procesu. Największy wzrost hydrofilowości dla wszystkich powłok uzyskano w przeciągu pierwszych 5 minut naświetlania. Całkowite rozpłynięcie kropli uzyskano dla powłoki TiO_2 o najmniejszej zawartości srebra po upływie 35 minut od rozpoczęcia naświetlania. Dla pozostałych powłok kąt ten osiągnął wartość poniżej 20 deg po upływie 30 minut.

Zależność zmian przeżywalności bakterii po naświetlaniu powłok o trzech różnych stężeniach srebra przedstawia RYS. 2.

Najniższą przeżywalność wykazały powłoki TiO_2-Ag o zawartości srebra wynoszącej 0,03 i 1,1%. Przeżywalność bakterii na nich wyniosła poniżej 45%. Przeżywalność dla zawartości srebra 1,1% była niemal dwukrotnie niższa niż dla 3,80% zawartości tego pierwiastka w powłoce. Wydłużenie czasu naświetlania z 2 do 4 minut nie wpłynęło znacząco na poprawę efektu bakteriobójczości.

Wnioski

Wyniki przeprowadzonych badań pozwalają na sformułowanie następujących wniosków:

- możliwe jest wykonanie domieszkowanych srebrem powłok TiO_2 wykazujących właściwości fotokatalityczne i bakteriobójcze za pomocą techniki RF PECVD z wykorzystaniem związku stałego jako źródła domieszki.
- temperatura sublimatora wpływa bezpośrednio na ilość domieszki w powłoce.
- pomimo antybakteryjnych właściwości srebra najsilniejszy efekt bakteriobójczy zaobserwowano dla niskiej jego zawartości w powłoce (ok.1%).

Podziękowania

Badania przedstawione w niniejszej pracy były finansowane przez Narodowe Centrum Nauki w ramach grantu No N 508 482 638.

TiO_2-Ag coatings of 0.03 and 1.1% silver content exhibit the lowest survival rate of bacteria (lower than 45%). The survival rate for 3.8% content of silver was almost twice as big as for 1.1%. An increase of the radiation time from 2 to 4 minutes did not influence much the bactericidal effect.

Conclusions

From the results presented above the following conclusions are to be drawn:

- With the help of RF PECVD technique and use of constant state compound as a dopant source, it is possible to prepare silver doped TiO_2 coatings characterized with photocatalytic and bactericidal properties.
- The temperature of sublimator effects directly an amount of dopant in the coating.
- The strongest antibacterial activity was observed for low content of silver in the coating, although silver is known as a strong bactericidal element.

Acknowledgments

The work was supported by the National Science Centre in the framework of the project No N 508 482 638.

Piśmiennictwo References

[1] Duncan T. V.: Applications of nanotechnology in food packaging and food safety:barier materials, antimicrobals and sensors.Journal of Colloid and Interface Science 363 (2011) 1-24.
[2] Alexander W. J. : History of the medical use of silver. Surgical Infections 10(3) (2009) 289-292.
[3] Kong H., Jang J. : Antibacterial properties of novel poly(methyl methacrylate) nanofiber containing silver nanoparticles. Langmuir: The ACS journal of surfaces and colloids 24 (2008) 2051-2056.
[4] Kubacka A., Ferrer M., Martinez-Arias A., Fernandez-Garcia M.: Ag promotion of TiO2-anatase disinfection capability: study of Escherichia coli inactivation. Applied catalysis B: Enviromental 84 (1, 2) (2008) 87-93
[5] Seery M. K., George R., Floris P., Pillai S. C. : Silver doped titanium dioxide nanomaterials for enhanced visible light photocatalysis. Journal of Photochemistry and Photobiology A; Chemistry 189 (2-3) (2007) 258-263.

PODATNOŚĆ MODYFIKOWANYCH POWŁOK SiO_2 NA ZASIEDLENIE PRZEZ BAKTERIE

Katarzyna Porębska, Witold Jakubowski, Anna Sobczyk-Guzenda, Bożena Pietrzyk*

Instytut Inżynierii Materiałowej, Wydział Mechaniczny Politechniki Łódzkiej,
ul.Stefanowskiego 1/15, 90-924 Łódź
*bozena.pietrzyk@p.lodz.pl

Streszczenie

Zasiedlanie przez bakterie powierzchni różnych materiałów może być zarówno źródłem infekcji jak również stanowić przeszkodę dla prawidłowego funkcjonowania niektórych konstrukcji i urządzeń biomedycznych. Wytwarzanie powłok antybakteryjnych może być skuteczną metodą zabezpieczania powierzchni przed ich kolonizacją przez bakterie. W niniejszej pracy modyfikowane powłoki SiO_2 wytwarzano metodą zol-żel na podłożach szklanych i stalowych. Zole przygotowano na bazie tetraetoxysilanu (TEOS), modyfikując ich właściwości za pomocą methyltrimethoxysilanu (MTMS) i domieszki azotanu cynku. Właściwości antybakteryjne powłok sprawdzono poprzez zbadanie ich podatności na kolonizację przez bakterie Escherichia coli. Stwierdzono, że dodatek antybakteryjny w postaci azotanu cynku ogranicza podatność na zasiedlanie bakterii a hydrofobowość nie ma zasadniczego wpływu na poziom zasiedlenia bakterii E.coli.

Słowa kluczowe: *powłoki SiO_2, zol-żel, domieszkowanie Zn, powłoki antybakteryjne, powłoki hydrofobowe.*

[Inżynieria Biomateriałów, 128-129, (2014), 67-71]

Wprowadzenie

Większość powierzchni dotykowych może być źródłem drobnoustrojów i sprzyjać ich łatwemu przenoszeniu. Adhezja mikroorganizmów do powierzchni materiałów jest wstępnym warunkiem ich kolonizacji. Wynikiem kolonizacji powierzchni przez bakterie może być rozwinięcie się biofilmu bakteryjnego, stanowiącego źródło oportunistycznych infekcji towarzyszące stosowaniu tych materiałów [1]. Ponadto bakterie kolonizujące powierzchnie materiałów mogą powodować problemy w prawidłowym funkcjonowaniu konstrukcji inżynierskich, zwłaszcza biomedycznych [1]. Dlatego też bardzo pożądane jest uzyskanie takiej antybakteryjnej powierzchni, która byłaby w stanie zapewnić sterylność i w znacznym stopniu zminimalizować problem zakażeń, które spowodowane są tworzeniem się biofilmu bakteryjnego na różnych powierzchniach.

Przykładem tego typu antybakteryjnych powierzchni mogą być modyfikowane powłoki krzemionkowe. Powłoki te mogą pomóc w walce ze wzrastającą ilością problemów zdrowotnych spowodowanych niekontrolowaną i niechcianą ilością drobnoustrojów w otoczeniu.

Powłoki SiO_2 mogą być wytwarzane za pomocą wielu technik jak np. metody CVD i PVD [2], lecz także za pomocą metody zol-żel, która cieszy się coraz większym zainteresowaniem. Metoda zol-żel jest prosta (łatwe domieszkowanie), ekonomiczna (niski koszt wyposażenia) oraz efektywna - możemy uzyskiwać powłoki wysokiej jakości bez konieczności wygrzewania powłok.

THE SUSCEPTIBILITY OF MODIFIED SiO_2 COATINGS TO BACTERIAL COLONIZATION

Katarzyna Porębska, Witold Jakubowski, Anna Sobczyk-Guzenda, Bożena Pietrzyk*

The Institute of Materials Engineering,
Lodz University of Technology
1/15 Stefanowskiego Str., 90-924 Lodz, POland
*bozena.pietrzyk@p.lodz.pl

Abstract

Colonization of surfaces of materials by bacteria can be a source of infection, as well as an obstacle for the proper functioning of some of the biomedical equipment. Preparation of anti-bacterial coating may be an effective method of protecting of the surface prior to colonization by the bacteria. In this paper, modified SiO_2 coating have been prepared by the sol-gel method on glass and stainless steel substrates. As the precursor of sols tetraethoxysilan (TEOS) was used. The properties of sols were modified using additives of methyltrimethoxysilan (MTMS) and zinc nitrate. Antibacterial properties of coatings were determined by examining of their susceptibility to colonization by the bacteria Escherichia coli. It was found that the addition of zinc nitrate reduces the risk of bacterial colonization and hydrophobicity is not essential to the level of E. coli colonization.

Keywords: *SiO_2 coating, sol-gel, Zn doping, anti-bacterial coatings, hydrophobic coatings.*

[Engineering of Biomaterials, 128-129, (2014), 67-71]

Introduction

Most of the touched surfaces can be a source of microorganisms and can promote their easy transfer. Adhesion of microorganisms to the surface of materials is a prerequisite for their colonization. The result of bacterial colonization of the surface may be a bacterial biofilm development, acting as a source of opportunistic infections associated with the use of these materials [1]. Moreover, bacteria which exist on surfaces of materials can cause problems in proper functioning of engineering structures, especially biomedical [1]. Therefore, it is very desirable to obtain such antibacterial surface that would be able to ensure sterility and substantially minimize the problem of infections, which are caused by the formation of bacterial biofilm on various surfaces.

An example of this type of antimicrobial surface may be modified silica coatings. These coatings can help in the fight against the growing number of health problems caused by uncontrolled and unwanted amount of microorganisms in the environment.

SiO_2 coatings can be produced using a number of techniques, such as CVD and PVD [2], as well as sol-gel method, which is becoming more and more popular. Sol-gel method is simple (easy doping), economic (low cost equipment) and effective – high quality coatings can be obtained even without annealing process.

Sol to produce coatings are prepared by mixing the precursor with a solvent and a catalyst. The preparation of the sol occurs by a process: hydrolysis of the precursor and condensation of the hydrolysis products leading to the formation of Si-O-Si [3]. The condition for the success of the synthesis is a very thorough mixing of all components of [4].

Zol do wytworzenia powłok przygotowuje się przez zmieszanie prekursora z rozpuszczalnikiem i katalizatorem. Wytworzenie zolu zachodzi w wyniku procesów: hydrolizy prekursora i kondensacji produktów hydrolizy prowadzącej do wytworzenia wiązań Si-O-Si [3]. Warunkiem powodzenia syntezy jest bardzo dokładne wymieszanie wszystkich składników [4]. Następnym etapem jest nanoszenie otrzymanego zolu na podłoże. Na powierzchni, w wyniku procesów żelowania, uzyskuje się jednorodną powłokę, która poddawana jest suszeniu w temperaturze pokojowej.

Właściwości antybakteryjne powłok można zapewnić poprzez dodatek atomów cynku. Właściwości cynku koncentrują się na działaniu przeciwzapalnym, antybakteryjnym, antygrzybiczym oraz łagodzącym efekty podrażnień. Ponadto potwierdzono jego rolę w procesach regeneracji uszkodzeń tkanek powstałych wskutek ekspozycji na promieniowanie UV lub kontaktu ze substancjami o właściwościach toksycznych. Wykorzystywany jest także w organizmie w ochronie przed wolnymi rodnikami [5]. Cechą, która może wpływać na właściwości antybakteryjne jest także hydrofobowość. Większa hydrofobowość może powodować łatwiejsze usuwanie bakterii, wpływając przez to na zmniejszenie adhezji bakterii do różnych materiałów biomedycznych [6,7]. Modyfikacja powierzchni materiałów prowadząca do ograniczenia ich podatności na zasiedlenie bakteriami pozwoli na poprawę właściwości użytkowych materiałów.

Materiały i metody

Przygotowano następujące rodzaje zoli krzemionkowych:

a) Zol A wykonano poprzez rozpuszczenie tetraetoxysilanu (TEOS) w alkoholu etylowym i dodanie jako katalizatora hydrolizy kwasu solnego HCl (36%). Stosunki molowe składników TEOS/C_2H_5OH/HCl to 1:20:0,6.

b) Zol Ahydr wykonano poprzez dodanie methyltrimethoxysilanu (MTMS) do zolu A, tak by stosunek molowy TEOS/ MTMS wynosił 1:0,64. Przed dodaniem MTMS do zolu rozpuszczono go w małej ilości etanolu.

c) Zol AZn wykonano poprzez dodanie 0,5% azotanu cynku do zolu A

d) Zol AhydrZn wykonano poprzez dodanie 0,5% azotanu cynku do zolu Ahydr

Procent domieszki azotanu cynku był wyliczany przez ustalenie procentowego stosunku wagowego azotanu cynku do ogólnej masy zolu.

Przed nanoszeniem powłok zole starzono w temperaturze pokojowej przez pięć dni. Powłoki osadzono metodą wynurzeniową (dip-coating) poprzez zanurzenie podłoża w zolu, a następnie wynurzanie go ze stałą prędkością 0,2 mm/s. Po nałożeniu powłoki zostawiano do wysuszenia w temperaturze pokojowej. Jako podłoża używane były podstawowe szkiełka mikroskopowe oraz krążki ze stali austenitycznej 316L o średnicy 15 mm i grubości ok. 4 mm, które poddane zostały szlifowaniu, a następnie polerowaniu. Wszystkie podłoża przed procesem osadzania powłoki poddano myciu w alkoholu etylowym w myjce ultradźwiękowej.

Chropowatość powierzchni badano poprzez określanie parametrów Ra za pomocą profilometru Hommel Tester z detektorem Waveline -20. Pomiar prowadzono na odcinku pomiarowym 4,8 µm.

Kąt zwilżania powłok określano za pomocą urządzenia Kruss Easy Drop Contact Angle System. Kąt zwilżania definiowany jest jako kąt utworzony pomiędzy płaszczyzną szkła, na którym osadzono kroplę wody, a powierzchnią styczną do kropli w punkcie jej zetknięcia z powierzchnią szkła [8].

The next step is the application of sol on the substrate. Due to gelation processes on the surface, the uniform coating is obtained which is subjected to drying at room temperature.

Antibacterial properties of coatings can be achieved by the addition of zinc atoms. Function of zinc consist on an anti-inflammatory, antibacterial, and antimycotic effect as well as on mitigating of irritation. In addition, its role was confirmed in the regeneration of tissue damage resulting from exposure to UV radiation or contact with substances which are toxic [5]. The feature which can affect the antimicrobial properties is also hydrophobicity. Increased hydrophobicity may result in easier removal of bacteria, thereby affecting the reduction of bacterial adhesion to various biomedical materials [6,7]. Surface modification of materials leading to reduce their susceptibility to colonization of bacteria will improve the performance of materials.

Materiałs and methods

The following types of silica sols were prepared:

a) Sol A was prepared by dissolving tetraetoxysilanu (TEOS) in ethanol and adding hydrochloric acid HCl (36%) as hydrolysis catalyst. Molar ratios TEOS/C2H5OH/HCl was 1:20:0.6.

b) Sol Ahydr was made by adding of methyltrimethoxysilan (MTMS) to sol A, so that the molar ratio of TEOS/ MTMS was 1:0.64. MTMS was dissolved in a small amount of ethanol before adding to the sol

c) Sol AZn was made by adding 0.5% the nitrate zinc to sol A

d) Sol AhydrZn was prepared by adding 0.5% zinc nitrate for sol Ahydr.

The percentage of zinc nitrate admixture was calculated by determining the percentage weight ratio of zinc nitrate to the total weight of the sol.

Before deposition of coatings sols were aged at room temperature for five days. The coatings were deposited by dip-coating method. The substrate was immersed in the sol, and then emerged from it at a constant speed of 0.2 mm/s. After deposition the coating was allowed to dry at room temperature.As substrates glass microscope slides were used as well as a discs of 316L austenitic stainless steel with a diameter of 15 mm and a thickness of approx. 4 mm, which were subjected to grinding and polishing. All of the substrate prior to deposition of the coating was subjected to washing in ethanol in an ultrasonic bath.

The surface roughness was investigated by determining the parameters of Ra by profilometer Hommel Tester detector Waveline 20. The measurement was carried out at the measuring section 4.8 microns.

The contact angle of the coatings was determined by means of a Drop Easy Kruss Contact Angle System. The contact angle is defined as the angle formed between the plane of the glass, the deposited water droplet and the surface tangent to the drop at the point of contact with the glass surface [8].

Susceptibility to bacterial colonization Escherischia coli has been studied for the coatings prepared from sols A, Ahydr and for coatings with the corresponding sols modified with additions of zinc nitrate (sol AZN and AhydrZn). Bacteria in the amount of $2 \cdot 10^3$ cells were introduced into 200ml of YPG medium. Sample with coating were immersed in the medium and placed in the incubator (37°C) for 24 hours. After removal of samples from the incubator, non adherent bacterial cells were removed from the surface of samples by gently rinsing with physiological saline. Then applied to the surface of two kinds of fluorescent dyes (propydyne iodide and bis-benzimidyne) in order to distinguish between live and dead bacteria using a fluorescence microscope GX71.

Podatność na zasiedlenie bakterii Escherischia coli badano dla powłok wytworzonych z zoli A, Ahydr oraz dla powłok z analogicznych zoli modyfikowanych domieszkami azotanu cynku (zol AZn i AhydrZn). Bakterie w ilości $2*10^3$ komórek wprowadzano do 200 ml pożywki YPG. Próbki z powłoką zanurzono w pożywce i wstawiono do cieplarki (37°C) na 24 godziny. Po wyjęciu z cieplarki usunięto niezaadherowane komórki bakterii z powierzchni próbek przepłukując delikatnie solą fizjologiczną. Następnie nałożono na powierzchnię dwa rodzaje barwników fluorescencyjnych (jodek propydyny i bis-benzimidyna) w celu rozróżnienia bakterii żywych i martwych z wykorzystaniem mikroskopu fluorescencyjnego GX71. Próbkami odniesienia były odpowiednio stal 316L i szkło. Próbkę kontrolną stanowiło podłoże ze stali 316L (stosowane jako standard dla prowadzonych badań zasiedlania bakterii [9]).

Wyniki i dyskusja

Wyniki badań zdolności zasiedlania bakterii na powierzchniach powłok osadzanych na podłożach szklanych przedstawiono na RYS. 1. Badanie prowadzono dla powłok wytworzonych z zoli Ahydr, AZn i AhydrZn w odniesieniu do powierzchni czystego szkła. Próbkę kontrolną stanowiła polerowana powierzchnia stali 316L.

W przypadku powłok osadzonych na szkle stwierdzono, że powierzchnia niepokrytego szkła jest mniej podatna na zasiedlanie bakterii E. coli niż kontrolna powierzchnia stali, a ilość bakterii zaadherowanych do jego powierzchni wynosi około 65% ilości bakterii obserwowanych na powierzchni stali. Na powierzchni próbki z powłoką wytworzoną z zoli A i Ahydr ilość zasiedlonych bakterii jest wyższa niż na powierzchni szkła bez powłoki (około 90%). Wzrost ilości bakterii na powłoce SiO_2 (powłoka z zolu A) w porównaniu z podłożem szklanym, może wynikać ze wzrostu chropowatości powierzchni Ra, która wynosił dla szkła R_a=0,014 μm, natomiast dla wytworzonych powłok jest podobna i wynosi R_a=0,04 μm.

Stwierdzono, że na powierzchni powłoki wytworzonej z dodatkiem Zn (zol AZn) ilość obserwowanych bakterii jest niższa w porównaniu do powłok bez dodatku Zn. Jednak najniższy poziom kolonizacji przez bakterie uzyskano dla powłoki z zolu hydrofobizowanego i domieszkowanego azotanem cynku AhydrZn (około 15% w odniesieniu do kontroli). Zdolność zasiedlania powierzchni przez bakterie wiązana jest z wieloma czynnikami w tym także z oddziaływaniami hydrofobowymi [10]. Z przedstawionych wcześniej badań własnych wynika, że poziom zwilżalności nie ma zasadniczego wpływu na zachowanie bakterii na powierzchni powłok SiO_2 [1]. Jednak w przypadku powłok SiO_2 domieszkowanych Zn wzrost hydrofobowości poprawia właściwości antybakteryjne. Wyniki pomiarów kąta zwilżania badanych powłok przedstawiono na RYS. 2.

Reference samples were respectively 316L and glass. The control sample was a 316L stainless steel substrate (used as a standard for the study of bacterial colonization [9]).

Results and discussion

The results of the ability of bacteria to colonize surfaces of coatings deposited on glass substrates are shown in FIG. 1. The study was conducted for the coatings prepared from the sols Ahydr AZN and AhydrZn with respect to the surface of clean glass. The control sample was a polished surface steel 316L.

In the case of coating deposited on the glass, it was found that the uncoated surface of the glass is less susceptible to the colonization of E. coli to the control surface of the steel, and the amount of bacteria adhering to the surface is approximately 65% of the number of bacteria observed on the steel surface. On the surface of the sample with the coating formed from the sol A and sol Ahydr the number of adhered bacteria is higher than on the surface of uncoated glass (approximately 90%). Increase in the number of bacteria on a SiO_2 coating (coating sol A) compared to the glass substrate, may be due to the increase of surface roughness Ra. The roughness of glass was R_a=0.014 microns, while the roughness of produced coatings was similar and amount to R_a= 0.04 microns.

It was found that on the surface of the coating formed with the addition of Zn (sol AZn) number of bacteria observed is lower compared to the coating without the addition of Zn. However, the lowest level of colonization by bacteria was obtained for the coating deposited using sol AhydrZn (approximately 15% in relation to controls). The ability of bacterial colonization of the surface result of many factors among others including hydrophobic interaction also [10]. In the previously described studies was shown that the level of wettability is not substantially affect the behavior of bacteria on the surface of SiO_2 coating [1]. However, in the case of Zn-doped SiO_2 coatings increase the hydrophobicity improves the antibacterial properties. Results of contact angle measurements coatings tested are shown in FIG. 2.

Regardless of the number of bacteria adhering to the tested surfaces, it is also important to determine the share of live bacteria compared of total amount present on the surface. This is an indicator of toxic properties of the surface in relation to existing thereon microorganisms.

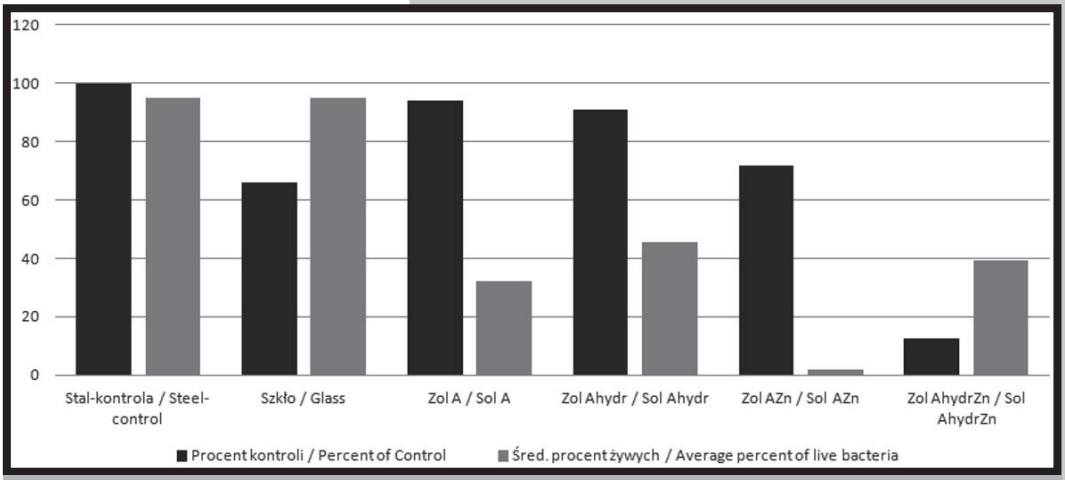

RYS. 1. Liczba bakterii na powłokach wytworzanych z zoli A, Ahydr, AZn i AhydrZn w porównaniu do stalowego i szkłanego podłoża.
FIG. 1. The number of bacteria on coatings produced with sol A, Ahydr, AZn i AhydrZn compared to steel and glass substrates.

Niezależnie od liczby bakterii zaadherowanych na powierzchniach badanych podłoży istotną informacją jest także określenie udziału bakterii żywych wśród wszystkich bakterii obecnych na powierzchni. Jest to wskaźnik toksycznych właściwości powierzchni w stosunku do obecnych na niej mikroorganizmów. Wszystkie otrzymane powłoki wykazywały właściwości podwyższonej toksyczności w porównaniu do powierzchni wyjściowej, jaką było czyste szkło (RYS. 1).

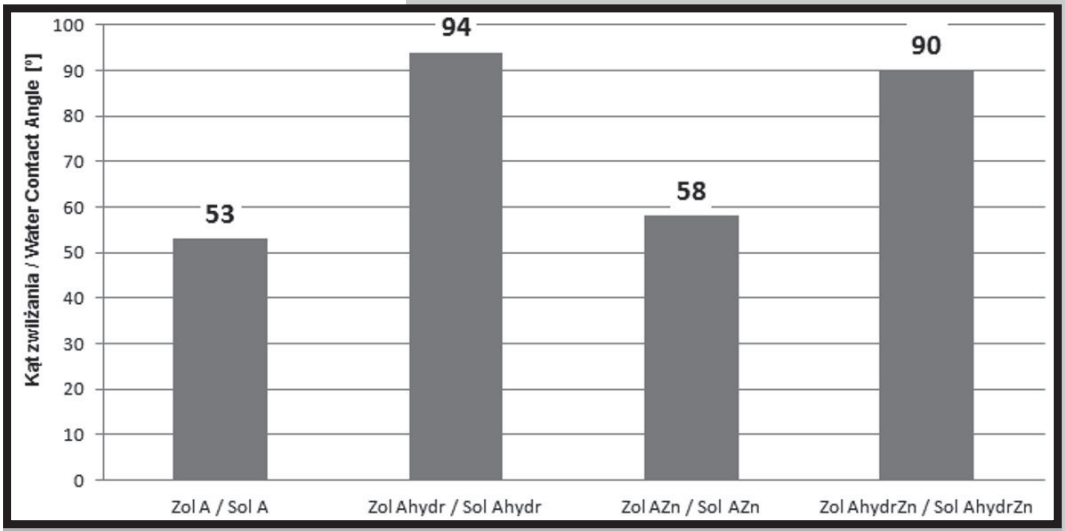

RYS. 2. Liczba bakterii na powłoce wytworzonej z zolu AhydrZn w porównaniu do stalowego podłoża wzorcowego.
FIG. 2. The number of bacteria on th coating procuded from sol AhydrZn compared to standard substrate steel.

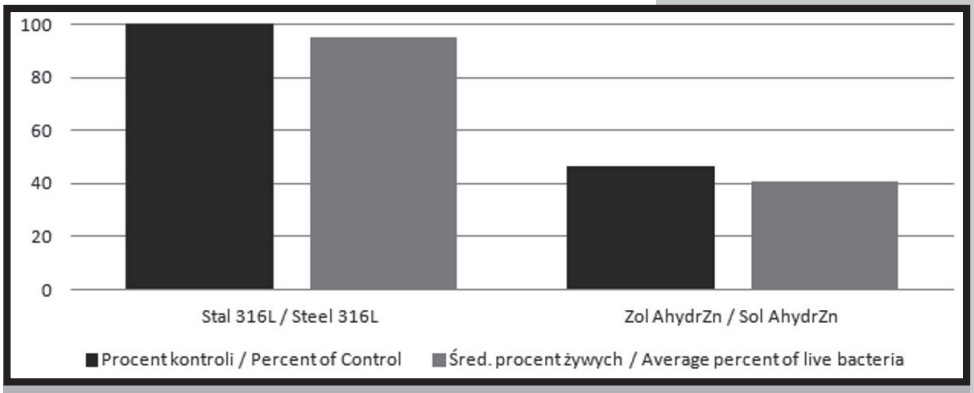

RYS. 3. Kąty zwilżania otrzymanych powłok.
FIG. 3. The contact angles of produced coatings.

Także w przypadku powłoki z zolu AhydrZn osadzonej na podłożu stalowym stwierdzono, że poziom zasiedlenia przez bakterie jest znacząco niższy w porównaniu do stalowej próbki wzorcowej i wynosi około 45%. Udział bakterii żywych dla tej powłoki jest również niższy niż dla stali 316L, co za tym idzie poziom toksyczności tej powłoki jest wyższy niż dla niepokrytej stali austenitycznej 316L. Wyniki tych badań przedstawiono na RYS. 3.

Podsumowanie i wnioski

W artykule przedstawiono badania dotyczące poziomu kolonizacji przez bakterie powłok krzemionkowych modyfikowanych za pomocą domieszkowania atomami Zn oraz dodatków zwiększających hydrofobowosc powłoki. Stwierdzono, że:

• Wzrost hydrofobowości powłoki SiO_2 nie ogranicza poziomu adhezji bakterii do powierzchni .

• Dodatek Zn (0,5%) obniża ilość bakterii na powierzchni w porównaniu z powłokami bez domieszki Zn.

• Najlepsze efekty ograniczenia ilości bakterii uzyskano dla powłok hydrofobowych z dodatkiem Zn (0,5%). Wpływ energii powierzchniowej na właściwości antybakteryjne powłok powinno być przedmiotem dalszych badań.

• Efekt ograniczenia ilości bakterii zaadherowanych do powierzchni powłok SiO_2 domieszkowanych Zn zaobserwowano na obu typach badanych podłoży

All the obtained coatings show high toxicity properties compared to the refer surface, which was clean glass (FIG. 1).

Also, in the case of coating of the sol AhydrZn deposited on a steel substrate, it was found that the level of colonization by the bacteria was significantly lower compared to the steel reference sample and amounted approximately 45%. Contribution of live bacteria on the coating is also less than on the surface of 316L stainless steel, thus the toxicity of the coating is higher than that of the uncoated 316L steel. The results of these tests are shown in FIG. 3.

Summary and conclusion

The article presents a study on the level of colonization by bacteria of silica coatings modified by doping Zn atoms and by additives that increase the hydrophobicity of the coating. It was found that:

• An increase in the hydrophobicity of the coating of SiO2 does not restrict the level of adhesion of bacteria to the surface.

• Addition of Zn (0.5%) lower the amount of bacteria on the surface when compared to coatings without dopant Zn.

• The best results of reduction the amount of bacteria on the surface was achieved on hydrophobic coatings containing Zn (0.5%). The influence of surface energy on the antibacterial properties of coatings should be the subject of further studies.

• The effect of limitation the amount of bacteria zaadherowanych to the surface of Zn-doped SiO_2 coatings were observed on both types of substrates examined

Piśmiennictwo

[1] Porębska K., Pietrzyk B., Jakubowski W. Podatność hydrofobowych powłok krzemionkowych na zasiedlenia bakterii Escherichia coli. Inżynieria Materiałowa nr 6/2013, str. 802-805
[2] Pulker H. Coatings on Glass. Elsevier Science B.V. Amsterdam 1999
[3] Kickelbick G. Hybrid Materials. Synthesis, Characterization, and Applications. Weinheim (2007), Rozdz. 1, 2.
[4] Wu L.Y.L., Tan G.H., Qian M. and Li T.H.. Formulation of transparent hydrophobic sol-gel hard coatings. SIMTech technical reports Volume 6 Number 2 Jul-Sep (2005), 1-4.
[5] Schoeder G. Nanotechnoligia, kosmetyki, chemia supramolekularna. Wydawnictwo Cursiva. 2010
[6] Sobolewska E., Frączak B., Błażewicz S., Seńko K., Lipski M. Porównanie kąta zwilżalności podstawowych materiałów protetycznych stosowanych w wykonawstwie protez ruchomych w badaniach in vitro. Protet. Stomat. LIX, 6 (2009) 401-406

References

[7] Yang H., Deng Y. Preparation and physical properties of superhydrophobic papers. Journal of Colloid and Interface Science 325 (2008) 588–593.
[8] Atkins P.W. Chemia fizyczna. Wydawnictwo Naukowe PWN. Warszawa 2012.
[9] Jakubowski W. Biofilm on biomateriale surface. NANODIAM, PWN Warszawa 2006, 189-197
[10] Doyle R.J. Contribution of the hydrophobic effect to microbial infection. Microbes and Infection (2000), 391-400
[6] Reguła T.: Badanie wpływu obróbki cieplnej na właściwości mechaniczne odlewniczego stopu AZ91, AGH im. Stanisława Staszica, Kraków, 2007.

HYDROŻELE KOLAGENOWE SIECIOWANE PRZY UŻYCIU KWASU SKWARYNOWEGO

Joanna Skopińska-Wiśniewska[1]*, Joanna Kuderko[1], Anna Bajek[2], Alina Sionkowska[1]

[1]Uniwersytet Mikołasja Kopernika, Wydział Chemiczny Gagarina 7, 87-100 Torun, Polska,
[2]Uniwersytet Mikołaja Kopernika Collegium Medicum, Karłowicza 24, 85-092 Bydgoszcz, Poland
*e-mail: joanna@chem.uni.torun.pl

[Inżynieria Biomateriałów, 128-129, (2014), 71-73]

Wstęp

Kolagen to jeden z najważniejszych biopolimerów. Występuje w skórze, kościach, mięśniach i wielu innych organach. Jest podstawowym skalnikiem macierzy zewnątrzkomórkwej (ECM) większości tkanek łącznych zapewniając im wytrzymałość mechaniczną. Białko to jest także, dobrze znane ze względu na inne właściwości, np. nietoksyczność, biozgodność z większością żywych organizmów i stosunkowo łatwą dostępność. Te cechy sprawiają, że kolagen znajduje szereg zastosowań w medycynie, farmacji i inżynierii tkankowej [1-3].

Sieciowanie jest metodą pozwalającą na modyfikowanie właściwości fizykochemicznych materiałów białkowych. Przez wiele lat przetestowano różnorodne czynniki sieciujące, jednakże badacze nadal poszukują nowych, bardziej efektywnych, a przede wszystkim bezpieczniejszych reagentów. Kwas skwarynowy to związek posiadający charakter aromatyczny. W jednej z form rezonansowych, ma dwa elektrony π i ujemny ładunek na każdym z karbonylowych atomów tlenu. W związku z tym, kwas ten łatwo ulega reakcjom z grupami aminowymi, co sprawia, że wykazuje on doskonałe właściwości sieciujące [4,5].

Celem badań było określenie wpływu dodatku 5%, 10% i 20% kwasu skwarynowego na właściwości materiałów kolagenowych.

THE USE OF SQUARIC ACID FOR CROSS-LINKING OF COLLAGEN MATRICES

Joanna Skopińska-Wiśniewska[1]*, Joanna Kuderko[1], Anna Bajek[2], Alina Sionkowska[1]

[1]Nicolaus Copernicus University, Faculty of Chemistry, 7 Gagarina Str., 87-100 Torun, Poland,
[2]Nicolaus Copernicus University, Collegium Medicum, 24 Karlowicza Str., 85-092 Bydgoszcz, Poland
*e-mail: joanna@chem.uni.torun.pl

[Engineering of Biomaterials, 128-129, (2014), 71-73]

Introduction

Collagen is one of the most important natural polymer. It is present in our skin, bones, muscles and other organs. It is a main component of extracellular matrix most of the connective tissues and provides them mechanical strength. This protein is widely known for its biological properties like non-toxicity, biocompatibility with all living organisms and easy availability. These attributes make the collagen ideal for many applications in medicine, pharmacy and tissue engineering [1-3].

The cross-linking is well known method of improving the physicochemical properties of protein materials. For many years various cross-linking factors have been tested. However, researcher still are looking for new, more secure reactants. Squaric acid, also called quadratic acid, is a molecule that has significant aromatic character. In one resonance form it has two π electrons and a negative charge on each of the carbonyl oxygen atoms, therefore the squaric acid willingly reacts with amino groups [4,5].

The main aim of our work was to determine the influence of 5%, 10% and 20% addition of squaric acid on the properties of collagen materials.

Materiały i metody

Z kolagenu wyizolowanego ze ścięgien ogonowych młodych szczurów albinosów sporządzono roztwór w 0,1 M kwasie octowym. Do próbek 1% roztworu kolagenu dodano odpowiednio 5%, 10% i 20% wagowych kwasu skwarynowego. Roztwory poddano dializie w tubach dializacyjnych względem wody dejonizowanej [3].

Wyniki i dyskusja

Sieciowanie przy użyciu kwasu skwarynowego w znaczący sposób wpływa na właściwości mechaniczne otrzymanych żeli kolagenowych. W wyniku tego procesu obniżeniu ulega wartość modułu sprężystości (TABELA 1). Najniższą sztywność wykazują próbki zawierające 20% kwasu skwarynowego, jednakże obserwowane zmiany nie są wprost proporcjonalne do ilości zastosowanego czynnika sieciującego.

Otrzymane materiały wykazują zdolność chłonięcia dużej ilości buforu fosforanowego (RYS. 1). Niemodyfikowane hydrożele kolagenowe absorbują około 3000% cieczy względem suchej masy materiału. Sieciowanie przy użyciu kwasu skwarynowego powoduje znaczne obniżenie stopnia spęcznienia badanych hydrożeli. Warto jednak zaznaczyć, że stopień spęcznienia wszystkich sieciowanych materiałów jest podobny, niezależnie od ilości zastosowanego czynnika sieciującego.

Właściwości powierzchniowe materiałów kolagenowych także ulegają zmianie na skutek sieciowanie przy użyciu kwasu skwarynowego (TABELA 2). Wartość swobodnej energii powierzchniowej oraz jej składowej dyspersyjnej wzrasta po dodaniu 5% i 10% czynnika sieciującego. Najwyższą wartość składowej polarnej swobodnej energii powierzchniowej zanotowano dla niemodyfikowanego hydrożelu, gdyż sieciowanie obniża polarność powierzchni badanych materiałów kolagenowych.

TABELA 1. Wartości modułu ściskania (E) dla hydrożeli kolagenowych.
TABLE 1. The values of compressive modulus (E) for collagen hydrogels.

Specimen/Próbka	E [kPa]
Coll	1.5286 ± 0.2770
Coll + 5% SqAc	1.0599 ± 0.3219
Coll + 10% SqAc	1.4176 ± 0.5737
Coll + 20% SqAc	0.9993 ± 0.5228

TABELA 2. Wartości swobodnej energii powierzchniowej (IFT) i ich składowych, polarnej i dyspersyjnej, dla materiałów kolagenowych.
TABLE 2. The values of surface free energy (IFT) and its dispersive and polar components of collagen samples.

Specimen/Próbka	IFT(s)	IFT(s,D)	IFT(s,P)
Coll	31.26	20.93	10.32
Coll + 5% SqAc	33.87	25.79	8.08
Coll + 10% SqAc	34.04	24.54	9.5
Coll + 20% SqAc	30.8	23.24	7.56

Materials and methods

The solution of collagen from tail tendons of young albino rats in 0,1M acetic acid was obtained in our laboratory. The 5%, 10% or 20% (weight percent based on the dry weight of the protein) of the squaric acid to 1% of collagen solution was add. Then the every mixture was poured into dialysis bag and neutralized during dialysis process against deionised water [3].

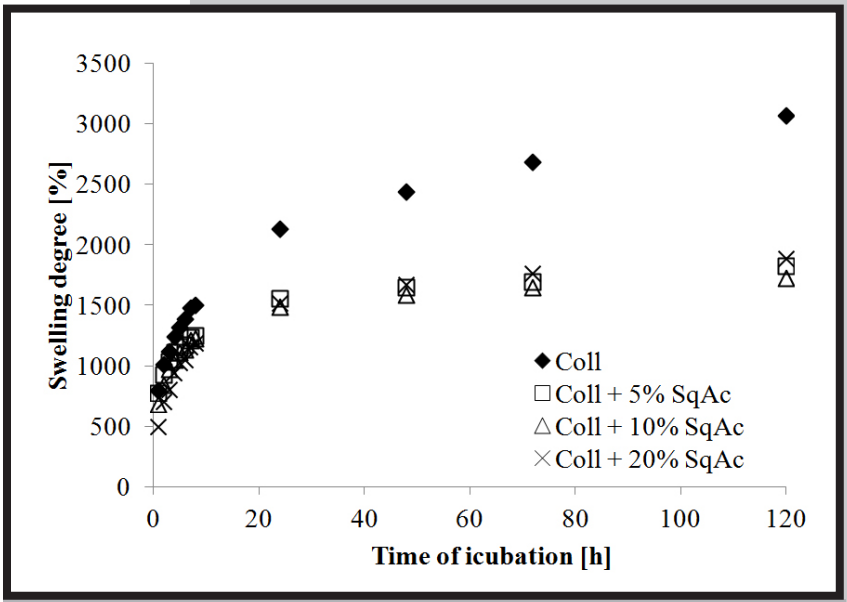

RYS. 1. Stopień spęcznienia E_s [%] żeli kolagenowych.
FIG. 1. The swelling degreeE_s [%] of collagen gels.

Results and discussion

The cross-linking by squaric acid significantly affects mechanical properties of the obtained collagen hydrogels. Unexpectedly, cross-linking process reduces the values of compression modulus (TABLE 1). The sample containing 20% of squaric acid exhibits the lowest stiffness. However, the changes are not directly proportional to the squaric acid content in the sample.

The obtained materials are capable of absorbing a large quantity of phosphate buffer (FIG. 1). The unmodified collagen hydrogel absorbs around 3000% of liquid. The addition of squaric acid causes significant decrease of swelling degree of the hydrogels. It is worth to notice, that the swelling ability of all cross-linked samples are similar, regardless of the amount of applied squaric acid.

The surface properties are modified by the cross-linking using squaric acid (TABLE 2). The surface free energy (IFT(s)) increases with the addition of 5% and 10% of the reagent, as well as the dispersive component of the IFT. The polar component of surface energy has the largest value in the case of pure collagen. The addition of the squaric acid cause a reduction of the surface polarity.

Wnioski

Przeprowadzone badania wykazały, że na skutek sieciowania przy użyciu kwasu skwarynowego właściwości hydrożeli kolagenowych ulegają znacznej zmianie. Obniżeniu ulega zdolność pęcznienia oraz polarność powierzchni. Jednocześnie, sieciowanie nie powoduje sztywnienia otrzymywanych żeli.

Podziękowania

Przeprowadzone badania były finansowane z grantu Narodowego Centrum Nauki (NCN, Poland, Grant no: UMO-2011/03/D/ST8/04600).

Conclusions

The our study showed that the properties of collagen gels were changing due to cross-linking by squaric acid. The swelling ability and the polarity of the surface decrease after cross-linking, but at the same time, the gels do not became stiffer.

Acknowledgements

The authors would like to thank the National Science Centre (NCN, Poland, Grant no: UMO-2011/03/D/ST8/04600) for providing financial support to this project.

Piśmiennictwo

[1] A.J.Bailey, Molecular mechanisms of ageing in connective tissues, Mechanisms of Ageing and Development, 2001, 122, 735-755
[2] A.Sionkowska, J.Kozlowska, Properties and modification of porous 3-D collagen/ hydroxyapatite composites, International Journal of Biological Macromolecules 2013, 52, 250-259
[3] J.Skopinska-Wisniewska, K.Olszewski, A.Bajek, A.Rynkiewicz, A. Sionkowska, Dialysis as a method of obtaining neutral collagen gels, Materials Science and Enginnering C, 2014, 40, 65-70

References

[4] M.B.Onaran, A.B.Comeau and C.T.Seto, Squaric Acid-Based Peptidic Inhibitors of Matrix Metalloprotease-1 (MMP-1), The Journal of Organic Chemistry, 2005, 70, 10792-10802
[5] A.L.Tatarets, I. A. Fedyunyaeva, E.Terpetschnig, L.D.Patsenker, Synthesis of novel squaraine dyes and their intermediates, Dyes and Pigments, 64 (2004) 125

WŁAŚCIWOŚCI I PARAMETRY PAMIĘCI KSZTAŁTU BIODEGRADOWALNYCH MIESZANEK OTRZYMANYCH Z KOPOLIMERU L-LAKTYD/ GLIKOLID I POLI(BURSZTYNIANU BUTYLENU)

Anna Smola[1]*, Piotr Dobrzyński[1,2], Michał Sobota[1], Natalia Śmigiel-Gac[2]

[1]Centrum Materiałów Polimerowych i Węglowych PAN,
ul. M. Curie-Skłodowskiej 34, 41-819 Zabrze
[2]Wydział Matematyczno-Przyrodniczy,
Akademia im. Jana Długosza w Częstochowie,
Al.Armii Krajowej 13/15, 42-200 Częstochowa
*e-mail: asmola@cmpw-pan.edu.pl

Streszczenie

W pracy przedstawiono wstępne wyniki badań nad otrzymywaniem i charakterystyką bioresorbowalnych mieszanek polimerowych L-laktydu-co-glikolidu z oligomerem bursztynianu butylu o zawartości 10, 20 lub 40 %w. Porównano własności termiczne, mechaniczne oraz parametry pamięci kształtu otrzymanych mieszanek jak i samego kopolimeru. Na podstawie przedstawionych wyników badań określono, że dodatek oligomeru prowadzi do obniżenia temperatury zeszklenia oraz zmniejszenia sztywności materiału, oraz poprawienia własności pamięci kształtu.

[Inżynieria Biomateriałów, 128-129, (2014), 73-76]

PROPERTIES AND SHAPE MEMORY BEHAVIOUR OF BIODEGRADABLE BLENDS BASED ON L-LACTIDE/ GLYCOLIDE COPOLYMER AND POLY(BUTYLENE SUCCINATE)

Anna Smola[1]*, Piotr Dobrzyński[1,2], Michał Sobota[1], Natalia Śmigiel-Gac[2]

[1]Polish Academy of Sciences,
Centre of Polymer and Carbon Materials
34 M. Sklodowskiej-Curie str., 41-819 Zabrze
[2]Jan Długosz University in Czestochowa, Institute of Chemistry, Environmental Protection and Biotechnology
13/15 Armii Krajowej Ave.., 42-200 Czestochowa
*e-mail: asmola@cmpw-pan.edu.pl

Abstract

The paper presents preliminary results on the preparation and characteristic of bioresorbable polymer blends of L-lactide-co-glycolide with oligo(butylene succinate) in ratios of 10, 20 and 40 %wt. Compared the thermo-mechanical properties and shape memory parameters of obtained copolymer and blends. On the basis of the results were determined that the addition of oligomer lead to reduction in glass transition temperature and to reduce the stiffness of the material, and to improve shape memory properties.

[Engineering of Biomaterials, 128-129, (2014), 73-76]

Wprowadzenie

Kopolimer L-laktyd-co-glikolid (PGLA) jest klasycznym materiałem, o doskonale poznanej biokompatybilności, stosowanym powszechnie w chirurgii małoinwazyjnej. Główną niedogodnością tego materiału jest stosunkowo wysoka temperatura wymagana do zainicjowania procesu powrotu do kształtu pierwotnego, co mocno ogranicza zastosowania tych polimerów w medycynie [1,2,3]. Poli(bursztynian butylenu) jest również poliestrem alifatycznym w pełni biodegradowalnym i biokompatybilnym [4]. W pracy przedstawiono możliwość otrzymania mieszanek PGLA z oligomerem bursztynianu butylenu (oBS), które wykazują interesujące własności fizykochemiczne, szczególnie w zastosowaniach tego materiału w kontrolowanym uwalnianiu leków, czy formowaniu bioresorbowalnych implantów o dużej elastyczności.

Materiały i metody

Metoda syntezy opartej na polimeryzacji otwarcia pierścienia (ROP) kopolimeru PGLA (85/15) w obecności niskotoksycznego inicjatora $Zr(acac)_4$ oraz otrzymywania oligomeru oBS polegająca na transestryfikacji diestru metylowego kwasu bursztynowego z 1,4-butandiolem została przedstawiona w naszych wcześniejszych pracach [5,6]. Wykorzystując PGLA otrzymano jego mieszaniny polimerowe z oligomerem oBS metodą wtrysku za pomocą mikro-wytłaczarki Haake MiniLab IIS (zestaw ślimaków stożkowych współbieżnych 100 obr./min, temperatura wytłaczania 180°C, ciśnienie wtrysku 300-600 bar). Skład otrzymanych mieszanek oznaczono na podstawie pomiarów protonowego rezonansu jądrowego NMR (Bruker Avans 600Mhz, rozpuszczalnik deuterowany chloroform). Analizę termiczną dokonano za pomocą różnicowej kalorymetrii skaningowej DSC (Du Pont1090B, kalibracja galem i indem, szybkość grzania 20°C/min). Badania mechaniczne wytrzymałości na rozciąganie materiałów przeprowadzono na maszynie wytrzymałościowej Instron 4200 (szybkość rozciągania 20 mm/min, rozstaw szczęk 50 mm). W celu scharakteryzowania parametrów efektu pamięci kształtu mierzono czas powrotu kształtki do kształtu pierwotnego (t_R) oraz stopień powrotu (RR). Kształtki rozciągano o 100% długości w temperaturze zeszklenia materiału. Kształt przejściowy utrwalany był poprzez ochłodzenie w temperaturze pokojowej. Po ponownym umieszczeniu kształtki w łaźni wodnej, w odpowiedniej temperaturze obserwowano przebieg procesu powrotu do kształtu permanentnego.

Wyniki i dyskusja

Założeniem pracy było sprawdzenie wpływu dodatku oligomeru oBS na właściwości termomechaniczne oraz parametry pamięci kształtu kopolimeru PGLA. W tym celu scharakteryzowano otrzymany oligomer oBS jak i kopolimer PGLA a następnie mieszaniny PGLA z oligomerem stosując dodatek 10, 20 i 40%. Właściwości termiczne wyznaczone za pomocą DSC dla oligomeru oBS przedstawiono w TABELI 1. Poliester ten wykazywał dużą semikrystaliczność. Na podstawie widma ^{1}H NMR, w wyniku analizy grup końcowych, wyznaczono masę molową oligomeru, równą 4000 Da.

Kolejno otrzymano mieszanki polimerowe PGLA z dodatkiem 10, 20 i 40% wag oligomeru BS, których skład i właściwości zebrano w TABELI 2. Rzeczywisty skład mieszanek wyznaczono na podstawie analizy widm 1H NMR.

Introduction

A copolymer of L-lactide-co-glycolide (PLGA) is a classic material with excellent biocompatibility, is commonly used in minimally invasive surgery. A major disadvantage of this material is relatively high temperature required to initiate the process to return to the programed shape, which severely limits the use of these materials in medicine application [1,2,3]. Poly(butylene succinate) is fully biodegradable and biocompatible aliphatic polyester too [4]. The paper presents the possibility of obtaining polymeric mixtures of PLGA with oligo(butylene succinate) (oBS), which exhibit interesting physico-chemical properties, especially in applications for controlled release of drugs, or the formation of bioresorbable implants with high flexibility and shape memory behavior.

Materials and methods

Copolymer PGLA (85/15) was obtained on the ring opening polymerization way in presence of low toxic initiator $Zr(acac)_4$ according to the method described previously [5]. Oligomer oBS was synthesized by transestrification of succinic acid methyl di-ester with 1,4-butanediol which was described detailed too [6]. The polymeric blends of PLGA with oligomer oBS was formed by extrusion with the device type Haake MiniLab IIS (synchronous conic screws 100 obr/min, temperature of extrusion 180°C, pressure of injection 300-600 bar). Composition of obtained blends was determined based on nuclear magnetic resonance measurements (Bruker Avans 600Mhz, deuterated chloroform solvent). Thermal analysis of formed materials was specified with using differential scanning calorimetry (DSC apparatus Du Pont1090B, calibration of gallium and indium, heating rate 20°C/min). Mechanical test of tensile strength was done on Instron 4200 (rate of stretching 20 mm/min, grip distance 50 mm). In order to determine the shape memory behavior basic parameters such as; time of returning to the original shape ($t_{R)}$ and shape recovery ratio (RR) were assigned. Before measurements, the blends in the form of dumbbells were stretched 100% in length at their glass transition temperature. Then temporary shape of samples was fixed by cooling at room temperature under constant stress. Return to the permanent shape was conducted in a water bath at suitable temperature.

Results and discussions

Objective of presented study was to examine the effect of the oligomer oBS addition on thermomechanical properties and shape memory parameters of PLGA copolymer. The resulting polyester oBS demonstrated high semi-crystallinity degree (TABLE 1). On the basis of the 1H NMR spectra, by analysis of end groups, molar mass of synthetized oligomer equal 4000 Da was determined.

Subsequently PLGA polymer blends was prepared with 10, 20 and 40 wt% oligomer BS, the composition and properties was listed in TABLE 2.

The second heating runs at 20°C/min after rapid cooling from melt (FIG. 1), shows glass transition temperature (TABLE 2). The actual glass transition temperatures are higher than the values calculated theoretically from the Fox equation [7]. The reason for this difference is the presence hydrogen bonding interactions between PLGA and oBS (which was confirmed by FTIR analysis). Single glass transition temperature which decreases with increasing amounts of added oligomer was shown by blends PLAGA with 10 and 20% oBS.

TABELA 1. Charakterystyka termiczna oligomeru BS.
TABLE 1. Characteristics of oligomer BS.

T_g [°C]	T_m [°C]	ΔH [J/g]
-27,5	115,6	79,2

Analizując II przebieg DSC prowadzony z szybkością grzania próbki 20°C/min, po jej uprzednim stopieniu i szybkim ochłodzeniu (RYS. 1) wyznaczono temperatury zeszklenia otrzymanych materiałów (TABELA 2). Wartości T_g wyznaczone za pomocą DSC są wyższe od obliczonych teoretycznie na podstawie równania Fox'a [7]. Powodem takiej różnicy jest występowanie, potwierdzonych badaniami FTIR oddziaływań typu wiązania wodorowe pomiędzy PGLA a oBS. Blendy z dodatkiem 10 i 20% oBS wykazują jedną temperaturę zeszklenia, która odpowiednio spada ze wzrostem ilości dodanego oligomeru. W przypadku mieszanki PGLA/oBS 60/40 występują dwie temperatury zeszklenia co może wskazywać na to, że otrzymana mieszanka polimerowa o tej zawartości o-PBS nie jest już w pełni kompatybilną. Dodatkowo materiał ten ma tendencję do krystalizacji związanej z obecnością tworzących się domen krystalicznych związanych z zwiększoną ilością bursztynianu butylenu. W TABELI 2 przedstawiono także właściwości mechaniczne omawianych materiałów. Testy mechaniczne prowadzono w temperaturze pokojowej oraz w temperaturze ciała królików (39°C) – modelu zwierzęcego w planowanych dalszych badaniach in vivo. Dla badanych mieszanek stwierdzono uelastyczniający wpływ dodatku oligomeru PBS, wraz ze wzrostem jego ilości w mieszance zanotowano zmniejszanie modułów Younga tego materiału oraz naprężeń w punkcie maksymalnego obciążenia.

In the case blend of a PLGA 60% wg. with oBS 40% wg. two glass transition temperature was observed, which may indicate that the resulting polymer mix is no longer fully compatible. In addition, this blend has a tendency to form the crystalline domains, which size increase with contain of butylene succinate. TABLE 2 shows also the mechanical properties of these materials. Mechanical tests were carried out at room temperature and body temperature of rabbits (39°C) - an animal model in the planned further studies in vivo.

Based on conducted studies it was found the flexibilizing effect of the oligomers addition. With increasing its quantities in blends, decrease of the Young's modules of the material and increase of maximal elongation was observed.

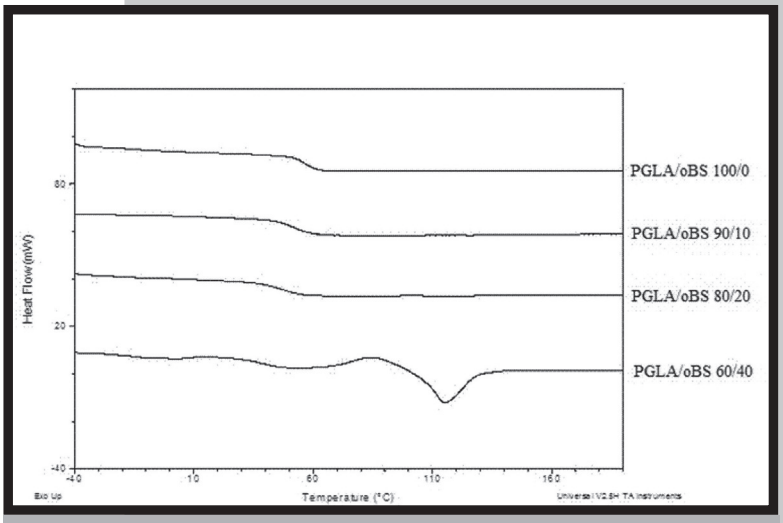

RYS. 1. Porównanie drugich przejść otrzymanych z DSC dla mieszanek PGLA/oBS. Szybkość ogrzewania 20°C/min.
FIG. 1. DSC second scans of PGLA/oBS blends with different composition at a heating rate of 20°C/min.

TABELA 2. Charakterystyka oraz własności mechaniczne mieszanek polimerowych PGLA/oBS.
TABLE 2. Characteristic and mechanincal properties of obtained blends.

Composition of blend / Skład blendy	Tg_1 [°C]	Tg_2 [°C]	T_{gT} [°C]	E_{25} [MPa]	σ_{25} [MPa]	E_{39} [MPa]	σ_{39} [MPa]
PGLA/oBS 100/0	56.5	-		2480±160	77±1	2020±30	58±0.1
PGLA/oBS 90/10	52.5	-	45.3	1968±117	72±0.9	1464±205	42±0.6
PGLA/oBS 80/20	47.0	-	35.4	1645±328	52±7.7	460±200	14±1.2
PGLA/oBS 60/40	-17.3	37.2	17.2	1504±11	49±2.3	255±30	14±0.9

TABELA 3. Charakterystyka oraz własności mechaniczne mieszanek polimerowych PGLA/oBS.
TABLE 3. Characteristic and mechanincal properties of obtained blends PGLA/oBS.

Composition of blend / Skład blendy	T_R [°C]	t_R [°C]	R_r [%]	V_R [%/s]	IRT [°C]
PGLA/oBS 100/0	48	2760	97.8	0.03	45
	52	420	98.8	0.23	
	56	30	99.8	3.33	
PGLA/oBS 90/10	42	3000	95.8	0.03	38
	47	1320	96.0	0.07	
	52	120	99.9	0.83	
PGLA/oBS 80/20	39	1800	54.0	0.03	36
	42	900	77.8	0.09	
	47	540	86.7	0.16	
PGLA/oBS 60/40	28	3000	21.5	0.01	27
	33	1680	26.6	0.02	
	38	1200	37.7	0.03	

Parametry charakteryzujące pamięć kształtu otrzymanych mieszanek przedstawiono w TABELI 3. Dodatek oBS do kopolimeru PGLA ma znaczny wpływ na zachowanie pamięci kształtu. Dla wszystkich materiałów najszybszy powrót do zaprogramowanego kształtu jak i jego największy stopień zachodzi w temperaturze zbliżonej do temperatury zeszklenia badanego materiału. Im większy dodatek oBS tym znacznie spada początkowa temperatura powrotu kształtu (IRT). W przypadku kopolimeru PGLA IRT wynosi 45°C a dodatek 20% oligomeru powoduje spadek tej temperatury do 36°C co jest bardzo korzystne z punktu widzenia zastosowań medycznych. Obecność oligomeru umożliwia także ułatwienie w nadawaniu kształtu tymczasowego, deformację próbki można prowadzić w niższych temperaturach, nawet poniżej temperatury otoczenia, wobec czego możliwym się staje uzyskanie wysokich wartości naprężeń podczas powrotu materiału do zaprogramowanego kształtu.

Wnioski

Na podstawie przedstawionych wyników wstępnych badań można określić, że dodatek oligomeru oBS do kopolimeru PGLA ma znaczny wpływ na temperaturę zeszklenia, sztywność materiału oraz parametry pamięci kształtu. Spośród przebadanych mieszanek, jako perspektywiczne w zastosowaniach biomedycznych są materiały PGLA/oBS o składzie 90/10 oraz 80/20. Mieszanki te wykazują kompatybilność składników, wykazują jedną tempereturę zeszklenia, a obserwacje mikroskopowe nie wykazują występowania wyraźnych granic poszczególnych faz. Zaobserwowane wyższe temperatury zeszklenia w porównaniu do temperatur wyznaczonych z klasycznego równania Fox'a związane są z silnymi oddziaływaniami międzycząsteczkowymi pomiędzy składnikami mieszanki, których istnienie potwierdziły nie przedstawione w tej pracy badania FTIR.

Podziękowania

Pracę wykonano w ramach projektu MNiSW Nr 2011/01/N/ST5/02257 „Wpływ struktury łańcucha, składu, wiązań wodorowych na właściwości bioresorbowalnych kopolimerów z pamięcią kształtu"

The parameters characterizing the shape memory obtained blends are shown in TABLE 3. Addition oBS to PLGA copolymer has a significant impact on the shape memory behavior. For all obtained blends, the fastest time of restoring the permanent shape and greatest shape recovery from the temporary stage occurs at a temperature close to the glass transition temperature. The larger addition of oBS decreases significantly the initial recovery temperature (IRT). In the case of PLGA copolymer IRT is 45°C, the addition of 20% of the oligomer resulted of the temperature decrease to 36°C which is very advantageous from the point of view of medical applications. The presence of the oligomer in blend facilitates of deformation of the sample and forming a temporary shape can be carried out at lower temperatures, even below the ambient temperature, so that it becomes possible to achieve a high stress during the return of the material to the permanent and previously programmed shape.

Conclusions

On the basis of obtained results it can be concluded that the addition of oligomer oBS to copolymer PLGA has major influence on glass transition temperature (Tg), stiffness of material and shape memory parameters. From examined blends, the materials PLGA/oBS of composition 90/10 and 80/20 are promising in biomedical application. The blends show compatibility of components, single Tg and additionally microscopic observations don't indicate the occurrence of clear boundaries individual phases. Higher glass transition temperatures, which were observed, in comparison with temperatures calculated with classic Fox equation, are associated with strong intermolecular interaction between components of blends, which existence was confirmed by FTIR.

Acknowledgments

A financial support has been provided by NCN, project No. 2011/01/N/ST5/02257 "Effect of chain structure, composition, the importance of hydrogen bonding on the properties of shape memory bioresorbable copolymers".

Piśmiennictwo

[1] Ignatius A.A., Claes L.E.: In vitro biocompatibility of bioresorbable polymers: poly(L, DL-lactide) and poly(L-lactide-co-glycolide). Biomaterials 17 (1996) 831-839.
[2] Athanasiou K.A., Niederauer G.G., Agrawal C.: Sterilization, toxicity, biocompatibility and clinical applications of polylactic acid/polyglycolic acid copolymers. Biomaterials, 172 (1996) 93-102.
[3] Pamuła E., Rutkowska M.M.: Hydrolytic and enzymatic degradation of poly(glycolide-co-L-lactide). Engineering of Biomaterials 47-53 (2005) 49-52.
[4] Ba C., Yang J., Hao Q., Liu X., Cao A.: Syntheses and physical characterization of new aliphatic triblock poly (L-lactide-b-butylene succinate-b-L-lactide)s bearing soft and hard biodegradable building blocks. Biomacromolecules, 4 (2003) 1827-1834.

References

[5] Dobrzynski P., Kasperczyk J., Janeczek,H., Bero, M.: Synthesis of biodegradable copolymers with the use of low toxic zirconium compounds. 1. Copolymerization of glycolide with L-lactide initiated by Zr(Acac)4. Macromolecules, 34 (2001) 5090-5098.
[6] Śmigiel N., Smola A., Janeczek H., Kasperczyk J., Dobrzyński P.: Synthesis and characterization of bioresorbable L-Lactide/Glycolide/Butylene succinate terpolymers with shape memory behavior. Engineering of Biomaterials, 114 (2012) 15-20.
[7] Brostow W., Chiu R., Kalogeras I.M., Vassilikou-Dova A.: Prediction of glass transition temperatures: Binary blends and copolymers. Materials Letters, 62 (2008) 3152-3155.

MICROSTRUCTURE AND PROPERTIES OF ALLOYED SILVER-GOLD NANOPARTICLES

O.Prymak[1], S.Ristig[1], W.Meyer-Zaika[1], D.Raabe[2], M.Epple[1]

[1]Institute of Inorganic Chemistry and Center for Nanointegration Duisburg-Essen (CeNIDE), University of Duisburg-Essen, Essen, Germany
[2]Microstructure Physics and Alloy Design, Max-Planck-Institut für Eisenforschung, Max-Planck-Str. 1, 40237 Düsseldorf, Germany

Abstract

Alloyed silver-gold nanoparticles recently raised an interest in biomedicine as potential antibacterial and surface-functionalized agents for imaging, drug-delivery, and tumor thermo-therapy [1,2]. The here synthesized alloyed AgAu nanoparticles with different compositions of silver and gold, as determined by atomic absorption spectroscopy (AAS), were prepared by reduction with citrate and tannic acid in aqueous media and subsequently functionalized by the addition of polyvinylpyrrolidone (PVP) [3]. UV spectroscopy confirmed that the particles consisted of alloyed Ag:Au and are not of a separate core-shell structure. The resulting nanoparticles were monodisperse and had a uniform size of ~6 nm, except pure Ag and Ag:Au-90:10, as shown by differential centrifugal sedimentation (DCS) and transmission electron microscopy (TEM). By means of X-ray powder diffraction (XRD) and use of Rietveld refinement [4], the precise lattice parameters, crystallite size and microstrain were determined. Based on the results by XRD, DCS and TEM it was shown, that the nanoparticles were not twinned, except pure Ag and Ag:Au-90:10. Additionally, a distinct deviation from Vegard's linear rule of alloy mixtures for the lattice parameter was found for the nanoparticles. This effect was also found for AgAu bulk materials, but was much more pronounced in the nanostate. Further investigations of the crystal structure of the alloyed nanoparticles by means of synchrotron radiation might be helpful to gain more information about the interactions of silver and gold atoms.

[Engineering of Biomaterials, 128-129, (2014), 77]

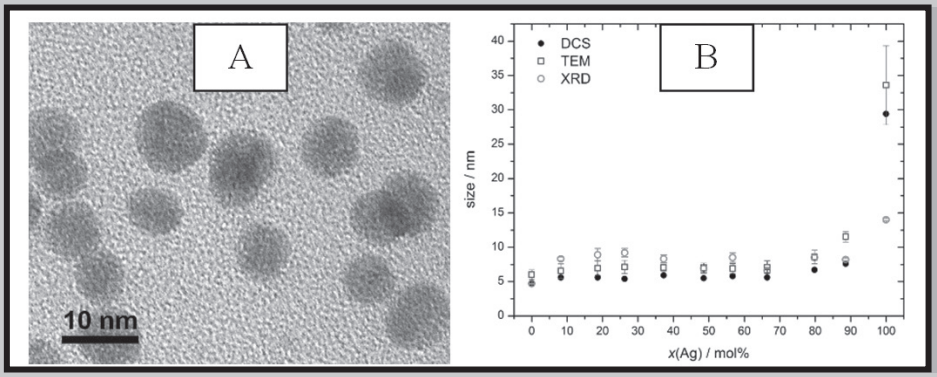

FIG. 1. (A) Representative TEM image of Ag:Au-40:60 nanoparticles, stabilized with PVP and (B) average particle size from DCS (hydrodynamic diameter), TEM (metallic core), and XRD (crystallite size).

References

[1] S. Chernousova, M. Epple, Angewandte Chemie International Edition 52 (2013) 1636
[2] D. Giljohann, D. Seferos, W. Daniel, M. Massich, P. Patel, C. Mirkin, Angewandte Chemie International Edition 49 (2010) 3280
[3] D. Mahl, J. Diendorf, S. Ristig, C. Greulich, Zi-An Li, M. Farle, M. Köller, M. Epple, Journal of Nanoparticle Research 14 (2012) 1153
[4] O. Prymak, S. Ristig, W. Meyer-Zaika, A. Rostek, L. Ruiz, J.M. Gonzalez-Calbet, M. Vallet-Regi, M. Epple, Russian Physics Journal 10 (2014) 1111

CALCIUM PHOSPHATE NANO-PARTICLES FOR DELIVERING SYNTHETIC DRUG MOLECULES ACROSS THE CELL MEMBRANE

O.Rotan[1], V.Sokolova[1], T.Schrader[2], M.Epple[1]

[1]Institute for Inorganic Chemistry and Center for Nanointegration, University of Duisburg-Essen, Universitätsstr.7, 45117 Essen, Germany
[2]Institute of Organic Chemistry, University of Duisburg -Essen, Universitätsstr.7, 45117 Essen, Germany

[Engineering of Biomaterials, 128-129, (2014), 77-78]

Introduction

Many synthetic drug molecules have their targets sites inside the cells. Typically, large molecules are not able to cross the cell membrane on their own and in order to bring them across it, an efficient carrier is needed [1]. We have loaded calcium phosphate nanoparticles with different synthetic drug molecules, i.e. a polyfunctional anionic polymer, a cationic calixarene dimer and a molecular tweezers. A polyfunctional anionic polymer was developed for selective inhibition of lysozyme as a model of enzyme inhibition [2]. A calixarene dimer due to its chemical and topological characteristics has the ability to specifically bind to the major groove of the DNA molecule that result in cell death [3]. Molecular tweezers inhibit the specific protein-protein interactions that lead to the formation of amyloidogenic aggregates inside the cells[4]. These aggregates are the cause of multiple incurable diseases, for example, Alzheimer's disease, Parkinson's disease and type-2 diabetes [5].

Materials and methods

Calcium phosphate nanoparticles were prepared by rapid precipitation, followed by functionalization with drug molecules. The polyfunctional anionic polymer and the cationic calixarene dimer were highly charged and therefore able to colloidally stabilize the nanoparticles. In the case of the molecular tweezers, first the cationic polymer polyethyleneimine (PEI) was adsorbed onto the nanoparticle surface, and then the molecular tweezers themselves. Afterwards, all particles were ultracentrifuged to separate them from dissolved counter-ions and non-adsorbed molecules and subsequently redispersed in pure water.

All nanoparticle dispersions were characterized by dynamic light scattering (DLS), nanoparticle tracking analysis (NTA), and scanning electron microscopy (SEM). By means of quantitative UV spectroscopy the amount of the fluorescing synthetic molecules on the nanoparticles was estimated.

The cell experiments were carried out on the HeLa cell line. The cells were incubated with the drug-loaded nanoparticles as well as with controls (the same concentration of the drug molecules dissolved in water, but without calcium phosphate nanoparticles). For quantifying the viability of the cells after incubation the MTT test was performed. Light and fluorescence microscopy along with confocal laser scanning microscopy were used to determine the uptake efficiency.

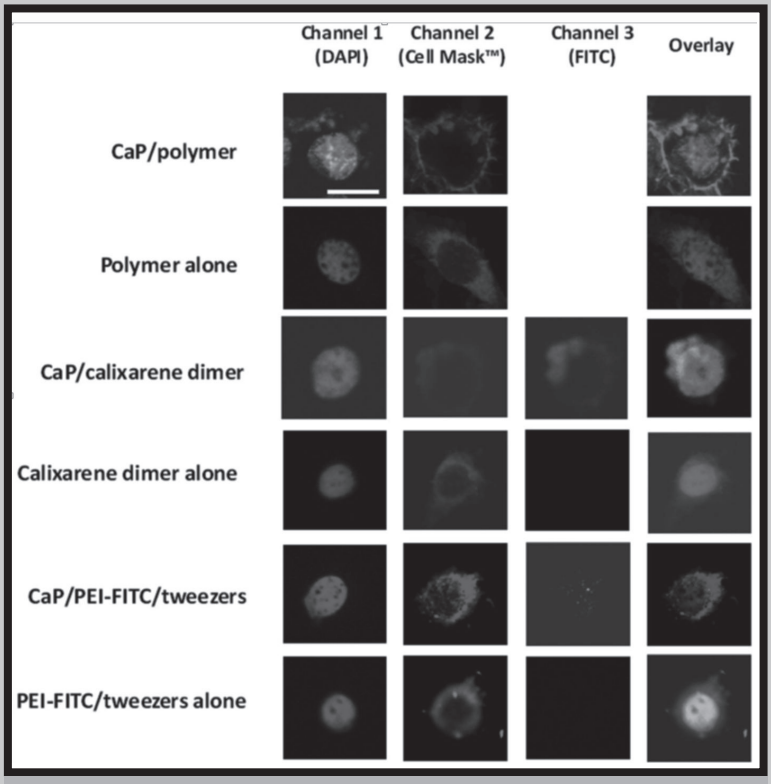

FIG. 1. Confocal laser scanning microscopy micrographs of HeLa cells after 3 h incubation with functionalized calcium phosphate nanoparticles and with the dissolved drug molecules. The blue channel represents the cell nucleus (DAPI) and the polymer, the red channel represents the cell membrane stained with Cell MaskTM, and the green channel represents the calixarene dimer and FITC-PEI/tweezers. Scale bar is 5 µm.

Results

The functionalized nanoparticles had spherical morphology with the size of 150-200 nm. The UV-spectroscopy data showed that, the amount of adsorbed drug molecules on the nanoparticles was between 22 and 51% of the initially present amount of drug molecules. The MTT test showed no toxic effects for the cells after interaction with the drug-loaded nanoparticles as well as with dissolved molecules, except for the ones with calixarene dimer. These results are in accordance to the purpose of the used molecules. The results of the uptake investigations (FIG. 1) had shown that together with calcium phosphate nanoparticles, all three drug molecules were easily detectable inside the cells, whereas the synthetic molecules alone were not taken up by cells [6].

Conclusions

We have shown the loading of calcium phosphate nanoparticles with three chemically different synthetic drug molecules. Fluorescence microscopy and confocal laser scanning microscopy showed that the functionalized calcium phosphate nanoparticles were easily taken up by HeLa cells after three hours incubation, whereas the dissolved drug molecules were not able to penetrate the cell membrane. We conclude that drug-loaded calcium phosphate nanoparticles represent a suitable carriage system for such molecules into the cell where they can exert their therapeutic action.

References

[1] V.Sokolova, O. Rotan, J.Klesing, P.Nalbant, J.Buer, T. Knuschke, A.Westendorf, M.Epple, Calcium phosphate nanoparticles as versatile carrier for small and large molecules across cell membranes. J. Nanopart. Res, 2012, 14, 910.
[2] K.Wenck, T.Schrader, A noncovalent switch for lysozyme. J. Am. Chem. Soc. 2007, 129, 16015-16019.
[3] W.Hu, C.Blecking, M.Kralj, L.Šuman, I.Piantanida, T.Schrader, Dimeric calixarenes – a new family of major groove binders. Chem. Eur. J. 2012, 18, 3589-3597.
[4] P.Talbiersky, F.Bastkowski, F.-G.Klärner, T.Schrader, Molecular clip and tweezer introduce new mechanisms of enzyme inhibition. J. Am Chem. Soc. 2008, 130, 9824-9828.
[5] S.Dutt, C.Wilch, T.Schrader, Artificial synthetic receptors as regulators of protein activity. Chem. Commun. 2011, 47, 5376-5383.
[6] O.Rotan, V.Sokolova, P.Gilles, W.Hu, S.Dutt, T.Schrader, M.Epple, Transport of supramolecular drugs across the cell membrane by calcium phosphate nanoparticles. Mat.-wiss. u.Werkstofftech. 2013, 44, 176–182.

INFLUENCE OF STRUCTURE AND SURFACE OF TERPOLYMER MATRICES ON RISPERIDONE RELEASE

Artur Turek[1,2]*, Janusz Kasperczyk[1,2], Aleksandra Borecka[1], Bartosz Warwas[2], Joanna Jaworska[1], Małgorzata Pastusiak[1], Piotr Dobrzyński[1], Henryk Janeczek[1], Marcin Libera[1]

[1]Centre of Polymer and Carbon Materials,
Polish Academy of Sciences,
34 M.Curie-Sklodowskiej Street, 41-819 Zabrze, Poland
[2]Medical University of Silesia in Katowice,
Faculty of Pharmacy, Department of Biopharmacy,
8 Jedności Street, 41-200 Sosnowiec, Poland
*e-mail: aturek@vip.interia.pl

[Engineering of Biomaterials, 128-129, (2014), 79]

Introduction

Therapy with risperidone (RSP) is one of the frontline treatments for most psychotic disorders. It should be noted that RSP is administrated mainly in oral formulations, i.e., tablets and orodispersible tablets, capsules or solutions. Recently, implantable formulations with prolonged release have been proposed to improve the efficiency of current therapies. The most popular solutions are based on aliphatic polyesters, i.e., poly(lactide-co-glycolide) (PLGA) with various content of lactidyl and glycolidyl segments, and different configurations of lactide. Nowadays, only one medicinal product with RSP based on D,L-PLGA 75:25 microspheres is available on the market. There are various opinions on the efficiency of this product and the rationale for its administration, pointing to both advantages and disadvantages. It should be noted that microspheres cannot be removed in the event of clinical complications.

In this study, an alternative solution has been developed. A basic research on solid formulation obtained from terpolymer material, i.e., L-lactide−glycolide−trimethylene carbonate (PLLAGATMC) terpolymer has been performed. The use of terpolymer may open a broader possibility of obtaining a solid formulation with optimized mechanical properties and release profile.

Materials and methods

The matrices (10 mm diameter) were obtained from PLLAGATMC terpolymer in the molar ratio of termonomers 56.7:18.1:25.2. Terpolymer was synthesized at the Centre of Polymer and Carbon Materials of Polish Academy of Sciences in Zabrze in bulk with the use of $Zr(Acac)_4$ as a low toxic initiator. Matrices were prepared with the use of the solution casting method. RSP (Teva Kutno S.A.) was introduced in the amount of 0.11 g to 1 g of terpolymer matrix.

The matrices were incubated in a PBS buffer (pH 7.4) under constant agitation (240 revs per minute) at the temperature of 37°C. Before measurements, the matrices were air dried at room temperature in a laminar box and then under reduced pressure.

The amount of released RSP was determined by high-performance liquid chromatography using Elite LaChrom HPLC system (VWR Hitachi, Merck) with UV absorbance detector (Diade Array Detector L -2355, VWR Hitachi, Merck) set at 280 nm.

The changes in terpolymer composition and chain microstructure (the average length of L-lactidyl, glycolidyl and trimethylene carbonate blocks were determined by ^1H and ^{13}C nuclear magnetic resonance (NMR) spectroscopy. ^1H NMR spectra were recorded at 600 MHz and ^{13}C NMR at 125 MHz with AVANCE II Ultra Shield Plus, Bruker 600 MHz spectrometer and a 5-mm sample tube. DMSOd6 was used as solvent.

Thermal characteristics of terpolymer matrices were assessed with DSC, using the TA DSC 2010 apparatus (TA Instruments, New Castle, DE) at a heating rate of 20°C/min, in the range from -20°C to +200°C, under nitrogen atmosphere (flow = 50 mL/min). The instrument was calibrated with high purity indium and gallium.

Glass transition temperature (Tg) was taken as the midpoint of the increase of the specific heat associated with the transition.

The matrices' morphology was assessed with a SEM (Quanta 250 FEG, FEI Company, USA). The micrographs were obtained under low vacuum. The samples stuck to the microscopic stubs with a double-sided adhesive carbon tape.

Results and discussions

The profile representing the cumulative release of RSP from terpolymer matrix showed a sigmoidal shape. Moreover, a burst effect was not noted.

The NMR study revealed changes in the composition for L-LA and GA during 127 days. The increase of L-LA with the decrease of GA was noted, i.e., from 56.7 to 63.0 and from 18.0 to 13.0, respectively. The least intense changes were found with respect to TMC.

The changes in the microstructure of the chain were also observed. The shortening of lactidyl blocks from 3.9 to 3.5 was noted during 127 days. The average length of the glycolidyl and trimethylene carbonate blocks remained unchanged (i.e., 1.1 and 1.5, respectively).

The DSC measurement shows to the changes in Tg from 39.9°C to 29.0°C during 127 days of degradation. This decrease demonstrated a gradual tendency.

SEM revealed the solid nature of native matrices without a differentiated morphology. Moreover, no pores were observed. Matrices degradation enhanced the diversity. However, no radical changes were noted.

The presented study exhibits a stable process of degradation. No intense changes in the analyzed parameters were shown. Moreover, a sigmoidal character of the curve showed RSP release without a burst effect, indicative of a great potential to obtain solid formulations obtained from PLLAGATMC terpolymer.

Conclusions

The results reveal the potential of PLLAGATMC in drug technology for the obtaining of an implantable biodegradable formulation for a prolonged release of RSP.

Acknowledgments

This work was financially supported by the National Centre for Research and Development, grant RYSPCONT no. PBS1/A7/2/201.

ON THE NATURE OF SILVER IONS IN COMPLEX MEDIA

K.Loza[1], J.Diendorf[1], C.Sengstock[2], M.Köller[2], M.Epple[1]

[1]Inorganic Chemistry and Center for Nanointegration Duisburg-Essen (CeNIDE), University of Duisburg-Essen, Universitaetsstr. 5-7, 45117 Essen, Germany
[2]Bergmannsheil University Hospital/Surgical Research, Ruhr-University of Bochum, Buerkle-de-la-Camp-Platz 1, 44789 Bochum, Germany

Abstract

Antimicrobial biocides are commonly used to prevent the growth of bacteria on surfaces and within materials. They are typically added in small quantities to many applications to prevent bacterial growth on the treated object. Silver is increasingly used in many applications due to the aim to replace organic chemical agents by inorganic additives. Examples of applications are bacteriostatic water filters for household use or swimming pool algaecides and numerous devices, ranging from consumer commodities like mobile phones, refrigerators, and clothes to medical devices like catheters, implant surfaces, and plasters. To meet the diversity of application types, many different forms of silver compounds have been developed to serve this market. In particular, there is little information on the types of transformations that silver nanoparticles will undoubtedly undergo in real, complex environments during long-term aging, and the impact of these transformations on their distribution in the environment, bioavailability, and toxicity potential.

The biocidal action results from the interaction of silver ions with bacteria. The most potent compounds for a high silver release are soluble silver salts like silver nitrate or silver acetate. These are fully water soluble with a high silver ion release rate. Therefore they are often used as control in cell experiments to elucidate the biological effect of silver nanoparticles. However, in the case of free silver nanoparticles the interactions can be more complex and catalytic reactions on the particle surface which depend on the size and shape of the nanoparticles can render the system very complex.

If $AgNO_3$ is used as control, it is tacitly assumed, that the free silver ion concentration is the same as that in the added $AgNO_3$. This obviously cannot be true because of the presence of a whole set of proteins, biomolecules and inorganic ions like Cl^- and $H_2PO_4^-$ in the biological medium. These will react with the silver ions in one or the other way.

We report on experiments on the behaviour of silver ions in biologically relevant concentrations in different media, from physiological salt solution over phosphate-buffered saline solution to cell culture media. For dissolution and immersion experiments PVP-coated silver nanoparticles were synthesized by reduction with glucose in the presence of PVP. The final silver concentration in all dispersions was determined by atomic absorption spectroscopy. The dissolution of silver nanoparticles was followed in long-term experiments out of a dialysis tube which was permeable only for silver ions. In case of immersion experiments, the nanoparticles and all precipitates were isolated by ultracentrifugation, redispersed in pure water and again subjected to ultracentrifugation. The particles were analyzed by scanning electron microscopy, energy-dispersive X-ray spectroscopy and X-ray powder diffraction.

The dissolution requires the presence of dissolved oxygen. If no oxygen is present, only a very small fraction of silver is dissolved, possibly by traces of oxygen in the experimental setup. An oxidizing agent like H_2O_2 clearly enhances the dissolution. The presence of NaCl, either in pure form or as PBS, strongly slows down the dissolution, probably due to silver chloride formation. Cysteine has a clearly inhibiting effect with almost no dissolution of the silver nanoparticles whereas glucose has a decelerating effect but leads to a similar final dissolved fraction. This suggests that cysteine adsorbs onto the silver nanoparticle surface with its thiol group and prevents the oxidation. In contrast, glucose slows down the dissolution, but clearly did not prevent the oxidation on a longer time scale.

We have extended the studies by mixing silver nanoparticle dispersions with different media of increasingly biological nature. The solutions/dispersions were stirred for equilibration and then subjected to ultracentrifugation. All precipitates and nanoparticles were isolated by this way and then analyzed. The results show that both initially present silver ions and released silver ions are mainly precipitated as AgCl if chloride is present. Only in the absence of chloride, glucose is able to reduce Ag^+ to Ag^0. The initially present silver nanoparticles were recovered in all cases. Silver phosphate was not observed in any case, probably due to the moderate pH (around 7) at which phosphate is mostly protonated to hydrogen phosphate and dihydrogen phosphate.

We can conclude that released silver ions precipitate mostly as AgCl in biological media, and that most cell culture studies where silver ions are used as control are in fact studying the effect of colloidal silver chloride on the cells. To prove this assumption, human mesenchymal stem cells (hMSC) were cultured in the presence of silver chloride nanoparticles (diameter 120 nm), and the viability of the cells was analyzed by fluorescence microscopy. In general, we clearly observed that pure silver nanoparticles have lower toxicity to hMSC compared to silver chloride nanoparticles with a comparable total silver dose. Silver acetate in the biological medium had a comparable toxicity to hMSC compared to silver chloride nanoparticles with the same total silver dose.

[Engineering of Biomaterials, 128-129, (2014), 80]

TECHNOLOGICAL ISSUES OF ADDITIVE MANUFACTURING OF PREPROTOTYPES OF THE MULTISPIKED CONNECTING SCAFFOLD FOR NON-CEMENTED RESURFACING ARTHROPLASTY ENDOPROSTHESES

Ryszard Uklejewski[1,2*], Mariusz Winiecki[1,2], Piotr Rogala[3]

[1]Department of Medical Bioengineering Fundamentals,
Institute of Technology, Casimir the Great University,
30 K.Chodkiewicza Street, 85-064 Bydgoszcz, Poland
[2]Laboratory of Medical Biomaterials and Bioprocess Engineering, Department of Process Engineering,
Institute of Technology and Chemical Engineering,
Poznan University of Technology,
2 Marii Sklodowskiej-Curie Street, 60-965 Poznan, Poland,
[3]Department of Spine Surgery,
Oncologic Orthopaedics and Traumatology,
Poznan University of Medical Sciences,
135/147 28 Czerwca 1956 St., 61-545 Poznan, Poland
*e-mail: uklejew@ukw.edu.pl

[Engineering of Biomaterials, 128-129, (2014), 81-82]

The biomimetic MultiSpiked Connecting Scaffold (MSC-Scaffold) is the essential innovation in fixation technique of the components of the resurfacing arthroplasty (RA) endoprostheses providing theirs entirely non-cemented and bone tissue preserving fixation in the periarticular trabecular bone – invented by Rogala [1-3] and designed, manufactured and tested in our research team [4-7]. The spikes of the MSC-Scaffold were designed to mimic the interdigitations of the periarticular subchondral bone and for this reason it is a biomimetic structure and it can be manufactured only in one of Direct Metal Manufacturing (DMM) technology. This fixation technique of RHA endoprosthesis components in surrounding bone preserves the femoral head blood vessels and the near-physiological regional blood supply and circulation. Consequently, the proper remodeling potential of the trabecular bone of femoral head can be preserved. In this way, the near-physiologic biodynamics and remodeling of bone tissue around the implant will be ensured and the desired promotion of bone tissue ingrowth into the MSC-Scaffold can be reasonably expected. In FIG.1a there is presented the 3D diagram of articular hyaline cartilage and subchondral bone with interdigitations interlocking with trabeculae of cancellous bone. In FIG.1b there is showed the prototype of the stemless and entirely cementless total resurfacing hip arthroplasty (TRHA) endoprosthesis with the MSC-Scaffold manufactured in Selective Laser Melting (SLM) technology. In FIG.1c there is demonstrated the femoral head component of our prototype of innovating THRA endoprosthesis – designed to preserve the subcapsular arteriae retinaculares: superior (3), and inferior (4); (1) – a.circumflexa femoris lateralis, (2) – ramus ascenens of (1).

The presented here pre-prototypes of the MSC-Scaffold were comprehensively designed as fragments of the central part of the TRHA endoprosthesis femoral component (see FIG.1b), for various tasks of the research project (no. NN518412638, Polish Ministry of Science), i.e.: the electrothermochemical modification of theirs spikes' surfaces contacting with bone [8], the optimization of the MSC-Scaffold general design on the basis of: the preliminary preclinical in vivo evaluation on animal models and the biological evaluation with human osteoblasts cultures [9] and also the biomechanical push-in tests performed to evaluate the implant push-in force [10].

Our attempts to manufacture the MSC-Scaffold pre-prototypes using various technologies from group of the DMM technologies, like Selective Laser Sintering (SLS) or Electron Beam Melting (EBM), despite referred in literature good potential to manufacture titanium porous structures or bone scaffolds [11-12], were not satisfying, because of disqualifying defects found in the interspike space of the MSC-Scaffold, as well as, in its microsections (high corrugation of the lateral surface of the MSC-Scaffold, the large quantity of the unmelted and unremovable powder granulates accumulated between the spikes' bases in case of EBM, the high number of discontinuity and microcracks revealed at their surface and in microsections in case of SLS). The DMM technology experimentally chosen for manufacturing our MSC-Scaffold preprototypes – the Selective Laser Melting (SLM) – also revealed some limitations, but was judged to have best potential to manufacture the MSC-Scaffold preprototypes in comparison to EDM or SLS. The variety of the CAD models of the biomimetic MSC-Scaffold pre-prototypes arranged as they were set up in one CAD file and then transferred into one STL file is presented in FIG.2a; in FIG.2b there is shown the screen presenting the pre-processing step – the formation of supports for all pre-prototypes of the MSC-Scaffold to be generated in SLM technology, while in FIG.2c the exemplary pre-prototype of the MSC-Scaffold is shown as seen directly after manufacturing with support to be cut out. The SLM machine (Realizer II 250, MTT Technologies, Germany) and the stages of the manufacturing process of the MSC-Scaffold pre-prototypes are presented in FIG.3: (1) selective laser melting of the first layer of TiAl6V4 powder, (2) selective laser melting of one of last layers of TiAl6V4 powder, (3) cleaning of the working chamber of not melted TiAl6V4 powder and (4) the set of the MSC-Scaffold pre-prototypes fixed to the platform pedestal via supports to be later cut out.

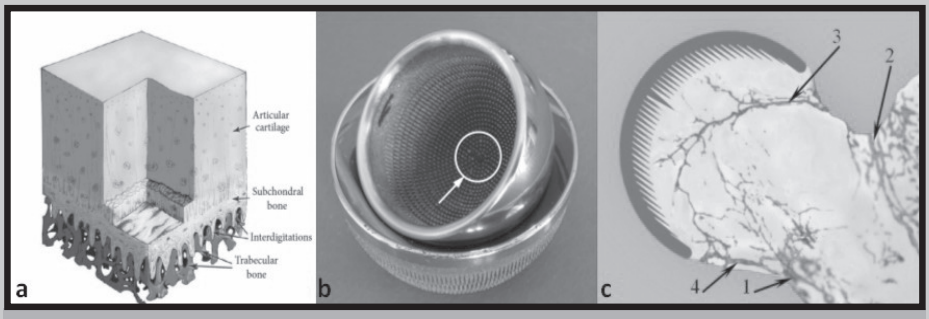

FIG. 1. a) The 3D diagram of articular hyaline cartilage and subchondral bone with interdigitations interlocking with trabeculae of cancellous bone; b) the prototype of the stemless and entirely cementless total resurfacing hip arthroplasty (TRHA) endoprosthesis with the multispiked connecting scaffold (MSC -Scaffold) manufactured in Selective Laser Melting (SLM) technology; c) the femoral head component of our prototype of innovating THRA endoprosthesis – designed to preserve the subcapsular arteriae retinaculares: superior (3), and inferior (4); (1) – a.circumflexa femoris lateralis, (2) – ramus ascenens of (1).

The major purpose of the presented here work is the examination of the MSC-Scaffold design to improve the inter-spike structural osteoconductive potential of the MSC-Scaffold and, having regard to technological limitations of the SLM, to provide the key information about the necessary modification in CAD model design of the MSC-Scaffold taking into account the adjustments of the appeared technological limitations in this case. Before the essential research there had to be also worked out and performed the additional non-standard technological tasks, like removing of the supports from the SLM-manufactured MSC-Scaffold pre-prototypes, threading of the special grips in case of some specific MSC-Scaffold specimens, and the glass pearl blasting treatment which is useful in removing the powder aggregates from the lateral surface of MSC-Scaffold's spikes.

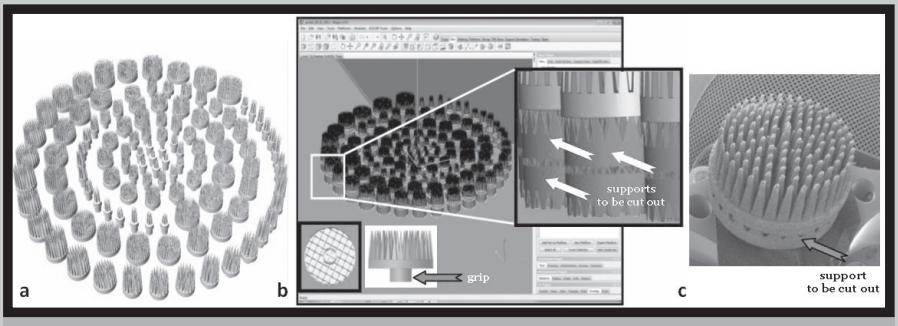

FIG. 2. a) The screen presenting variety of the CAD models of the biomimetic MSC-Scaffold pre-prototypes (designed with special grip for biomechanical push-in tests provided to evaluate the implant push-in force) arranged as they were set up in one CAD file and then transferred into one STL file; b) the screen presenting the pre-processing step – the formation in Magic 13.0 software of supports for all pre-prototypes of the MSC-Scaffold to be generated in SLM technology; c) the exemplary pre-prototype of the MSC -Scaffold directly after manufacturing with support to be cut out.

The applied SLM post-processing treatment is indispensable before the surface modification of the MSC-Scaffold's spikes, but still requires the improvement or alternative post-treatment process to be worked out. The change in the MSC-Scaffold prototype design (i.e.: optimal enlarging of the distances between the spikes base edges) is expected to increase the effectiveness of the glass pearl blasting of spikes surface of the MSC-Scaffold prototypes and cleaning this region from the metallic remains from SLM manufacturing process. The review of the most important technological issues of the additive manufacturing of the MSC-Scaffold will be presented in series of photos in our poster at the PSB Conference 2014.

FIG. 3. The SLM machine (Realizer II 250, MTT Technologies, Germany) and the main stages of the manufacturing process of the MSC-Scaffold pre-prototypes.

Aknowledgements

This research was supported by the Polish Ministry of Science by research Project no. NN518412638: "The thermochemical surface modification of preprototypes of the minimally invasive RHA endoprostheses and porous intraosseous implants" (Head: R. Uklejewski).

References

[1] Rogala P., Endoprosthesis; EU patent nr 072418 B1, 1999.
[2] Rogala P., Acetabulum endoprosthesis and head, US patent nr 5,91,759, 1999.
[3] Rogala P., Method and endoprosthesis to apply this implantation, Canadian patent nr 2,200,064, 2002.
[4] Uklejewski R., Rogala P., Winiecki M., Mielniczuk J.: Prototype of innovating bone tissue preserving THRA endoprosthesis with multi-spiked connecting scaffold manufactured in selective laser melting technology. Inżynieria biomateriałów (Engineering of Biomaterials) 12 (87), 2009, 2-6.
[5] Uklejewski R., Rogala P., Winiecki M., Mielniczuk J.: Prototype of minimally invasive hip resurfacing endoprosthesis – bioengineering design and manufacturing. Acta of Bioengineering and Biomechanice 11(2), 2009, 65-70.
[6] Uklejewski R., Rogala P., Winiecki M., Mielniczuk J.: Projektowanie i kształtowanie przyrostowe minimalnie inwazyjnej endoprotezy powierzchniowej stawu biodrowego z wieloszpilkowym rusztowaniem łączącym. Mechanik 83(7), 2010, 464-467.
[7] Uklejewski R., Winiecki M., Rogala P., Mielniczuk J.: Selective laser melted prototype of original minimally invasive hip endoprosthesis. Rapid Prototyping Journal 17(1), 2011, 76-85.
[8] Uklejewski R., Winiecki M., Tokłowicz R.: Effect of the process parameters of electrochemical cathodic deposition of Ca-P on the modified surface properties of multispiked connecting scaffold prototypes for non-cemented resurfacing arthroplasty endoprostheses – submitted to the journal 'Engineering of Biomaterials (Inżynieria Biomateriałów).
[9] Uklejewski R., Rogala P., Winiecki M., Kędzia A., Ruszkowski P.: Preliminary results of implantation in animal model and osteoblast culture evaluation of prototypes of biomimetic multispiked connecting scaffold for noncemented stemless resurfacing hip arthroplasty endoprostheses. BioMed Research International, 2013 (2013), 10 pages, doi:10.1155/2013/689089.
[10] Uklejewski R., Winiecki M., Tokłowicz R., Kowalski S., Musielak G., Rogala P.: Mechanical behaviour of preprototypes of MSC -Scaffold for non-cemented stemless joints endoprostheses during push-in tests into periarticular cancellous bone. Work in progress.
[11] Van Bael S., Chai Y.C., Truscello S., Moesen M., Kerckhofs G., Van Oosterwyck H., Kruth J-P. and Schrooten J.: The effect of pore geometry on the in vitro biological behavior of human periosteum-derived cells seeded on selective laser melted Ti6Al4V bone scaffolds, Acta Biomater, 8, 2012, 2824–2834.
[12] Liu F.H., Lee R.T., Lin W.H., Liao Y.S.: Selective laser sintering of bio-metal scaffold. Procedia CIRP 5, 2013, 83-87.

DEVELOPMENT OF GRAPHENE-BASED BIOSENSOR FOR MEDICAL DIAGNOSTICS

P.Sobolewski[1], K.Penkala[2], J.Podolski[3], E.Mijowska[4], M.El Fray[1]

[1]Polymer Institute, Department of Biomaterials and Microbiological Technologies, West Pomeranian University of Technology, Szczecin, Poland
[2]Faculty of Systems, Signals and Electronics Engineering, Department of Electrical Engineering, West Pomeranian University of Technology, Szczecin, Poland
[3]NZOZ Meditest Diagnostic Medicine, 14D Bronisławy Street, Szczecin, Poland
[4]Division of Nanotechnology, Department of Chemical Engineering, West Pomeranian University of Technology, Szczecin, Poland

Abstract

The explosion of information provided by the "-omics," (genomics, proteomics, etc.) has resulted in a pressing need to develop matching diagnostic technologies, so-called biosensors. Rapid, sensitive, selective, and cost-effective analysis of different biomolecules and microorganisms is crucial in clinical diagnosis and efficient treatment of patients. Further, there is a growing demand for decentralized laboratory methodologies that can be implemented in doctor's office, emergency room or in the field for the analysis of such analytes as DNA, RNA, proteins, antibodies, bacteria, viruses, small compounds etc. Lab-on-a-chip platforms and miniaturized point-of-care devices based on biosensors fulfill these demands and are foreseen to revolutionize the future of medical diagnostics. Because of excellent electric and optical properties, graphene has recently found to be highly attractive in biosensing applications and may thrust new possibilities into the field of miniaturized medical diagnostic devices. The main objective of this project is to develop a multifunctional graphene biosensor for effective electrochemical detection of specific DNA microbial targets in biological samples. Novel nanocomposites consisting of chitosan and nanoparticle-modified graphene will be combined with locked nucleic acid molecular beacons with the goal of producing "ink" for ultrasonic non-contact printing of electrical circuits. The developed technology will allow fabrication of low cost, highly sensitive biosensors for point-of-care diagnosis.

[Engineering of Biomaterials, 128-129, (2014), 83]

CHEMICAL PURITY OF NEW SEGMENTED POLYESTER BIOMATERIALS

Agnieszka Piegat, Małgorzata Walenia, Mirosława El Fray

West Pomeranian University of Technology in Szczecin, Polymer Institute, Division of Biomaterials and Microbiological Technologies, Piastow Ave 45, 70-311 Szczecin, Poland

[Engineering of Biomaterials, 128-129, (2014), 83-85]

Introduction

Chemical purity is the crucial property of polymers for biomedical applications. All materials before in vitro testing and especially clinical studies needs to be purified and characterized with respect to potential leachable substances. The characterization pathway is described in PN-EN ISO: 10993 12:2009 standard, part 12, 13 and 18 1–3 and PN-83/P-04607 4.

In this research project new multiblock copolymer are developed, as potential materials for producing elements of extracorporeal heart assisting devices. Currently used polyurethanes (PU) possess following advantages: blood compatibility, transparency and easy processing, but their main drawbacks are poor mechanical stability and number of significant chemical changes on the polymer surface 5. Due to the disadvantages of commercially available PUs we proposed new multiblock copolymer consist from poly(ethylene terephthalate) (PET) hard segments and ethylene ester of dilinoleic dimer acid as soft segments (DLA). The aim of this work was to establish purification methodology of new PET-DLA copolymer and evaluate their chemical purity ,as potential materials for blood contacting product. A detailed characterization of physical and chemical properties of aqueous and non- polar extracts, as well as the purified product was performed.

Experimental

Materials

PET-DLA copolymer with the 50:50 hard:soft segments ratio (wt%) was obtained by two step polycondensation method. Briefly, transesterification between dimethyl terephthalate and ethylene glycol was carried out at the temperature range 150-190°C, then dimer fatty acid (DLA) was added and polycondensation reaction was carried at p=0,4mbar and temperature 255-260°C. α-Tocopherol was used as natural thermal stabilizer. The intrinsic viscosity of 0,724 dl/g was measured, and the melting temperature of 198°C was determined. The proposed chemical structure is demonstrated in FIG. 1.

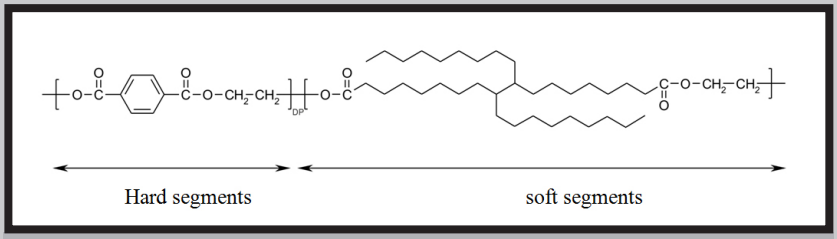

FIG. 1. Chemical structure of PET-DLA copolymer; DP - degree of polymerization for 50:50 copolymer 2,98.

Methods

Organic solvent extraction

Different alcohols: ethanol, methanol and isopropanol were examined as polar solvents. As a non-polar solvent for leachable substances, we used petroleum ether (boiling temperature 40-60°C). The extraction was carried out in Soxhlet apparatus according to the PN/P-04607:1983 and PN-EN ISO 10993-12: 2009 standards.

Water extraction

Water extraction was carried out on material previously purified by solvent extraction. Polymer granules were immersed in water at 37°C for 3, 7, 14, 21 and 28 days in shaking incubator. As reference material, commercially available thermoplastic elastomer polycarbonate polyurethane (PCU) was used. Water extracts were used for determination of total organic carbon (TOC), turbidity, conductivity and total dissolved solids.

Results and discussion

Four different solvents were used for Soxhlet extraction, and UV-Vis spectra of model solutions reflecting the main components of new polymers (thermal stabilizer, α-tocopherol, and dimethyl terephthalate, DMT) and the extracts are presented in FIG.2.

The absorbance spectra of all solutions shows maximum between 200 and 300 nm (200, 240, 280nm). This absorbance region is characteristic for π- π* absorption in aromatic compounds. The analysis of the polymer composition suggests that polymer extract contains unreacted DMT or short oligomers and/or α-tocopherol (FIG. 2b).

Total carbon (TC) analysis was carried out on purified and the neat materials and TC values were calculated according the equation: TC=TOC+IC, where: TC- total carbon amount (mg/dm^3), TOC- total organic carbon (mg/dm^3), IC- inorganic carbon (mg/dm^3), respectively. The results of total dissolved solids (TDS) and the conductivity of water extracts are presented in FIG. 3.

The obtained results allow to draw the following conclusions:

- Purification of new PET-DLA materials was successfully performed in different media (solvents), including petroleum ether commonly used for purification of medical-grade polymers;
- The chemical composition of PET-DLA copolymer were unchanged after Soxhelet extraction
- The parameters of water extracts were comparable with thofor commercially available PCU

Acknowledgements

The authors would like to thank the National Center of Research and Development (Grant no: PBS1/A5/2/2012) for providing financial support to this project.

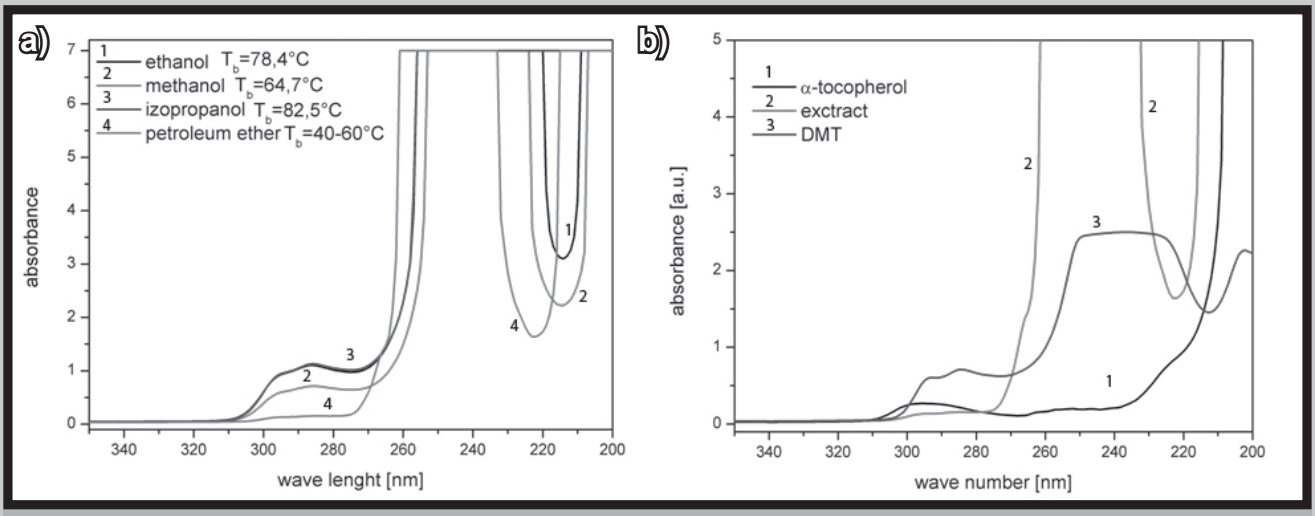

FIG. 2. UV-Vis spectra od different extracts (a) from PET-DLA polymer and the model solutions (b).

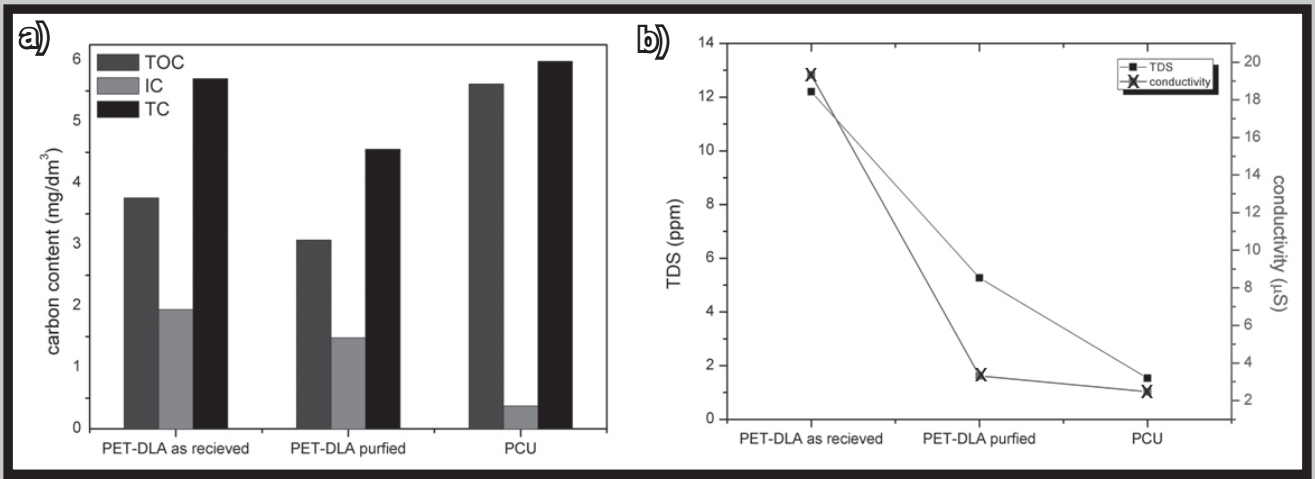

FIG. 3. The carbon content (a); TDS and conductivity (b) of water extracts from analysed materials.

References

[1] PN-EN ISO 10993 Biological evaluation of medical devices; Part 18: Chemical characterization of materials. In: ; 2009.
[2] PN-EN ISO 10993 Biological evaluation of medical devices; Part 12: Sample preparation and reference materials. In: ; 2009.
[3] PN-EN ISO 10993 Biological evaluation of medical devices; Part 13: Identification and quantification of degradation products from polymeric medical devices. In: ; 2009.
[4] PN-83/P-04607 Metody badań surowców włókienniczych i przędzy -- Wyznaczanie zawartości substancji niewłóknistych. In: ; 1974.
[5] Santerre JP, Woodhouse K, Laroche G, Labow RS. Understanding the biodegradation of polyurethanes: from classical implants to tissue engineering materials. Biomaterials. 2005;26(35):7457-70. doi:10.1016/j.biomaterials.2005.05.079.

IN VITRO STUDY OF A NOVEL COLLAGEN - CALCIUM PHOSPHATE COMPOSITES

Justyna Kozłowska[1], Alina Sionkowska[1], Anna Bajek[2], Aldona Rynkiewicz[2]

[1]Department of Biomaterials and Cosmetics Chemistry, Faculty of Chemistry, Nicolaus Copernicus University, Torun, Poland
[2]Tissue Engineering Department, Chair of Medical Biology, Collegium Medicum, Nicolaus Copernicus University, Bydgoszcz, Poland
e-mail: justynak@chem.umk.pl

[Engineering of Biomaterials, 128-129, (2014), 85]

Introduction

Reconstruction of bone defects lost due to trauma, cancer, or congenital defects is a major issue in orthopedic surgery [1]. Calcium phosphate (CaP) ceramics are widely used in bone regeneration. Excellent biocompatibility, bioactivity and biodegradability make CaP an ideal starting material for bone tissue engineering applications [2,3].

The aim of this work was to produce 3-D bioengineered composites of collagen and calcium phosphates (Col/CaP) by deposition of calcium phosphate within collagen matrix. The objective of the current study is the preliminary investigation of the in vitro cytotoxicity of a biomimetic collagen–calcium phosphate scaffold for orthopaedic.

Materials and methods

The high porous scaffolds were produced from a collagen solution using a freeze–drying technique. Collagen solutions with concentrations 2% (w/w) was prepared from lyophilized collagen in deionized water. Then, calcium phosphate formation in collagen scaffold was achieved. Collagen scaffolds were into a solution containing sodium ions for 3h, then were immersed into a calcium chloride solution for 3h. The next step were freezing and lyophilizing of scaffolds. After drying scaffolds were briefly washed in deionized water and freeze-dried.

Mouse fibroblast cell line 3T3 were seeded in the number of 1×10^6 cells/1 cm^2 and incubated for 7 days. After incubation, MTT assay was performed to assess the viability of 3T3 cells.

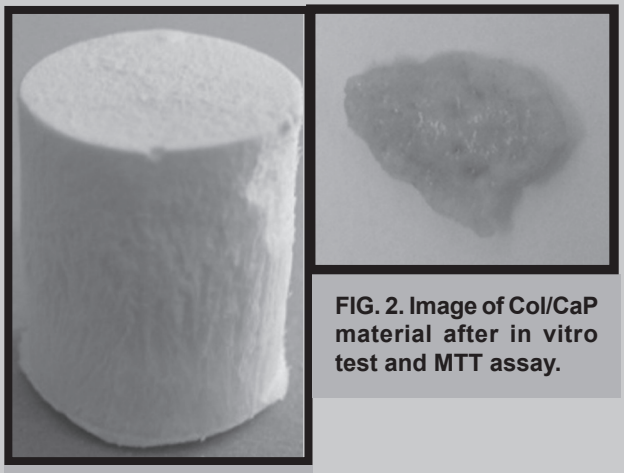

FIG. 2. Image of Col/CaP material after in vitro test and MTT assay.

FIG. 1. Image of Col/CaP material.

Results

In FIG. 1. image of 3D Col/CaP material is presented and FIG. 2 shows a photograph of this material after in vitro testing.

The qualitative analysis of color intensity resulting from MTT assay showed that Col/CaP sample was quite well tolerated by the cells. As can be seen the cells were distributed only on the surface of the scaffold. Although the structure of the material was porous, the fibroblasts did not migrate into the material. The results from this study suggest, that calcium phosphate is precipitated primarily on the surface of the collagen matrix. Moreover, there may be a closing of pores in the material during the precipitation of the inorganic particles. These conditions are not conducive to cell adhesion and proliferation into collagen matrix.

Conclusion

In conclusion, our method allows to obtain 3D, porous Col/CaP materials. However, calcium phosphate was precipitated most of all on the surface of this material. Results concerning cell viability/proliferation evaluated by MTT assay showed viable cells on the surface of Col/CaP material.

Acknowledgements

Financial support from the National Science Centre (NCN, Poland) Grant No UMO-2012/05/N/ST8/02283 is gratefully acknowledged.

References

[1] Dimitriou R., Jones E,. Gonagle D., Giannoudis P.V., Bone regeneration: current concepts and future directions, BMC Med. 2011;9:66-75.
[2] Sopyan I., Mel M., Ramesh S., Khalid K.A., Porous hydroxyapatite for artificial bone applications. Sci. Technol. Adv. Mater. 2007;8:116-123.
[3] Bose S., Tarafder S., Calcium phosphate ceramic systems in growth factor and drug delivery for bone tissue engineering: A review, Acta Biomater. 2012; 8:1401-1421.

CHITOSAN-BASED NANOCOMPOSITES AS POTENTIAL MATERIALS FOR NERVE REGENERATION

Anna Turek[1], Kamil Dudziński[2], Ewa Stodolak-Zych[3]*

AGH University of Science and Technology,
30 A.Mickiewicza Ave., 30-059 Krakow, Poland:
[1]Faculty of Electrical Engineering, Automatics,
Computer Science and Biomedical Engineering
[2]Faculty of Mechanical Engineering and Robotics
[3]Faculty of Materials Science and Ceramics
*e-mail: stodolak@agh.edu.pl

Abstract

The nanocomposite material based on chitosan was obtained and characterized. Commercially produced biopolymer at 85% deacetylization degree was used. The biopolymer matrix was modified with carbon nanofillers such as graphite oxide (GO), carbon nanotubes (CNTs) and nanontubes with the surface affected by carboxyl groups (CNT-COOH). The obtained nanocomposites were formed by means of two methods: casting (to manufacture nanocomposite foils) and liofilization (to manufacture porous nanocomposite materials). Their electrical properties and microstructure were examined. The tests proved that adding the carbon nano-filler results in high resistivity (graphite foils, carbon nanotubes) and also the average size of pores in liofilized materials. Additionally, the electric potential of the materials may be improved by surface processing (EPD- electrophoretic deposition). The described materials are an alternative to polymer nerve implants e.g. tubes or hydrogels which are already present on the market and applied to regenerate nerves.

Keywords: *nanocomposites, chitosan, carbon fillers, guided nerve regeneration (GNR)*

[Engineering of Biomaterials, 128-129, (2014), 86-87]

Introduction

Peripheral nervous system disorders (OUN) are a serious social problem, as approximately 2-5% of patients never fully recover from the damage and most of them (about 3%) are considered disabled. Both neurosurgery and neurology have proven that peripheral nerves display a potential for recovery. Biomaterials engineering focusing on designing specific materials may also facilitate the process of nerve regeneration. Guided nerve regeneration (GNR) means creating paths to direct the axons' growth. Such implants are most often manufactured from pure and modified polymers. Their objective is to provide the proper durability of the material in vivo conditions, efficient mechanical and functional properties, and such a microstructure that will facilitate the migration of growth factors and nutrients. Using degradable products means that a patient does not have to be reoperated on to remove the unnecessary material.

The in vivo durability of the material might be modified both by the type of the material and its porosity (the more porous material, the faster degradation). That is why the most popular polymers applied in GNR techniques are: polylactides (PLA), polyglicolides (PGA), their copolymers (e.g. PLGLA) and natural biopolymers such as chitosan (CS).

Another desirable feature is high electrical conductivity of the implant that will stimulate the regeneration of the damaged nerves. The conductivity phenomenon is present in every animal tissue. Unfortunately, it is often neglected in the process of designing nerve implants.

There are two methods to improve the electrical properties of the implant. One method involves the necessity to use piezoelectric polymers, such as PVDV (polydifluorovinylidene), PTFE (polytrifluoroethylene) or their copolymers, that are able to generate the surface charge under the influence of slight mechanical stresses. In the other method a certain number of carbon fillers is introduced into the polymer matrix in order to cross the percolation threshold and induce electrical conductivity of the material [1]. In the latter method carbon nanotubes (CNT), graphite (GR) and, as of late, graphene (G) are used. Since the volume modification is often not efficient enough, the electrophoretic deposition method (EPD) is used to increase the material's electrical conductivity. In this procedure carbon particles are introduced to improve electrical properties of the surface [2].

This paper presents the implant designed for guided nerve regeneration. The implant is made of two different materials: the outer chitosan membrane and the scaffolding filling. The chitosan membrane is modified in volume by means of CNT,GR,G, whereas its surface is modified with different carbon nanoforms (CNT). The porous scaffolding constitutes the filling of the membrane; its role is to facilitate the axial pathfinding.

In our work nanocomposite chitosan membranes were obtained by casting and their structure was modified by depositing the layer of carbon nanotubes (EPD). The porous scaffolding was obtained through liofilization, using various forms of carbon (GR, CNT) as fillers.

The microstructure of the porous background was examined using SEM imaging. It was also established how different types of modifiers affect the shape and size of pores. Electrical properties of the surface were tested both for initial nanocomposite chitosan membranes and the EPD-modified ones. The most advantageous material composition was selected, which is the scaffolding with the highest porosity and the most resistive membrane.

Materials and method

The base polymer was chitosan (CS) of viscosity 200-800cT and 75-85% degree of deacetylation (purchased from Sigma-Aldrich). The carbon fillers were: commercially available carbon nanotubes (purchased from NanoAmor, US), graphite oxide (AO-4, from Graphene Supermarket) and graphene (Graphene Supermarket). Producent date showed TABLE 1. The porous background with 2%wt filler was prepared in the shape of cylinders measuring 0.9x1cm. 3% acetic acid was used as a solvent. The membranes contained 1%wt of nano-filler. Both forms of the nanocomposite were air-dried. Then the materials were observed using a scanning miscroscope (Nova NanoSEM). The electrical properties of nanocomposite membranes were established with a multimeter (EAT 200). Both the volume-modified foils and the volume- and surface-modified foils were tested.

TABLE 1. Producent date of nanofillers.

Nanofillers	Shape and size of nanofillers	Specific surface area [m^2/g]
MWCNT (Nano Amor)	d=2-5 [nm], l=10-12 μm	450-560
MWCNT-COOH (NanoAmor)	d=0,7-2 [nm], l=15-30 μm	660
A6 (Graphen Supermarket)	d=6nm, a=2-3 μm	120
AO-4 (Graphene Supermarket)	d=60 nm, a=3-7 μm	<15

Results and discussion

Adding the nano-filler to the chitosan matrix changes the electrical potential of the material in a significant way. Using 1%wt of unmodified nanotubes set the material resistivity at the level of 350-78 kΩ, while the CNTs modified with carboxyl groups increased the value to 8-9 MΩ. It was established that additional surface modifications with different forms of carbon increase the resistivity of the system only if the modified material is carbon nanotubes. However, this change is rather slight, as compared to the initial material's value in the applied conditions (increase by 15-20% only). Meanwhile, the presence of fillers has a strong influence on the shape and size of pores in the liofilized systems. Introducing the carbon nanotubes results in elliptical and irregular pores. Introducing graphene and graphite oxide makes the pores more circular and homogenous (FIG. 1).

Conclusions

The proposed nanocomposite systems: active electrical foil and porous fulfilling nanocomposite material seem to meet the requirements for material used in guided nerve regeneration concerning damages in the peripheral nervous system.

References

[1] K. Haastert-Talini, S. Geuna, L. B. Dahlin, C. Meyer, L. Stenberg at all, Chitosan tubes of varying degrees of acetylation for bridging peripheral nerve defects Biomaterials, Vol 34, Issue 38, 2013, 9886–9904

[2] F.Sun, X. Pang, I. Zhitomirski, Electrophoretic deposition of composite hydroxyapatite chitosane heparine coatings, Journal of materials processing technology, Vol 209, 2009, p 1597-1606

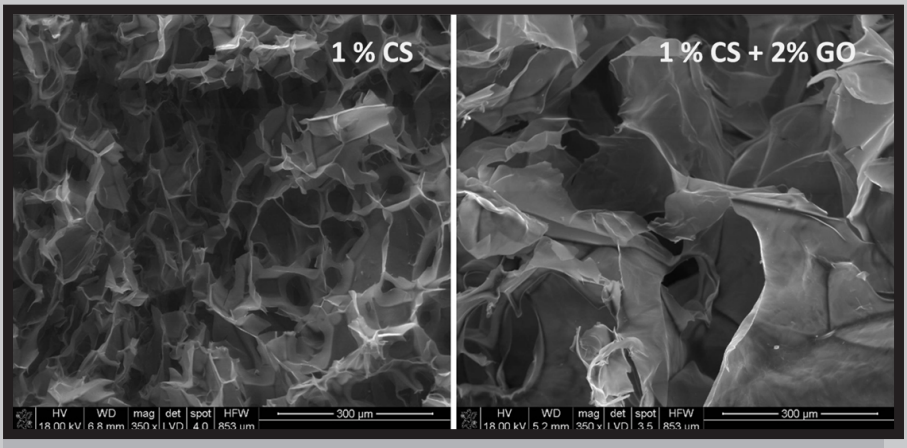

FIG. 1. Mictrostructure of liophilised chitosane and chitosane witf graphite.

COMPARISON OF DURABILITY OF RESORBABLE POLYMER PINS IN IN VITRO AND IN VIVO CONDITIONS. PRELIMINARY STUDY

Ewa Stodolak-Zych[1*], Krzysztof Pałka[2], Tomasz Szponder[3], Katarzyna Nowicka[1], Stanisław Błazewicz[1]

[1]AGH University of Science and Technology, Faculty of Materials Science and Ceramics, Department of Biomaterials, al. Mickiewicza 30, 30-059 Kraków
[2]Lublin University of Technology, Department of Materials Engineering, Nadbystrzycka St. 36, 20-618 Lublin, Poland
[3]University of Life Sciences in Lublin, Faculty of Veterinary Medicine, 20-950 Lublin, 13 Akademicka Street , Poland
* e-mail: stodolak@agh.edu.pl

Abstract

The work focuses on polymeric cartilage/bone pins (pegs) that were manufactured and tested to assess their application in meniscus injuries. The bone pins measuring 1,2 and 4 mm in diameter were produced from certified resorbable PLDLA by means of hot pressing (at 126°C). In order to establish the material characteristics, tests of mechanical properties, structural testing and stability tests were performed in vitro (an immersion medium: water/ PBS buffer). It was established that after three months of incubation the initial implant's bending strength (120 MPa) decreased by 35%, whereas its tensile strength (52 Pa) weakened by 60%. The degree of degradation did not affect the pH of the immersion fluid. The observed physical changes of the implant, such as: the mass decrease, the change of shape, the increase of crystallinity (DSC/TG), the number of polymer terminal groups (-OH, -COOH), proved the advanced degradation process of PLDLA pins. Implants of particular behaviour were inoculated into the tibia of a New Zealand rabbit. In vivo tests were conducted to confirm the changes observed in vitro. Monitoring of the degradation process was performed after three months following the implantation by means of control X-ray and computed microtomography (μCT).

Keywords: *meniscus, bone pins, polylactide, regeneration*

[Engineering of Biomaterials, 128-129, (2014), 87-89]

Introduction

Meniscus injuries concern mainly young and physically active people. Doing competitive and amateur sports may result in meniscal tears. Injury to the meniscus occurs during the sudden bend-and-twist motion of the knee. Unfortunately, meniscal tears often happen at the same time other components of the knee are injured - a common injury among athletes involves simultaneously the anterior cruciate ligament (ACL) and the posterior cruciate ligament (PCL). Apart from the trauma-induced injuries, the congenital knee deformities (such as dysplasia or deviation of the knee joint) as well as degenerative process contribute to the incidence of meniscal injuries. The methods of treatment depend on the location of the injury, i.e. whether the injured area is well or poorly supplied with blood. In the first case the suture is usually recommended, using stitches, pins or staples made of plastic. The disadvantage of this method is the patient's longer immobilization and recovery time in comparison to meniscectomy (the surgical removal of all or part of a torn meniscus). In particular cases the faulty meniscus may be replaced by allogenic graft (from Tissue Banks) or the scaffolding implant. The porous material improves regeneration of the injured meniscus and may be applied in surgery. When the injured area is with the good blood supply, the preferable treatment is meniscectomy. The materials used in meniscus surgery are mainly polyhydroxy acids, among which the most popular ones are polylactide and polydioxanone (PDS). This polymer, depending on the isomer type (right or left, isomer mixture L/DL), is characterized by various time of durability and differentiation of mechanical properties tested in vitro/in vivo (strength, Young's modulus). Additionally, the thermoplastic material may be formed by means of heat treatment used in the polymer technology (injection moulding, drawing, blow moulding). Thus it is possible to form pins, pegs, staples, scaffolds or membranes used in surgical procedures of meniscus. The well recognized products on the market such as RigidFix pin, Steinman pin are manufactured mainly from polylactide due to its high endurance and crystallinity. In order to expand the implant/tissue interface, the pins are often roughened (Steinman pin). The main problem indicated by orthopaedists is migration of the pin during the recovery time and long degradation of polylactide (over two years). Because of the possibility of combining the meniscus treatment with the ligaments reconstruction, it seems advantageous to apply the material suitable for the soft tissue/bone interface. Thus the tested pin was made from poly-L/DL-lactide (80:20, L/DL), whose durability tested in vitro is 12-14 months, according to the manufacturers. The material is approved by FDA for medical applications and the proposed processing does not affect its biocompatibility. The aim of this work was to verify the material both in vivo and in vitro after three months. To assess its durability the following properties were tested in vitro: mechanical, thermal and structural (FTIR), and macroscopic (shape/mass). For in vivo testing an animal model was used – a PLDLA pin was implanted into the tibia of a New Zealand rabbit. Monitoring of the degradation process was performed by means of control X-ray and X-ray computed microtomography (μCT).

Materials and method

Polymer implants (PLDLA, by PURAC Biochem) were manufactured by means of hot pressing (at 160°C). Three types of the nozzle were used measuring respectively: 1, 2 or 4 mm in diameter. All the implants had 2cm in length. The prepared implants were measured, paying special attention to the mass and shape. The immersed medium were: PBS and water (1:100). Every month the pH and conductivity values were registered to establish the degradation rate. The mechanical bending and tension tests were performed first on the initial implants and after three months of in vitro incubation (37°C/water/PBS buffer) using Zwick 1435 machine. The initial values of tensile and bending strength were established. The thermal properties of the implant were measured in the atmosphere of nitrogen using the Netzsch thermal analyzer STA 449F3. The degradation rate of the material was established by means of analyzing the crystallinity alterations. The structural changes of polymer were monitored by means of FTIR-ATR (FTS 3000 Excalibur, Bio-Rad) equipped with a diamond ATR (PIKE Technology). This method made it possible to follow the changes taking place on the surface of the material (penetration depth of 2 μm).

In vivo testing was conducted on three groups of New Zealand rabbits. Under general anaesthesia (using xylazine 5 mg/kg and ketamine 25mg/kg) a lateral approach to the stifle joint was made in sterile conditions. Following lateral arthrotomy and medial patellar luxation, the femoral trochlea was visualized. A cylindrical hole (2 mm in diameter, 4 mm in depth) was drilled in the trochlear groove to imitate the osteochondral defect. Then the defect was filled with an implant using press-fitting method. The joint capsule, fascia and skin were closed in a routine manner. After the operation all rabbits were allowed to move freely in cages without any splints. The animals were sacrificed after three months of implant loading. The femoral trochleas were harvested, fixed in 4% paraformaldehyde solution and submitted to further analysis.

Skyscan 1174 system equipped with the dedicated control software (Bruker microCT, Belgium) was used for X-ray microtomography analysis. During scanning the sample was rotated within angular range of 0°÷180° with a step of 0.7°. After each step, three photographs were taken in order to average the exposure levels. In total, 257 photographs were taken. To eliminate possible artefacts, the sample was randomly moved for each projection. An aluminium 0.25 mm-thick filter was used at the source to reduce beam hardening effect. The images were then reconstructed into cross-sections using NRecon software (Bruker microCT, Belgium). After the reconstruction, the isotropic voxel size for the set of images was 18.3 mm in each axis. The set was then analyzed to establish geometrical measurements, using CTAn software (Bruker microCT, Belgium).

Results and discussion

The pins had the same measurements in diameter and length (TABLE 1) and the mass of the implants was also comparable, which confirms the possibility to achieve the statistically homogeneous group for further research. The applied degradation time does not affect the pH values or the conductivity of the immersion medium (water/PBS buffer). A slight change is noted in the shape of implants, especially noticeable in pins initially measuring 1 and 2 mm in diameter. Yet such a change concerns only 10% of the tested pins. As for the 4- mm pins, no change of shape or mass was noted. The tests assessing mechanical properties of the thin pins (φ=1; φ=2 mm) revealed the tensile strength decrease by 60% and the bending strength fall by 35% in comparison to the initial implant (TABLE 2). The pins of φ=4 mm do not record strength decrease (following the applied degradation time). Additionally, the analysis of the curves in the force-deformation system shows that the implant material becomes brittle after three months of incubation.

TABLE 1.

	Pin φ=1	Pin φ=2	Pin φ=4
Size	d=0.85-1.05 mm	d=1.95-2.12 mm	d=3.75-4.15 mm
Size after durability test	d=0.98-1.26 mm	d=1.97-2.15 mm	d=3.83-4.05 mm

TABLE 2. Mechanical properties of pins after durability test.

	Rm [MPa]	E [GPa]
Pin φ=2	122±2.11	2,12±0.5
Pin φ=2 after durability test	41.2±2.62	0.95±0.7

The reason for such a significant decrease in durability is the growing crystallinity value – from the initial 18% up to 38% after three months of incubation. The advanced degradation of the implant is also visible in the analysis of FTIR spectroscopy data. In the range of wavelengths characteristic for the groups -OH (3200-3600 cm^{-1}) and -COOH (1240-1380 cm^{-1}) there is the increase in intensity. It confirms their increased concentration in the implant signifying the molecular weight decrease (groups -OH i -COOH are the terminals of the polymer chain PLDLA). The X-ray images of rabbits' bones taken three months after the surgery showed a visible outline of the implant. No negative changes were noticed in the implantation area. The three-month clinical observation of the rabbits did not reveal any pathology concerning the rabbits' knees, all the animals moved ably. The μCT confirmed the in vitro results – firstly the bone implant swells as the degradation proceeds (the pin's diameter changes from 1,78 to 1,94 mm). None of the implanted pins underwent the disintegration (FIG. 1). Probably the degradation process in vitro is faster than the one in vivo, which might be connected with the immediate surroundings of the implant. In the tissue the implant is press-fitted, while in the immersion fluid the penetration is unlimited and happens all over the surface.

Conclusions

To conclude the preliminary research on the durability of polymeric pins, it may be assumed that in vitro testing does not entirely reveal the changes taking place in the pin implanted in the tissue. Still such a testing "in glass" is a probable prediction concerning the degradation rate and the stages of the process. The presented results prove PLDLA to be a material of high mechanical potential and relatively short degradation time. The particular properties of the implant's material seem to recommend it for a bone pin.

References

[1] Ole A. Raustol, Kornelis A. Poelstra, Annikar Chhabra, David R. Diduch, The Meniscal Ossicle Revisited: Etiology and an Arthroscopic Technique for Treatment, The Journal of Arthroscopic and Related Surgery, Vol 22, 2006: pp 687

[2] Dirk Stengel, Gerrit Matthe, Julia Seifert, Volker Tober, Sven Mutze, Grit Rademacher, Axel Ekkernkamp, Kai Bauwens, Michael Wich, Dirk Casper, Resorbable screws versus pins for optimal transplant fixation (SPOT) in anterior cruciate ligament replacement with autologous hamstring grafts: rationale and design of a randomized, controlled, patient and investigator blinded trial, BMC Surgery 2005, 5:1 doi:10.1186/1471-2482-5-1

[3] Mirco Herbort, Sandra Zelle, Dieter Rosenbaum, Nani Osada, Michael Raschke, Wolf Petersen, and Thore Zantop, Arthroscopic Fixation of Matrix-Associated Autologous Chondrocyte Implantation: Importance of Fixation Pin Angle on Joint Compression Forces The Journal of Arthroscopic and Related Surgery, Vol 27, 2011: pp 809-816

[4] P. J. Atkinson, R. L. Lancaster, T. S. Atkinson, S. P. Arnoczky, R. C. Haut, S. E. Weisbrode, Breaking Strength Retention and Histologic Effects Around 1.3-mm. ORTHOSORB® Polydioxanone Absorbable Pins at Various Sites in the Rabbit, The Journal of food & ankle surgery 37(1):42-47, 1998

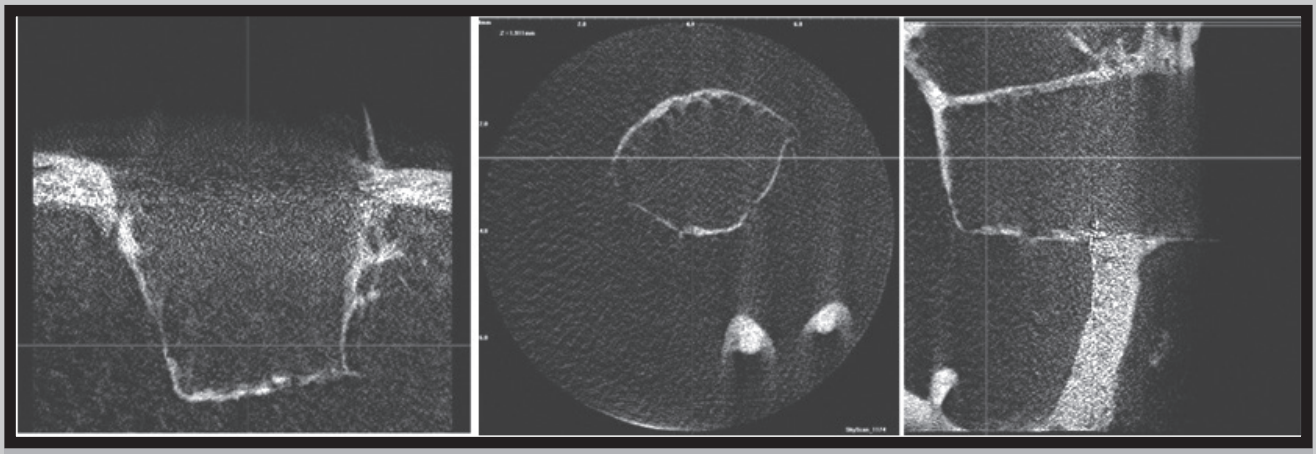

FIG. 1. Place of implanted pin in μCT photographs.

INJECTABLE BONE SUBSTITUTES BASED ON POLYURETHANE AND β-TCP

Piotr Szczepańczyk*, Kinga Pielichowska, Jan Chłopek

AGH University of Science and Technology
Faculty of Materials Science and Ceramics
Department of Biomaterials
30 Mickiewicza Av. 30-059 Kraków
*e-mail: pszczepa@agh.edu.pl

[Engineering of Biomaterials, 128-129, (2014), 90-91]

Introduction

Structure of segmented polyurethanes (PU) determines their widespread properties. PU/β-tri-calcium phosphate (β-TCP) open-celled foams may be used as three-dimensional scaffolds which successfully support cell adhesion, proliferation, angiogenesis, nerve and bone tissue regeneration [1]. The aim of this study was to investigate the influence of varying PEG/PCL ratios on properties of polyurethane hierarchical foams. Poly(ethylene glycol) (PEG) is an uncharged, hydrophilic and nonimmunogenic polymer used as component of blood-contacting devices [2]. Poly(ε-caprolactone) (PCL) is widely used in regenerative medicine due to good mechanical properties, nontoxicity and biocompatibility [3]. Li et al. developed hemocompatible PEG/PCL based PU which supported attachment, growth and proliferation of rat glial cells. The research carried out by Li et al. showed potential of PU based on PCL and PEG as nerve regeneration scaffolds [4]. PU synthesized by Gong et al. exhibited higher hydrophilicity with increasing PEG content. On the other hand higher PCL content prolonged degradation time [5]. This study focused on the relationship between composite structure and properties.

Materials and methods

β-TCP microparticles (with particle size ca 150 μm) were produced by Fluka Chemie GmbH. Composites were manufactured with different mass fractions of β-TCP (0, 20, 40, 60 and 80%). 4,4'- diphenylmethane diisocyanate (MDI), poly(ethylene glycol) (PEG) of average molecular weight (Mw) of 2000, poly(ε-caprolactone) diol (PCL) of Mw amounting to 2000 and 1, 4-butanediol (BDO) were purchased from Sigma Aldrich. Sulphonated castor oil (SCO) from Fluka Chemie GmbH and calcium stearate (CS) from POCH S.A. One-step synthesis was performed by mixing all the above mentioned substrates. SCO and CS were used for better porosity control and to obtain open porous systems. SCO played role of surfactant.

Fourier transform infrared (FTIR) spectra of the composites were obtained with a BIO-RAD FTS60V FTIR spectrometer in the middle infrared range with samples mixed with the KBr powder (about of 0.1-2% of the KBr amount) and pressed into pellets. The contact angles were measured by the sessile drop method using an automatic drop shape analysis system DSA 10 Mk2 (Kruss, Germany). Ultra high quality (UHQ) water droplets with a volume of 0.2 μl were placed on each sample surface and the contact angles were obtained by averaging the results of ten measurements. Compressive tests were carried out with the aid of a mechanical testing machine Zwick on dry samples.

Results and discussions

The structure of obtained polyurethane was confirmed by FTIR method. The FTIR spectra (FIG. 1) revealed structure changes occurring by different PEG/PCL ratio. Characteristic absorptions corresponding to functional groups in PEG and PCL differ from each other. This allows to detect structural changes with aid of infrared spectroscopy.

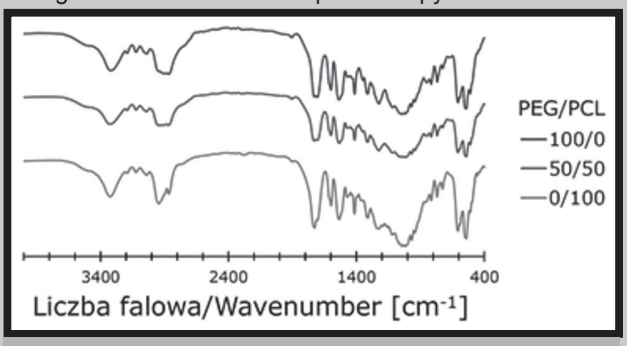

FIG. 1. FTIR spectra for PU/β-TCP composite samples containing 80% β-TCP.

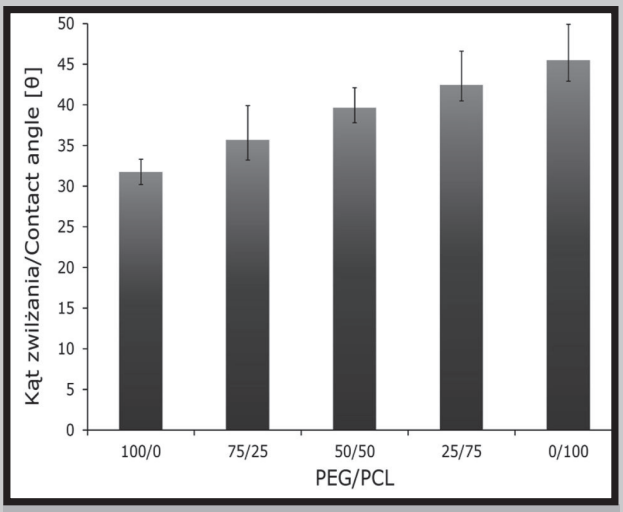

FIG. 2. Contact angle values measured on surface of the composites containing 80% β-TCP.

The characteristic peak at 1100 cm^{-1} corresponds to the ether linkage C-O-C present in PEG. The absorbance at 1730 cm^{-1} corresponds to the ester carbonyl linkage present in PCL. The band located at 3330 cm^{-1} proves presence of N-H stretching vibrations and band at 2934 and 2850 cm^{-1} is assigned to asymmetric and symmetric vibrations of group CH_2. Backbone vibrations causing stretch of the C-C binding within aromatic ring absorb radiation in range 1600-1585 cm^{-1} and 1500-1400 cm^{-1}. Stretching vibration C-N, in turn, absorbs radiation of wavenumber 1222 cm^{-1}. The band at 1535 cm^{-1} is assigned to bending vibrations of N-H group. The bands at 570 cm^{-1} and 600 cm^{-1} are assigned to the O–P–O bending mode in β-TCP.

Contact angle was measured on surface of the samples to assess the contribution of PEG into hydrophilicity. The measured values are shown in the FIG. 2.

The values are average of measurements from 10 readings for each sample. The above results indicate that PEG is more hydrophilic than PCL. The increasing PCL content caused higher contact angle. This complies with previous research [6]. Different PEG/PCL ratios may be used to manipulate hydrophilicity of the composite samples. Additionally β-TCP influenced hydrophilic nature of the surface. Pure PU surface is more hydrophobic in comparison with composites containing β-TCP microparticles.

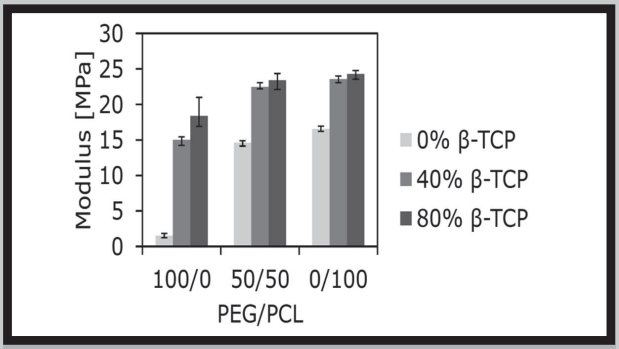

FIG. 3. Modulus of composite samples.

Compressive tests were carried out on dry samples. The modulus was calculated on basis of force-strain relationship curvatures. The results are shown in the FIG. 3.

The above results show an increase of modulus with increasing PCL and β-TCP content. These results comply with previously carried out research [7]. Both PCL and β-TCP can be used to manipulate mechanical properties. However the values are much lower than in case of cancellous bone of which Young's Modulus amounts to 60-260 MPa [8].

Conclusions

Porous composite materials containing bioactive ceramics were synthesized and characterized. They have potential to be applied as injectable biomaterials. However there is still need to investigate their properties considering tissue engineering application.

Acknowledgements

This work was financed by statutory research 11.11.160.256 of Faculty of Materials Science and Ceramics, AGH University of Science and Technology.

References

[1] Pereira I.M., Gomide V., Oréfice R.L., De Fátima Leite M., Arcoverde Cavalcanti Zonari A., Goes A.M.: Proliferation of human mesenchymal stem cells derived from adipose tissue on polyurethanes with tunable biodegradability. Polímeros 20 (2010) 280-286.
[2] Guo J., Feng Y., Ye Y., Zhao H.: Construction of hemocompatible polycarbonate urethane with sulfoammonium zwitterionic polyethylene glycol. Journal of Appplied Polymer Science 122 (2011) 1084-1091.
[3] Valence S.D., Tille J.C., Mugnai D., Mrówczyński W., Gurny R., Möller M., Walpoth B.H.: Long term performance of polycaprolactone vascular grafts in a rat abdominal aorta replacement model. Biomaterials 33 (2012) 38–47.
[4] Li G., Li D., Niu Y., He T., Chen K.C., Xu K.: Alternating block polyurethanes based on PCL and PEG as potential nerve regeneration materials. Journal of Biomedical Materials Research Part A 102 (2014) 685-97.
[5] Gong, C.Y., Fu S.Z., Gu Y.C., Liu C.B., Kan B., Deng H.X., Luo F., Qian Z.Y.: Synthesis, Characterization, and Hydrolytic Degradation of Biodegradable Poly(ether ester)-Urethane Copolymers Based on ε-Caprolactone and Poly(ethylene glycol). Journal of Applied Polymer Science. 113 (2009) 1111-1119.
[6] Sarkar D., Yang J-C., Klettlinger N., Lopina S.T.: Blends of L-tyrosine based polyurethanes for biomaterial applications. eXPRESS Polymer Letters 1 (2007) 724-733.
[7] Szczepańczyk P., Pietryga K., Pielichowska K., Chłopek J.: Porous composites polyurethane/β−TCP for orthopaedic applications. Engineering of Biomaterials 16 (2013) 33-41.
[8] Liu S., Qi W., Zhang Y., Wu Z-X., Yan Y-B., Lei W.: Effect of bone material properties on effective region in screw-bone model: an experimental and finite element study. Biomedical Engineering 13:83 (2014)

APPLICATION OF INJECTION METHOD TO MODIFY TITANIUM ALLOY Ti6Al4V

Justyna Klimas [1]*, Adrian Łukaszewicz[1], Michał Szota[1], Marcin Nabiałek[2]

[1]Czestochowa University of Technology, Faculty of Production Engineering and Materials Technology, Institute of Material Engineering,
19 Armii Krajowej Ave., 42-200 Częstochowa
[2]Czestochowa University of Technology, Faculty of Production Engineering and Materials Technology, Institute of Physics,
19 Armii Krajowej Ave., 42-200 Częstochowa
*e-mail: justynaklimas88@gmail.com

Abstract

In the present work, the samples were subjected to a comparative analysis of the titanium alloy Ti6Al4V prepared by various methods. The research included a comparison of the following properties of manufactured elements: microstructure, phase composition and surface roughness. The test results clearly showed that these properties are different when using different method of casting. These changes allows the use of prepared elements in medicine.

Keywords: *biomaterials, titanium alloy Ti6Al4V, massive amorphous alloy*

[Engineering of Biomaterials, 128-129, (2014), 91-92]

Introduction

Long-term studies lasting over metallic materials suitable for biomedical applications have shown, that a group of alloys based on titanium is safe to implant applications. Since the forties of the last century there are attempts selecting the ideal chemical composition of the alloy, which would be completely neutral to the human body. One of the most widely used implant material is titanium alloy Ti6Al4V, although that alloy doesn't have only advantages [1,2]. Currently, studies are carried out of the attempt to obtain amorphous materials based on titanium, thereby resulting in improved mechanical properties, more developed surface, higher biochemical resistance. Obtaining materials with such properties allows the injection method, which the liquid is injected into the metallic copper mold cooled with a suitable rate [3,4].

Materials and methods

The first test sample was cut by waterjet from purchased rod made of titanium alloy Ti6Al4V, the second was produced by a novel method of injection. The chemical composition of materials tested are given in TABLE 1.

Samples were subjected to microscopic analysis, qualitative X-ray analysis, assessment of surface topography.

TABLE 1. Chemical composition of titanium alloy Ti6Al4V.

Chemical composition	Al	V	C	Fe	O	N	H	Ti
%	6	4	0,03	0,1	0,15	0,01	0,003	rest

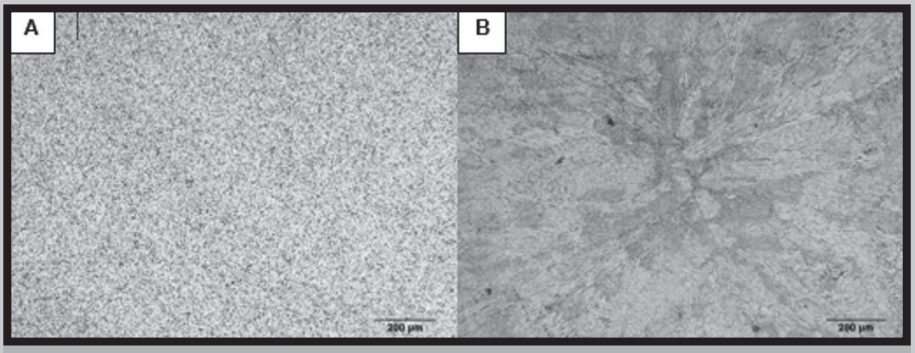

FIG. 1. Microstructure of titanium alloy Ti6Al4V produced by: a) conventional method, b) injection method.

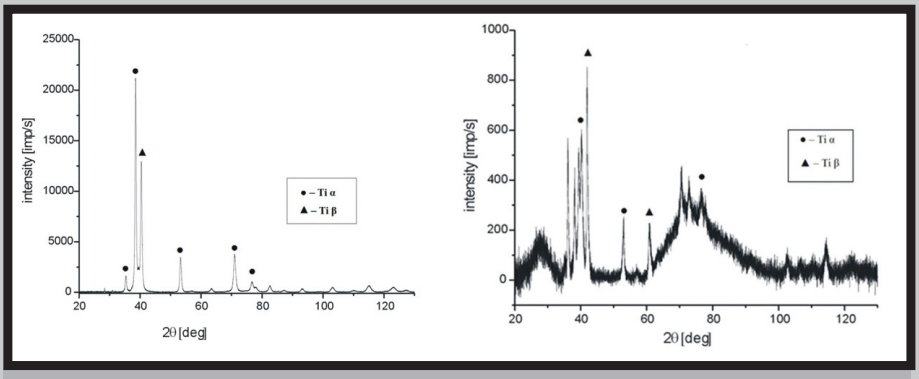

FIG. 2. Diffraction patterns of titanium alloy Ti6Al4V produced by: a) conventional method b) injection method.

TABLE 2. Summary of roughness parameter Ra of surface samples.

Sample	Numer of masurement	Parametr					
		R_t	RS_m	R_z	R_a	R_p	R_{max}
Conventional method	masurement I	3,21	0,02	1,86	0,19	1,71	3,21
	masurement II	6,46	0,03	3,47	0,31	2,55	6,50
	masurement III	2,24	0,01	1,59	0,33	0,99	2,56
	Average	3,97	0,02	2,31	0,28	2,08	4,09
Injection method	masurement I	2,53	0,11	1,78	0,44	1,30	2,53
	masurement II	2,48	0,08	1,40	0,34	1,50	2,48
	masurement III	2,96	0,09	1,74	0,42	1,21	2,81
	Average	2,66	0,09	1,64	0,4	1,34	2,61

Results and discussion

Samples were submitted for microstructure using an optical microscope Axiovert. The resulting microstructures are shown in FIG. 1.

Microstructural observations using light microscopy of samples produced by two methods allowed for finding, that the samples obtained by the conventional method have a crystal structure typical of a two-phase materials. Material produced by injection is characterized by a lack of regularity and short-range ordering.

The samples were prepared by two methods was subjected qualitative X-ray analysis, in order to determine the phase composition. Graphical representation of the X-ray studies show the diffraction patterns presented in FIG. 2.

The diffraction pattern of the titanium alloy produced by the conventional method shows crystal structure, and discloses the two peaks of the titanium phase. For samples produced through injection, diffraction pattern has a characteristic waveform for the partly crystalline material. There are wide angle peaks forming the typical backdrop of amorphous samples, as well as occur peaks of the crystallite phase.

In order to determine the surface topography, and its parameters studies were carried out with using a Hommel T1000 profilometer. Determination of surface roughness parameter R_a made in contact with the test surface by the engagement of the needle with a differential measuring arrangement. The results roughness parameter R_a are shown in TABLE 2.

Analyzing the arithmetic average ordinates of profile R_a, obtained during the study of surface geometry can be stated that a smaller development of the surface characterized samples produced by conventional method as compared to the samples produced by injection method.

Conclusions

Microstructural observations allowed the determination of the structure depending on the method of production. Traditionally manufactured titanium alloys have a crystal structure, with regular arrangement of grains, while the injection method allow produce a massive amorphous materials, with lack of regularity, this material is present in only a long-range ordering. Confirmation of the structural test records are obtained with a qualitative analysis of the diffraction of X-ray. Evaluation of surface topography allowed to state, that elements produced by the injection have higher surface roughness, than the same alloys produced by the conventional method, which from the point of view of application components such implants is very advantageous phenomenon.

References

[1] Jurczyk M., Jakubowicz J.: Biomateriały, Wydawnictwo Politechniki Poznańskiej, Poznań 2008.
[2] Klimas J., Dudek A. Klimas M.: Surface Refinement of Titanium Alloy Ti6Al4V ELI, Engineering of Biomaterials R.15 nr 116 -117, 2012.
[3] Klimas J., Szota M., Nabiałek M., Łukaszewicz A., Bukowska A.: Comparative Description of Structure and Properties of Ti-6Al-4V Titanium Alloy for Biomedical Applications Produced by Two Methods: Conventional (Molding) and Innovative (Injection) Ones. Journal of Achievements in Materials and Manufacturing Engineering Vol.61 Iss.2, 2013, s.195 - 201.
[4] Nabiałek M.: Wytwarzanie oraz właściwości amorficznych i nanokrystalicznych stopów żelaza, Wydawnictwo Politechniki Częstochowskiej, Częstochowa, 2012.

IDEAL SELECTION OF COLOR. EFFECTIVENESS OF VISIONARY TECHNIQUE IN THE DENTAL PRACTICE

Jacek Kasperski, Magdalena Cieślik, Katarzyna Sutkowska, Patrycja Sikorska, Ewa Białożyt

Medical University of Silesia,
School of Medicine with the Division of Dentistry
17 Akademicki Place, 41-902 Bytom Poland

Abstract

Introduction: *Aesthetic restorations also have a significant impact on the success of prosthetic treatment which recreates the proper functioning of the teeth. Suitable aesthetic effect is determined by the appropriate restoration of tooth shape and colour. Selecting the proper colour of artificial teeth is difficult and may suffer from many problems in everyday dentistry. In addition, visual assessment for the help of the unique is subjective and may give erroneous results. On the market there are auxiliary device for the instrumental assessment of the colour of teeth: spectrophotometers, calorimeters, colour analyzers computer. They are not commonly used in everyday medical practice.*

Goal: *The aim of the study is to assess the applicability of Sopro 717 intraoral camera in the correct assessment of the colour of teeth.*

Methods: *The study was conducted based on the evaluation of the natural tooth colour visually using the unique "Lumin - Vacuum" by the patient's dental and medical students in natural light and using the intraoral camera having their own source of light. The experiment involved 40 people aged 22-46 years. The study was conducted to assess the colour of the surface of the cheek teeth 11 or 21 and 32 Takes into account a number of factors affecting the proper assessment of the colour of teeth such as colour space, light intensity, eye fatigue investigator.*

Results: *The evaluation of the occurrence of differences in colour of the teeth within the two mentioned methods.*

Conclusions: *Intraoral camera helps us to choosing the right colour of the tooth. Although this is still a subjective method allows us to reduce the number of errors made in the selection of the proper shade of hard tissues of the tooth.*

Keywords: *selecting colour of teeth, intraoral camera, shade guide*

[Engineering of Biomaterials, 128-129, (2014), 93]

PHYSIOCHEMICAL AND BIOLOGICAL EVALUATION OF THIN CNTS LAYERS

Aleksandra Benko[1]*, Agata Przekora[2], Marek Nocuń[1], Aleksandra Wesełucha-Birczyńska[3], Grażyna Ginalska[2], Marta Błażewicz[1]

[1]AGH University of Science and Technology,
Faculty of Materials Science and Ceramics,
Department of Biomaterials,
30 Mickiewicza Ave., 30-059 Krakow, Poland
[2]Department of Biochemistry and Biotechnology,
Medical University of Lublin,
Faculty of Pharmacy with Medical Analytics Division,
1 Chodzki Str., 20-093 Lublin, Poland
[3]Department of Chemical Physics, Faculty of Chemistry,
Jagiellonian University,
3 Ingardena Str., 30-060, Krakow, Poland
*e-mail: abenko@agh.edu.pl

Abstract

Carbon nanotubes are nanometric-sized materials which possess a set of interesting features that favor their applications in various fields of materials engineering, including biomedical applications. However, their usage as implants or in nanomedicine raises many questions, regarding their potential cytotoxicity, relative to their length, diameter, structure and functional groups, present on their outer walls. The given study presents a physiochemical and biological in vitro (in accordance with EN-ISO 10993-5) evaluation of thin carbon nanotubes films, deposited on the surface of titanium, by means of the EPD process. Experiments were carried out on commercially available, pre -functionalized with OH groups, multi-walled carbon nanotubes. The obtained material is proven to be biocompatible, with no cytotoxic effect on the human fetal osteoblast cell line. During the study, selectivity of the EPD process was proven - performed experiments revealed that the process favors deposition of CNTs with chosen set of features from the stock solution. Presented results point out that the EPD process can be successfully applied as a method for fractioning the CNTs, aimed to fabricate non-toxic layers that might be considered for various biomedical applications.

Keywords: *EPD, MWCNTs, thin layers, biocompability*

[Engineering of Biomaterials, 128-129, (2014), 93-94]

Introduction

Due to their extremely high mechanical properties [1] and good electric and thermal conductivity [2], carbon nanotubes are nowadays a widely considered material for various applications – either as a reinforcing phase in composites or as electrodes for electrochemistry, supercapacitors and actuators. However, in terms of their biomedical application, a real potential lies within good biocompability and a possibility to promote growth and differentiation of various tissues. These promising features have already been proven by some of the scientists and published in numerous reports, which propose usage of the CNTs either in tissue engineering [3], in nanomedicine [4,5] or as implantable electrodes that would aid in treatment of assorted diseases [6].

Despite many promising results presented independently by scientists worldwide, a road towards actual biomedical application of the CNTs is still bumpy, due to many controversies regarding their potential cytotoxicity. In the literature, one can find many contradictory results, with some scientists pointing out adverse cytotoxic responses and others proving very good biocompability. We believe that the reason of such large discrepancy in the reported studies lies within heterogeneity of the studied materials, having different dimensions, type and amount of functional groups or level of structural perfection – all reported to be determinants of the outcome CNTs toxicity, both in vitro and in vivo [7]. What is more, in some of the cytotoxicity studies, very poor physiochemical evaluation is performed and no connection between the outcome cells response and properties is established.

The aim of the study was to fabricate thin layers of the MWCNTs on the surface of biocompatible titanium, study their physiochemical properties and perform cytotoxicity evaluation in order to establish some of the very basic correlations between physiochemistry and outcome cell's reaction. In the study, EPD process was used as a fractioning tool for obtaining dense layers of well adhered CNTs of uniform, strictly desired properties. The proposed method not only allows for fabrication of the CNTs layers of well-defined characteristics but also creates a vast possibility for further modifications of the properties.

Materials methods

In the study, physiochemical evaluation of the stock MWCNTs, modified with OH groups, provided by the NanoAmor (Stock#: 1249YJF), is performed by means of SEM, Raman, XPS and goniometer. Next, the as-received CNTs are used to create a stable suspension in ethanol and acetone (1:3), which is consecutively applied in the EPD process. Layers are obtained for two different times of deposition and their physiochemical properties are evaluated. Finally, a thicker layer, showing no titanium peaks in the XPS spectrum is used in the in vitro both indirect and direct contact cytotoxicity studies (in accordance with ISO 10993-5, using hFOB 1.19 cell line - normal human fetal osteoblasts), guaranteeing that only influence of the CNTs on cells is studied.

Results and discussions

Physiochemical evaluation of both stock MWCNTs and the obtained layers proves that the EPD process favors deposition of different kinds of tubes in the function of time. The preliminary in vitro study indicates that by means of the deposition, highly biocompatible material is obtained, with even less-pronounced indirect contact cytotoxicity than the negative control sample (PS of the culture well). During direct contact cytotoxicity evaluation, no dead cells on the surface of the material were observed, compared to very little on pure titanium.

Conclusion

The applied EPD method was proven to be a good fractioning tool for the CNTs containing different chemical species on their surface. Preliminary in vitro biocompatibility assessment revealed promising applicability of the method for fabricating nontoxic layers of strictly desired, potentially steerable properties, for various biomedical applications, including implantable electrodes or scaffolds for tissue engineering.

Acknowledgements

This work has been supported by National Science Centre (NCN) grants Nos.: 2011/01/B/ST5/06424.

References

[1] Demczyk, B.G., et al., Direct mechanical measurement of the tensile strength and elastic modulus of multiwalled carbon nanotubes. Materials Science and Engineering: A, 2002. 334(1–2): p. 173-178.
[2] Kwon, O.-S., et al., Fabrication and characterization of inkjet-printed carbon nanotube electrode patterns on paper. Carbon, 2013. 58(0): p. 116-127.
[3] Harrison, B.S. and A. Atala, Carbon nanotube applications for tissue engineering. Biomaterials, 2007. 28(2): p. 344-353.
[4] Foldvari, M. and M. Bagonluri, Carbon nanotubes as functional excipients for nanomedicines: I. pharmaceutical properties. Nanomedicine: Nanotechnology, Biology and Medicine, 2008. 4(3): p. 173-182.
[5] Foldvari, M. and M. Bagonluri, Carbon nanotubes as functional excipients for nanomedicines: II. Drug delivery and biocompatibility issues. Nanomedicine: Nanotechnology, Biology and Medicine, 2008. 4(3): p. 183-200.
[6] Justino, C.I.L., et al., Advances in point-of-care technologies with biosensors based on carbon nanotubes. TrAC Trends in Analytical Chemistry, 2013. 45(0): p. 24-36.
[7] Lanone, S., et al., Determinants of carbon nanotube toxicity. Advanced Drug Delivery Reviews, 2013. 65(15): p. 2063-2069.

MATERIALS AND METHODS SUPPORTING NERVE REGENERATION IN PERIPHERAL AND CENTRAL NERVOUS SYSTEM

Jadwiga Laska[1]*, Paulina Bednarz[2], Anna Lis[1], Dariusz Szarek[3]

[1]AGH University of Science and Technology,
Faculty of Material Science and Ceramics,
30 Mickiewicza Ave., 30-059 Krakow
[2]State Higher Vocational School in Tarnow,
8 Mickiewicza Str., 32-100 Tarnow
[3]T.Marciniak Lower Silesian Specialist Hospital - Emergency Center, Department of Neurosurgery,
116 Traugutta Str., 53-127 Wroclaw
*e-mail: jlaska@agh.edu.pl

Keywords: *polyurethane, polylactide, polymer blends, implants, neuroregeneration*
[Engineering of Biomaterials, 128-129, (2014), 95-96]

Typical problems strictly connected with injuries of both peripheral and central nervous system are sensor and motor disabilities, and sometimes even paralysis. In addition, minor nerve damage can cause a formation of benign tumors - neuroma. The most common reasons for nerve injuries are car and construction accidents, tumors and cancers and iatrogenic side effects of many surgical procedures such as orthopedic or dental.

The injuries of the peripheral nerves and the spinal cord are treated differently. This is mainly due to the fact that the peripheral nerves are capable of autoregeneration and the interruption of the spinal cord triggers the formation of the glial scar which prevents growth of axons. When the peripheral nerve is disrupted, connection or bridging the nerve stumps is used. To bring back the nerve function transplant from other place in the body or nerve fibers from another organism can be taken as well as synthetic implant can be used. Synthetic implant, most often a tube connecting nerve stumps, provides protective environment, limits fibrous infiltration and enhances concentration of locally produced growth factors. Nerve functions properly when the anatomic continuity of nerve fibers and proper synaptic connection is ensured between nerve fiber and its effector. The success of the repair process depends on the level of nerve damage. Regeneration of neural tissue significantly differs from the healing process taking place in the other tissues in the body. The spinal cord requires a more comprehensive approach associated with the need to inhibit glial scar formation and to provide a place of loss scaffold to facilitate directed growth of axons.

In this study polymers that found application as a implantable materials were chosen. Attention was focused on a mixture of two polymers, namely, polyurethane an polylactide, mixed with weight ratio 80/20. The choice of that mixture was not made unintentional, material of that composition shows good surgical handiness and posses suitable mechanical properties for the needs of neurosurgery and angioplasty. The thermal and surface properties were characterized as well as tests in vitro on cells (fibroblasts and mesenchymal cells) and in vivo on group of rats (for peripheral nerve regeneration assessment), and geckos (for spinal cord regeneration assessment) were done.

Polyurethane, produced by Bayer, built up of hexamethylenediisocyanate and ε- oxycaproic (PCL of mass 530 Da) segments was used. Isosorbitol was applied as a chain extender. Poly(L-lacide-co-DL-lactide) consisting of 80% of L-lactide and 20% of DL-lactide was purchased from Purac. Both polymers received medical certificate and can be used in medical applications. Sodium and calcium alginate (NaAlg and CaAlg, respectively) fibers, obtained by wet method from alcohol solution, were produced in Department of Man-Made Fibres on Faculty of Material Technologies and Textile Design, Łódź University and Technology. Films were prepared by dissolving polyurethane and polylactide in dimethylformamid at temperature of ~45 °C, in order to obtain 10% solution. Series of films with different weight ratio of polyurethane to polylactide. Polymeric tubes were manufactured by vertical immersing of mandrels in a polymer solution or in their mixture. Polymer coated mandrels were then placed into cold distilled water, where they were allowed for 10-15 minutes, then tubes were slipped off the mandrels and placed in vacuum dryer at temperature of 45-50°C for at least 48 hours.

When porosity was needed, suitable amount of porogen was added to the polymeric mixture for manufacturing films and tubes. Pentane, sodium phosphate, sodium chloride, polyethylene glycol of different viscisities and different molecular weights, were used as a porogenic substance. To obtain a homogeneous mixture and to prevent sedimentation the suspension was homogenized with the use of ultrasounds. After evaporation of the solvent the porogen was washed out form the polymer blend with ultrapure distilled water.

The resulting mixture of polymer in the form of solid films, porous films, sponges, microtubules, and various forms of implants for spinal cord were subjected to comprehensive material testing. Mechanical evaluation on tensile and compressive strength, spectroscopic tests with using of total internal reflection technique (ATR) in the range of mid-infrared (500-4000 cm^{-1}), wettability determination using sessile drop method on DSA (Drop Shape Analysis) 10 Kruss at ambient temperature in air, and surface roughness were performed. The pore size distribution of the tested materials PU/PLA was determined using a porosimeter PoreMaster 60, Quantachrome Instruments company. Porosity measurements on small pores were made on the multi-function automatic apparatus ASAP 2010, Micromeritics Company with using of volumetric sorption of nitrogen method. The microstructure of the PU/PLA films as well as tubes was observed under a scanning electron microscope (SEM Nano Nova 200, FEJ EUROPE Company, USA). The rate of degradation was evaluated in the conductivity and pH values changes of the incubated solution and on the basis of cubes weight degraded during incubation. Materials used in biological tests in vitro and in vivo were sterilized with the use of peroxide cold plasma. In order to determine the effect of the sterilization method on properties of a polymeric material, ethylene oxide sterilization and ultraviolet radiation in a laminar was also carried out.

The sterilized films were placed in 24-well plate (Nunclon, Denmark), both surfaces of the films (top surface, i.g. air-cured, and bottom surface, i.g. glass-cured) were tested and as a control the bottom of the well tissue culture polystyrene-TCPS was used. NIH 3T3 mouse embryonic fibroblast cells were cultured on the studied materials in DMEM (PAA, Austria) supplemented with 10% FBS, 1% penicilin/streptomycin at 37ºC under 5.0% CO_2 atmosphere for 24 hours and 7 days. MTT test was used for cells viability measurements. Morphology of the cells was observed under fluorescence microscopy (Zeiss Axiovert, Carl Zeiss, Germany).

The cultured cells were fixed in 4% paraformaldehyde for 1 h, then washed in PBS and stained with acridine orange solution (1 mg/mL). Examination of the viability and proliferative activity of stem cells was carried out using the test Alamar Blue (Sigma Aldrich, Germany). To the culture medium DMEM / F12 Ham's with 10% bovine serum and 1% antibiotics was applied.

In vivo studies of peripheral nerve regeneration were carried out on groups of male rats (Wistar, each approx. 300 g), and the regeneration of the spinal cord was observed on a group of leopard gecko after implantation in the animal's tail.

Acknowledgements

The authors gratefully acknowledge the National Science Center (Poland) for financial support (grant no. 2011/01/B/STB8/07795 and N N403 176540).

THE INFLUENCE OF PRE-COARSENING ON ARCHITECTURAL AND MECHANICAL PROPERTIES OF HIGHLY POROUS TITANIUM DIOXIDE SCAFFOLDS FOR BONE TISSUE ENGINEERING

Katarzyna Reczyńska[1], Łucja Rumian[1], Elżbieta Pamuła[1], Havard J. Haugen[2], Hanna Tiainen[2]

[1]AGH University of Science and Technology,
Faculty of Materials Science and Ceramics,
Department of Biomaterials,
30 Mickiewicza Ave., 30-059 Krakow, Poland
[2] University of Oslo, Institute for Clinical Dentistry,
Department of Biomaterials,
PO Box 1109 Blindern, 0317 Oslo, Norway

[Engineering of Biomaterials, 128-129, (2014), 96-98]

Introduction

Highly porous titanium dioxide (TiO_2) scaffolds are very interesting among other bone substitutes. TiO_2 is proved to be fully biocompatible with bone tissue and it promotes proliferation of bone cells [1]. TiO_2 scaffolds can be manufactured by polymer sponge replication method, which enables obtaining materials with preferable pore architecture. However, high porosity significantly reduces compressive strength of the scaffolds [2]. In ceramics, a lot of defects are introduced to the material during sintering, in which powder particles are irreversibly fused into one piece. Any inhomogeneity in green body can lead to formation of microstructural flaws and reduction of mechanical strength of the material [3]. Pre-coarsening of the material can eliminate the smallest pores and particles and allow obtaining more homogenous and fine grained ceramics [4-6].

In the present study, pre-coarsening was used in order to improve mechanical properties of the TiO_2 scaffolds manufactured by polymer sponge replication method. To this end four different dwelling times (2, 5, 10 or 30 h) at 1100°C were tested prior final sintering at 1500°C for 20 h. The main goal of the study was to find out what is the most preferable time of pre-coarsening treatment from the point of view of increase in compression strength.

Materials and methods

Manufacturing of titanium dioxide scaffolds

TiO_2 powder (Kronos 1171, Kronos Titan GmbH, Leverkusen, Germany) was cleaned prior to use in order to remove phosphate ions from the surface of the particles. Raw powder was soaked in 1M NaOH solution and then rinsed several times with deionized water. After drying, powder was sieved and particles between 0-100 μm were collected for further processing. For preparation of the slurry, 65 g of cleaned TiO_2 powder was gradually mixed with 25 ml of deionized water at low stirring rate (1000 pm). After 10 min of initial homogenization, pH of the slurry was measured and adjusted with 1M HCl solution to 1.5-1.7. Stirring was continued for 2.5 h at 15°C and stirring rate of 5001 rpm. Polyurethane sponge (60 ppi, Bulbren S, Eurofoam GmbH, Wiesbaden, Germany) was cut into cylinders (10 mm in height and 12mm in diameter), washed and dried. Templates were immersed in a slurry and compressed few times. Excess slurry was removed by squeezing templates between two polyurethane foam sheets using a self-made device. Dried scaffolds were hated up at 0.5°C/min to 450°C and kept for 1h in order to remove polymeric material. Then scaffolds were heated up at 1°C/min to 1100°C, dwelled for 2, 5, 10 or 30 h (20 samples for each group) and cooled down at -5°C/min. 10 samples from each group were withdrawn, the remaining ones were sintered at 1500°C for 20 h.

Material characterization

In order to investigate the influence of pre-coarsening on architectural parameters of the scaffolds, 5 sintered samples from each group were examined using micro-computed tomography (micro-CT). Samples were scanned using desktop 1172 micro-CT imaging system (Skyscan, Kontich, Belgium). Data were reconstructed using standard SkyScan software (NRecon) and analyzed with standard SkyScan software (CTan). The microstructure of the non-sintered and sintered scaffolds was analyzed using scanning electron microscopy (Hitachi TM3030, Hitachi High-Technologies Corporation, Tokyo, Japan). The main interest was put in compressive strength of the scaffolds. All of the samples were examined using Zwicki (Zwick/Roell, Ulm, Germany) according to DIN EN ISO 3386. Statistical analyses were performed using SigmaPlot 12.0 software (Systat Software Inc., San Jose, United States of America).

Results and discussion

TABLE 1 presents selected architectural parameters of the sintered scaffolds. No statistically significant differences were found between different groups, which proves that the pre-coarsening treatment does not affect architecture of the scaffolds.

FIG. 1 presents microstructure of the selected samples. In the case of non-sintered samples (upper panel), it can be found that after 2 h of dwelling powder particles are barely connected with each other, while after 5 and 10 h, necks between particles are much wider. After 30 h initial sintering of particles occurred. The microstructure of sintered samples is very similar, with the presence of large and irregular grains (lower panel). However, scaffolds heat-treated for 5 h at 1100°C seem to be more uniform than the others.

TABLE 1. Selected architectural parameters of the sintered scaffolds dwelled at 1100°C for different period of time and sintered for 20 h at 1500°C (n=5).

Sample	Strut thickness [μm]	Pore size [μm]	Closed porosity [%]	Open porosity [%]
2 h at 1100°C 20 h at 1500°C	63.8 ± 6.7	437 ± 7	0.91 ± 0.28	90.1 ± 1.0
5 h at 1100°C 20 h at 1500°C	61.6 ± 3.1	427 ± 22	0.78 ± 0.29	90.3 ± 1.1
10 h at 1100°C 20 h at 1500°C	61.4 ± 8.1	434 ± 11	1.23 ± 0.39	90.1 ± 1.0
30 h at 1100°C 20 h at 1500°C	62.0 ± 5.1	431 ± 24	0.97 ± 0.29	89.7 ± 1.0

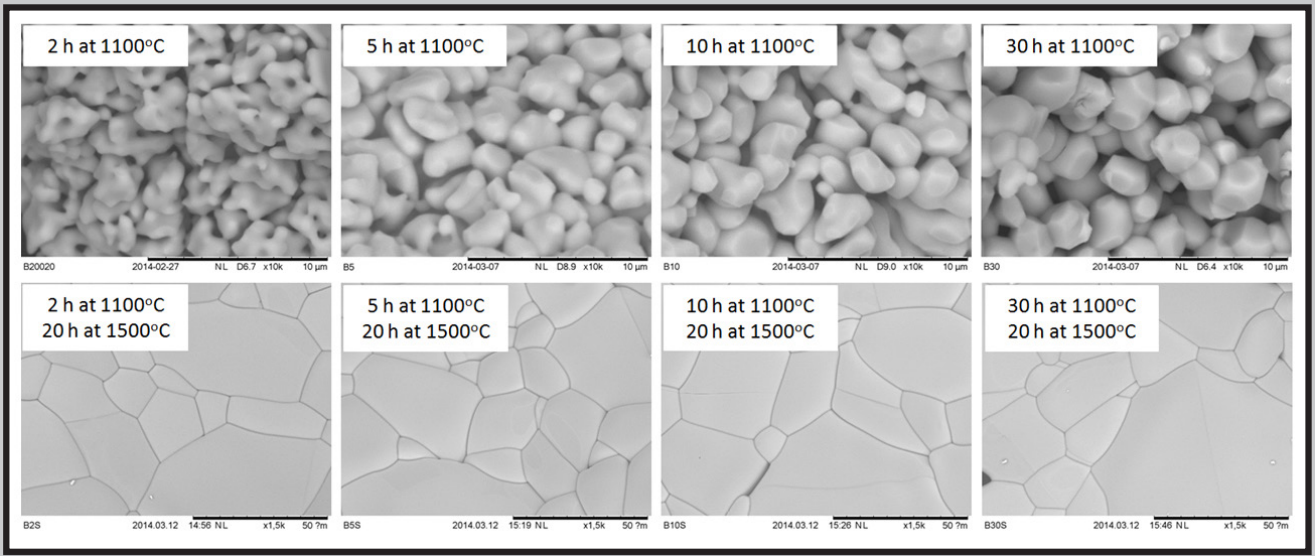

FIG. 1. SEM images of samples after pre-coarsening phase (upper panel) and corresponding samples after sintering (lower panel).

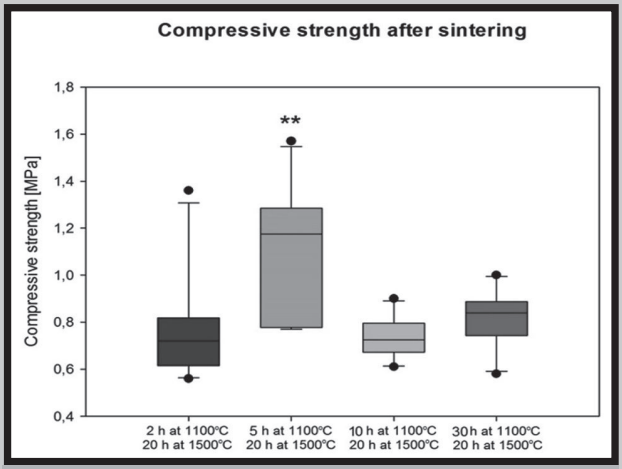

FIG. 2. Comparison of compressive strength of scaffolds after sintering (P < 0.01 against all other groups). The bottom and the top of the box represent the first and third quartiles, the band inside the box - the second quartile (median). The whiskers stand for the minimal and maximal values, excluding outliers (values lower than 3/2 of the first quartile or greater than 3/2 of the third quartile, marked with dots).**

Compressive strength of non-sintered scaffolds was very similar for all groups, but in the case of sintered samples significant differences were found (FIG. 2). The highest compressive strength was measured for the samples dwelled at 1100°C for 5 h. One-way ANOVA confirmed that difference between group pre-coarsened for 5 h and the other groups was significantly higher with the probability level $P<0.01$. No significant differences had been found between groups dwelled for 2, 10 and 30 h.

Improved compressive strength of the scaffolds pre-coarsened for 5 h at 1100°C resulted probably from more uniform microstructure. Higher concentration of grain boundaries inhibited propagation of the cracks and strengthened the material. When large grains were present, cracks were more likely to propagate through the grains and they spread more easily in the whole volume of the material.

What is noteworthy, closed porosity of the scaffolds pre-coarsened for 5 h was slightly lower than in the other samples, which indicates that densification of the material and porosity reduction was the most successful after 5 h of pre-coarsening. Increase in dwelling time could cause initial sintering of particles, isolation of pores and in the end, might preclude effective densification.

Conclusions

Pre-coarsening did not affect architectural parameters of the titanium dioxide scaffolds such as pore size or porosity. However, it significantly improved the compressive strength of the scaffolds. 5 h of dwelling at 1100°C followed by sintering at 1500°C for 20 h was found as the most favorable in terms of microstructural and mechanical properties of the scaffolds.

Acknowledgements

Polish National Science Centre (Grant no: 2013/09/N/ST8/00309) is acknowledged for financial support.

References

[1] Tiainen, H et al.Processing of highly porous TiO_2 bone scaffolds with improved compressive strength. Journal of the European Ceramic Society. 2013. 33(1): p. 15-24.
[2] Tiainen, H. et al.. Bone formation in TiO_2 bone scaffolds in extraction sockets of minipigs. Acta Biomaterialia. 2012. 8:p. 2384-2391.
[3] Rahaman. M.N..Ceramic processing and sintering. 1995. New York: Marcel Dekker. Inc.
[4] Chu. M.Y. et al..Precoarsening To Improve Microstructure And Sintering Of Powder Compacts. Journal of the American Ceramic Society. 1991. 74(11): p. 2902-2911.
[5] Shen. Z.-Y. et al..Influence of Sintering Temperature on Grain Growth and Phase Structure of Compositionally Optimized High -Performance Li/Ta-Modified (Na.K)NbO3 Ceramics. Journal of the American Ceramic Society. 2009. 92(8): p. 1748-1752.
[6] Gupta, T.K. et al. Sintering of ZnO: I. Densification and Grain Growth. Journal of the American Ceramic Society. 1968. 51(9): p. 521-525.

CARBON FIBROUS MATERIAL FOR CARTILAGE TISSUE TREATMENT

Jaroslaw Markowski[1]*, Jan Pilch[1], Wojciech Ścierski[2], Aleksandra Benko[3], Elżbieta Menaszek[4], Marta Błażewicz[3]

[1]E.N.T. Department, Medical University of Silesia,
20-24 Francuska Street, 40-027 Katowice, Poland
[2]St. Joseph Hospital,
27 Okrzei Street, 43-190 Mikołów, Poland
[3]AGH University of Science and Technology,
Faculty of Materials Science and Ceramics,
Department of Biomaterials,
30 Mickiewicza Ave., 30-059 Krakow, Poland
[4]Jagiellonian University (UJ), Collegium Medicum,
Department of Cytobiology,
9 Medyczna Street, 30-068 Cracow, Poland
*e-mail: jmarkow1@poczta.onet.pl

Abstract

The work presents in vitro and in vivo experiments related to the evaluation of the biological properties of the two groups of carbon fibrous (micro, nano) materials. We investigated the carbon materials in the form of a biomimetic scaffolds made from carbon nanotubes and a composite membrane made from carbon micro-fiber and biocompatible polymer to induce regeneration of missing cartilage tissues. Evaluation of biological properties of both materials clearly showed that carbon fibrous material is biocompatible with cartilage cells and stimulates regeneration of cartilage tissue.

Keywords: *cartilage, chondrogenic materials, tissue engineering, carbon fibrous composite*
[Engineering of Biomaterials, 128-129, (2014), 98-99]

Introduction

Reconstruction of upper respiratory tract in case of neoplasms, traumas (of mechanical, thermal or chemical origin), as well as post-intubation and post-trauma stenoses is a medical problem, which still remains without a solution. The materials used so far (autogenic as well as plastic ones) fail to give results that would be satisfying for patients as well as doctors, in early as well as late follow-up. Developing a biologically active material for making up the defects in upper respiratory tract shall allow to reconstruct the defective structures, which occurred in patients due to neoplasms, as well as in treatment of stenoses or traumas of mechanical, thermal and post-intubation origin. As is it evident from our previous studies and papers of other authors, the carbonaceous material in fibrous forms (micro and nano) were successfully applied in the treatment of defects of cartilage. Numerous findings support the hypothesis that fibrous carbon components due to their unique chemical and physical properties (biomimetic form, functional groups on the surface, electrical conductivity, thermal conductivity, mechanical properties) can act as chondrogenic materials [1-7].

Materials methods

Our studies comprise in vitro and in vivo assessment of carbon micro and nano materials. The subjects of the experiments are membranes made of carbon fibers (micro-fibers made from PAN precursor, carbonized at 1100°C) and a biocompatible polymer (PVDF- polyvinylidene fluoride) – in vivo experiments. Carbon nanotubes - based scaffold has been prepared on a titanium substrate by use EPD method (Multi-Walled Carbon Nanotubes -MWCNT, length: 1-2 microns; outside diameter: 10-30 nm; were purchased from Nanostructured & Amorphous Materials, Inc., USA. MWCNT were chemically oxidized in concentrated H_2SO_4 and HNO_3 acids mixture) - in vitro tests. Human chondrocytes isolated from tissues of the larynx and trachea, collected during surgical procedures, were used for in vitro study. These cells were seeded with scaffolds prepared from carbon fibrous materials for various periods of time. In order to assess the impact of carbon materials on the cultured chondrocytes, cytotoxicity and genotoxicity tests were carried out. In vivo studies were carried out using carbon fibers /polymer membranes to rebuild experimentally prepared defects of the trachea of animals (sheep). The in vivo experiments were performed for various periods of time, from one to nine months. FIG. 1 shows chondrocytes adhering to the scaffolds made of carbon nanotubes, and FIG. 2 presents the histological image of tissue formed in the presence of the implant (carbon fibers/polymer membrane).

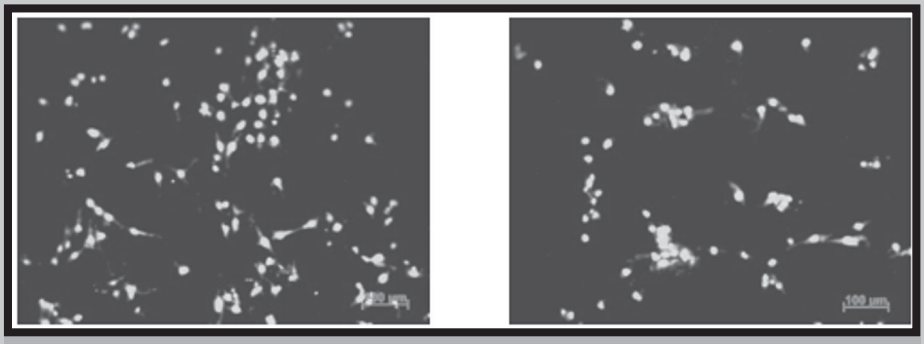

FIG. 1. Chondrocytes adhering to the surface of the scaffolds made of carbon nanotubes (acridine orange).

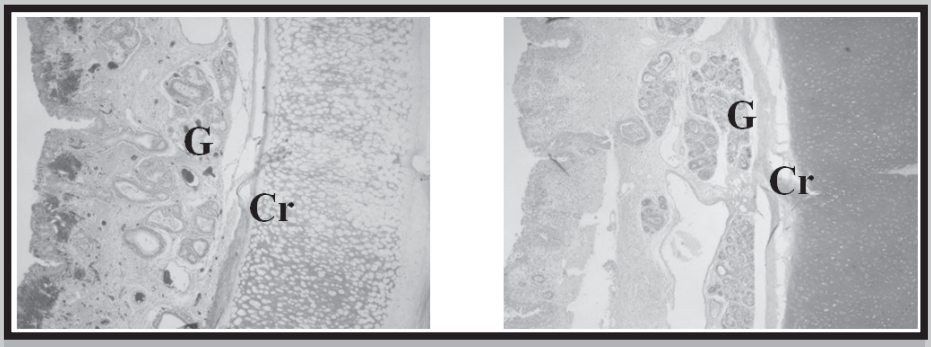

FIG. 2. Histological images of tissue formed in the presence of the implant (carbon fibers/biocompatibile polymer membrane), one month after implantation. Proper construction of the tracheal wall: stratified columnar epithelium, visible layer of active sero-mucous glands (G) and cartilage (C). Masson-Goldner staining of (A) and PAS (B), magnification 10x.

Results and discussions

The preliminary in vitro study indicates that all carbon fibrous scaffolds are neither genotoxic nor cytotoxic. The cells adhering to the scaffold made of carbon nanotubes retain the shape characteristic for chondrocytes. Analysis of tissue remodeling in contact with the composite; microcarbon fibers / polymer, revealed the chondrogenic properties of the material. Cartilage tissue in contact with the carbon composite material includes elements such as the natural tissue of a tracheal tissue.

Conclusion

The positive preliminary in vitro and in vivo assessment of nano and microfibrous carbons indicates that such materials provide structures which seem to be promising as scaffolds for the treatment of cartilage.

Acknowledgements

This work has been supported by National Science Centre (NCN) grants Nos.: 2011/01/B/ST5/06424.

References

[1] E.B. Hunziker, Articular cartilage repair: basic science and clinical progress. A review of the current status and prospects; Osteoarthritis and Cartilage, 10 (2002) 432-463.
[2] M. Błażewicz, Węgiel jako biomateriał: badania nad biozgodnością włókien węglowych, Polska Akademia Nauk. Oddział w Krakowie: Ceramika, 2001.
[3] M. Blazewicz, Carbon materials in the treatment of soft and hard tissue injuries; Eur Cell Mater, 2 (2001) 21-29.
[4] M.S. Dresselhaus, A. Jorio, A.G. Souza, R. Saito, Defect characterization in graphene and carbon nanotubes using Raman spectroscopy; Philosophical Transactions of the Royal Society a-Mathematical Physical and Engineering Sciences, 368 (2010) 5355-5377.
[5] R.J. Minns, M. Flynn, Intra-articular implant of filamentous carbon fibre in the experimental animal; J Bioeng, 2 (1978) 279-286.
[6] P. Pongor, J. Betts, D.S. Muckle, G. Bentley, Woven carbon surface replacement in the knee: independent clinical review; Biomaterials, 13 (1992) 1070-1076.
[7] M. Brittberg, E. Faxen, L. Peterson, Carbon fiber scaffolds in the treatment of early knee osteoarthritis. A prospective 4-year followup of 37 patients; Clin Orthop Relat Res, (1994) 155-164.

CORROSION PROPERTIES OF Ca-DOPED TiO_2 COATINGS

Barbara Burnat*, Justyna Robak, Andrzej Leniart, Sławomira Skrzypek, Mariola Brycht

University of Lodz, Faculty of Chemistry,
Department of Inorganic and Analytical Chemistry,
12 Tamka Str., 91-403 Lodz, Poland
* e-mail: burnat@chemia.uni.lodz.pl

Abstract

The paper presents the preparation and characterization of TiO_2 coating doped with Ca produced by the sol-gel method using titanium alkoxide as the precursor of titania as well as calcium nitrate as dopant source. These coatings were used to modify the biomedical alloy M30NW. Using the optical microscopy and the atomic force microscopy the topography of synthesized coatings was characterized. Whereas using electrochemical methods the corrosion measurements were carried out. Anticorrosion properties of calcium-doped TiO_2 coating were determined in PBS solution on the basis of corrosion potential Ecor, polarization resistance Rp, corrosion rate CR, current density in the passive range i0.5 and also breakdown Eb and repassivation Erep potentials. Analogous corrosion tests were also made for the uncoated alloy as well as for alloy coated with pure TiO_2 coating.

It was stated that modification of M30NW alloy surface by calcium-doped TiO_2 coating shows anticorrosion properties in PBS solution. These properties are slightly lower compared to a pure TiO_2 coating. The analysis of the topography of TiO_2-based coatings showed that calcium doping increases the surface development and roughness of the obtained coatings.

***Keywords**: biomaterial, surface modification, sol-gel method, doping, corrosion*

[Engineering of Biomaterials, 128-129, (2014), 100-102]

Introduction

Ceramic materials: carbides, nitrides, borides, silicides and oxides are often used to modify the surface of metallic biomaterials to improve their mechanical properties and corrosion. Very good results are achieved through the use of titanium dioxide (TiO_2), which increases the resistance to high temperatures, wear and corrosion of metals and alloys [1-3]. Increased corrosion resistance amounts to increasing the biocompatibility of biomaterials.

An important feature of biomaterials is their bioactivity. The formation of biologically active apatite, whose structure is similar to that of the human bone, is decisive for the integration between the implant and the bone (osseointegration). Studies carried out on titanium implants have shown that the process of spontaneous formation of the apatite layer can be accelerated by modifying the surface of titanium, for example by implanting calcium ions into its surface [4]. In a similar way it is possible to increase the bioactivity of the titanium dioxide layers applied to modify the steel implants [5]. Such modification can be carried out by various methods. In this study, a sol-gel method was used, both as coating and modification method. It shows many advantages compared to other commonly used coating methods: very good control of stoichiometry, homogeneity, purity and chemistry of produced coatings.

The main objective of this study was to determine the effect of calcium ions doping on anticorrosion properties of titanium dioxide coating obtained by the sol-gel method on surface of biomedical alloy M30NW. Corrosion measurements were carried out in PBS solution. Anticorrosion properties of TiO_2 and Ca/TiO_2 coatings were specified based on the determined values of corrosion potential E_{cor}, polarization resistance Rp, corrosion rate CR, current density in passive range i0.5 and also breakdown E_b and repassivation E_{rep} potentials.

Materials and methods

The single-layer titanium dioxide coatings were applied on the surface of biomedical alloy M30NW (AUBERT & DUVAL, France) by the sol-gel method using the dip-coating technique. The samples of alloy, which meets the requirements of ISO 5832-9 standard [6], had the shape of discs with a diameter of 22 mm and a thickness of about 3 mm. Prior to modification alloy samples were ground and polished according to the procedure described in [7]. For pure and calcium-doped TiO_2 coatings titanium tetraisopropoxide was used as the precursor, hydrochloric acid as catalyst, 2-propanol as solvent, and calcium nitrate (1.33 mol/l) as dopant source. The amount of added calcium nitrate solution was chosen so that the molar ratio of Ti/Ca was 20. The composition of sols used for TiO_2 coatings are summarized in TABLE 1.

TABLE 1. The chemical composition of sols with a molar ratio of the reagents.

	Precursor	Solvent	Catalyst	Additive
TiO_2				
	$Ti[OCH_2(CH_3)_2]_4$	C_3H_8O	$HCl_{stęż}$	H_2O
V [ml]	1.256	16.92	0.18	0.1597
Molar ratio	1	52	0.5	2
Ca/TiO_2				
	$Ti[OCH_2(CH_3)_2]_4$	C_3H_8O	$HCl_{stęż}$	$Ca(NO_3)_2$
V [ml]	1.256	16.92	0.18	0.1597
Molar ratio	1	52	0.5	0.05

In the final step, TiO_2 and Ca/TiO_2 coatings was subjected to a heat treatment at temperature of 400°C for 1 hour.

Microscopic analysis of surface of obtained TiO_2 and Ca/TiO_2 coatings was carried out using a metallographic microscope MMT800BT (Mikrolab) and atomic force microscope Dimension Icon (Bruker).

Corrosion measurements were carried out in deoxygenated PBS (Phosphate Buffered Saline) solution with a pH 7.4 and temperature of 37°C, that simulates the human body fluid environment. A potentiostat - galvanostat PGSTAT 30 (Autolab) were used for the measurements. With the use of electrochemical measurement techniques following corrosion parameters were calculated: corrosion potential, polarization resistance, corrosion rate, breakdown potential, repassivation potential, passive current density. All potentials reported in this paper are given versus calomel electrode (E°=0.236 VSHE). Working area of each sample was ca. 0.64 cm^2.

Results and discussions

The TiO_2 coatings obtained showed a very good adhesion to the substrate of biomedical alloy M30NW. There were no cracks or delamination of coatings. Titanium dioxide coating had a golden color and had a thickness of ca. 30 nm regardless of the doping.

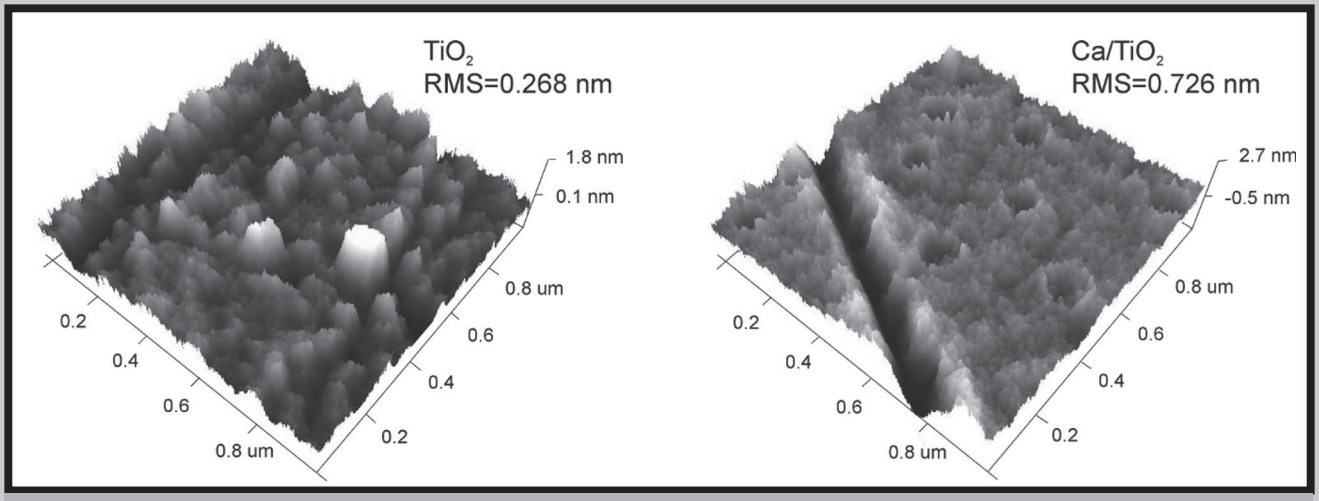

FIG. 1. AFM 3D images of TiO_2 and Ca/TiO_2 coatings.

It was found that doping of calcium ions increases the surface development and roughness of the obtained TiO_2 coatings (FIG. 1). RMS determined from AFM measurements for the undoped coating is 0.26 nm while doping of Ca^{2+} increases its value to 0.726 nm. Differences in RMS are due to the spherical cavities with a diameter of ca. 100 nm and a depth of 2 nm visible on the surface of Ca/TiO_2 coating (FIG. 2).

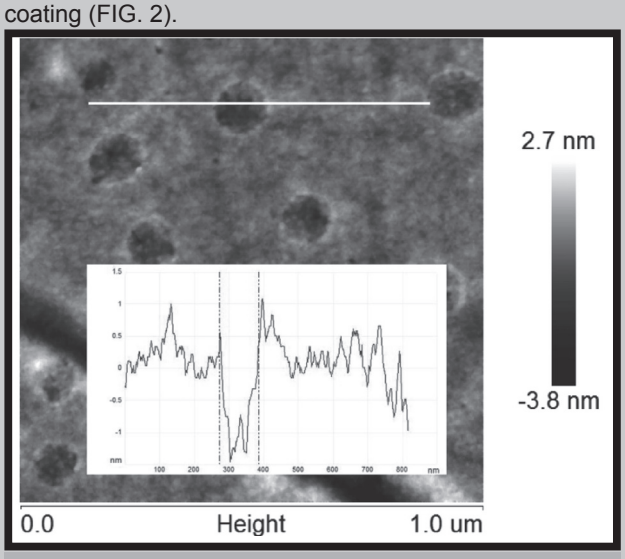

FIG. 2. AFM 2D image and cross section of Ca/TiO_2 coating.

TABLE 2 presents the values of parameters characterizing the corrosive properties of the investigated alloy M30NW both uncoated and coated with TiO_2 coatings: corrosion potential E_{cor}, polarization resistance R_p and corrosion rate CR. The values of corrosion rate were calculated based on determined values of Rp, according to the assumptions of standard ASTM G 102–89 [8], that the corrosion processes at Ecor potential occurs as uniform corrosion.

TABLE 2. Values of corrosion parameters of M30NW alloy in PBS solution.

coating	E_{cor} (V)	R_p (Mohm cm^2)	CR (mm/yr)	p (%)
uncoated	-0.117±0.011	3.4±0.5	(6.1±0.9)×10^{-5}	-
TiO_2	0.213±0.019	39.6±6.3	(5.3±0.8)×10^{-6}	8.8±1.3
Ca/TiO_2	0.232±0.026	26.2±8.4	(8.5±2.5)×10^{-6}	14.1±4.2

Surface modification of M30NW by TiO_2 coating significantly improves its corrosion resistance in PBS solution - coated alloy shows higher values of corrosion potential and polarization resistance, as well as ca. 10-times lower values of corrosion rate. Whereas the calcium ions doping procedure causes a slight deterioration in anticorrosion properties of TiO_2 coating - in case of Ca/TiO_2 - coated alloy the corrosion rate is higher compared to pure TiO_2 - coated alloy.

Results of electrochemical measurements were also used to determine the porosity of the coatings, which is calculated as a ratio of Rp for uncoated alloy and Rp for coated alloy, and it is expressed in percentage. Calcium doping of TiO_2 coatings increases the thus calculated porosity from ca. 9% to ca. 14% (TABLE 2), which in case of biomaterials is advantageous and desirable effect, because higher porosity of the surface promotes osseointegration.

Surface modification of M30NW alloy by TiO_2 coating results in a significant change in the shape and position of the potentiodynamic characteristics in wide range of anodic polarization recorded in PBS solution. Based on potentiodynamic characteristics gathered in wide range of anodic polarization (FIG. 3) following quantities were determined: current density in the passive range (at arbitrary chosen potential E=0.5V) i0.5, breakdown potential E_b and repassivation potential E_{rep}. The values of these quantities are collected in TABLE 3.

In the case of alloy samples coated with TiO_2 the current density in the passive range at a potential equal to E=0.5V is about 3 orders of magnitude lower than for the uncoated alloy.

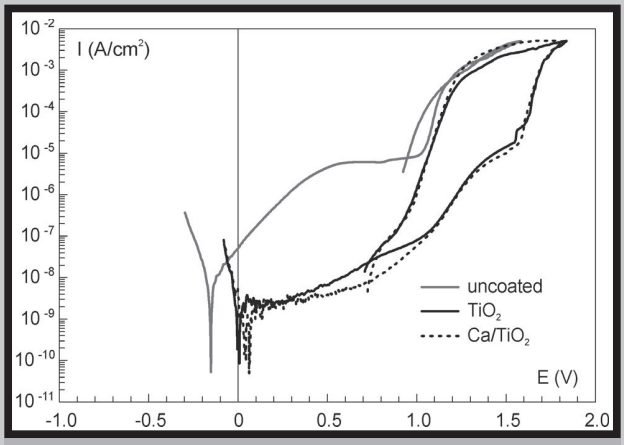

FIG. 3. Potentiodynamic characteristics in anodic range of polarization (scan rate of 1 mV/s).

TABLE 3. Values of corrosion quantities determined from potentiodynamic characteristics.

coating	$i_{0.5}$ (A/cm^2)	E_b (V)	E_{rep} (V)
uncoated	(4.3 ± 0.4) x 10^{-6}	1.047 ± 0.006	0.948 ± 0.001
TiO_2	(6.7 ± 1.1) x 10^{-9}	1.585 ± 0.067	0.759 ± 0.053
Ca/TiO_2	(3.4 ± 1.0) x 10^{-9}	1.598 ± 0.013	0.732 ± 0.001

Also, the breakdown potential values are significantly shifted toward the anodic direction, which confirms the protective properties of titanium dioxide coatings against pitting corrosion. These properties remain unchanged also after doping with calcium ions. Furthermore, for Ca-doped TiO_2 coating the average value of current density read at a potential of 0.5V is even lower, which is a beneficial effect.

Conclusions

Sol-gel method allows to obtain homogeneous coating of titanium dioxide from organic precursor. It is also possible to modify the synthesized sol-gel coating by calcium ion doping using calcium nitrate solution. The doping does not affect the thickness of the coating, but it affects the surface development and roughness of the coating. Synthesized TiO_2-based coatings exhibit anticorrosion properties in PBS solution both at corrosion potential as well as during the anodic polarization. The studies carried out at corrosion potential show that coatings containing calcium ions have a slightly weaker anticorrosive properties compared to pure TiO_2 coatings. Whereas no significant effect of doping were stated during anodic polarization.

Acknowledgements

The investigations were supported by grant UŁ 506/1118. The M30NW biomedical alloy was bought from MEDGAL (Bialystok, Poland).

References

[1] Siva Rama Krishna D., Sun Y., Thermally oxidised rutile-TiO_2 coating on stainless steel for tribological properties and corrosion resistance enhancement, Applied Surface Science, 252 (2005) 1107–1116.
[2] Shen G.X., Chen Y.C., Lin C.J., Corrosion protection of 316 L stainless steel by a TiO_2 nanoparticle coating prepared by sol–gel method, Thin Solid Films, 489 (2005) 130–136.
[3] Shan C.X., Hou X., Choy K.-L., Corrosion resistance of TiO2 films grown on stainless steel by atomic layer deposition, Surface & Coatings Technology, 202 (2008) 2399–2402.
[4] Krupa D., Baszkiewicz J., Sobczak J.W., Biliński A., Barcz A., Modifying the properties of titanium surface with the aim of improving its bioactivity and corrosion resistance, Journal of Materials Processing Technology, 143–144 (2003) 158–163.
[5] Krzak-Roś J., Filipiak J., Pezowicz C., Baszczuk A., Miller M., Kowalski M., Będziński R., The effect of substrate roughness on the surface structure of TiO_2, SiO_2, and doped thin films prepared by the sol–gel method, Acta of Bioengineering and Biomechanics, 11 (2009) 21-29.
[6] ISO Standard 5832-9:2007 Implants for surgery - Metallic materials - Part 9: Wrought high nitrogen stainless steel
[7] Burnat B., Błaszczyk T., Leniart A., Scholl H., The effect of TiO_2 sol-gel layers on corrosion properties of M30NW biomedical alloy in 0.9% NaCl solution, Engineering of Biomaterials, 106-108 (2011) 133-139.
[8] ASTM G 102-89:2004 Standard Practice for Calculation of Corrosion Rates and Related Information from Electrochemical Measurements

STEM CELLS AND THEIR DERIVATIVES – HOPES AND CHALLENGES IN REGENERATIVE MEDICINE

Ewa K. Zuba-Surma

Jagiellonian University,
Faculty of Biochemistry, Biophysics and Biotechnology,
Department of Cell Biology,
Krakow, Poland

Abstract

Major goals of contemporary regenerative medicine focus on improvement of irreversible damage of multiple organs and tissues by employing several approaches including recent achievements of cell-based therapies and tissue engineering.

Several types of stem cells (SCs) such as bone marrow (BM)- derived mesenchymal stem cells (MSCs), hematopoietic stem cells (HSCs) as well as SCs with multi- and pluripotent characteristics (PSCs) have been postulated as potential source of cells for therapy. Recently, embryonic stem cells (ESCs) and so called induced pluripotent stem cells (iPS cells) representing "genetically induced" SCs with high differentiation potential, have brought great hope to the field of regenerative medicine and clinical applications. When combined with modern accomplishments of tissue engineering including biocompatible carriers and scaffolds, SCs become leading targets for cell -based regenerative applications.

Although the variety of stem/ progenitor cells have been applied in experimental therapies of several organs injuries, there is still no agreement in scientific and clinical world which subpopulation/s of cells would be the most efficient in such treatment. Moreover, multiple obstacles needs to be overcome prior to optimal application of SCs in regeneration including optimization of ex vivo isolation and expansion conditions or limiting vast adverse features of some SC fractions such as teratogenic potential of ESCs and iPS cells.

Recently, stem cell- derived bioactive components such as cellular microvesicles (MVs) are postulated to play important role in mediating SC activity following transplantation. MVs representing bioactive components carrying SC- derived transcripts (mRNA, miRNA), proteins, enzymes and receptors may participate in tissue regeneration via stimulation of endogenous repair mechanism by activating endogenous target cells in damaged organs.

Thus, the newest trends in regenerative medicine would focus not only on combined applications of biocompatible materials with SC subpopulations, but also with their bioactive acellular components including microvesicles. Unquestionably, successful applications of stem/ progenitor cells and their derivatives in regenerative medicine would need to be safe, ethically acceptable and therapeutically efficient. Sources and application protocols for such optimal stem cell therapy are still being optimized and need scientific discussion.

[Engineering of Biomaterials, 128-129, (2014), 102]

NEW FUNCTIONAL ALIPHATIC POLYCARBONATES – MATERIALS FOR ADVANCED BIOMEDICAL APPLICATIONS

Malgorzata Pastusiak[1]*, Michal Kawalec[1], Joanna Jaworska[1], Piotr Kurcok[1,2], Henryk Janeczek[1], Piotr Dobrzynski[1,2]

[1]Polish Academy of Sciences,
Centre of Polymer and Carbon Materials,
Zabrze, Poland
[2]Jan Dlugosz University,
Faculty of Mathematics and Natural Science,
Czestochowa, Poland
*e-mail: mpastusiak@cmpw-pan.edu.pl

Abstract

The aim of this study is to develop a new method of synthesis of functional (co)polycarbonates by ring -opening polymerization of ethyl 5-methyl-2-oxo-1,3-dioxane-5-carboxylate (MTC-Et), benzyl 5-methyl-2-oxo-1,3-dioxane-5-carboxylate (MTC-Bz) and their copolymerization with 1,3-trimethylene carbonate (TMC) with potential application in the formation of bioresorbable scaffolds for living cells and drug delivery, systems for achieving controlled drug release. (Co)polymerizations were conducted in bulk, in the presence of low toxic lanthanum acetylacetonate - $La(acac)_3xH_2O$ as catalyst. All synthesized materials were obtained at 120°C.

The results are very promising. A series of (co) polymers were obtained with high conversion and relatively high molecular weights. The composition of the comonomers and their sequence lengths were determined by means ^1H NMR and ^{13}C NMR measurements. Higher reactivity during the investigated copolymerizations presented carbonates with pending ethyl or benzyl group than 1,3-trimethylene carbonate. The thermal properties obtained (co)polymers were characterized by differential scanning calorimetry.

Keywords: *bioresorbable polymers, cyclic carbonates (co)polymerization, 1,3-trimethylene carbonate, functional polymers*

[Engineering of Biomaterials, 128-129, (2014), 103-106]

Introduction

Copolymers based on 1,3-trimethylene carbonate are promising materials for medical and pharmaceutical applications due their high elasticity, biocompatibility and susceptibility to biodegradation. Copolymers of TMC with glycolide [1-2], lactide [3-4] and ε-caprolactone [5-6] have been described in numerous publications. However, in other applications, polymer materials with specific functionalities are desirable. Functional synthetic polymers are significant, for example, as components for injectable gels [7], systems for targeted drug delivery [8] and materials for specific interactions with biological systems [9]. Therefore, the need for suitable methods for the preparation of a wide variety of functional biomaterials, seem to be pressing problem.

In this work, we present a new method of synthesis of functional (co)polycarbonates by ring-opening polymerization of ethyl 5-methyl-2-oxo-1,3-dioxane-5-carboxylate (MTC-Et), benzyl 5-methyl-2-oxo-1,3-dioxane-5-carboxylate (MTC-Bz) and their copolymerization with 1,3-trimethylene carbonate (TMC). Lanthanum acetylacetonate, compound simple in structure, stable and low toxicity, was used as catalyst.

Develop of a new methods of synthesis of functional (co) polycarbonates allows to obtain biomaterials with potential application in the formation of drug delivery systems for achieving controlled drug release and in tissue engineering as materials for forming bioresorbable scaffolds with novel properties such as hydrophilicity control, flexibility, as well as with bioactivity and possibility to curing of proteins or peptides on the surface.

Materials and methods

Monomers and initiators

Monomer: 1,3-trimethylene carbonate (TMC) was obtained from FORUSORB (Huizhou Foryou Medical Devices Co., Ltd, China). It was purified by re-crystallization from dried ethyl acetate and then dried in a vacuum oven at room temperature. Both: benzyl 5-methyl-2-oxo-1,3-dioxane-5-carboxylate (MTC-Bz) and ethyl 5-methyl-2-oxo-1,3-dioxane-5-carboxylate (MTC-Et) were synthesized in our laboratory according to the previously published procedure [10]. The commercially available catalyst: Lanthanum (III) acetylacetonate hydrate, $La(acac)_3xH_2O$ (Sigma-Aldrich) was used as received.

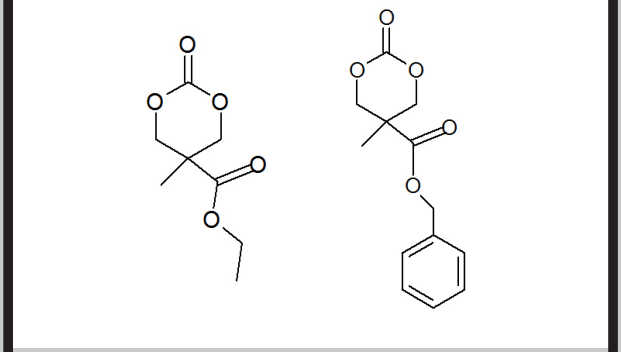

benzyl 5-methyl-2-oxo--1,3-dioxane--5-carboxylate (MTC-Bz) | **ethyl 5-methyl-2-oxo--1,3-dioxane-5-carboxylate (MTC-Et)**

Polymerization and copolymerization procedure

The ring-opening (co)polymerization was carried out in a glass flask equipped a magnetic stirrer, using $La(acac)_3xH_2O$ as catalyst. Selected amounts monomer(s) and catalyst were introduced in argon atmosphere into a flask. The flask was immersed in an oil bath at 120°C. After the selected reaction time, the flask was quenched to room temperature. The resulting (co)polymers were purified by dissolving in chloroform and dropwise to cold methanol. Finally, the purified material was dried in a vacuum at room temperature.

Measurements

The conversion of the monomers and the microstructure of the obtained copolymers were determined by ^1H and ^{13}C NMR spectroscopy. The ^1H NMR spectra were recorded at 600 MHz using a Avance II Bruker TM at 25ºC. Dried dimethyl sulfoxide-d6 (DMSO-d6) was used as the solvent, and tetramethylsilane (TMS) was applied as the internal standard. The ^1H NMR spectra were obtained with 64 scans, 2.65s acquisition time, and 11 μs pulse width.

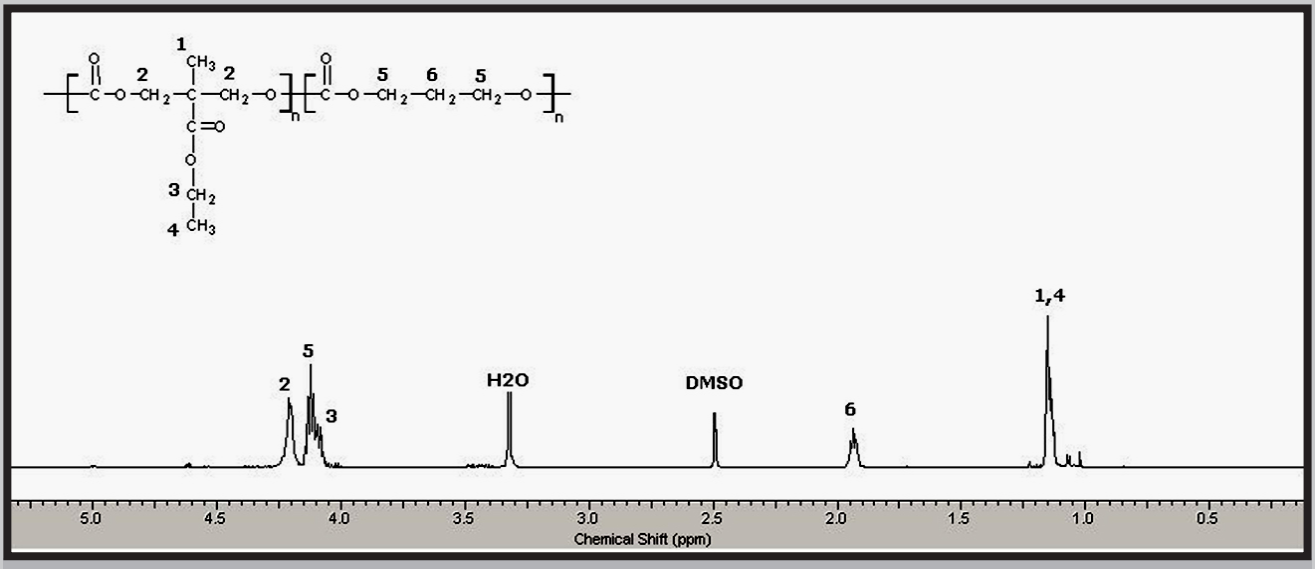

FIG. 1. ^{1}H NMR spectrum (in DMSO-d6) of equimolar TMC/ MTC-Et copolymer obtained with $La(acac)_3xH_2O$.

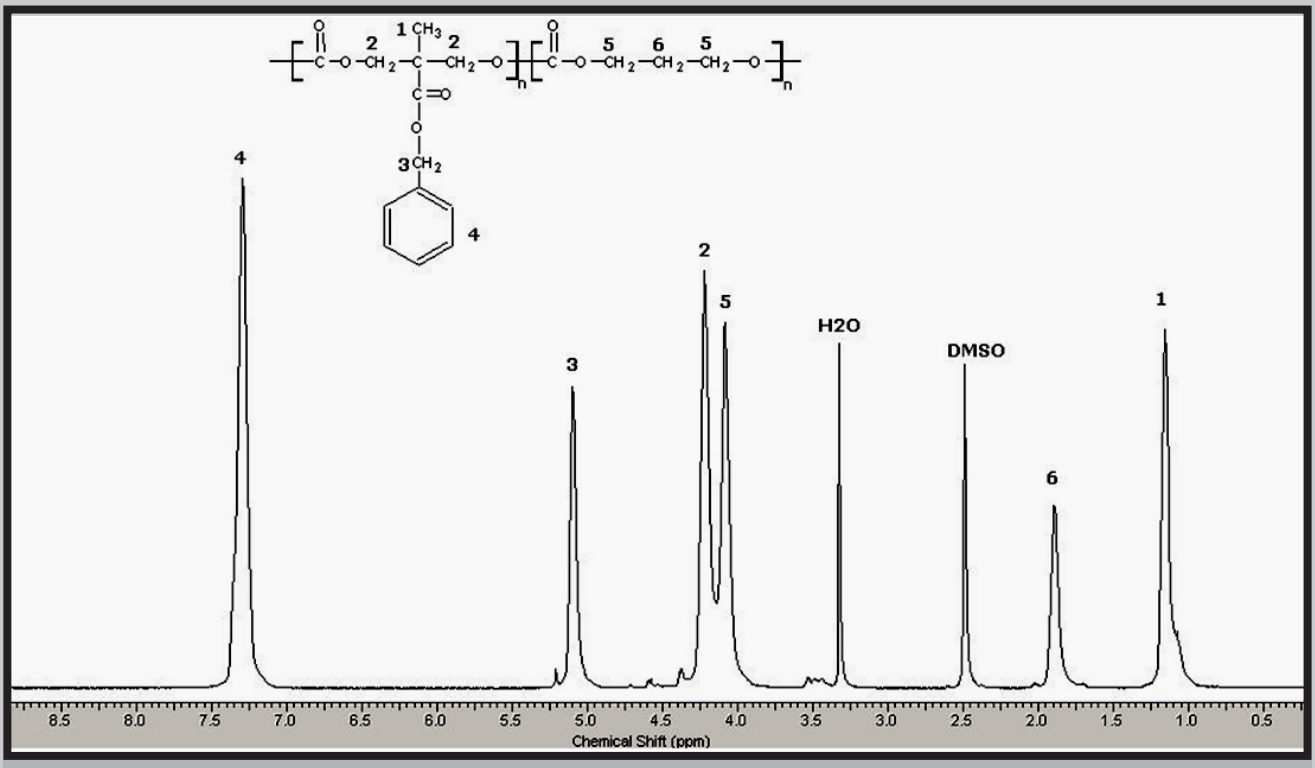

FIG. 2. ^{1}H NMR spectrum (in DMSO-d6) of equimolar TMC/ MTC-Bz copolymer obtained with $La(acac)_3 xH_2O$.

The ^{13}C NMR spectra were recorded at 150 MHz with 19500 scans, 0.91s acquisition time, and 9.1 μs pulse width.

The weight-average molar masses and dispersity indexes of the homopolymers and copolymers were determined by gel permeation chromatography (GPC) with a Viscotek RImax chromatograph. Chloroform was used as the eluent, and the temperature and the flow rate were 35°C and 1mL/ min, respectively. Two PL Mixed C columns with a Viscotek model 3580 refractive index detector were used. The molecular weights were calibrated with polystyrene standards.

Thermal properties (T_g, T_m and ΔHm) were examined by differential scanning calorimeter with a DuPont 1090B apparatus, calibrated with gallium and indium (heating and cooling rate of 20°C/min in the range from -100°C to 220°C).

Results and discussions

Ring-opening polymerization of ethyl 5-methyl-2-oxo-1,3-dioxane-5-carboxylate (MTC-Et) and benzyl 5-methyl-2-oxo-1,3-dioxane-5-carboxylate (MTC-Bz) and their copolymerization with 1,3-trimethylene carbonate (TMC) were conducted in bulk in the presence of $La(acac)_3xH_2O$ as catalyst. The results are summarized in TABLE 1 and 2.

A series of copolymers 1,3-trimethylene carbonate with MTC-Et were obtained with high conversion 99% (TABLE 1, run 1-4). The time required to obtain a full conversion ranged from 24 to 28 hours in case of copolymerization of equimolar mixture of TMC with MTC-Et (FIG. 3). The composition of the copolymers were determined by ^{1}H NMR spectrum (FIG. 1). The area of the signal of [CH_2-CH_2-CH_2] group of TMC unit at (δ=1.84-1.98 ppm) and the signals of [CH_2O] group of MTC-Et unit at (δ=4.16-4.28 ppm) were employed to calculate the composition of the copolymers.

TABLE 1. Properties of 1,3-trimethylene carbonate/ MTC-Et copolymers with various composition[a].

No.	(TMC: MTC-Et)^0 [% mol]	Time [h]	Conv. [%]	(TMC: MTC-Et)^N [% mol.]	M_w [kDa]	D	L_{TMC}	L_{MTC-Et}	T_g [°C]	T_m [°C]	H_m [J/g]
1.	100 : 0	2	100	100 : 0	56,6	2,1	-	-	-13,4	-	-
2.	80 : 20	24	99	80 : 20	60,9	15	7,4	1,8	-7,6	41	5,4
3.	50 : 50	28	99	49 : 51	27,1	3,3	4,2	4,4	-12,3	30	8,2
4.	20 : 80	24	99	21 : 79	75,7	15	2,3	5,9	-3,2	42,4	9,5
5.	0 : 100	3	97	100 : 0	143	13	-	-	-0,5	29,7	7,5

[a] (Co)polymerizations were performed at 120°C with the $La(acac)_3 \times H_2O$ to monomer ratio (I/ M) averaged 1 : 1000
Where: (TMC:MTC-Et)^0 – initial feed molar fraction TMC and MTC-Et, **Conv.** - total conversion of copolymerization, **(TMC: MTC-Et)^N** – feed molar fraction of TMC and MTC-Et, **M_w** – weight-average molecular weight were determined by GPC and calibrated with polystyrene standards, **$D=M_w/M_n$** – dispersity, **L_{TMC}, L_{MTC-Et}** - average length of carbonates microblock, calculated with NMR, **T_g** – glass-transition temperature, **T_m** – melting temperature of the crystalline phase, **ΔH_m**- heat of melting of the crystalline phase

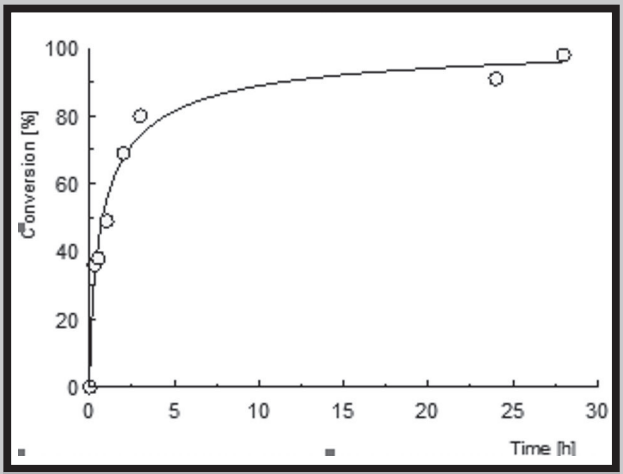

FIG. 3. The rate of conversion of monomers as a function of copolymerization time (copolymerization of equimolar mixture of TMC with MTC-Et).

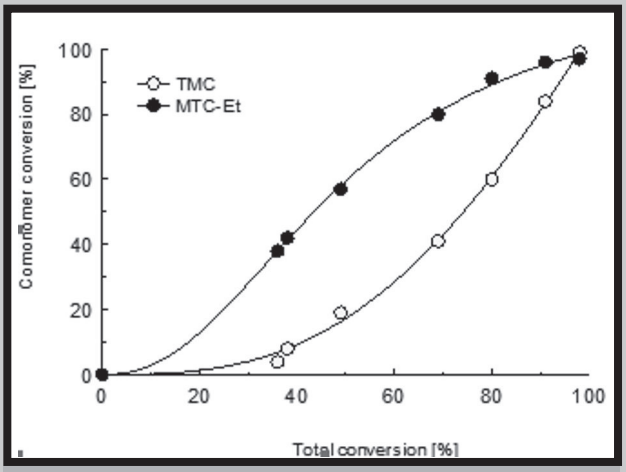

FIG. 4. Dependence of the TMC and MTC-Et conversion on the total conversion of the copolymerization (TMC/ MTC-Et molar ratio was of 1:1)

TABLE 2. Properties of 1,3-trimethylene carbonate/ MTC-Bz copolymers with various composition[a].

No.	(TMC: MTC-Bz)^0 [% mol]	Time [h]	Conv. [%]	(TMC: MTC-Bz)^N [% mol.]	M_w [kDa]	D	L_{TMC}	L_{MTC-Bz}	T_g [°C]	T_m [°C]	H_m [J/g]
1.	100 : 0	2	100	100 : 0	56,6	2,1	-	-	-13,4	-	-
2.	80 : 20	2	~100	80 : 20	33,7	10,5	8,5	2,2	16,2	-	-
3.	50 : 50	2	~100	43 : 57	23,6	14,7	8,0	10,7	21,2	-	-
4.	20 : 80	2	~100	15 : 85	31,1	9,6	2,0	11,2	17	-	-
5.	0 : 100	3	97	0 : 100	36	7,6	-	-	4,1	42	15,2

Where: (TMC: MTC-Bz)^0 – initial feed molar fraction TMC and MTC-Bz, **Conv.** - total conversion of copolymerization, **(TMC: MTC-Bz)^N** – feed molar fraction of TMC and MTC-Bz, **M_w** – weight-average molecular weight were determined by GPC and calibrated with polystyrene standards, **$D=M_w/M_n$** – dispersity, **L_{TMC}, L_{MTC-Bz}** - average length of carbonates microblock, calculated with ^{13}C NMR, **T_g** – glass-transition temperature, **T_m** – melting temperature of the crystalline phase, **ΔH_m**- heat of melting of the crystalline phase
[a] (Co)polymerization was performed at 120 °C with the $La(acac)_3 \times H_2O$ to monomer ratio (I/ M) averaged 1 : 1000

The mole compositions of copolymers were in accordance with the monomers feed ratio. The resulting copolymers were characterized by relatively high molar masses Mw. High dispersion of copolymers containing 20 and 79 mole% MTC-Et (TABLE 1, row 2,4), indicates relatively strong intermolecular transesterification of functional carbonate (MTC-Et) ester bonds.

During the investigated copolymerization, MTC-Et comonomer presented higher reactivity than 1,3-trimethylene carbonate (FIG. 4), contrary to the case of TMC/ 2,2-dimethyltrimethylene carbonate copolymerization conducted with the use of $Zn(acac)_2xH_2O$, described in a previous publication [11].

The thermal properties of the copolymers of 1,3-trimethylene carbonate with MTC-Et were verified by DSC analysis. All obtained copolymers are semi-crystalline. We observed that the glass-transition temperature (T_g) and melting temperature decreases with increasing content of TMC in copolymer.

Other hand, the copolymerization of 1,3 trimethylene carbonate/ MTC-Bz has proceeded faster and the time required to achieve complete conversion was only 2 hours (FIG. 5).

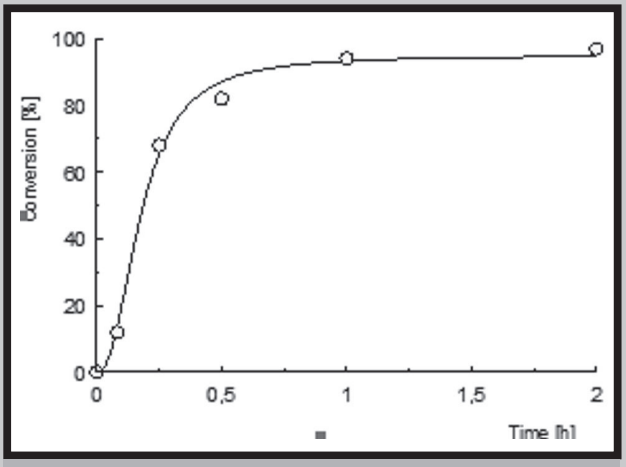

FIG. 5. The rate of conversion of monomers as a function of copolymerization time (copolymerization of equimolar mixture of TMC with MTC-Bz).

The copolymer composition was characterized by ^{1}H NMR spectrum (FIG. 2). The area of the signal of [CH_2-CH_2-CH_2] group of TMC unit at δ=1.79-1.97 ppm) and the signals of [CH_2O] group of MTC-Bz unit at (δ=4.96-5.16 ppm) were employed to calculate the composition of the copolymers. The molar masses (Mws) were determined for soluble fraction only since gel fraction was present in the products. High dispersion indicates relatively strong intermolecular transesterification of functional carbonate (MTC-Bz) ester bonds, also in the case of 1,3-trimethylene carbonate/ MTC-Bz copolymers (TABLE 2, row 2, 3, 4),

For the copolymerization of 1,3-trimethylene carbonate / MTC-Bz the higher reactivity observed for the carbonate with benzyl group (MTC-Bz) relative to TMC (FIG.6).

The thermal analysis showed that copolymers of 1,3-trimethylene carbonate with MTC-Bz, irrespective of the composition, are completely amorphous whereas poly(MTC-Bz) is semi-crystalline.

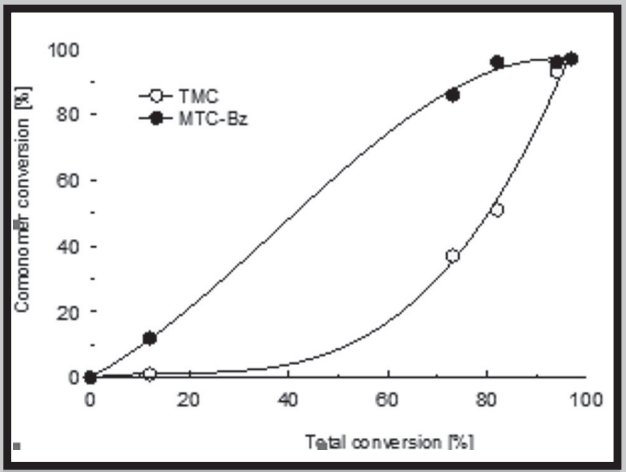

FIG. 6. Dependence of the TMC and MTC-Bz conversion on the total conversion of the copolymerization (TMC/ MTC-Bz molar ratio was of 1:1).

Conclusions

Lantanum (III) acetylacetonate was shown to be effective catalyst for homopolymerization both functional carbonates and their copolymerization with 1,3-trimethylene carbonate. The preliminary results are very promising. We obtained of a new (co)polymers with high conversion and relatively high molecular weights.

Received copolymers, especially semi-crystalline 1,3-trimethylene carbonate/ MTC-Et copolymers, are promising materials for forming scaffolds used in tissue engineering or carriers in controlled drug release systems.

Acknowledgements

This study was supported by the National Science Centre Poland, project No. UMO-2012/07/B/ST5/00616 "Novel copolymers of functionalized cyclic carbonates. Investigation of synthesis of novel, functional and biocompatible materials by coordination ring-opening polymerization"

References

[1] Warner J. J., Miller M. D., Marks P., Fu F. H.: Arthroscopic Bankart repair with the Suretac device. Part I: Clinical observations. Arthroscopy 11 (1995) 2-13.
[2] Lee S.C., Kim K. J., Kang S. W., Kimet C.: Microstructural analysis and structure-property relationship of poly(glycolide-co-1,-3-trimethylene carbonate). Polymer 46 (2005) 7953–7960.
[3] Jelonek K., Kasperczyk J., Li S., Dobrzyński P., Jarząbek B.: Controlled poly(L-lactide-co-trimethylene carbonate) delivery system of cyclosporine A and rapamycine - the effect of copolymer chain microstructure on drug release rate. International Journal of Pharmaceutics 414 (2011) 203–209.
[4] Pospiech D., Komber H., Jehnicken D., Häussler I., Eckstein K., Scheibner H., Janke A., Kricheldorf H. R., Potermann O.: Multiblock Copolymers of L-lactide and Trimethylene Carbonate. Biomacromolecules 6 (2005) 439-446.
[5] Bat E., Plantinga J. A., Harmsen M. C., M. van Luyn J. A., Zhang Z., Grijpma D. W., Feijen J.: Trimethylene Carbonate and epsilon-Caprolactone Based (co)Polymer Networks: Mechanical Properties and Enzymatic Degradation. Biomacromolecules 9 (2008) 3208-3215.
[6] Pêgo A. P., Zhong Z., Dijkstra P. J., Grijpma D. W., Feijen J.: Influence of Catalyst and Polymerization Conditions on the Properties of 1,3-Trimethylene Carbonate and εCaprolactone Copolymers. Macromolecular Chemistry and Physics 204 (2003) 747-754.
[7] Bergman, K., Engstrand, T., Hilborn, J., Ossipov, D., Piskounova, S., Bowden, T.: Injectable cell-free template for bone-tissue formation. Journal of Biomedical Materials Research Part A 91A (2009) 1111–1118.
[8] Seow W. Y., Xue J. M., Yang Y. Y.: Targeted and Intracellular Delivery of Paclitaxel using Multi-functional Polymeric Micelles. Biomaterials 28 (2007) 1730–1740.
[9] Yin M. Z., Ding K., Gropeanu R. A., Shen J., Berger R., Weil T., Mullen K.: Dendritic Star Polymers for Efficient DNA Binding and Stimulus-Dependent DNA Release. Biomacromolecules 9 (2008) 3231–3238.
[10] Kawalec M., Dove A. P., Mespouille L., Dubois Ph.: Morpholine-functionalized polycarbonate hydrogels for heavy metal ion sequestration. Polymer Chemistry 4 (2013) 1260-1270.
[11] Pastusiak M., Dobrzynski P., Kasperczyk J., Smola A., Janeczek H.: Synthesis of biodegradable high molecular weight polycarbonates from 1,3-trimethylene carbonate and 2,2-dimethyltrimethylene carbonate. Journal of Applied Polymer Science 131 (2014) 40037.

BIOLOGICAL PROPERTIES OF NEW CHITOSAN-FATTY ACIDS DERIVATIVES

A.Niemczyk, M.El Fray

West Pomeranian University of Technology, Szczecin,
Biomaterials and Microbiological Technologies,
Al. Piastow 45, 71-311 Szczecin, Poland

[Engineering of Biomaterials, 128-129, (2014), 107-108]

Introduction

Chitosan is a natural polysaccharide that is nontoxic, biodegradable, biocompatible, and has antimicrobial properties. Due to the presence of amine groups, chitosan is amenable to chemical modification, which can widen the range of potential applications.

In our previous work, we modified chitosan obtaining chitosan-fatty acid derivatives with improved physical and antimicrobial properties. The aim of this work was to investigate the blood compatibility of the chitosan-fatty acid derivatives.

Experimental

Materials and coating preparation

Chitosan-fatty acid derivatives were obtained by N-acylation of low molecular weight chitosan (CH) (ChitoClear 4300 – hqg10, Primex) with linoleic acid (LA), α-linolenic acid (ALA) (Sigma-Aldrich), and dilinoleic acid (DLA) (Croda, The Netherlands), natural hydrophobic compounds, intended to improve the physical and biological properties of chitosan. Synthesis details and characterization of antibacterial properties of the derivatives, CHLA, CHALA and CHDLA, are described elsewhere [1], [2]. Coatings were prepared by dip-coating activated polyester (copolymer of poly(ethylene terephthalate) and dilinoleic acid blocks, PET/DLA). Before coating, the surface of polyester disks was treated with argon plasma and oxygen flushing (FIG. 1, step I) to create functional groups on the surfaces. Next, disks were dipped in aqueous EDC (step II), in order to activate carboxylic groups. Carbodiimide catalyst promotes the reaction of carboxylic groups with the amine groups of chitosan in the next step (step III), the dip-coating in CH or Chitosan-FA solutions (in 1% acetic acid).

Hemocompatibility tests

The study was conducted with human whole blood (HWB), from the Regional Blood Center in Katowice, stored in citrate/phosphate/dextrose/adenine (CPDA). Flat discs (8 mm diameter) were rinsed in deionized water, dried, and sterilized with ethylene oxide, followed by contact with HWB for 24 h at 37°C. The two test groups were: negative control, HWB without contact with the test materials, and material group, samples contacted with the HWB. Hemocompatibility was evaluate by measuring:

1. free hemoglobin concentration in plasma, fHGB (g/L); measured using a spectrophotometer
2. morphological parameters of blood and red blood cell indices; measured with a hematology analyzer
3. blood cell morphology
4. the degree of hemolysis; determined by calculating the index of hemolysis (IH)

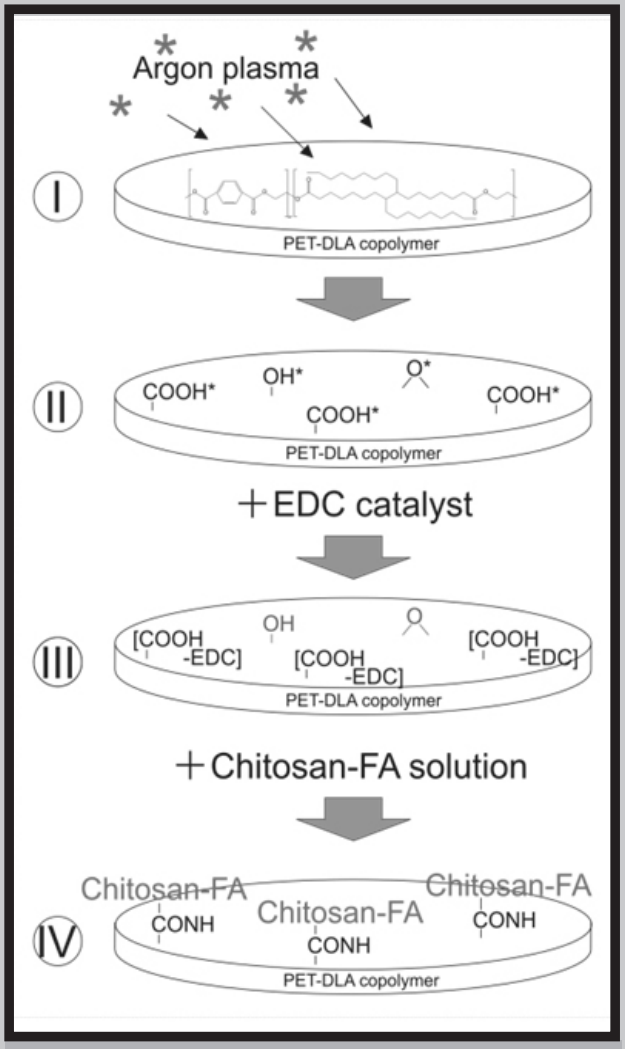

FIG. 1. Coating process.

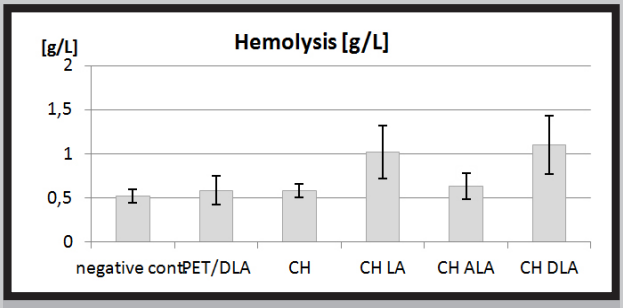

FIG. 2. Concentration of free hemoglobin released into the plasma.

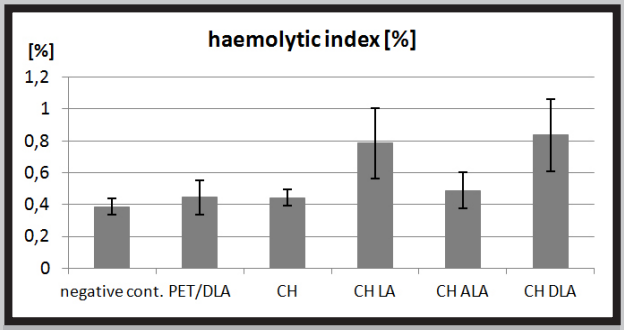

FIG. 3. The index of hemolysis for negative control, referenced materials PET/DLA and chitosan and its derivatives coating.

Results and discussion

The free hemoglobin concentration in plasma from HWB exposed to uncoated PET/DLA samples, chitosan, and chitosan-ALA coatings was similar to that of the negative control. Samples coated with chitosan-DLA and chitosan-LA resulted in the higher concentrations of fHGB, around 1,0-1,1g / L (FIG. 2).

The Index of Hemolysis for all material is summarized in FIG. 3. The calculations were performed according to standard ASTM F 756-00. On the basis of the IH value, the degree of hemolysis was considered to be:

I. IH = 0-2% : not hemolytic,
II. IH = 2-5% : slightly hemolytic,
III. IH> 5% : hemolyzing.

Based on the above ranges of hemolysis, all of the tested materials can be classified as not hemolytic, because the IH did not exceed 2%.

Summary

In this study, we examined the hemocompatibility of chitosan-fatty acid derivative coatings on plasma-activated PET/DLA. In general, the hemocompatibility studies indicate that the tested materials are not hemolytic; however, the ALA derivative may be particularly promising for further testing.

Acknowledgements

This project has received funding from the National Science Centre grant N N507 319440 (chitosan derivative synthesis). Additionally, the project received partial financial support from the European Union's Seventh Framework Programme for research, technological development and demonstration under grant agreement no. 286174 "UNITISS". We thank the Foundation for Cardiac Surgery Development in Zabrze for performing blood compatibility tests and dr A. Piegat and dr P. Sobolewski for useful discussions.

References

[1] M. El Fray, A. Niemczyk, and B. Pabin-Szafko, "Chemical Modification of Chitosan with Fatty Acids," Prog. Chem. Appl. Chitin Its Deriv., vol. XVII, pp. 29–36, 2012.
[2] A. Niemczyk and M. El Fray, "Novel Chitosan Derivatives as Films with an Antimicrobial Effect," Prog. Chem. Appl. Chitin Its Deriv., vol. XVIII, pp. 59–66, 2013.

OSTEOSYNTHESIS ON THE BASIS OF RESORBABLE POLYMERS IMPLANTS - SELECTED PROBLEMS

R. Będziński[1], J. Chłopek[2], R. Frątczak[3], I. Kotela[4]

[1] Division of Biomedical Engineering, Institute of Mechanical Engineering and Machine Operation, University of Zielona Gora,
50 Podgórna Str., 65-246 Zielona Góra, Poland
[2] AGH University of Science and Technology, Faculty of Materials Science and Ceramics, Department of Biomaterials,
30 Mickiewicza Ave.30, 30-059 Krakow, Poland
[3] NOBO Solutions S.A., al. Kasztanowa 3a-5
53-125 Wrocław, Poland
[4] Central Clinical Hospital Ministry of Interior in Warsaw, 137 Wołoska Str, 02-507 Warsaw, Poland

Abstract

Use of bioresorbable materials in bone surgery opens up new possibilities in treatment of injuries and orthopaedic illnesses. Lack of necessity for implant removal surgery enables faster treatment and substantial reduction in costs of treatment. In recent years, these advantages have caused growing interest in materials of this type. It must be noted that bioresorbable materials in most cases are based on macromolecular materials – polymers which have completely different mechanical characteristics than traditional materials used in bone surgery. Bioresorbable properties give enormous possibilities but also present difficult challenges related to construction of new types of implants based on materials of this type.

Full characteristics of new materials is indispensable in construction process, especially of mechanical properties and surface properties. The latter is responsible for contact with biological environment and bioactivity is determined on the basis of hydroxyapatite precipitations amount on material surface. In case of polymer based composites, influence of phases in powder and fibre form on properties is fundamental to be proved. Addition of particle modifier into polymer matrix causes reduction in strength of polymer. This phenomenon is mostly associated with homogenic particle distribution difficult to be achieved in case of higher filler content. However biological interplay is insufficient by low filler contents. Therefore in the below presented investigations different filler contents were applied and their influence on mechanical properties was investigated to achieve compromise between mechanical properties and bioactive, antibacterial or anti-inflammatory effect of the applied particles. Acquaintance with these results allowed for elaboration of full range of material and constructive solutions for implants in bone surgery.

Biodegradable biopolymers have low mechanical properties (Young's modulus, strength, viscoelasticity). Construction process of bioresorbable implants requires to be completely changed in way of conduction. Computer simulation based investigations of stress-strain characteristics is necessary to be carried out in each stage of research. Bigger cross-sections and different shapes of implants are required to achieve suitable stiffness.

Application of bone screws made of resorbable materials requires design of these elements from the bottom up. Design of optimal shape of screw thread and point of contact between screw head and bone plate is particularly important.

9 different implants were designed within the confines of conducted research – including for tibia, humerus, radius, ulna, phalanges, clavicle, calcaneus, pelvis and metatarsus. Stress values were determined in analyzed implants. Acceptable loads were determined for individual types of plate.

Plates made of PLA can bear small loads and play role mainly as grasping and holding bone element. In most cases additional immobilization of operated bone is required in order to prevent plate or screw destruction. In case of stabilization function for resorbable materials – as many screws as possible are recommended – thanks to it, screws are less loaded and the plate-bone system is more immobilized.

[Engineering of Biomaterials, 128-129, (2014), 108]

HYDROGELS BASED ON IONICALLY AND COVALENTLY CROSSLINKED ALGINATES

Joanna Walczak, Jakub Marchewka*, Jadwiga Laska

AGH University of Science and Technology,
Faculty of Materials Science and Ceramics,
30 A.Mickiewicza Ave., 30-059 Krakow
*e-mail: jmar@agh.edu.pl

Abstract

In the presented research sodium alginate modified by ionic and covalent crosslinking in the form of hydrogel beads was examined. In the first step, sodium alginate was ionically crosslinked by treatment with calcium chloride. Different forms of crosslinked alginate were obtained depending on the calcium chloride concentration. The forms varied from shapeless gel to dense agglomerated spheres. The optimal structure were spherical beads separated from each other. Ionically crosslinked alginates were then subjected to covalent crosslinking with epichlorohydrin. For additional reinforcement the crosslinked beads of alginate were modified with cellulose nanofibers. The products were compared in terms of water absorption in the dry samples, their morphology was observed by scanning electron microscopy. Calcium ions distribution in the composites was evaluated by energy dispersive spectroscopy analysis. In vitro biodegradation of the crosslinked alginates was also investigated.

Keywords: *hydrogels, alginate beads, crosslinking, cellulose*

[Engineering of Biomaterials, 128-129, (2014), 109-110]

Introduction

Hydrogels are materials composed of hydrophylic polymers, which have high ability to absorb and retain water. Water absorption is essential property influencing mechanical properties of the material, ability to release drugs inside the organism and biocompatibility. Hydrogels in order to maintain their structure and prevent dissolution in the aqueous phase can be subjected to crosslinking process, in which ionic or covalent crosslinks are formated [1]. Alginates are naturally occurred polysaccharides consisting of β-D-mannuronic acid and α-L-guluronic acid linked together by glycosidic bond. Alginates are characterized by their high biocompatibility, biodegradability and diversity of processing. In the present work crosslinked alginate hydrogel beads were obtained by the ionic and covalent crosslinking. Covalent crosslinking which was implemented as an additional process in ionically bonded alginates, is an effective strategy to improve the alginate beads biostability in physiological media [2,3].

Materials and methods

Alginic acid sodium salt, epichlorohydrin (≥99%) and cellulose in the form of medium fibers were purchased from Sigma Aldrich, Germany. Calcium chloride (anhydrous, ≥99.9%), ethyl alcohol (anhydrous, 99.8%), sodium hydroxide (anhydrous, ≥99.9%) and nitric acid (65%) were purchased from POCH, Poland.

Sodium alginate was ionically crosslinked by treatment with a calcium chloride solution. For this, sodium alginate (1,5 g) was dissolved in 75 ml of a distilled water, and the calcium chloride solutions of various concentrations, i.e., 0,05, 0,075, 0,1, 0,2, 0,3, 0,5 and 0,7 M, were prepared. The sodium alginate solution was added to a calcium chloride solution via syringe with the needle diameter of 0,9 mm. Alginate beads were formed, and left over 24h in the solution. Finally the product was filtered, washed with distilled water and dried at 45°C. The obtained alginate beads were additionally crosslinked covalently with epichlorohydrin. 1 g of the alginate beads was immersed in 30 ml of the ethanol/water mixture (60% v/v). Next 0,729 ml (2 eq) of the epichlorohydrin were added to the reaction vessel. A 1 M solution of sodium hydroxide was added dropwise until pH of 13 was obtained. The reaction was stirred for 90 minutes at room temperature. Then concentrated nitric acid was carefully added to decrease pH of the reaction mixture to 7. Finally the product was filtered, washed with distilled water and dried at 45°C. Cellulose modified alginates were produced by addition of the specific additive during the ionic crosslinking process. Cellulose nanofibers were introduced into 75 ml of distilled water and stirred magnetically until uniform suspension was created. Then an appropriate amount of sodium alginate was added and stirred until dissolved. Weight ratios of cellulose to sodium alginate were: 25:75, 40:60, 50:50 and 70:30. Effectiveness of mixing the components was gained by sonication with ultrasonic homogenizer SONICS Vibra-Cell (Sonics and Materials, USA). The ionic crosslinking using 0,1 M solution of calcium chloride, as well as subsequent covalent crosslinking with epichlorohydrin were carried out as described above.

Samples were characterized with scanning electron microscopy analysis, performed with the use of Nova NanoSEM 200 (FEI, Netherlands) and energy dispersive spectroscopy analysis with EDS detector (EDAX, USA). In vitro biodegradation was examined by incubating the samples in PBS at the temperature of 37°C in INE 400 incubator (Memmert, Germany). Changes of pH and conductivity of the solutions were measured periodically.

Results and discussions

All of the products of ionic crosslinking were varying in their physical properties as a result of various concentrations of calcium chloride solutions and the differences in crosslinking densities. The alginate beads resulting from the use of 0,05M calcium chloride solution formed a shapeless gel while these from 0,7 M formed a block of agglomerated spheres. Separate regular beads were produced for $CaCl_2$ various concentrations in the range of 0,075–0,5M. The amounts of the crosslinked products, though, were moderate and decreasing with increasing the calcium chloride concentration, while the crosslinking density and the hardness of the beads increased. As ionic bonding is sensitive to polarity of solvents, including water, additional covalent crosslinking was performed. The chemical reaction in this case is based on ring opening of oxirane group of epichlorohydrin catalyzed with sodium hydroxide. The reaction occurs at room temperature. The yield of this process was high (up to 95%), however, similarly as in case of ionic croslinking, it also decreased with increasing calcium chloride concentration. For additional mechanical reinforcement the alginate beads were modified with cellulose nanofibers as described in the chapter Materials and methods.

The water absorption by a crosslinked material strongly depends on the crosslinking density. For the comparison, all kinds of the obtained alginate beads were investigated for water absorption by immersing them in distilled water for 24h and 48h. Water intake was determined by weight raise in relation to initial mass of a dry product. For the lower calcium chloride solution concentrations the water absorption was decreasing with icreasing the $CaCl_2$ concentration, but for the concentrations higher than 0,3 M the water absorption was stabilized at similar level. This effect could be observed in both ionically and covalently crosslinked beads and both after 24h and 48h. The water was fastest absorbed at the beginning and then the process rate was decreasing until the saturation of the material. The water absorption is strictly connected to the density of crosslinking. The higher $CaCl_2$ concentration the higher density of crosslinking and the lower water absorption. For cellulose reinforced alginate beads the water absorption was decreasing with increasing the amount of the additive. The relation between the time and the mass of absorbed water was similar as for the materials not containing cellulose. In case of ionically and covalently crosslinked alginate beads a change in the highest range of the concentration did not affect the yield of the process so it was occurring only to some maximal degree.

Morphology of the surface of all alginate beads independently on the crosslinking density was very similar. The surface of the beads has high roughness. The flatness is a result of contiguousness of the beads to each other or to the substrate during drying. Reinforcment of the beads with cellulose allowed to obtain the spheres of undisturbed shape. Qualitative elemental analysis was obtained with the energy dispersive spectroscopy. The ionically crosslinked product still containes certain amount of sodium and chloride ions, while after covalent crosslinking the contents of these elements were significantly lower, however calcium content decrease can be also seen. It means that the cations are eliminated during the reaction of epichlorohydrin with alginate molecules, and as a consequence it means that carboxyl groups are involved in the reaction. The in vitro biodegradation process was examined by incubating 200mg a sample in 20ml of PBS buffer for 14 days at the temperature of 37°C. The pH value change is directly connected with the degree of the biodegradation. The most intense biodegradation occurred during the first day of the incubation. Then the pH change were insignificant. For all of the products the observations were very similar.

Conclusions

The beads possessing various hardness corresponding to the degree of the crosslinking were fabricated. Crosslinking was conducted by two ways - ionically and covalently. The alginate beads were additionally reinforced by addition of cellulose fibers. The water absorption in the products was investigated. It strongly depends on the density of crosslinking. For samples obtained in the CaCl2 solution of the lowest concentration (0,1 M) the water absorption was almost twice of the dry alginate mass while in the samples obtained in the solutions of 0,3 M and higher concentration it was three times lower. Analogically, the water uptake in ionically bonded alginates was visibly higher than in this additionally crosslinked by covalent intermolecular bonding. The samples were characterized with scanning electron microscopy and energy dispersive spectroscopy.

Acknowledgements

The authors gratefully acknowledge the National Science Center (Poland) for financial support (grant no. 2011/01/B/STB8/07795).

References

[1] Jejurikar A., Lawrie G., Martin D, Grøndahl L.: A novel strategy for preparing mechanically robust ionically cross-linked alginate hydrogels. Biomedical Materials 6(2) (2011) 025010
[2] Pal K., Banthia A.K. , Majumdar D.K.: Polymeric Hydrogels: Characterization and Biomedical Applications - A mini review. Designed Monomers and Polymers 12 (2009) 197-220
[3] Grasselli M., Diaz E.L., Cascone O.: Beaded matrices from cross-linked alginate for affinity and ion exchange chromatography of proteins. Biotechnology Techniques 7(10) (1993) 707-712

PRELIMINARY STUDY ON THE ELECTROSPUN PLA–BASED NANOFIBRES AS BIOMATERIALS FOR THE TREATMENT OF CARTILAGE

Anna Magiera[1], Jarosław Markowski[2], Marta Lesiuk[3], Aleksander L. Sieron[3], Jan Pilch[2], Stanisław Błażewicz[1]*

[1] AGH University of Science and Technology,
Faculty of Materials Science and Ceramics,
Department of Biomaterials,
al. A. Mickiewicza 30, 30-059 Krakow, Poland
[2] Medical University of Silesia,
Department of Laryngology,
ul. Francuska 20, 40-752 Katowice, Poland
[3] Medical University of Silesia,
Department of General, Molecular Biology and Genetics,
ul. Medyków 18, 40-752 Katowice, Poland
* e-mail: blazew@agh.edu.pl

Abstract

Electrospinning is a simple and universal way to produce fibres from a variety of materials having diameters ranging from submicrometers to nanometers. Such fibres can be formed from resorbable and non-resorbable polymers, ceramics and their different combinations containing nanoparticles. Such a method has gained a great interest in medicine due to its ability to form a fibrous space architecture, similar to the natural extracellular matrix [1,2]. On the other hand, due to a wide range of technical facilities of electrospun fibers the method allows to create directionally-dependent space architecture of nanofibres which mimic natural tissues [3]. Considering the similarities between the microstructure created by nanofibres and the extracellular matrix, nanofibrous materials made by ES technique seem to be promising scaffolds to regenerate cartilage [4] and neural tissue [5]. A material which is used for cartilage scaffolds should mimic native cartilage, which is known to have an oriented structure associated with its mechanical and physiological functions [5]. Scaffold with a biomimetic-oriented architecture is an important requirement for tissue-engineered cartilage.

In this study, PLA oriented and non-oriented fibrous scaffolds were manufactured. Selected properties of the materials were analysed and dissussed in view of the manufacture of optimal structure for cartilage tissue engineering.

Keywords: *electrospinning, nanofibrous scaffold, cartilage*

[Engineering of Biomaterials, 128-129, (2014), 110-111]

Acknowledgments

This work was supported by the National Science Centre, PRELUDIUM 6 research program and project no. 2013/11/N/ST8/01169.

References

[1] Spaddacio C., Rainer A., Trombetta M., Vadala G., Chello M., Covino E., Denaro V., Toyoda Y., Genovese J.A.: Poly-L-lactic acid/hydroxyapatite electrospun nanocomposites induce chondrogenic differentiation of human MSC. Annals of Biomedical Engineering 37 (2009) 1376-89

[2] Xin X., Hussain M., Mao J.: Continuing differentiation of human mesenchymal stem cells and induced chondrogenic and osteogenic lineages in electrospun PLGA nanofiber scaffold. Biomaterials 28 (2007) 316-25

[3] Jia S., Liu L., Pan W., Meng G., Duan C., Zhang L.: Oriented cartilage extracellular matrix-derived scaffold for cartilage tissue engineering. Journal of Bioscience and Bioengineering 113 (2012) 647-653

[4] Lia W.J., Tulia R., Okafora C., Derfoula A., Danielsonb K.G., Halla D.J., Tuan R.S.: A three-dimensional nanofibrous scaffold for cartilage tissue engineering using human mesenchymal stem cells. Biomaterials 26 (2005) 599-609

[5] Yang F., Qu X., Cui W., Bei J., Yu F., Lu S., Wang S.: Manufacturing and morphology structure of polylactide-type microtubules orientation-structured scaffolds. Biomaterials 27 (2006) 4923-4933

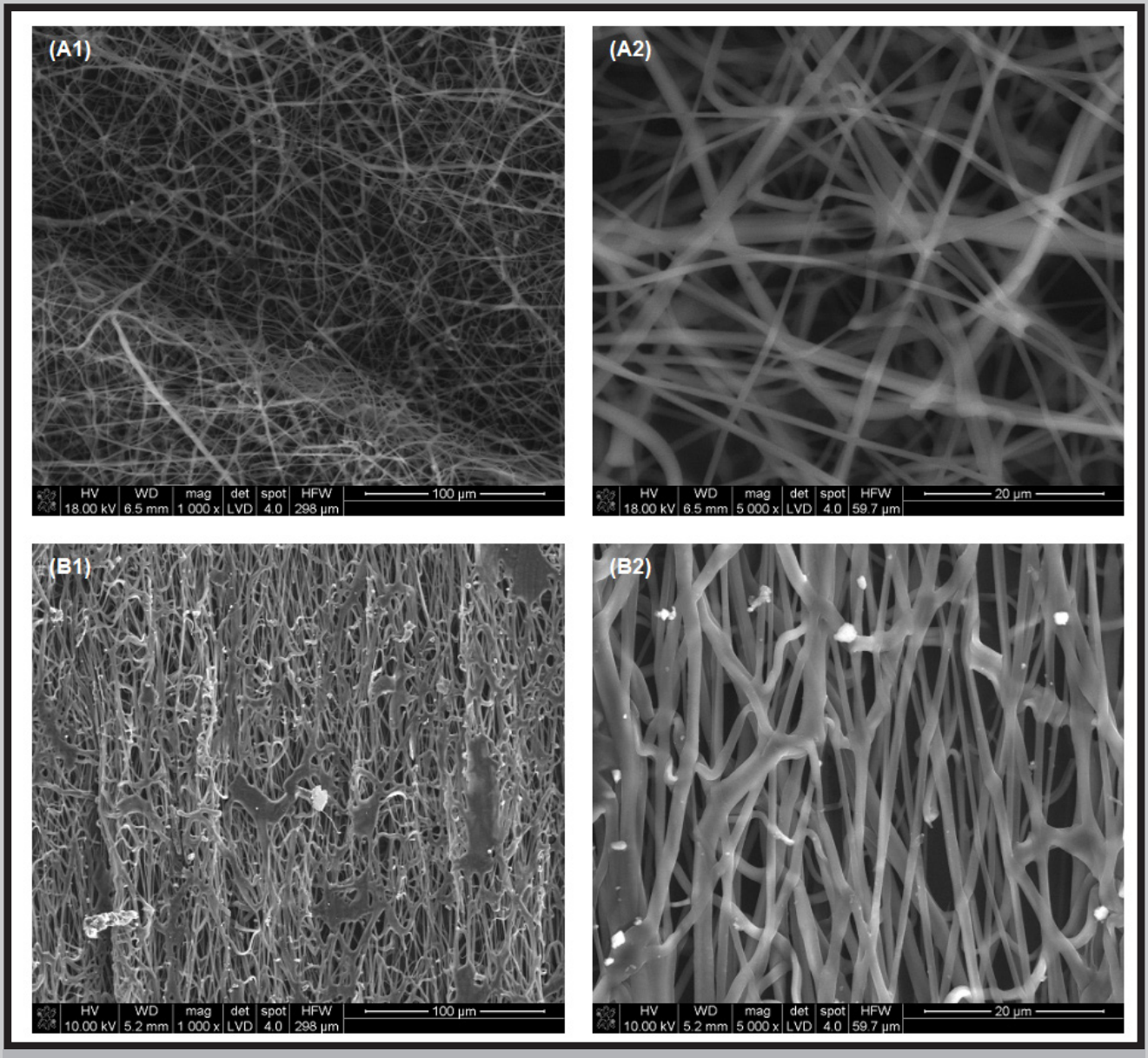

FIG. 1. SEM images of fibrous scaffolds: (A) non-oriented PLA, (B) oriented PLA. (Scale bars: (1) 100 µm, (2) 20 µm).

THE BIOCOMPATIBILITY IN VITRO STUDY OF AN INNOVATIVE ELASTOMER FOR HEART ASSIST DEVICES CONSTRUCTION

Magdalena Kościelniak-Ziemniak[1]*, Piotr Wilczek[2], Roman Kustosz[1], Małgorzata Gonsior[1], Alicja Błachowicz[1], Mirosława El Fray[3], Agnieszka Piegat[3], Marta Piątek-Hnat[3]

[1] Foundation for Cardiac Surgery Development, Artificial Heart Laboratory, Wolności Str. 345a, 41-800 Zabrze (AHL FRK)
[2] Foundation for Cardiac Surgery Development, Bioengineering Laboratory, Wolności Str. 345a, 41-800 Zabrze (BL FRK)
[3] West Pomerania University of Technology, Polymer Institute, Biomaterials and Microbiology Technologies Dept., (WPTU PI BMT Dept.) Pułaskiego Str. 10, 70-322 Szczecin,
* e-mail: mkoscielniak_ziemniak@frk.pl

[Engineering of Biomaterials, 128-129, (2014), 112-113]

Introduction

The progress in modern medicine would not have been possible without advanced medical devices application, basing on development of new biomaterials with improved biocompatibility properties. The new elastomeric biomaterial have been developed as a part of WPTU PI BMT Dept. study, dedicated to be used as a construction material of polish pulsatile extracorporeal ventricular assist device ReligaHeart EXT. The material is a co-polymer, basing on poly(terephthalate ethylene) (PET) modified by dimerized parts of fatty acids (DLA)- PET/DLA. The essential part of the new biomaterial investigation is its biocompatibility assessment in compliance with PN EN ISO 10993 [1]. The PET/DLA biocompatibility evaluation was performed for two biomaterial forms: the raw material and for the material technologically processed of high-pressure injection moulding.

Materials and Methods

The reaction of petroleum ether cleaned biomaterial PET/DLA with red blood cell components and fibroblasts was investigated in compliance with PN EN ISO 10993-1,4-5 [1]. Biomaterial was assessed in two forms: granulate before technological processing, and 8 mm diameter discs, manufactured using high-pressure injection moulding process. The biomaterial samples were prepared for study in accordance with guidelines defined for applied investigation technique, and in form representative for final medical device shape. The sterilization process of the PET/DLA biomaterial discs has been performed as 12 hours cycle of ethylene oxide exposure at temperature of 30°C, utilizing sterilization cabinet EOGas 4 series Andersen Products. After the sterilization process, the biomaterial has been submitted to a natural airing process for 28 days. The biomaterial granulate was indirectly contacted with the biological medium, while the biomaterial discs were tested using direct methods. The blood haemolysis examinations have been performed after biomaterial samples incubation with CPDA preserved Whole Blood, with increased temperature and natural slow mixing conditions, applied for period of 8 and 24 hours [1-4]. The following parameters were analyzed: blood morphology, concentration of free plasmatic haemoglobin (fHGB), red cells osmotic resistance. The Haemolysis Indexes (IH) have been calculated in compliance with ASTM 756 00. The cytotoxicity evaluation was performed on fibroblasts line - clone 929 L, treated with 5% CO_2 flow and temperature of 37°C for 48h [1]. The propidium iodide coloured cells have been investigated using fluorescence microscope.

Results

The free plasmatic haemoglobin (fHGB) concentration at the blood after contact with PET/DLA was retained on the level 0,5 g/L for both biomaterial forms: the raw material and material after technological processing (FIG. 1). The red blood cells parameters and osmotic resistance values were close to the preserved Whole Blood value and oscillated within referential values interval.

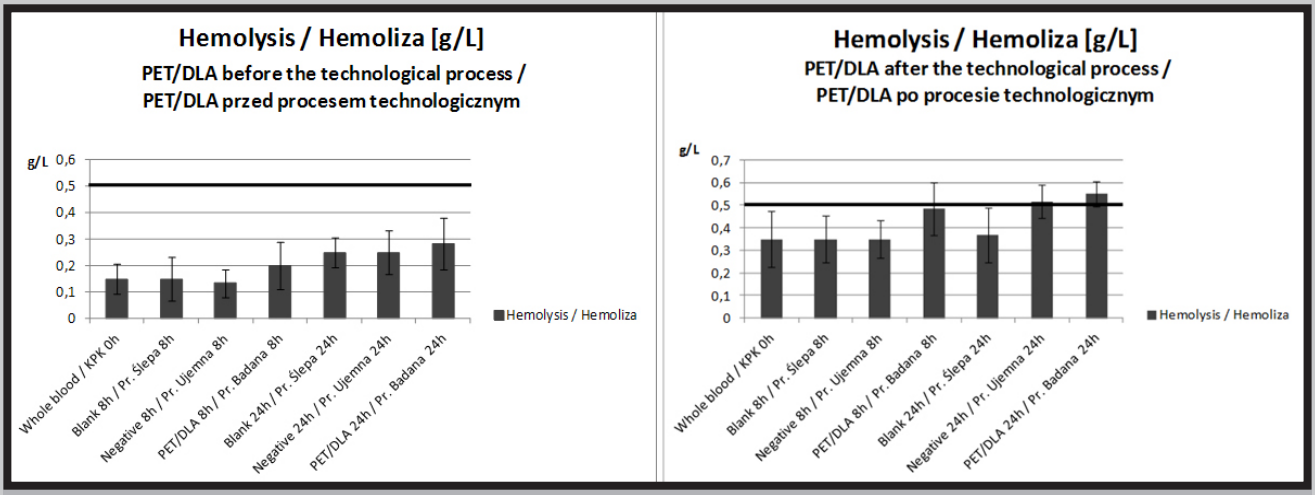

FIG. 1. Concentration of free osmotic haemoglobin for PET/DLA which were contacted with the preserved Whole Blood a) direct b) indirect. Legend: for the studied research groups:
• Whole Blood - the preserved Whole Blood; • Blank – Whole Blood standing at room temperature for 8 and 24 h, not subjected to the conditions of the experiment; • negative control - Whole Blood without contact with the test materials, subjected to the conditions of the experiment for 8 and 24 h (subject to natural slow mixing); • study group - tested biomaterials PET / DLA contacted with the preserved Whole Blood directly and indirectly, at the experimental conditions for 8 and 24 h.

The ASTM F 756-0 norm defines three intervals of haemolysis levels: IH from 0 to 2% - haemolysis level = non-haemolytic, IH from 2 to 5% - haemolysis level = slightly haemolytic, IH > 5% - haemolysis level = haemolytic. The Haemolysis Indexes of exanimated biomaterial have not exceeded 2% (FIG. 2). Pursuant to IH values, the assessed PET/DLA has been determined as non – haemolytic in both forms: row biomaterial and injection moulding processed.

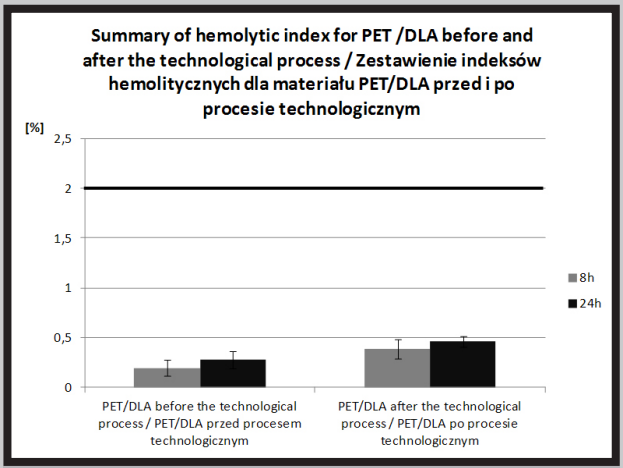

FIG. 2. Haemolysis Index for preserved Whole Blood after a contact with the PET/DLA in forms: granules (row material before technological process), and disc samples (after technological process).

Observation of culture for both: cells supplemented with extract of row material granulate, and cells after direct contact with injected biomaterial discs, haven't show the essential cytotoxicity feature. The number of necrotic cells has remained at the level from 0 to 0,83%. The remaining cells were positive in the presence of fluorescein diacetate (FDA) and classified as alive. Most of alive cells shown normal morphology, typical for fibroblasts. According to cytotoxicity assessment scale of ISO 10993-5 standard, there have been assigned: cytotoxicity level equal to 0 with no reactivity for studied extracts of row biomaterial PET/DLA before technological process, and cytotoxicity level equal to 1 with slightly reactivity for PET/DLA after the technological process.

TABLE 1. Results of fibroblasts cytotoxicity evaluation within indirect contact of PET/DLA before technological process (granulate of row material) and within direct contact of PET/DLA biomaterial injection moulded.

Biomaterial PET/DLA	Before technological process	After technological process
Cytotoxity Grade	0	1
Reactivity	None	Slight

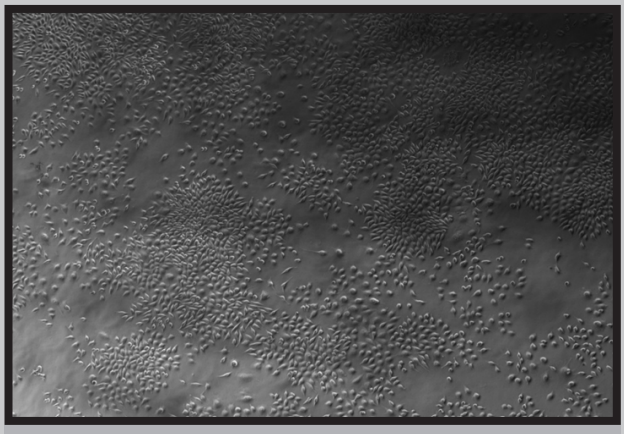

FIG. 3. Fibroblasts sample image after cytotoxicity tests for PET/DLA extract.

Conclusions

The performed initial biocompatibility investigations of biomaterials, in accordance with the Polish standard PN-EN ISO 10993, have shown that exanimated biomaterial PET/DLA is biocompatible in aspect of blood haemolysis and cytotoxicity - as well as a raw material and after technological process. Neither of investigated biomaterials have not negatively affected on morphological blood elements and have not caused cells cytotoxicity. The study will be continued in order to carry out the complete biocompatibility in vitro and in vivo evaluation of PET/DLA biomaterial after a technological injection moulding process, to confirm the full range of biomaterial biocompatible properties, essential for its application in the construction of heart prosthesis.

Acknowledgments

This study was realized as part of PBS1/A5/2/2012 project within the Applied Researches Program supported by the National Centre for Research and Development.

References

[1] PN EN ISO 10993 (Biological evaluation of medical devices – parts: 1, 4-5).
[2] ASTM F 756-00. Standard Practice for Assessment of Haemolytic Properties of Materials 2005
[3] H. Bomski. Podstawowe laboratoryjne badania hematologiczne. PZWL, Warszawa 1995.
[4] Monografia: Postępy inżynierii biomedycznej. Red. Lucyna Leniowska i Zbigniew Nawrat. Rzeszów 2013. Rozdział: Ocena wpływu oddziaływania polimerów konstrukcyjnych pompy Religa-HeartEXT na składniki czerwonokrwinkowe krwi. Magdalena Kościelniak-Ziemniak, Karolina Janiczak, Roman Kustosz, Małgorzata Gonsior. pp. 58-62.

THE EFFECT OF SURFACE MODIFICATION ON CORROSION RESISTANCE OF AISI 440B MARTENSITIC STAINLESS STEEL

Magdalena Łępicka, Małgorzata Grądzka-Dahlke*

Białystok University of Technology,
Faculty of Mechanical Engineering,
Department of Materials and Biomedical Engineering
* e-mail: m.dahlke@pb.edu.pl

[Engineering of Biomaterials, 128-129, (2014), 114-115]

Introduction

Issues concerning surface modification techniques are nowadays put in the context of biomaterials development directions. Efficient surface modification of finished products allows to increase their durability, corrosion resistance and improve their frictional properties. Both the diamond-like carbon coatings (DLC) and the low-temperature plasma nitrided (LTN) diffusion layers are mainly known for their good corrosion resistance [1-4] and excellent tribological properties [1,4-7]. However, relatively little attention is paid to matters concerning application of these layers in high-chromium martensitic steels.

Given the above arguments, searching for appropriate methods of surface modification of martensitic stainless steels, which are extensively used in e.g. surgical instruments manufacturing, seems reasonable. The aim of this study was to determine the effect of plasma nitriding and DLC coatings on corrosion characteristics of applied in surgical tools manufacturing PN-EN X90CrMoV18 (AISI 440B) steel.

Materials and methods

The research was made to determine the effect of surface modification on corrosion resistance of high-chromium martensitic steel PN-EN X90CrMoV18 (AISI 440B, DIN 1.4112). Potentiodynamic polarization scans and open-circuit potential tests of metallic materials were carried out on Radiometer analytical PGP201 potentiostat/galvanostat equipped with VoltaMaster 4 software, which comprise as an integral research kit. For the purposes of research the examined steel surface was treated with DLC coating (DLC – series 1). For comparison, analogous tests were carried out for steel plasma nitrided (seres 2) in 380°C (50% H_2 : 50% N_2). The reference sample was conventionally treated steel, tempered at 500°C (series 3).

Each open circuit potential (E_{OCP}) measurement and the potentiodynamic scan was performed in room temperature (21°C) 70 ml 0,9% $NaCl_{aq}$ solution. Using the included in the set software, the corrosion potential (E_{kor}), corrosion current (i_{kor}), polarisation resistance (R_p) and the corrosion rate were determined. All values were determined with respect to a saturated calomel electrode (SCE) as the reference electrode. The three-electrode electro-chemical cell consisted also of platinum auxiliary electrode with a contact area of 128 mm^2. Working electrode circular area of 50.24 mm^2 was left to mantain contact with the testing solution. An open circuit potential (E_{OCP}) was studied after two hours of immersion. The initial potentiodynamic polarisation scan potential was E_{OCP}-100 mV.

Once completed corrosion studies, microscopic observations were performed to determine the examined samples surface topography. Observations were carried out on a scanning electron microscope (SEM) Hitachi S-3000N equipped with and X-ray microanalyzer (EDX).

Results and discussion

The analyzed PN-EN X90CrMoV18 steel samples E_{OCP} change in time is presented in FIG. 1. Primarily, it can be noted that the initial potential of diamond-like carbon coated series (FIG. 1, series 1) is significantly more positive than other samples potentials. This implies that only DLC layer application allows refining the analyzed steel surface, making it chemically stable in physiological saline solution. Such properties are attributed to high density and low porosity of diamond-like carbon layers, thus the detail surrounding aqueous solutions and ions therein contained do not penetrate the surface layer [8]. Moreover, series 2 and 3 curves almost coincide, starting the potential drop from 300±20 mV. The observed for all series decrease in corrosion potential is related to the equilibrium processes, in which the corrosive dissolution is prevalent. Potentials stabilize after 80-100 minutes of immersion in physiological saline solution. What is important, approximately after 30 minutes of immersion first corrosion pits were visible on series 2 and 3 samples, whereas no changes were observed for series 1.

Corrosion behaviour of AISI 440B steel prepared samples during anodic polarization is given in FIG. 2. As it is depicted by the family of curves, there are significant differences of E_{kor} and i_{kor} values achieved by each series. Above all, as in open-circuit potential measurement, series 1 curve significantly differs from the others. Both decrease in i_{kor} and corrosion potential shift towards positive values are observed according to series 2 and 3. This means that applying DLC layer allows considerable delay in corrosion processes onset on finished product surface. In case of series 2 and 3, cathodic branches overlapping can be seen; differences between series are noted in anodic course. Course of the third curve is mild, while for series 2 pitting potential (-300 mV) can be noted. The occurrence of pitting potential is in literature attributed to development of corrosion pits on the anodically polarized sample.

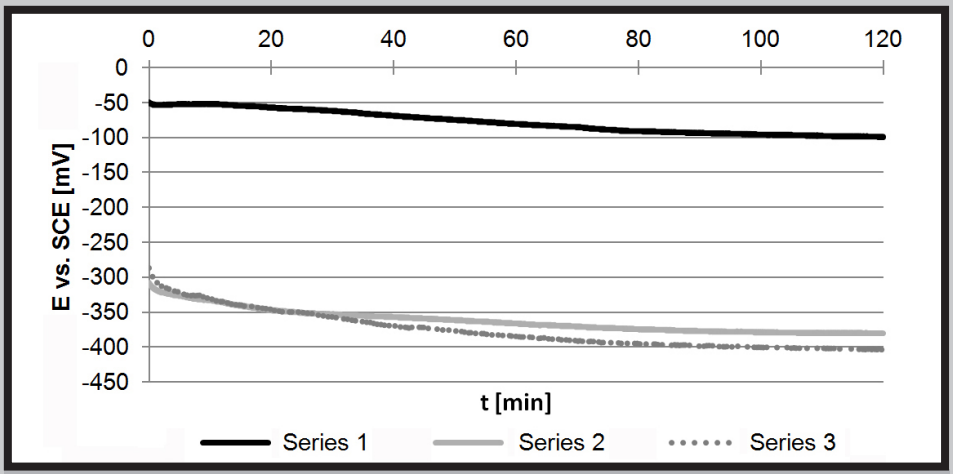

FIG. 1. An open-circuit potential of PN-EN X90CrMoV18 steel; 0,9% $NaCl_{aq}$ solution.

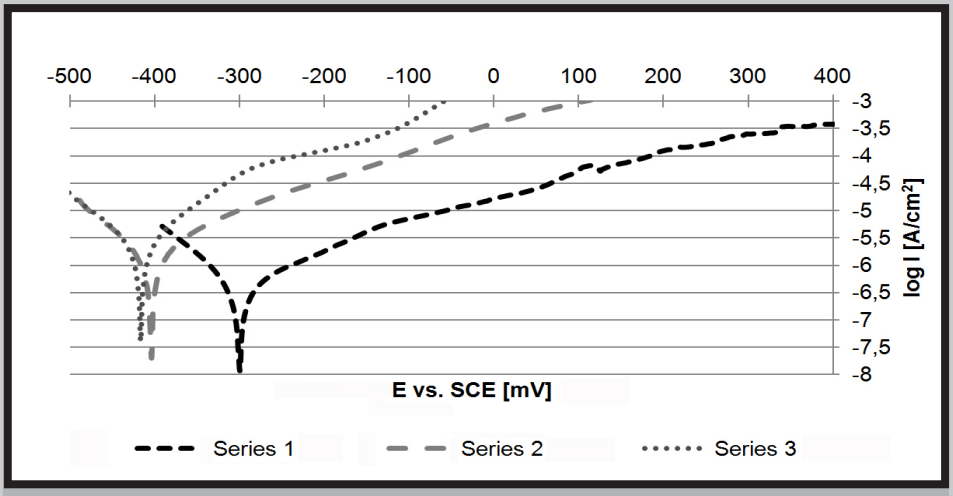

FIG. 2. Potentiodynamic curves of PN-EN X90CrMoV steel in 0,9% $NaCl_{aq}$ solution.

Conclusion

The obtained results suggest that DLC layers are promising coatings for use in manufacturing cutting surgical tools made of high-chromium martensitic stainless steel PN-EN X90CrMoV18. Unlike the low-temperature plasma nitriding, applying protective diamond-like carbon layer effects in increase of surface passivity, and thus – delays corrosive dissolution development. According to the authors, further analyses of suggested layer are needed, paying special attention to its friction properties and wear resistance in cutting tools applications.

Acknowledgements

This scientific work was supported by the Faculty of Mechanical Engineering, Białystok University of Technology, project No MB/WM/13/2014.

Author Magdalena Łępicka is a beneficiary of the project "Scholarships for PhD students of Podlaskie Vovoideship". The project is co-financed by European Social Fund, Polish Government and Podlaskie Vovoideship.

References

[1] Li C.X., Bell T.: Corrosion properties of plasma nitrided AISI 410 martensitic stainless steel in 3.5% NaCl and 1% HCl aqueous solutions. Corrosion Science 48 (2006) 2035-2049.
[2] Hadinata S.S., Lee M. T., Pan S.J., Tsai W. T., Tai C.Y., Shih C.F.: Electrochemical performances of diamond-like carbon coatings on carbon steel, stainless steel, and brass. Thin Solid Films 259 (2013) 12-416.
[3] Wang L., Su J.F., Nie X.: Corrosion and tribological properties and impact fatigue behaviors of TiN- and DLC-coated stainless steels in a simulated body fluid environment. Surface & Coatings Technology 205 (2010) 1599-1605.
[4] Xi Y., Liu D., Han D.: Improvement of corrosion and wear resistances of AISI 420 martensitic stainless steel using plasma nitriding at low temperature. Surface & Coatings Technology 202 (2008) 2577-2583.
[5] Azzi M., Amirault P., Paquette M., Klemberg-Sapieha J.M., Martinu L.: Corrosion performance and mechanical stability of 316L/DLC coating system: Role of interlayers. Surface & Coatings Technology 204 (2010) 3986-3994.
[6] Hauert R., Thorwarth K., Thorwarth G.: An overview on diamond-like carbon coatings in medical applications. Surface & Coatings Technology 233 (2013) 119-130.
[7] Love C.A., Cook R.B., Harvey T.J., Dearnley P.A., Wood R.J.: Diamond like carbon coatings for potential application in biological implants - a review. Tribology International 63 (2013) 141-150.
[8] Kim H.G., Ahn S.H., Kim J.G., Park S.J., Lee K.R.: Corrosion performance of diamond-like carbon (DLC)-coated Ti alloy in the simulated body fluid environment. Diamond & Related Materials 14 (2005) 35-41.